

**THE MINERALOGY, GEOCHEMISTRY AND
ORIGIN OF A LATE PRECAMBRIAN
ALTERATION PROFILE IN NW SCOTLAND :
AGALMATOLITE AND ITS LINKS WITH
CAMBRIAN SHALES**

LINDSAY KATHRYN FERGUSON

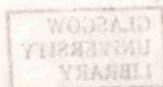
B.Sc. (Hons) STRATHCLYDE

A thesis submitted for the degree of Doctor of Philosophy

**Department of Geology & Applied Geology,
Faculty of Science,
University of Glasgow**

March 1992

© Lindsay K. Ferguson, 1992.



ProQuest Number: 13815413

All rights reserved

INFORMATION TO ALL USERS

The quality of this reproduction is dependent upon the quality of the copy submitted.

In the unlikely event that the author did not send a complete manuscript and there are missing pages, these will be noted. Also, if material had to be removed, a note will indicate the deletion.



ProQuest 13815413

Published by ProQuest LLC (2018). Copyright of the Dissertation is held by the Author.

All rights reserved.

This work is protected against unauthorized copying under Title 17, United States Code
Microform Edition © ProQuest LLC.

ProQuest LLC.
789 East Eisenhower Parkway
P.O. Box 1346
Ann Arbor, MI 48106 – 1346



The first carving of Scottish agalmatolite - by T. Daniels.
Sample from the 'cave' exposure [NC 438 661]

ABSTRACT

This thesis investigates the origin of an alteration profile developed beneath the Lewisian-Cambrian unconformity in Sutherland, NW Scotland and considers its postulated link with the genesis of shales of the overlying Cambrian succession.

Field investigation was carried out to determine the areal and vertical extent of the alteration. Samples were collected throughout the length of the unconformity and suites, containing samples from various depths in the alteration profile, were taken from different places along strike. Detailed investigation of the mineralogical changes with progressive alteration was carried out using optical microscopy, X-ray diffraction, Scanning electron microscopy, electron probe analysis and cathodoluminescence techniques. Geochemical behaviour was considered in light of results determined from X-ray fluorescence spectrometry, CO₂/H₂O and FeO determination and the ICP method of analysis was used for determination of boron concentration in samples. Stable isotope analyses and fluid inclusion investigation provided information on fluids and processes affecting the rocks. The K/Ar and ⁴⁰Ar/³⁹Ar dating techniques allowed the timing of formation of certain minerals to be ascertained.

Field evidence indicated that the alteration profile was developed in most places exposed beneath the unconformity throughout its length of outcrop. Its geometry suggests that the profile is a palaeosaprolite. The order of alteration of primary phases is consistent with that for stability of minerals during weathering, and the major secondary phases, pinite (very fine-grained muscovite) and pyrophyllite, are also found in other Precambrian palaeosaprolites. Geochemical behaviour was similar to that found in other Precambrian palaeosols with most elements being lost relative to Al₂O₃ (including all major element oxides apart from TiO₂ (and possibly ZrO₂)). Most of the criteria of Grandstaff *et al.* (1986, *Precamb. Res.* 32, 97-131) for identification of palaeosols are satisfied.

It is concluded that the alteration profile beneath the Lewisian/Cambrian unconformity in NW Scotland is a palaeosaprolite. The soil horizon was extensively developed throughout the area and formed during late Precambrian times prior to the

deposition of overlying strata. It developed under humid, tropical, oxidising conditions at moderate pH and was similar to a modern day pedalfers. However, only the lowermost 'C' horizon was preserved after the Cambrian marine transgression. The dominant clay weathering product, which was preserved beneath the Cambrian sediments, was illite, with kaolinite also preserved in places at the top of the profile. This indicates that the rocks retained had been weathered up to intermediate and advanced stages respectively.

Clays eroded from the soil formed the shales of the overlying succession and chemical weathering of the gneisses provided the cations for the formation of authigenic K-feldspar in the Cambrian succession. Boron was absorbed by illites from the seawater, which allowed the later development of tourmaline and which explains the regional geochemical boron anomaly over the Cambrian sedimentary rocks.

The present mineralogy of the palaeosaprolite developed after temperatures in the rocks reached $\sim 245^{\circ}\text{C}$ to 275°C , with pinites and pyrophyllite forming after illite and kaolinite respectively. This occurred at the end of the Caledonian orogeny at ~ 408 to 422 Ma in response to emplacement of the Caledonian thrust sheets.

ACKNOWLEDGEMENTS

I would like to start by acknowledging all those who have helped me in the various geology courses during my undergraduate studies. I am particularly indebted to the staff of the Department of Geology at the University of Strathclyde for their help and support. To them I am indebted.

Dr. Iain Allison, my supervisor, has been a great help and support throughout the project. His advice and encouragement have been invaluable. I am particularly indebted to him for his help and support. To him I am indebted.

DECLARATION

The material presented in this thesis summarises the results of four years of research carried out in the Department of Geology & Applied Geology of Glasgow University and the Department of Applied Geology of Strathclyde University under the supervision of Dr. Iain Allison. This study is based on my own individual research and any previously published or unpublished results of other researchers used in this thesis have been given reference in the text.

The material presented in this thesis summarises the results of four years of research carried out in the Department of Geology & Applied Geology of Glasgow University and the Department of Applied Geology of Strathclyde University under the supervision of Dr. Iain Allison. This study is based on my own individual research and any previously published or unpublished results of other researchers used in this thesis have been given reference in the text.

Lindsay K. Ferguson.

19/03/92

Through all this time I have been indebted to my family, particularly my mother, Mary, and my father, James, for their love and encouragement. I am particularly indebted to them for their help and support. To them I am indebted.

And, finally, to that Carpenter from Nazareth, Jesus Christ, who, through his love and whose grace has brought me into this world. To him, who is able to help you from falling and to present you before his glorious presence with great joy, to the only God and our Father, in glory, be majesty, power, and authority, through Jesus Christ our Lord, before all ages, now and for evermore. (Luke 24-25)

Through all this time I have been indebted to my family, particularly my mother, Mary, and my father, James, for their love and encouragement. I am particularly indebted to them for their help and support. To them I am indebted.

And, finally, to that Carpenter from Nazareth, Jesus Christ, who, through his love and whose grace has brought me into this world. To him, who is able to help you from falling and to present you before his glorious presence with great joy, to the only God and our Father, in glory, be majesty, power, and authority, through Jesus Christ our Lord, before all ages, now and for evermore. (Luke 24-25)

ACKNOWLEDGEMENTS

I would like to start by acknowledging all those members of staff who both instructed and inspired me in the various geological subjects during my undergraduate years at Strathclyde. It should not go unmentioned that the interest, concern and general attitude of members of staff at the Department of Applied Geology at the University of Strathclyde helped to endear many students both to that place and to the subject of Geology. To them I am indebted.

Dr. Iain Allison, my supervisor, who initiated this project, is thanked for his help, especially for his constructive criticism and support during writing up, and for allowing me the academic freedom to pursue research areas of my particular interest. This project was funded by the Natural Environment Research Council which is gratefully acknowledged.

Dr. George E. Bowes is thanked for his willing help with computer plots and general computing problems and Dr. Allan J. Hall for guidance with XRD work and general advice and direction. Grateful thanks are expressed to Professor Michael J. Russell for assuming responsibility during my supervisor's sabbatical, also for supporting me in my wish to do isotopic analysis, for the many references he has lent me and pointed out, and so much for his "empathy".

At the SURRC, Dr. Tony Fallick made available stable isotope facilities for work which has proved valuable to this project. Thank you, Tony, for helpful discussions and for proof-reading part of this thesis. Mitch McIntyre and Jim Imlach are also thanked for K/Ar work and Alison MacDonald for running oxygen samples. The $^{40}\text{Ar}/^{39}\text{Ar}$ laser probe analyses done with Dr. Ray Burgess proved important. My time in that lab was encouraging and Ray is thanked for his help, his willingness to answer my many questions and for proof-reading my Chapter pertaining to that work.

Thanks are due to Dr. Jeff Harris for important discussions over the years and for his help and concern. Dr. Brian Bell is thanked for valuable advice, for his interest and for proof-reading part of this thesis. Thanks also to Dr. R. Stuart Haszeldine for helpful discussion and for making available his computer during the closing stages of typing this thesis. Useful discussion from Professor Brian Bluck, Hilde Skauli, Dr. Colin Braithwaite, Dr. Ben Doody, Dr. Alan Owen and Professor Donald Ramsay is also appreciated.

Dugald Turner and Murdoch McLeod are thanked sincerely for their assistance with XRD and general geochemistry queries and for providing a friendly working atmosphere.. Thanks are due to Dugald for some important discussions. The technical assistance and expertise of Peter Ainsworth - SEM, Jim Gallagher and George Bruce - XRF, John Gilleece and Peter Wallace - Polished and thin sections, Roddy Morrison and Robert MacDonald for their general help are also appreciated. Douglas Maclean is also acknowledged for providing an excellent photographic service, which was of great value in the presentation of this thesis.

Dr. Pete Hill and Dr. Stuart Cairns at the Grant Institute of Geology, Edinburgh University, are thanked for their guidance and on-hand assistance (at all hours!) during my times on the probes in Edinburgh. Thanks also to Dr. Nick Walsh at the Royal Holloway and Bedford New College, London, who gave me instruction there on preparation of samples for boron analysis, and made available ICP(S) facilities.

Thanks are due to all those who sponsored my trip to China and who helped in some of my applications for that sponsorship, especially the Mineralogical Society of Great Britain, the NERC, the Department of Geology & Applied Geology, the West Lothian Education Trust, Livingston Rotary Club, my parents, Dr. Allan J. Hall, Dr. Iain Allison, Dr. Brian Bell and Dr. Jeff W. Harris. Also to Xinquan Ma for translating a paper from Chinese into English.

I would also like to thank all my family and friends who have encouraged and supported me over the period of this project, -to friends at St. George's Tron Parish Church and the 'Navigator' Bible Study Group, and especially to Pat and Garth Menzies, Helen Belford, Billy McQuade, David Ellis, Eric Alexander and the Murray family. From the Departments, Mark Osborne is thanked for his friendship and encouragement and also Ross Fulton, Nassir Benzitun, Iain McDonald and Miles Jordan. Miles is also thanked for assistance with some geochemical analyses. Thanks to staff and postgraduates in general, especially Maggie, Derek, Andy, Janey, Joe, Gian, Orla, Gary, Richard, Sharif, Clark, Janette Forbes and Shiela, the janitors, John and Eddie and many more, including some undergraduates who have made the Department of Geology & Applied Geology a friendly place to be in. Thanks also to my flatmates and other friends, especially Kirsty, Yvonne, Catie, David, Susan, Margaret and June, and to my brother, Ross. Sincere thanks are due to Heather Crichton for typing this thesis and for her friendly encouragement. Also to my mother for her ever willing help in proof-reading and Sheila Hall for help with final preparation of some graphs.

Through all this time I have been indebted to my parents, Kathleen and Robert, for their support, both financial and moral. Their love and encouragement has been invaluable.

And, finally, to that Carpenter from Nazereth, Jesus Christ, whose love constrains me, my God, whose Grace has brought me safe this far.

"To Him, who is able to help you from falling and to present you before his glorious presence without fault and with great joy, to the only God and saviour, be glory, be majesty, power and authority, through Jesus Christ our Lord, before all ages, now and for evermore" (Jude: 24-25).

CONTENTS

		Page
1	INTRODUCTION	1
2	HISTORY OF RESEARCH	4
	Derivation of the name "agalmatolite"	5
	Definition	5
3	MODERN WEATHERING PROFILES, PRECAMBRIAN PALAEOOLS, SIMILAR HORIZONS OF HYDROTHERMAL ORIGIN AND THEIR ECONOMIC POTENTIAL	7
	MODERN SOILS	7
	Primary mineral stability during weathering	8
	Secondary minerals and their order of formation in weathering environments	9
	Rate of formation and erosion	10
	PRECAMBRIAN PALAEOOLS	10
	SIMILAR HORIZONS OF HYDROTHERMAL ORIGIN	13
	ECONOMIC SIGNIFICANCE OF SUCH PYROPHYLLITE-MUSCOVITE-RICH ROCKS	16
	Pyrophyllite	17
	<i>China</i>	17
	<i>North America</i>	17
	<i>Southern Africa</i>	17
	<i>NW Scotland</i>	18
	Carving Stone	18
	<i>China</i>	18
	<i>North America</i>	19
	<i>Southern Africa</i>	19
	<i>NW Scotland</i>	19
4	FIELDWORK	20
	INTRODUCTION	20
	Background	20
	FIELD OCCURRENCES	21
	Description of unconformity	24
	Northern Area	24
	Central Area	27
	Cranstackie	27
	Arkle	27
	Ben Stack	28
	Southern Area	29
	REASONS FOR THE VARIATION IN EXTENT OF DEVELOPMENT OF AGALMATOLITE	32
	Regional	32
	Local	33
	1 Precambrian faulting	33
	2 Irregular bottom surface	34
	DISCUSSION	34
6	CONCLUSION	34
5	MINERALOGY AND MINERAL CHEMISTRY	36
	INTRODUCTION	36
	ANALYTICAL TECHNIQUES	37
	GENERAL MINERALOGICAL VARIATIONS	39

	Hand specimen changes	39
	Thin section	40
	CHANGES OBSERVED IN SPECIFIC MINERALS	45
	Progressive alteration of Primary Minerals	46
	Plagioclase	46
	Progressive replacement	46
	Chemical analysis	49
	K-feldspar	50
	Progressive replacement	50
	Biotite	53
	Progressive alteration	53
	Mineral chemistry	54
	Quartz	61
	Progressive replacement	61
	Surface features	66
	Quartz/Secondary mineral interface textures	66
	Dissolution textures	66
	Secondary silica	69
	Low-T cristobalite	69
	Progressive development of Secondary Minerals	71
	Pinite	71
	Texture	71
	X-ray diffraction	75
	Methods	77
	Results	78
	Errors in measurement of peak positions and intensity	83
	Mineral Chemistry	83
	Qualitative	83
	Quantitative	86
	Tourmaline	87
	Tourmaline in tourmaline/quartz veinlets	87
	Tourmaline in rock body	88
	Development of tourmaline associated with remnant biotite	88
	Texture of tourmaline 'suns' from SEM investigation	91
	Tourmaline composition	97
	Blue 'sun' and green tourmaline	97
	Vein tourmaline	98
	Displaying results	98
	Results and mineral interpretation	100
	Pyrophyllite	102
	Optical and SEM investigation	102
	Mineral chemistry	106
	Opaques	107
	Introduction	107
	Suite CG-rutile	107
	Agalmatolite at [NC 4361 6240]	107
	Zones of deep red staining	112
	Steely grey minerals	112
	White material	113
6	GEOCHEMISTRY	115
	INTRODUCTION	115
	RESULTS	115
	INDEXING WEATHERING	120
	Chemical Index of Alteration	121
	Results	121

	BORON	Interpretation	122
	GAINS AND LOSSES		125
	1 Gresens' analysis		125
	Composition-volume diagrams		126
	Application and Results		127
	2 Isocon Diagram		132
	Plotting the diagram		132
	Application and Results		133
	DISCUSSION		137
	Alumina, Titania, Silica and their implications concerning pH		137
	Alkalis		139
	Alkaline Earths		140
	CO ₂ , H ₂ O		141
	P ₂ O ₅		142
	Iron		142
	Fe ³⁺ /Fe ²⁺		143
	Mn		143
	Co, Cr, Ni		144
	Ga		145
	Lanthanides; La, Ce		145
	Actinides; U, Th		146
	Y and Zr		146
	Zn, Cu, Pb		147
	Au		148
	CONCLUSION		148
7	INTERPRETATION OF MINERAL PARAGENESIS, INCLUDING STABLE ISOTOPE INVESTIGATIONS		150
	PINITE		150
	PYROPHYLLITE		151
	PLAGIOCLASE		155
	BIOTITE		155
	QUARTZ	Primary	156
		Secondary	156
	K-FELDSPAR		157
	Oxygen isotope investigation of K-feldspar (separates)		157
	Samples		158
	Results		158
	Interpretation		162
	TOURMALINE		163
	Stable isotope investigation		163
	Results		163
	Interpretation		168
	DISCUSSION		169
		Mineral paragenesis of the alteration profile	169
		Comparison with profiles in North America	172
8	GEOCHEMICAL LINKS BETWEEN THE ALTERATION PROFILE AND CAMBRIAN SHALES OF NW SCOTLAND		176
	INTRODUCTION		176
	Geological context	Mineralogical and Field Evidence	180
	Hydrothermal alteration	K ⁺ supply	180
	K/Rb RATIOS	Metamorphism	181

	BORON		186
	Introduction		186
	Methodology		188
	Analyses and determination of Bppm		188
	Samples		189
	Results		189
	Interpretation		194
	DISCUSSION		196
	<i>Tephra derivation</i>		197
	<i>Genesis related to later mineralising events</i>		198
9	AGE DETERMINATION OF CAMBRIAN SHALES AND PINITE FROM THE PALAEOSOL		200
	⁴⁰ Ar/ ³⁹ Ar LASER PROBE INVESTIGATION OF AGES OF CAMBRIAN SHALES		200
	Introduction		200
	Material studied		200
	1 Green shale (Eriboll sandstone (Lower Member) -0988)		201
	Sample description		201
	Results		202
	Interpretation and Discussion		207
	Reasons for resetting of clasts and not matrix		209
	2 Banded black shaly rock (Furoid beds member -0100)		210
	Results and Interpretation		210
	Discussion		212
	3 Black shale (Eriboll sandstone (Lower Member) -0589)		213
	Sample description		213
	Analyses and analytical problems		213
	Results		215
	<i>Feldspars</i>		215
	<i>Black shale</i>		215
	<i>Brown crystals</i>		217
	Interpretation		217
	Discussion		218
	K/Ar DETERMINATION OF THE AGE OF PINITE FORMATION		221
	Introduction		221
	Results		221
	Interpretation and Discussion		222
	CONCLUSIONS		223
10	IMPLICATIONS OF THIS STUDY		224
	SUMMARY OF THE GEOLOGICAL HISTORY		224
	WIDER IMPLICATIONS		226
	FURTHER WORK		228
11	CONCLUSIONS		230
	REFERENCES		236
	APPENDICES		249
	1 Agalmatolite (Shoushan Stone) of China		249
	INTRODUCTION		249
	Number of deposits and locations in China		249
	Geological environments of formation		250
	1 Hydrothermal pyrophyllite		250
	2 Metamorphic pyrophyllite		251

LIST OF FIGURES

	a) <i>Dynamic metamorphism</i>	251
	b) <i>Burial metamorphism</i>	251
	c) <i>Regional metamorphism</i>	251
CHAPTER 1	Chinese nomenclature	252
	Uses	252
1.1	FUJIAN PROVINCE	253
	Dongzi deposit	253
CHAPTER 3	Geological setting	253
	Orebodies	256
3.1	Processing the pyrophyllite at Dongzi	259
	Crushing	259
3.2	Shoushan deposit	261
	Extraction methods	261
	Original site of Shoushan Stone	263
CHAPTER 4	CARVING "SHOUSHAN STONE"	263
	Types of pyrophyllite used for carving	264
4.1	Carving procedures (Fuzhou carving factory)	264
4.2	Workshop procedure for carving	265
	Finished carvings	266
CHAPTER 5		
2	Samples used in this project	267
3.1	3 Instrument conditions used on the XRD machine	271
5.2	4 Test statistic ('t-test')	271
5.3	5 Alteration of plagioclase	272
5.4	6 Major element chemistry of biotites	273
5.5	7 Major element chemistry of pinites	275
5.6	8 Major element chemistry of tourmaline	278
	a Vein tourmaline	278
5.7	b Blue 'sun' tourmaline rosettes	279
5.8	c Green tourmaline	281
5.9	9 Major element chemistry of pyrophyllite	282
5.10	10 Methods used for whole rock geochemical analysis	283
5.11	11 Whole rock major, minor and trace element compositions	285
5.12	12 Variation diagrams	291
5.13	13 Chemical Index of Alteration values for samples in Fig. 6.2	294
CHAPTER 6	14 Precambrian palaeosols referenced in the text	295
	15 Whole rock geochemistry of shales	298
6.1	16 a) Preparation procedure for determination of boron by ICPMS	300
	b) Operating conditions for the ICP	302
	c) Intensities determined by ICP spectrometry	303
	d) Determination of Bppm from intensities	304
6.2a	e) Determination of seawater column required to supply boron	
6.2b	concentration found in agalmatolite	305
6.3	17 Experimental methods for $^{40}\text{Ar}/^{39}\text{Ar}$ laser probe investigation	306
6.4	18 Quantitative EDS analyses of minerals in sample 0988	308
6.5	19 Ages determined from $^{40}\text{Ar}/^{39}\text{Ar}$ laser probe analysis	309
6.6	Relative behaviour of different elements with progressive alteration	149
CHAPTER 7		
7.1	Phase diagrams for the muscovite → kaolinite → pyrophyllite and muscovite → pyrophyllite.	153
7.2	Variation in $\delta^{18}\text{O}$ of K-feldspar with depth below the unconformity.	161
7.3	Oxygen isotope composition of quartz and tourmaline, compared with published data.	165

LIST OF FIGURES**CHAPTER 1**

- 1.1 Outcrop of Lewisian and Cambrian rocks in NW Scotland. 2

CHAPTER 3

- 3.1 Cartoon sections of the alteration sequences in rocks of Newfoundland and NW Scotland. 14
- 3.2 Sketch section of secondary minerals in hydrothermally altered dacitic tuff, Dongzi. 15

CHAPTER 4

- 4.1 Outcrop of Lewisian/Cambrian unconformity north of Assynt. 23
- 4.2 1:50,000 O.S. map of Arkle with unconformity marked. 28

CHAPTER 5

- 5.1 Mineralogical variations as a function of depth. 44
- 5.2 Comparison of fresh and altered biotite by qualitative EDS analysis. 58
- 5.3 Weight % oxide of biotite vs. whole-rock for selected major element oxides. 60
- 5.4 X-ray diffractograms of typical igneous muscovite and pinite. 76
- 5.5 X-ray diffractogram traces of four pinite samples. 79
- 5.6 X-ray diffractograms of pinite and muscovite analysed under the same conditions. 84
- 5.7 Graphical output from qualitative analyses across a mass of pinite. 85
- 5.8 Cartoons of the formation of tourmaline at the expense of biotite. 90
- 5.9 Plot of compositions of tourmalines. 99
- 5.10 Relationships between tourmalines analysed and values given by Deer *et al.* (1986) 101
- 5.11 Mole ratio plot. 106

CHAPTER 6

- 6.1 Variation diagrams for major element oxides and trace elements from [NC 4385 6614] (a) Gneiss suite, 117
(b) Pegmatite suite, 118
(c) Amphibolite suite 119
- 6.2a Variation in Chemical Index of Alteration with depth at [NC 4385 6314]. 123
- 6.2b Variation in Chemical Index of Alteration with depth from other locations. 124
- 6.3 Composition-volume diagrams for (a) rocks in the cave gneiss suite 129
(b) rocks in the cave pegmatite suite. 131
- 6.4 Isocon diagrams comparing rocks from the cave gneiss suite [NC 478 661]. 135
- 6.5 The solubility of silica and alumina as a function of pH. 139
- 6.6 Relative behaviour of different elements with progressive alteration. 149

CHAPTER 7

- 7.1 Phase diagrams for the transformations kaolinite → pyrophyllite and muscovite → pyrophyllite. 153
- 7.2 Variation in $\delta^{18}\text{O}$ of K-feldspar with depth below the unconformity. 161
- 7.3 Oxygen isotope composition of quartz and tourmaline, compared with published data. 165

7.4	Oxygen and hydrogen isotope compositions of tourmaline, compared with published data.	165
7.5	Homogenisation temperatures for fluid inclusions in the veinlet quartz.	167
7.6	$\delta^{18}\text{O}_{(\text{SMOW})}$ and $\delta\text{D}_{(\text{SMOW})}$ fields for naturally occurring waters.	167

CHAPTER 8

8.1	Stratigraphic log of Cambrian clastic sediments.	177
8.2	$\text{K}_2\text{O}(\%)$ vs. Rb (ppm) of Precambrian rocks and Cambrian shales - this project.	183
8.3	$\text{K}_2\text{O}(\%)$ vs. Rb (ppm) of Precambrian rocks and Cambrian shales - other data.	185
8.4	Whole-rock boron concentrations for altered and fresh Lewisian rocks (vs depth below unconformity) and Cambrian shales.	191
8.5	Boron (ppm) vs. Al_2O_3 (wt%) for altered and fresh sub-unconformity rocks and Cambrian shales.	192
8.6	Whole-rock B/ Al_2O_3 concentrations for altered and fresh Lewisian rocks (vs depth below unconformity) and Cambrian shales.	193

CHAPTER 9

9.1	$^{40}\text{Ar}/^{39}\text{Ar}$ ages for minerals from green shaly sand, 0988.	206
9.2	$^{40}\text{Ar}/^{39}\text{Ar}$ laser probe ages from traverses in Fucoid Beds sample (0100).	211
9.3	$^{40}\text{Ar}/^{39}\text{Ar}$ ages for minerals from black shale, 0589.	216
9.4	Comparison between ages of detrital feldspars from 0589 and K-feldspar from Ohio, U.S.A.	219

APPENDIX 1

A1.1	Chinese provinces with known pyrophyllite deposits.	250
A1.2	Sketch of orebody 4 (Dongzi).	256

LIST OF TABLES

CHAPTER 3

3.1	Criteria for identification of palaeosols.	12
-----	--	----

CHAPTER 5

5.1	dÅ and I/I_1 values for peak positions of pinites and other muscovites from JCPDS.80	
5.2	Peak ratios and I/I_1 values for selected pinites samples.	82

CHAPTER 6

6.1	General variations in weight% of major element oxides with alteration at [NC 4385 6314].	116
-----	--	-----

CHAPTER 7

7.1	$\delta^{18}\text{O}$ isotopic values for K-feldspar separates.	160
7.2	$\delta^{18}\text{O}_{(\text{SMOW})}$ and δD results from tourmaline and quartz mineral separates.	163

CHAPTER 9

9.1	Samples investigated in this project.	201
-----	---------------------------------------	-----

9.2	K/Ar ages for pinite samples from west of Loch Eriboll.	221
APPENDIX 1		
A1.1	Chinese categories of Shoushan stone.	252
LIST OF PLATES		
	Carving of Scottish agalmatolite	Frontispiece
CHAPTER 4		
4.1	Regional view of Lewisian/Cambrian unconformity.	22
4.2	Agalmatolite at "the cave" [NC 438 661].	26
4.3	Agalmatolite ~2m below the unconformity at [NC 4387 6611].	26
4.4	Sheared agalmatolite at [NC 3154 3241].	30
4.5	Warped Lower Member units, east of Loch Glendhu [NC 3154 3241].	31
CHAPTER 5		
5.1	Progressive changes in pegmatite and gneiss suites with alteration.	42
5.2a	Altered Lewisian gneiss at [NC 4387 6611].	43
5.2b	Green and purple agalmatolite [NC 4361 6240].	43
5.3	Progressive replacement of plagioclase.	47
5.4	Cathodoluminescence image of overgrowth on plagioclase crystal.	48
5.5	Exposure containing deep pink K-feldspar crystals.	51
5.6	Progressive replacement of microcline.	52
5.7	Progressive replacement of biotite crystals.	56
5.8	Biotite at various stages during alteration.	57
5.9	Progressive replacement of quartz by pinite.	63
5.10	Progressive replacement of quartz by pyrophyllite.	64
5.11	Relationships between quartz and secondary minerals.	65
5.12	Pinite, quartz and secondary low-cristobalite.	67
5.13	Dissolution textures on quartz crystals.	68
5.14	Progressive stages of growth of low cristobalite.	70
5.15	Pinite textures.	73
5.16	Pinite aggregate with ghost precursor mineral boundaries.	74
5.17	Tourmaline in altered pegmatite and tourmaline/quartz veinlets.	92
5.18	Tourmaline/quartz veinlets.	93
5.19	a Blue 'sun' tourmaline and b green tourmaline.	94
5.20	Tourmaline formation associated with altering biotite.	95
5.21	SEM images of 'sun' tourmaline and tourmaline associated with biotite.	96
5.22	Pyrophyllite consuming quartz.	104
5.23	Pyrophyllite textures.	105
5.24	Altered gneiss from [NC 4361 6240].	109
5.25	Opagues from the alteration profile at [NC 4361 6240].	110
5.26	Colour backscatter image of opagues from [NC 4361 6240].	111
5.27	Opagues from haematite-rich zone.	114
CHAPTER 8		
8.1	SEM photomicrographs of black argillitic shale from the Fucoïd Beds member.	178
8.2	Boron concentrations from stream sediments in Scotland.	187

CHAPTER 9

9.1a	Sample 0988.	203
9.1b	SEM secondary electron image of a polished thin section of 0988.	203
9.2a	Backscatter electron image of 0988.	204
9.2b	Close-up of 9.2a.	204
9.3	Composition of matrix as compared with feldspar clasts.	205
9.4a	Black shale interleaving between quartzarenites of Eriboll sandstone.	214
9.4b	Thick section of black shale, 0589.	214

APPENDIX 1

A1.1	Geological map of the Dongzi pyrophyllite deposit.	254
A1.2	Dongzi pyrophyllite deposit.	255
A1.3	Field samples from orebody 4/1.	257
A1.4	Rock samples from the mineralised zone.	258
A1.5	Pronounced silicified ridge.	259
A1.6	The two stages of jaw crushing.	260
A1.7	Outlets for the 500# and 1000# fines.	260
A1.8	Faults associated with the caldera at Shoushan.	262
A1.9	Location of Tianhuang.	263
A1.10	Fuzhou carving factory.	264
A1.11	Sample at initial stages of sculpting.	265
A1.12	A complicated piece during the final stages of sculpting.	265
A1.13a	Carving of Tianhuang.	266
A1.13b	Shoushan stone horse.	266

CHAPTER 1

INTRODUCTION

Agalmatolite was rediscovered in Scotland in 1984. In search for evidence of a Precambrian weathered surface in Sutherland, Russell and Allison came across a peculiar alteration profile at the top of the Lewisian basement, immediately beneath the Cambrian unconformity. The crystalline basement had been altered to an attractive, soft, waxy rock, largely retaining the gneissic layering and displaying a variety of greenish colours in marked contrast to the grey and pink gneisses. Named agalmatolite by Heddle (1881), this rock had been unreported since the mapping of the NW Highlands by the Geological Survey around the turn of this century.

This peculiar profile has only been found immediately beneath this major unconformity in NW Scotland, where Proterozoic Lewisian gneisses, pegmatites and amphibolites are overlain by quartz arenites of the Cambrian succession. This unconformity extends from the north coast in a SSW direction for about 80km until it becomes covered by the Moine nappe (Fig. 1.1).

The agalmatolite of this profile is largely olive-green to yellow and consists predominantly of very fine grained muscovite of the form pinite. Peach *et al.* (1907) consider that it formed due to weathering. Cardenas (1986) also concludes, from his investigation of one exposure on the North coast at [NC 438 661], that it represents a fossilised soil profile. Based on this weathering hypothesis, Russell and Allison (1985) imagined that ionic potassium, ionic or colloidal aluminium as well as silica released by weathering, were transported by ground and river waters to the nearby marine shelf and Dalradian basin where they became constituents of the K-feldspar in the Fucoïd Beds of the Cambrian succession and in the hydrothermal celsian deposit of the Middle Dalradian respectively. The residual quartz was reworked to form the overlying Eriboll sandstones of the Cambrian succession (cf. Anderton *et al.* 1979).

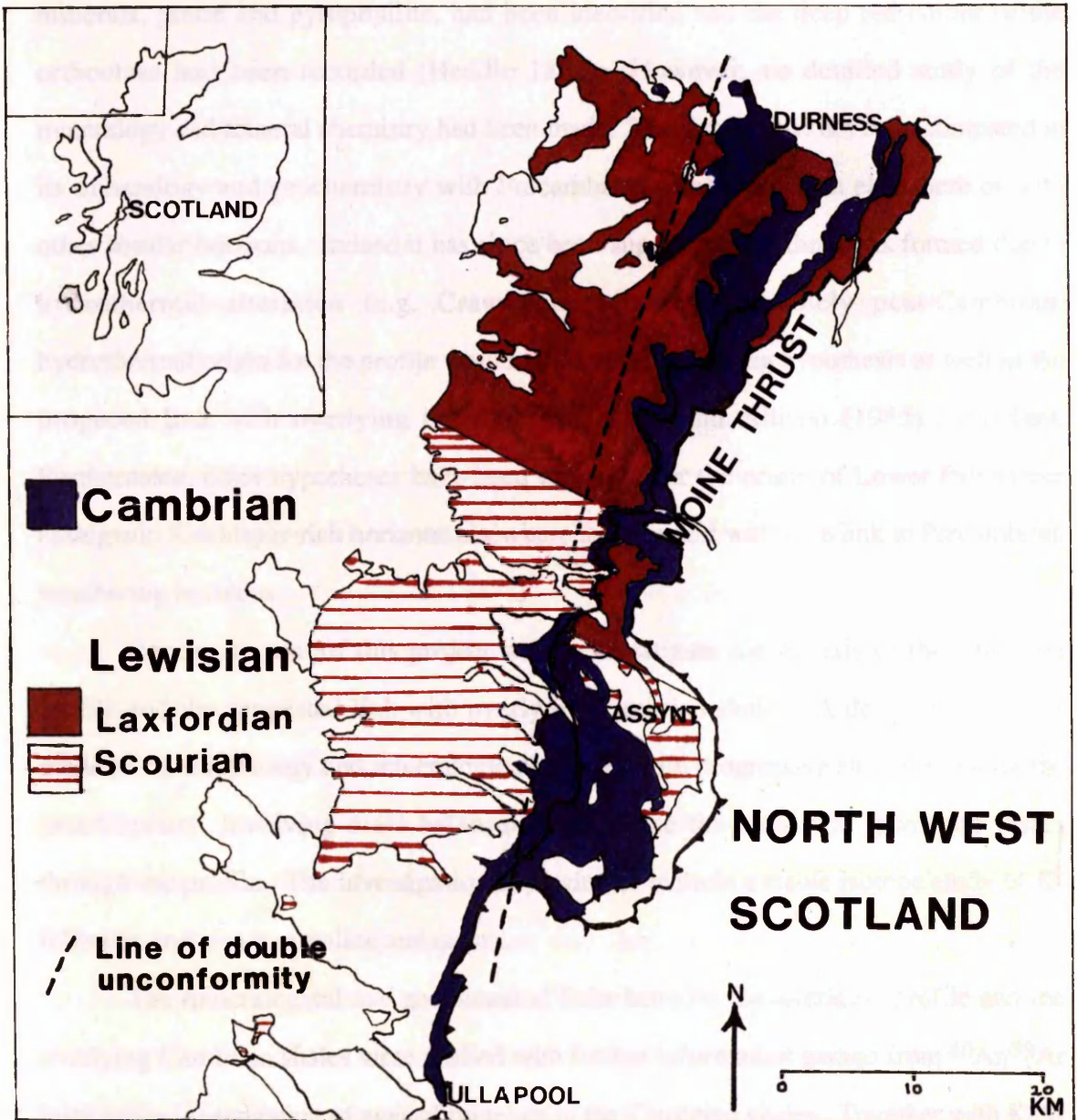


Fig. 1.1

Outcrop of Lewisian (Precambrian) and Cambrian (Phanerozoic) rocks in NW Scotland.

Although several exposures had been discovered, little was known about the extent of and variations in development of the alteration profile, with Cardenas drawing his conclusions almost completely from the study of one exposure. The secondary minerals, pinite and pyrophyllite, had been identified and the deep red colour of the orthoclase had been recorded (Heddle 1881). However, no detailed study of the mineralogy and mineral chemistry had been made. This profile had not been compared in its mineralogy and geochemistry with Precambrian palaeosols from elsewhere or with other similar horizons. Indeed it has since been suggested that the rocks formed due to hydrothermal alteration (e.g. Craw pers. comm.). A solely post-Cambrian, hydrothermal origin for the profile would render the weathering hypothesis as well as the proposed link with overlying horizons of Russell and Allison (1985) redundant. Furthermore, other hypotheses have been proposed for the origin of Lower Palaeozoic authigenic K-feldspar-rich horizons elsewhere in the world without a link to Precambrian weathering horizons.

Hence, the aim of this project was to investigate the genesis of the alteration profile and the suggested link with overlying Cambrian shales. A detailed study was made of the mineralogy and mineralogical changes with progressive alteration and of the geochemistry, involving mass balance to determine the elemental gains and losses through the profile. The investigation expanded to include a stable isotope study of K-feldspars and also tourmaline and quartz.

The mineralogical and geochemical links between the alteration profile and the overlying Cambrian shales were studied with further information gained from $^{40}\text{Ar}/^{39}\text{Ar}$ laser probe investigation of ages of minerals in the Cambrian shales. Together with K/Ar age determination of pinite from the profile, these data elucidated the sequence of events in the genesis of the profile.

After this time, however, the name disappeared from usage in Scotland and, moreover, the rock lay undisturbed and uninvestigated for scores of years. However, in the 1980s it was rediscovered by Russell and Allison (1985) when more detailed investigation began. In his Ph.D. thesis, Cardenas (1986) investigated geochemical

CHAPTER 2

HISTORY OF RESEARCH

In 1841, Cunningham discovered a peculiar green rock in Sutherland, NW Scotland. He said that, "near the village of Rispond, the gneiss makes a transition into a rock composed of large concretions of serpentine and quartz, between the two there being also every mode of gradation".

Cunningham's "serpentine" was named "indurated steatite" by Heddle (1881) until it was analysed. Analysis of the material showed it to be close to muscovite in composition, and it was then that Heddle named the "pea-green" material "agalmatolite" - thus linking this material with carvings imported to Europe from China - and "first proving agalmatolite to be British". Heddle found several more exposures. He suggested that the pea-green agalmatolite had probably resulted from a change of oligoclase and he noticed that the orthoclase was of "a heightened red colour, a greasy lustre and of markedly less than normal hardness".

With this established the name "agalmatolite" was used during the mapping of the NW Highlands at the end of the 19th Century by officers of the Geological Survey. On certain fieldmaps it is noted as green fine-grained muscovite where observed in the field and, therefore, possibly not all the mappers were familiar with the term. The Geological Survey officers recorded "that wherever the Lewisian gneiss can be examined underneath the Lower Cambrian basal quartzites, the feldspars in the rocks that formed the old sea-floor show a peculiar type of decomposition and in particular the feldspar has been changed into agalmatolite" Peach *et al.* (1907). They described this as due to "peculiar Precambrian weathering".

After this time, however, the name disappeared from usage in Scotland and, moreover, the rock lay undetected and uninvestigated for scores of years. However, in the 1980's it was rediscovered by Russell and Allison (1985) when more detailed investigation began. In his Ph.D. thesis, Cardenas (1986) investigated geochemical

changes in one exposure and discovered that pyrophyllite is also present at the top of the alteration profile and forms at the boundary between quartz and pinite.

Derivation of the name "agalmatolite"

Agalmatolite (literally "picture stone") is the English translation of the German word Agalmatolithus (in German literally Bildstein (same literal meaning)). This name was given by Klaproth (1797) to the carved rock imported into Europe from China. It had hitherto been called Speckstein - bacon stone (due to its often striped nature). Agalmatolite was derived from the Greek $\alpha\gamma\alpha\lambda\mu\alpha$, an image, as it was used for carving and lithos, which means stone. (The rock had also been known as pagodite as the Chinese carved such stone into miniature pagodas, images etc., Dana and Ford 1949).

Definition

The word agalmatolite, although not widely known even to many geologists and thus rarely used, is, notwithstanding, well established in geological literature. Definitions have been given by Heddle (1881), Dana and Ford (1949), Webster (1983), Bates and Jackson (1987). However, slight differences in definition exist from author to author. An all-encompassing definition which incorporates all these nuances and known information about agalmatolite may be as follows:-

AGALMATOLITE: ("Picture stone"). The name given to a rock usually composed of pinite but which may also include or be composed of pyrophyllite or steatite and quartz. Minor amounts of feldspar and mica may also be present. In Chinese varieties, dickite, kaolinite and alunite may also be found. The rock is dominantly olive-green to yellow but can also be white, greyish white, greyish green, brownish or reddish depending on the mineralogy and impurities present. It is waxy and translucent to

opaque. Its specific gravity ranges from approximately 2.77 (Heddle 1881) to 2.82 (Klaproth 1797), and its hardness ranges from 2 to 3.5 making it amenable for carving.

While agalmatolite is the rock name, the name "pinite" is here given to the generally green aggregate of very fine-grained muscovite of which agalmatolite is predominantly composed, following the definition of Dana and Ford (1949). i.e.

Pinite..."In composition essentially a hydrous silicate of aluminium and potassium corresponding more or less closely to muscovite, of which it is probably to be regarded as a massive, compact variety".

It is noted that more recent definitions consider pinite as a fine-grained chlorite-sericite aggregate (e.g. Webster 1983).

CHAPTER 3

MODERN WEATHERING PROFILES, PRECAMBRIAN PALAEOOLS. SIMILAR HORIZONS OF HYDROTHERMAL ORIGIN AND THEIR ECONOMIC POTENTIAL

Weathering profiles are formed at the Earth's surface as a result of the interaction of five main factors: climate, organisms, topographic relief, parent material and time (Jenny 1941). They vary in their character depending on the interplay of the above factors, the oxygen content of the atmosphere, humidity or aridity of the environment and pH of the fluids in the system. Hence, fossilised weathering profiles (palaeosols) may be useful indicators of Earth surface conditions when and where they developed.

The complete physically and chemically weathered profile is known as a regolith. Where the remnant weathered profile retains traces of its original texture and structure it is called a saprolite.

MODERN SOILS

Presented here is information about modern soils, sufficient to cover the information required by the reader to understand the rocks described in this thesis. More detailed information on soil development and weathering processes may be gained in e.g. Rose *et al.* (1979) and Ollier (1984).

Modern soils are divided into two major categories based on the humidity or aridity of the environment (Drever 1982), i.e:

Pedalfers -formed in humid environments, usually rich in Al and Fe and containing no calcium carbonate, as calcium released from primary minerals is removed in solution.

Pedocals Most stable -formed in less humid environments where there is insufficient fluid to remove all the calcium. Calcium carbonate may precipitate in the soil zone in the form of nodules called caliche. In modern soils caliche forms in alkaline conditions (Feakes and Retallack 1988).

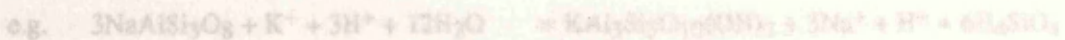
In temperate humid climates, soils show a characteristic sequence (after Drever 1982):-

(Uppermost)	O Horizon	Organic rich layer.
	A Horizon	Layer from which iron and aluminium have been leached.
	B Horizon	Layer in which iron and aluminium have accumulated.
	C Horizon	Partially altered bedrock.

In tropical humid climates, there is less accumulation of organic matter and leaching is so intense that quartz is dissolved and removed from the soil. Soils known as laterites are formed under extreme weathering conditions in this environment. These are rich in Al and Fe oxides and hydroxides. When the soil is predominantly Al hydroxide, with little Fe hydroxide, it is known as a bauxite.

Primary mineral stability during weathering

Goldich (1938) pointed out that the order of stability of minerals of igneous rocks during weathering is the reverse of their order in Bowen's reaction series, i.e. (after Mason 1982).....



Most stable



Quartz

Muscovite

Potash feldspar

Biotite

Alkali plagioclase

Alkali-calcic plagioclase

Hornblende

Calcic-alkali plagioclase

Augite

Calcic plagioclase

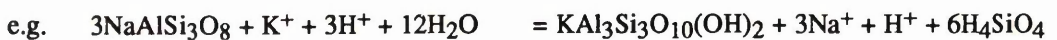
Least stable

Olivine

Secondary minerals and their order of formation in weathering environments

The degree of weathering in soils has been divided into three categories depending on the secondary minerals formed (e.g. Kronberg and Melfi 1987, Kronberg *et al.* 1987a)(with reactions from Nordstrom and Munoz 1986, after Helgeson *et al.* 1978). i.e.:-

1. Initial and Intermediate stages. Complex clay minerals, e.g. smectites, illite, chlorite. Complex clays incorporate cations released from primary silicate minerals, e.g. Na^+ , K^+ , Mg^{2+} , Ca^{2+} into their structures and have high capacities to exchange these ions. Formed from pore waters with high salinity:



albite

muscovite

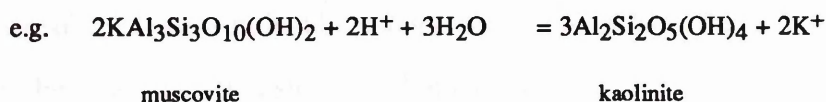


K-feldspar

muscovite

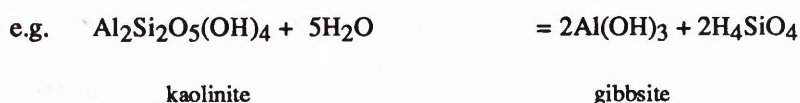
2. Advanced weathering.

Kaolin group minerals, e.g. kaolinite. As primary minerals are depleted surface waters are no longer replenished with rock derived constituents, e.g. Na^+ , K^+ , Mg^{2+} , Ca^{2+} . Dissolution of complex clays follows with formation of kaolin phases:



3. Extreme stage.

Aluminium oxide phases, e.g. gibbsite. Depletion of silica-rich minerals and accumulation of aluminium oxide phases:



Rate of formation and erosion

According to Kronberg *et al.* (1987), soil formation occurs at 2-3cm per century, with incipient to intermediate conditions found after thousands of years. A million years is required for the formation of deep profiles (20-100m) and millions of years for the formation of bauxite deposits (Kronberg *et al.* 1987). Modern erosion rates are considered to be 10-100m m.yr.⁻¹ (Kronberg 1985) and, without renewal of continental surfaces by tectonic activity, most continental surfaces would be reduced to sea level in 10-100 m.yr. (Kronberg *et al.* 1987).

PRECAMBRIAN PALAEOOLS

Palaeosols have been recognised throughout the geological record and have been identified as old as 3000 Ma. Palaeosols are most often found beneath major unconformities. They are important economically; for example, Button and Tyler (1979)

note that "a disproportionately large number of mineral deposits are associated" with Precambrian unconformities, e.g. Au and U deposits, and some authors even suggest that sub-Cambrian uppermost basement rocks have been a source of ions for the Mississippi Valley Type mineralisation in the North American mid-continent.

It is only in recent years that there has been an increase in interest in Precambrian palaeosols. Little work had been done before the 1970's. For example, Williams (1968) describes the pre-1.1Ga sub-Torridonian palaeosol at Sheigra, Scotland as representing "the remnants of the oldest known soil in the British Isles, possibly the world"! In 1984, Retallack *et al.* wrote that "very little has been written about them [palaeosols] especially those as old as the Precambrian". However, publications on Precambrian palaeosols increased throughout the 1980's and presently there is more information on Archean palaeosols, especially profiles in southern Africa and Canada, with much less about Proterozoic horizons.

Precambrian palaeosols are usually thin horizons, $\sim < 20\text{m}$ thick. They are recognised in the field by a change in colour and mineralogy of the protolith and often retain their original structure with the degree of alteration increasing towards the unconformity. The weathered rocks are most often greens, yellows and greys. Palaeosols are often mineralogically and chemically very similar, despite derivation from different protoliths (Nesbitt and Young 1982 and G-Farrow and Mossman 1990). They contain predominantly sericite (which, from descriptions, is generally equivalent to pinite), quartz \pm pyrophyllite, chlorite, opaques. Variations in colour and mineralogy may reflect the oxidation state of the minerals and may be related to oxygen content of the atmosphere. Most authors consider that the early atmosphere was reducing (e.g. see Kastner 1987). The change from reducing to oxidising is considered to be between 2.45 and 2.2 Ga (Prasad and Roscoe 1991) or around 2.0 Ga, from the appearance of significant red-beds (e.g. Waterberg Supergroup, Southern Africa, and other equivalents, Button and Tyler 1979) and positive excursions in $\delta^{13}\text{C}$ of seawater around 2.0 Ga (Baker and Fallick 1989). The presence of granular uraninite and pyrite in pre-2.2 Ga conglomerates is considered to be further evidence of an oxygen-deficient

atmosphere (Button and Tyler 1979). Button and Tyler (1979) stated that all pre-2200 Ma profiles they reviewed had iron "thoroughly leached", with "no evidence of haematite concentration". However in contrast, younger profiles may contain haematite (e.g. the pre-1.1 Ga profile reported by Kalliokoski 1975), consistent with the proposal of a change from a reducing to an oxidising environment.

It was hoped that the study of Precambrian palaeosols would provide "evidence of climate, including temperature, rainfall and chemical composition of the early atmosphere" (Retallack *et al.* 1984) although just how useful their study has been is as yet uncertain. Problems with interpretation are posed due to the later diagenesis, metamorphism, hydrothermal alteration or deformation that the profiles have suffered. Furthermore, Precambrian palaeosols may be difficult to differentiate from hydrothermally altered horizons and sub-unconformity alteration profiles have been interpreted in both ways (e.g. see Kalliokoski 1975 and Grandstaff *et al.* 1986). To aid the identification of palaeosols, Grandstaff *et al.* (1986) listed some criteria for their recognition (Table 3.1).

Table 3.1

Criteria for identification of palaeosols (from Grandstaff *et al.* 1986)

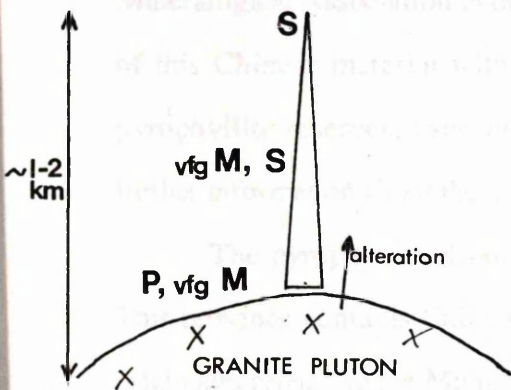
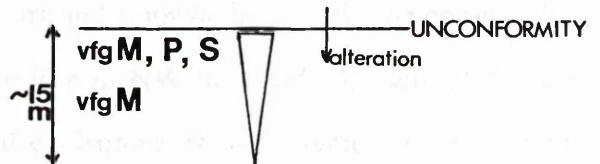
1. Stratiform.
2. Relatively thin (usually <20m).
3. Transitional lower boundary and a sharp upper boundary.
4. Colour variations.
5. Destruction of primary rock textures, often accompanied by formation of soil textures including clay coatings on grains, calcite or silica nodules or iron and manganese crusts, etc.
6. Mineralogical variations; destruction of primary minerals and formation of clay minerals or their metamorphic equivalents.

7. Major and trace element distributions; depletion of most cations, enrichment of Al, Ti, Zr and other elements forming insoluble compounds.
8. Dykes of material from overlying sediments washed down into desiccation cracks in the soil.
9. Rip-up clasts in overlying sediments.

SIMILAR HORIZONS OF HYDROTHERMAL ORIGIN

The dominant mineralogy of the profile in NW Scotland, i.e. very fine-grained muscovite (pinite)-pyrophyllite-quartz, is similar to that seen in some hydrothermally altered rocks, as well as sub-unconformity weathering profiles.

In North America, most pyrophyllite deposits are situated in a zone of Late Precambrian volcanic and sedimentary rocks, along the eastern side of the Appalachians, from Newfoundland to SE U.S.A. The minerals in these rocks, as described from North Carolina by Zen (1961) and Newfoundland by Papezik *et al.* (1978) and Bryndzia (1988), occur in the same chemical systems as those in the agalmatolite profile in NW Scotland, namely $K_2O-Al_2O_3-SiO_2-H_2O$ with the dominant mineralogy, pyrophyllite-sericite-quartz. Most authors consider that the pyrophyllite and sericite in the Appalachians formed as a result of hydrothermal alteration of acid to intermediate volcanics. However, after considering seven pyrophyllite deposits in North Carolina, Zen (1961) concludes that the protolith there had previously been weathered. Zen (1961) proposes that silica, alumina and ferric oxide-rich saprolites were later buried by volcanics and all was subsequently deformed and metamorphosed. Significantly, Zen (1961) states that "this picture of surface weathering of volcanic rocks implies disconformities or unconformities". For comparison, the alteration sequence of one of the pyrophyllite-sericite deposits of the Appalachians with that from NW Scotland is given in Fig. 3.1.

NEWFOUNDLAND (Papezik *et al.* 1978)**NW SCOTLAND** (This project)

vfgM = very fine-grained muscovite
 (= sericite (Papezik *et al.* 1978)
 = pinite (This project))

P = pyrophyllite

S = silica / primary quartz

(∇) ...degree of alteration)

Fig. 3.1

Cartoon sections of the alteration sequences in rocks of Newfoundland and NW Scotland.

In both cases, very fine-grained muscovite has formed as a replacement of primary feldspars and other phases. In more highly altered rocks, pyrophyllite is developed, becoming the major phase in the most intensely altered rocks. Areas containing significant finely disseminated haematite are also found in both cases. In contrast, the rocks are much thicker in Newfoundland, with alteration extending up to ~150 times further than in NW Scotland. However, the development is localised in Newfoundland (restricted to the extent of the granite) while in NW Scotland, it is extensive over a very large area (see below). Significantly, in Newfoundland the altering

fluids penetrated from depth upwards, while in NW Scotland alteration was from the surface downwards.

In China, the vast majority of pyrophyllite deposits were formed due to hydrothermal alteration of acid to intermediate igneous rocks (Song and Dong 1988). Two deposits, referred to in the literature as agalmatolite deposits, were visited in the course of this study during attendance at the 15th General Meeting of the International Mineralogical Association in order to compare and contrast the genesis and composition of this Chinese material with the agalmatolite in NW Scotland. (Details of China's pyrophyllite reserves, uses and geological environments of formation, together with further information about the pyrophyllite deposits below are given in Appendix 1).

The pyrophyllite deposits visited are situated in SE China, in Fujian province. This province contains China's richest reserves, with the pyrophyllite of hydrothermal origin and related to the Mingdong Volcanic belt. In the Dongzi deposit (China's largest deposit) pyrophyllite is found in lenses which formed due to hydrothermal alteration of Jurassic rhyolitic and dacitic tuffs (see sketch, Fig. 3.2).

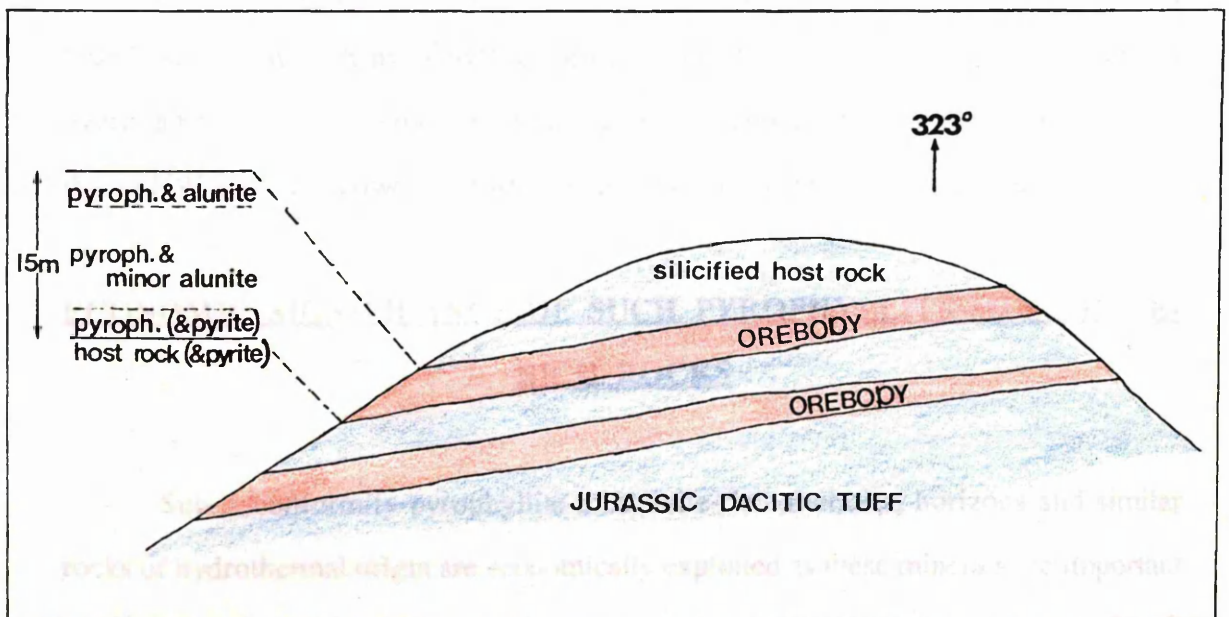


Fig. 3.2

Sketch section of a sequence of secondary minerals in the hydrothermally altered dacitic tuff of the Dongzi deposit.

The purest pyrophyllite is in the centre of the altered zone. Associated minerals alunite and pyrite (and also dickite and haematite) are found around the edges of this zone (Fig. 3.2). The host rock adjacent to the pyrophyllite is strongly silicified and in places the dacite has been oxidised and pyritised.

The Shoushan deposit in Fujian, some 60km from Dongzi, was also formed due to hydrothermal alteration of Lower Jurassic volcanic rocks. Radial faults around the centre of a volcanic caldera became conduits for hydrothermal fluids, resulting in the formation of pyrophyllite, sericite and silica in the country rocks. As at Dongzi, the pyrophyllite is found in lenses up to 12m thick with a symmetrical zonation from pyrophyllite in the centre, through sericite to quartz.

Although the secondary minerals of pyrophyllite and sericite, with pyrophyllite in the most altered rocks, is like that found in NW Scotland, the symmetry and geological environment of formation is completely different. Also the minor secondary phases alunite, dickite and pyrite are not present in NW Scotland. Indeed, dickite is generally of hydrothermal origin (Deer *et al.* 1962) and is mostly associated with metallic ores (Read 1980).

Pyrophyllite is also found in China related to unconformities and Song and Dong (1985) state that such pyrophyllite formed from Al-rich clay due to an increase in overlying pressure and temperature during burial. This geological setting is similar to that in NW Scotland; however, it was not possible to visit any of the localities.

ECONOMIC SIGNIFICANCE OF SUCH PYROPHYLLITE-MUSCOVITE-RICH ROCKS

Sub-unconformity pyrophyllite-muscovite-rich alteration horizons and similar rocks of hydrothermal origin are economically exploited as these minerals are important industrially and some are also used for ornamental carving. Notes on these uses of such rocks from China, North America and Southern Africa are given below, and the economic potential for the Scottish agalmatolite is discussed.

Pyrophyllite

Pyrophyllite is mined from palaeosols as well as larger scale hydrothermal deposits. The major uses for pyrophyllite include; ceramics, refractories, fillers, insecticide carriers, glass manufacture, concrete, paints, rubbers, plastic, paper making (Dickson 1985). Sericite-pyrophyllite mixes are considered even more useful for refractory purposes (Dickson 1985).

China:

China is the third largest producer and consumer of pyrophyllite (after Japan and South Korea) (Anon 1989). Approximately 90% of recoverable reserves were formed from hydrothermal alteration of acid to intermediate rocks. Unconformity-related pyrophyllite deposits constitute a small amount of recoverable reserves (Song and Dong 1988).

North America:

Four of the five pyrophyllite producers of North America, as recorded by Dickson (1985), are in the Appalachians - three in North Carolina and one in Newfoundland. Sericite as well as pyrophyllite is mined for refractory purposes (Dickson 1985). Most authors consider these rocks formed due to hydrothermal alteration of acid to intermediate volcanic rocks.

Southern Africa:

Sub-unconformity pyrophyllite developed on the 2800 Ma Dominion Reef group of acid lavas and tuffs, locally named "Wonderstone", has been quarried for several decades (Button and Tyler 1979). It is used in the production of synthetic diamonds and as an electrical insulator (Button and Tyler 1979). "Modest tonnages" of pyrophyllite are also mined from the pre-2200 My old palaeosaprolite on the basaltic surface of the Insuzi Subgroup, Swaziland (Button and Tyler 1979).

NW Scotland:

Although rocks with 50-70% pinite (\equiv sericite) are developed up to >10m beneath the unconformity, only minor and variable quantities of pyrophyllite are developed at the top of the alteration profile. This factor, coupled with the remoteness and inaccessibility of most of the outcrops, indicates that there is no real potential for the sub-Cambrian, Lewisian pyrophyllite as an industrial mineral.

Carving stone*China:*

Although mainly used as an industrial mineral in China, pyrophyllite and related minerals are traditionally very important for carving. Agalmatolite and pyrophyllite in China is traditionally known as "Shoushan stone", after the village of Shoushan in Fujian province where it was originally mined (Song pers. comm.). There are >100 different types of Shoushan stone, dependant on composition, colour and lustre (Song pers. comm.). These are divided into three categories; 1) Shankeng, 2) Shuikeng and 3) Tiangkeng (see Appendix 1), but generally only Shuikeng and Tiangkeng are carved. The art of carving has been passed down for >1500 years. Since the Qing Dynasty (1644-1911), two branches have developed; "Xiamen" - noted for life-likeness and simplicity and "Dongmen" - noted for delicately and intricately carved pieces (see Appendix 1 for examples). Many types of Shoushan stone are very valuable to the Chinese, and in ancient China the Emperor had a special seal made from it. Indeed, a sample of the rarest and most valuable variety, Tianhuang (translated "King of stones"), in the category Tiangkeng, can fetch 3 times the price of gold (by weight) (Song pers. comm.)! (See Appendix 1).

North America:

Although there is no known tradition of carving pyrophyllite or related sericite by indigenous North Americans, a small company has recently been established for this purpose in Newfoundland.

Southern Africa:

"Wonderstone" from western Transvaal has been carved for ornamental purposes (Webster 1983).

NW Scotland:

The large variety of colours and waxy lustre of the agalmatolite, coupled with its softness, makes this Scottish material both appealing and suitable as a carving stone. The first carving of Scottish agalmatolite was of rock from the cave at [NC 4385 6614] and was made by T. Daniels (see frontispiece). The finished object is valued at ~£1000.

Given the quantity of rock available for this purpose, its rarity as a Scottish stone and its value, it is suggested that the greatest economic potential for agalmatolite in NW Scotland is in utilising it as a carving stone for a small cottage industry.

CHAPTER 4

FIELDWORK

INTRODUCTION

Fieldwork was carried out to gain more information about the extent and nature of the development of agalmatolite in NW Scotland.

In the investigation of the extent of development of agalmatolite, questions that were addressed to understand further its genesis include:-

1. Whether agalmatolite occurs everywhere or rarely beneath the unconformity.
2. If it is developed to the same degree and in the same fashion wherever it occurs.
3. If it is affected by lower Palaeozoic tectonism.

Also, investigation of further exposures may reveal other features characteristic of a particular process.

Background

Although Peach *et al.* (1907) stated that wherever the unconformity was examined, the rocks underneath showed 'decomposition', neither the extent of the alteration at each exposure, nor the number of exposures upon which this statement was based is known.

On the original 6" geological maps, compiled between 1883 and 1896 by Peach, Home, Hinxman, Cadell and Gunn, the length of the outcrop of the Lewisian/Cambrian unconformity was examined. In addition, the maps along the Moine Thrust zone as far south as Skye were studied. In all of the 63 maps, there are only 7 places where 'agalmatolite' is mentioned, and all but one occur in the north, around Loch Eriboll. Of these, two occurrences were in the foreland and the remainder in the thrust belt.

With only one extensive exposure of agalmatolite known and studied in detail, and with very little knowledge of the condition of sub-unconformity rocks elsewhere, the aim of the fieldwork was to determine the extent of and variation in sub-unconformity alteration. After the unconformity had been surveyed, the most complete sections and other exposures of particular interest could be chosen for subsequent detailed analysis. All samples, including suites and individual samples of altered and fresh Lewisian rocks as well as individual samples from other Precambrian groups are tabulated in Appendix 2. (Samples from shaly horizons in the overlying Cambrian members are tabulated in Appendix 2c).

FIELD OCCURRENCES

The unconformity of Cambrian on Lewisian in NW Scotland crops out over a distance of ~65km in a SSW-trending zone from the north coast. To the west, the Cambrian rests on the Torridon Group strata and to the east the unconformity is obscured by the thrust sheets of the NW margin of the Caledonian orogen. Along its length, the unconformity is a pronounced topographic feature. This distinctively planar unconformity is marked by an abrupt change from the hummocky Lewisian rocks below, to the grey-white bedded quartzarenites above (Plate 4.1), and is often found at a distinct break in slope.

The outcrop of the unconformity is divided into three geographical areas based on differing topography and degree of exposure. These are : 1) Northern area (from the north coast to Meall nan Cra), 2) Central area (from Meall nan Cra to Ben Stack), 3) Southern area (from Ben Stack to Assynt) (Fig.4.1). These will be considered in turn.



Plate 4.1

The unconformity between the Lewisian basement and overlying Cambrian sandstones is distinctly seen along the centre of this mountain (Arkle) and the mountain behind to the left (Foinaven). Scree from the Cambrian rocks obscures most of the outcrop of the unconformity.

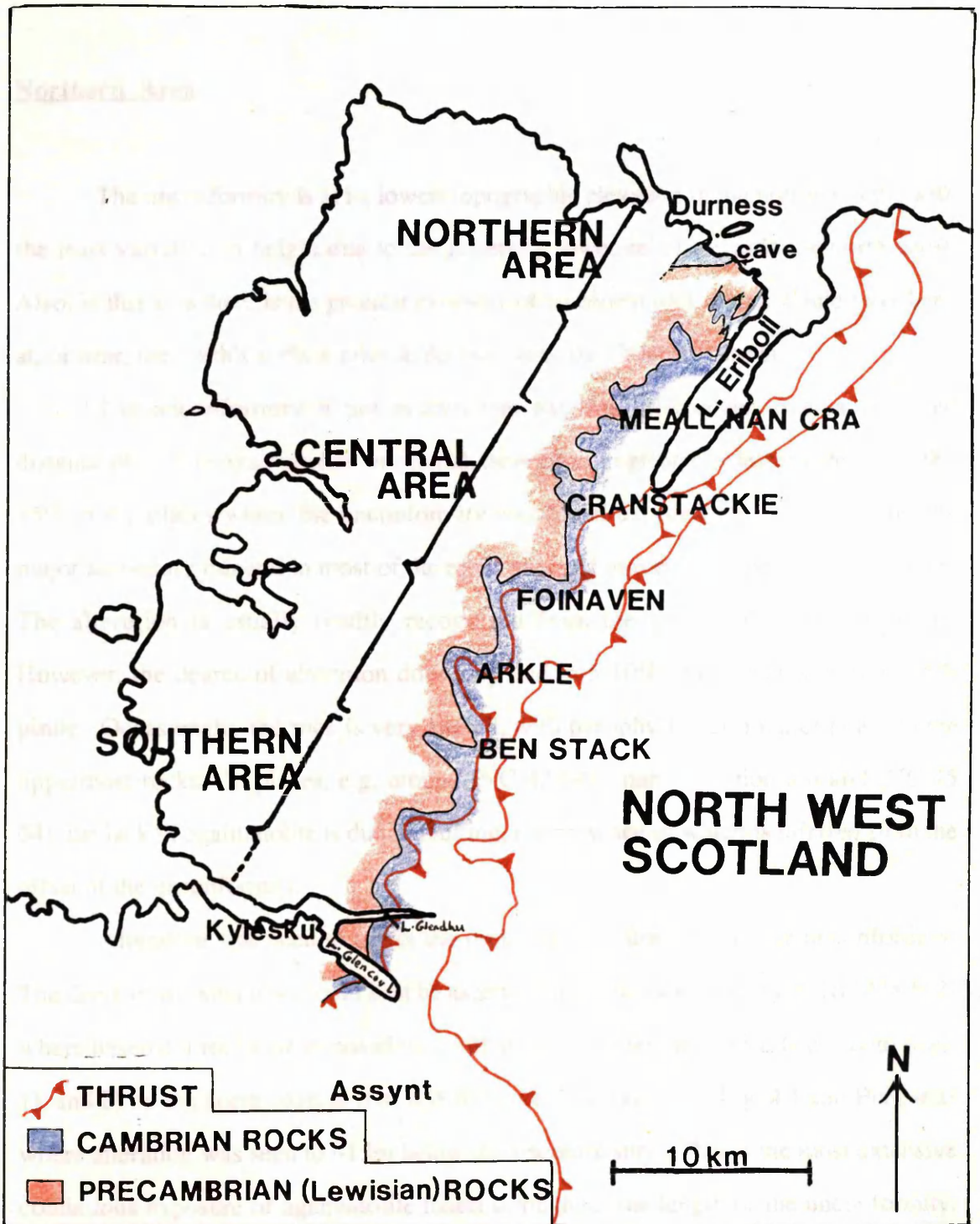


Fig. 4.1
Outcrop of Lewisian/Cambrian unconformity north of Assynt.

Some of the most interestingly altered rock observed was that of an Eboracian exposure, 5 km from the cave above 1 mile (Page 4.3).
Against this is exposed to the greatest extent to the north. This is directly due to the outcrop of Cambrian. The example, such as in the outcrops around [NC 438 638] as the Lower Member has been eroded and the unconformity and the topography have a

Description of unconformity

Northern Area

The unconformity is at its lowest topographic elevation in the northern area, with the least variation in height due to the generally lower relief towards the north coast. Also, in this area there is the greatest exposure of basement rock which would have been at, or near, the Earth's surface prior to deposition of the Cambrian strata.

The unconformity is not everywhere exposed. However, over a surveyed distance of ~15km agalmatolite was found, developed to greater or lesser extent, in ~90-95% of the places where the unconformity was found exposed. Pinite constitutes the major secondary mineral in most of the rocks exposed immediately beneath the contact. The alteration is usually readily recognised from the green colour of the pinite. However, the degree of alteration does vary and in 5-10% of exposures there is ≤5% pinite. Occasionally the rock is very altered, with pyrophyllite as a major phase in the uppermost rocks. In places, e.g. around [NC 43 64] (map 1, section ab) and [NC 45 64], the lack of agalmatolite is due to faulting, the presence of which is inferred from the offset of the unconformity.

Alteration was seen to affect the rocks up to ~20m beneath the unconformity. The depth of the alteration could best be ascertained at two locations; 1) at [NC 438 637] where basement rocks are exposed on a hill-slope and alteration extends to ~20m (map 1), and 2) on the north coast at [NC 438 611], i.e. "the cave" (cf. Fig. 4.1 and Plate 4.2) where alteration was seen to ~15m below the unconformity. This is the most extensive continuous exposure of agalmatolite found throughout the length of the unconformity. Some of the most intensely altered rock observed was found in an isolated exposure, ~50m from the cave across a fault (Plate 4.3).

Agalmatolite is exposed to the greatest extent in the north. This is directly due to the pattern of erosion. For example, much agalmatolite outcrops around [NC 438 638] as the Lower Member has been eroded and the unconformity and the topography have a

similar attitude, dipping gently towards Loch Eriboll (map 1, section cd). At [NC 44 63] a number of knolls on the hummocky landsurface are composed of agalmatolite, e.g. [NC 4435 6394] and [NC 4462 6394]. Neither has Cambrian strata on top, but the presence of agalmatolite is taken to infer that the unconformity was at some small distance above the top of the knolls. In particular the knoll at [NC 4462 6394] stands proud as an 'island' of agalmatolite surrounded by fresh Lewisian at a lower elevation.

Clasts of pinite were found above the unconformity in the Basal conglomerate of the Lower Member at [NC 4426 6387] ~10mm diameter (map 1) and [NC 4055 6110] ~1.2mm diameter (map 2). There and elsewhere the matrix is often greenish.



Plate 4.2

Agalmatolite at "the cave" [NC 438 661].

Here exposure is seen to ~15m beneath the unconformity in what was the largest continuous exposure of agalmatolite found.



Plate 4.3

Exposure of agalmatolite $\sim \leq 2$ m below the unconformity, with Cambrian rocks (Eriboll sandstone-Lower Member) in the background [NC 4387 6611].

Central area

The width of outcrop of the unconformity is greater in the central area due to the greater relief of the mountains. It crops out on four large mountains in the central area; Cranstackie, Foinaven, Arkle and Ben Stack (see Fig. 4.1).

Exposure is very poor in the central area, with scree of the overlying Cambrian quartzarenites resting on the Lewisian at the break in slope (Plate 4.1), over most (~70-75%) of this area. However, the unconformity was found exposed at several locations.

Cranstackie

Agalmatolite is not developed below the exposed unconformity at the top of Cranstackie. Interestingly, neither is there a basal conglomerate immediately above the unconformity at this location.

Arkle

The unconformity is exposed at [NC 3035 4444] (Fig. 4.2). Agalmatolite is poorly developed below the unconformity, with pinite constituting only up to ~10% of the rock. However, the feldspars are very pink (and opaque rather than translucent). Indeed, all along the break in slope the feldspars have this salmon pink colour and at [NC 3080 4351] a small amount of pinite (~10%) is also present, indicating that alteration has also affected much of the rock along this break in slope.

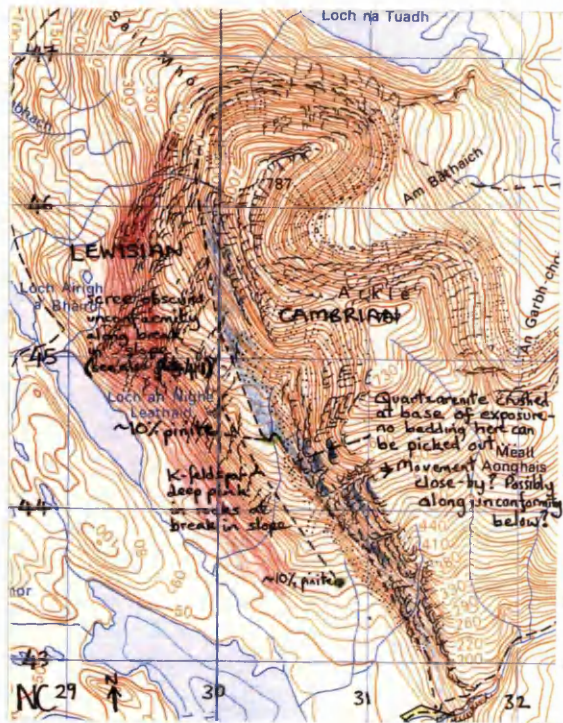


Fig. 4.2

1:50,000 Ordnance Survey map of Arkle with unconformity marked.

Ben Stack

The rocks immediately beneath the unconformity exposed at the top of Ben Stack show no sign of alteration. However, the matrix in the Basal conglomerate above the unconformity appears slightly greenish. Also, ~40m below the unconformity, a very small patch of pinite ~8cm x 4cm was found in an otherwise apparently fresh pegmatite ~0.8m x (0.03 to 0.07m). This was originally noted by Peach *et al.* (1907, p.148). No other agalmatolite was seen on this mountain.

Southern area

The unconformity in the foreland is also poorly exposed in the southern area. In the south, the double unconformity, i.e. where the Cambrian oversteps from Torridonian to Lewisian, occurs to the east of Loch Glencoul at [NC 24 30] and southwest of Loch Assynt at [NC 23 22]. However, no exposure of the unconformity was found by Loch Assynt, nor is it exposed at Loch Glencoul. The most southerly outcrop where the sub-unconformity rocks are known to be altered is on the slopes of Beinn na Fhuarain in the Assynt window at [NC 257 158] where samples of poorly altered rock were found in the scree around the unconformity (Allison pers. comm.).

The most interesting and informative exposure in the southern area was of sheared agalmatolite (noted on the original geological field maps) in an imbricated unit to the east of Loch Glendhu at [NC 3154 3241] (Plates 4.4a and b). Movement has been sufficiently intense that Lower Member beds within 1 to 2m of the contact have been warped (Plate 4.5), and agalmatolite is incorporated between the units, making the contact difficult to decipher. The orientation of the shearing is consistent with a Caledonian thrust sense, with slickensides indicating movement towards the west.



Plate 4.4a

A pearly lustre is seen on the exposed surface of the sheared agalmatolite at [NC 3154 3241].

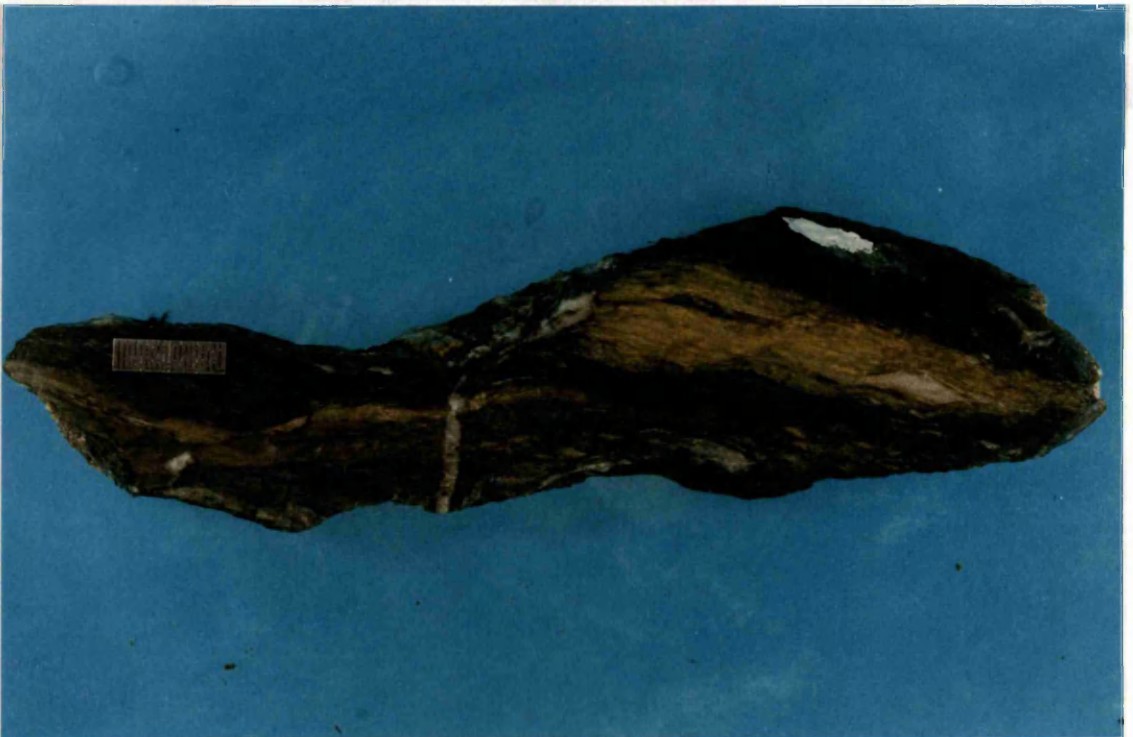


Plate 4.4b

A section of the sheared agalmatolite [NC 3154 3241].



Plate 4.5

Warped Lower Member units within 1 to 1.5m of the unconformity, above sheared agalmatolite. Location in thrust belt, east of Loch Glendhu [NC 3154 3241].

REASONS FOR THE VARIATION IN EXTENT OF DEVELOPMENT OF AGALMATOLITE

Regional

Although agalmatolite was found throughout the whole area, it was apparently better developed in the north than around the mountains farther south. Its poor development around the high ground in the central area may be for structural reasons.

At the cave [NC 4383 6614] and at Meall nan Cra [NC 3790 5974] in the north, the foliation in the gneisses has been rotated at the unconformity. In both instances the rotation of the gneissic foliation is consistent with a thrust deformation, i.e. to the west. This indicates that there has been movement along this plane. The lack of Basal conglomerate above the unconformity on Cranstackie could also have been due to movement. In the central area, the western limit of the thrust belt is found much closer to the unconformity than farther north (Fig. 4.1). On Arkle, the joints in the Eriboll sandstone are very closely spaced and ~3-4m above the exposed unconformity no bedding was visible as the rock has been crushed. Indeed, a major duplex is found within the Cambrian rocks on Arkle, with imbricate faults every 50 to 100m (Peach *et al.* 1907, Elliott and Johnson 1980).

It would be reasonable to suggest that there has been movement in the north, and the close proximity of major thrusts in the central area would suggest there is likely to have been much more deformation there. Since agalmatolite is very soft ($H = 2.5$ to 3) and if such a soft horizon was developed before Caledonian tectonism, then the thrusts of Caledonian age may have taken advantage of it as an easy-slip horizon. Hence, although there is presently less exposure, this does not necessarily indicate that it was less developed initially, as the agalmatolite may have been removed during movement. Indeed, one can consider that the alteration profile influenced the position of the sole thrust.

Local

The extent of alteration of the sub-unconformity rocks can vary over hundreds of metres: e.g. at [NC 4384 6264] (map 1), no agalmatolite is developed, while at [NC 4369 6252] and [NC 4372 6241] the rocks are highly altered. Two possible reasons for such variations are; 1) faulting and 2) an irregular bottom surface of the alteration horizon.

1. Precambrian Faulting

Differential movement in the late Precambrian prior to deposition of overlying sediments is the most probable explanation for one exposure and possibly others. Agalmatolite was extensively developed beneath the unconformity on the NE side of the N-S fault at [NC 406 610] (map 2) but very poorly developed on the SW side. This fault has moved since the deposition of the Eriboll sandstone. However, movement could have been initiated in Precambrian times. This is consistent with Anderton *et al.* (1979), who proposed that in late Precambrian times, the hitherto stable continental margin "began to break up into a series of blocks and basins". Also Craig (1983) remarked on evidence for N-S trending differential uplift in the Lewisian and Torridonian rocks prior to the deposition of the Cambrian. If faulting raised the SW side relative to the NE side, then after peneplanation, the SW side would have had more agalmatolite eroded, thus explaining the variation in development. The fault is noticeable here due to the displacement of Cambrian units and the unconformity, and the large erosional gully which runs along it. Elsewhere similar faults may account for the variations in development of agalmatolite.

2. Irregular bottom surface

Alteration need not have been equally as pervasive from one point to another. Such variation could be related to joint spacings or other factors affecting the rock's permeability.

DISCUSSION

Agalmatolite is developed throughout the length of outcrop of the Lewisian/Cambrian unconformity. Its presence in the thrust belt which, according to Elliott and Johnson (1980) has displacements of ~77km, indicates that the area where agalmatolite was developed exceeds ~80km x 65km. Agalmatolite was clearly not formed by a localised event. Very similar rocks are also found, though not present to such a great extent, beneath the equivalent Precambrian/Phanerozoic unconformity in Newfoundland and Labrador ~1200km west at that time (Allison pers. comm.).

The marked variation in degree of alteration from one side of the fault to the other at [NC 406 610] is good evidence to suggest that alteration had occurred in late Precambrian times, prior to the deposition of the Cambrian strata. Certainly, the agalmatolite in the thrust zone east of Loch Glendhu [NC 3154 3241], which was sheared during Caledonian tectonism, would restrict agalmatolite to be Caledonian or older.

CONCLUSION

The formation of agalmatolite in the Lewisian of NW Scotland is restricted to rocks immediately beneath the unconformity and alteration increases towards the unconformity. It is laterally continuous and developed over a large area with alteration of the basement up to thousands of square kilometres. Agalmatolite most probably formed prior to the deposition of the overlying Cambrian quartz arenites. It is similar in colour, mineralogy, vertical thickness and geological setting to palaeosaprolites of this age and

also older ones elsewhere in the world. For these reasons, a weathering origin for agalmatolite seems most likely.

However, the peculiar indurated and crystalline nature of the rocks is unlike modern weathered rock products, implying that later diagenetic or metamorphic processes, or both, were also involved in its formation.

CHAPTER 5**MINERALOGY AND MINERAL CHEMISTRY****INTRODUCTION**

The agalmatolite at and around [NC 4385 6614] (cave) gave the most information concerning progressive alteration of all the sub-unconformity exposures and rock suites examined throughout the length of the unconformity. Here the altered rock was exposed to ~15m depth. Also, samples could be confidently collected from the same gneissic/amphibolitic layer or pegmatite, therefore keeping natural variation in mineralogy from different samples of gneisses and pegmatites to a minimum.

To compare findings with fresher rocks (alteration pervading >15m beneath the unconformity (b.u.)), two samples of gneiss, pegmatite and amphibolite from ~5m apart in individual bands were taken from the nearest exposure of 'fresh' Lewisian rock, across a fault ~100m away. Their depths below the unconformity were unknown, but were probably markedly >15m- as compared with samples from [NC 4385 6614].

Watson (1975) estimates that 80% of the Scourian consists of acid to intermediate gneisses. Since these Proterozoic (Laxfordian) rocks are suggested to represent reworked equivalents of the Scourian (Sutton and Watson 1951), which were later injected by a suite of acid pegmatites, it can be deduced that >80% of the parent rocks of the alteration horizon consist of acid to intermediate gneisses and pegmatites, composed predominantly of feldspar (plagioclase and potash), quartz and biotite. Suites CG and CP, described in detail herein, show the progression in alteration of typical plagioclase-rich gneiss and K-feldspar-rich pegmatite respectively. More altered rocks than those in suites CG and CP were observed close-by in the isolated 'pod' at [NC 4387 6611] (Plate 4.3), the top of which was estimated to be <1.5m below the unconformity. Specific observations of yet further alteration are made from samples therein. The variations

described in this chapter typify the principal mineralogical changes the basement rocks exhibit with progressive alteration.

ANALYTICAL TECHNIQUES

Techniques used to investigate the mineralogy and mineral chemistry of the rocks of the alteration profile are listed below.

Hand specimen examination

Optical microscopy: Examination of polished thin sections. Point counting (500 points per slide) under optical microscope was used to determine modal mineral percentages.

X-ray diffraction: For mineral identification and characterisation and for qualitative determination of mineral constituents in rocks.

Electron Probe analysis: Mineral chemistry was determined quantitatively using Wavelength Dispersive Spectrometer analysis. Energy Dispersive system analysis (qualitative) was also used for mineral identification. The backscatter electron imaging facility allowed minerals with similar optical properties (especially very fine-grained minerals) to be differentiated. Analyses were made using Cameca Camebax and Cambridge Microscan 5 instruments.

Scanning Electron Microscopy: Principally used for detailed morphological and textural investigation - gained from high magnification secondary imaging of small sample chips. Qualitative EDS analysis was used for mineral identification. The cathodoluminescence facility was used to differentiate overgrowths from primary crystals in polished thin section. Quantitative EDS analysis of mineral chemistry (rarely

used) and backscatter and secondary imaging on polished thin sections were also employed for mineral identification. Analyses were made on a Cambridge Instruments Stereoscan 360 with integrated Link Analytical AN1000 EDX microanalyser.

Other techniques: i.e.....

Fluid inclusion studies

Stable isotope ($\delta^{18}\text{O}$ and δD) investigations of particular minerals were used to gain further geochemical information. Minerals were separated by hand picking and heavy liquid separation. (Heavy liquid used was tetrabromoethane).

GENERAL MINERALOGICAL VARIATIONS

Hand specimen changes

In hand specimen the Lewisian rocks, predominantly white, grey, pink and dark brown to black in varying proportions when fresh, generally become greener and even yellow and purple with alteration.

Progressive changes in hand specimen appearance of samples from suites CG and CP are shown in Plates 5.1a and b. In the pegmatite suite (5.1a), the areas of white plagioclase are first to become green (50A, 10.7m b.u.) while the K-feldspar becomes deeper pink. By 8.4m b.u., the K-feldspar has also started to alter - the rock now varying shades of green. Fine purple lines from haematite staining are also seen. At 2.8m, all the K-feldspar has been consumed and sites of precursor plagioclase and K-feldspar are green. Some yellow patches are present beside remnant grey quartz.

The plagioclase-rich, almost fresh, white grey and black gneiss, Plate 5.1b (4888,G,H & I) becomes predominantly olive-green by 10.4m b.u.. White flecks of altered biotite are seen and occasional deep pink areas of unconsumed K-feldspar. By 7.8m b.u., the remnant biotite crystals are creamy-yellow, with many flakes separated by green pinite. Areas of pink K-feldspar are absent. Haematite staining is seen at the end of altering biotites and concentrated in laminations, coloured pinkish and deep purple respectively. At 5.0m b.u., the size of the remnant biotite flakes has decreased. By 2.0m b.u., small dark minerals <1mm diameter are seen throughout the body of the rock. These are often situated close to, or along with, remnant biotite, although very little remnant biotite remains. The mass of pinite is mottled with some yellowish patches and a larger area of yellow cryptocrystalline material is seen adjacent to the coarser grained quartz-rich band (not shown). It should be noted that the pinite, which forms the predominant mineral from <10m to \geq 2m below the unconformity, becomes progressively paler towards the unconformity.

The distance beneath the unconformity at which alteration is initially seen in any one suite, is dependant on the composition of the precursor rock - e.g. a K-feldspar-rich rock will show much less sign of alteration between 10 and 15m below the unconformity in this exposure, than a plagioclase-rich band, but more dramatic changes will be seen higher up.

Although the above suites show typical changes with alteration, many altered rocks assume different appearances dependant on their primary mineralogy and degree of alteration. More altered rocks contain a larger proportion of the later secondary minerals and are frequently more yellow than green, any green being very pale. Gneisses containing more biotite give altered products more pink to deep purple from haematite staining. Boundaries between different colour zones are frequently very sharp, e.g. Plate 5.2a, but may be gradational over several cm, Plate 5.2b.

Occasional opaques up to ~10mm diameter are found. These are most often concentrated in zones (generally joints) around which the wallrock has been strongly haematized (see Plate 5.27a).

Thin section

Variations in modal mineral % with depth below unconformity for suites CG and CP are given in Fig. 5.1. With alteration, secondary 'pinitite' (very fine-grained muscovite, green in hand specimen) becomes more abundant, forming the dominant mineral at the top of the alteration profile in these suites. Plagioclase is the first mineral to start being replaced, followed by biotite, microcline and quartz. Towards the top of the profile, secondary tourmaline (small dark crystals in hand specimen), rutile and pyrophyllite (very fine-grained, yellow in hand specimen) develop. In these suites, pyrophyllite is a minor phase, but in more altered rocks it becomes a major phase. Indeed e.g. in the purple bands at [NC 4387 6611] (Plate 5.2a) it supersedes pinitite as the dominant secondary mineral.

Replacement of primary minerals generally progressed from the outside and penetrated inwards, preferentially along cleavages and cracks in the crystals. However, in plagioclase the more calcic cores were preferentially replaced. In biotite, the penetration of pinitite along cleavages caused remnant flakes to splay. Further alteration resulted in pinitite and then pyrophyllite developing at the expense of these remnant biotite flakes, with development of tourmaline at the end of and in sites of precursor biotites. Tiny crystals of rutile also formed within sites of precursor biotites. Quartz was slightly replaced by pinitite initially but much more pervasively consumed by pyrophyllite towards the top of the profile.

Opaques in the profile are predominantly haematite and also rutile. Magnetite is also present but most magnetite is replaced by haematite.

Replacement of primary minerals generally progresses from the outside and penetrated inwards, preferentially along cleavages and cracks in the original silicates. In plagioclase the more calcic cores were preferentially replaced. In the early generation of quartz along cleavages coarsened or remained in place. This resulted in quartz and then pyrophyllite developing in the cores of the original feldspar flakes, with development of corundum at the ends and in the cracks between the flakes. Tiny crystals of rutile also formed within sites of the original feldspar. The feldspar was replaced by quartz initially but much was later replaced by pyrophyllite. In some cases the top of the profile.

Features in the profile are predominantly textural and mineralogical.

also present but most corundum is replaced by hematite.

PLATE 5.1

Changes in pegmatite and gneiss suites with progressive alteration. (Scale bar = 2cm).

- | | | |
|------------|--------------------|----------------|
| Plate 5.1a | Pegmatite suite CP | [NC 4385 6614] |
| Plate 5.1b | Gneiss suite CG | [-----"-----] |

Sample No Depth Below Unc. (m)

5-1a

4988 2.8



5088 8.4



50A 10.7



5188 14.7



E ~20



F ~25



Sample No Depth Below Unc. (m)

5-1b

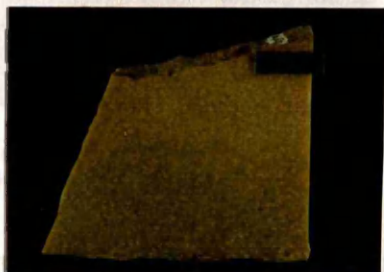
4688 2.0



46A 5.0



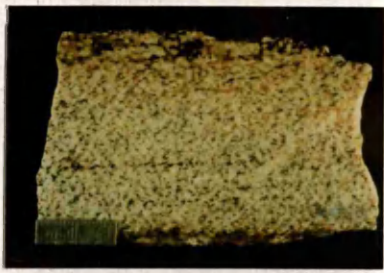
4788 7.8



47A 10.4



4888 15.0



G ~20



H & I ~25





Plate 5.2a

Altered Lewisian gneiss and pegmatite (agalmatolite) <2m below unconformity at [NC 4387 6611]. Boundaries between purple and yellow, and yellow and black and white bands are sharp. (Purple colour due to haematite staining).

Yellow bands	=	pinite
Purple band (RHS)	=	predominantly pyrophyllite, with pinite and quartz.
Black mineral in rock	=	tourmaline.



Plate 5.2b

Green and purple agalmatolite. The colour banding grades from dark green to light green to pink and to purple over 15 to 80mm. [NC 4361 6240].

Green bands:	pinite and quartz in altered feldspar and quartz pegmatite.
Purple bands:	precursor gneiss contained sufficient biotite to give agalmatolite purple colour on alteration..

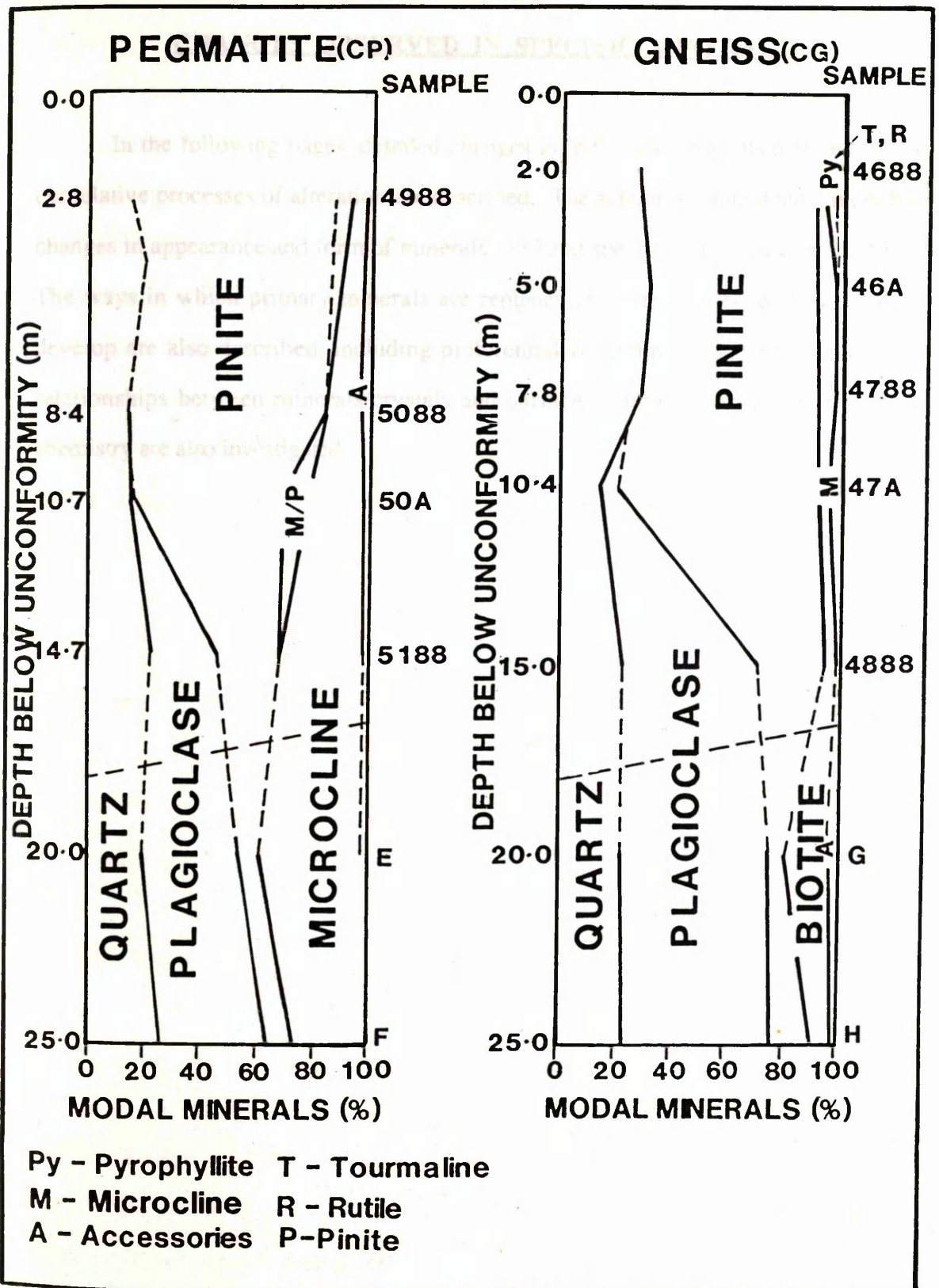


Fig. 5.1

Mineralogical variations as a function of depth in (a) pegmatite and (b) gneissic layers of the alteration profile at [NC 4385 6614]. (Suites CP and CG respectively).

Note: Samples 0 - 15m are from the same gneissic layer/pegmatite.
 Samples ~20m and ~25m are from the same gneissic layer/pegmatite but different from those at 0m - 15m. They were collected at [NC 4390 6609] (see text).

CHANGES OBSERVED IN SPECIFIC MINERALS

In the following pages, detailed changes in individual minerals affected by the cumulative processes of alteration are described. The accounts relate details including changes in appearance and form of minerals - in hand specimen, thin section and SEM. The ways in which primary minerals are replaced and alter and secondary minerals develop are also described, including preferential consumption and growth, textural relationships between minerals/crystals and surface features. Variations in mineral chemistry are also investigated.

Progressive Alteration of Primary Minerals...

Plagioclase

In hand specimen, the white translucent areas of fresh plagioclase became green when consumed by secondary minerals. The plagioclase in the rocks examined is almost entirely albite, and is the first mineral both to start being replaced and to be completely consumed. Alteration commences at >15m beneath the unconformity.

Progressive replacement

Plagioclase replacement occurred initially at grain boundaries and along cracks in the crystals and pinite (lighter grey in backscatter) developed laterally from the cracks at the expense of plagioclase (darker grey in backscatter) (Plate 5.3a). The main body of the crystals started to be replaced along cleavage planes (Plate 5.3b, left). The cleavages remained the major zones along which secondary minerals formed. As alteration progressed, decomposition of the rest of the crystal pervaded laterally from the cleavages, along crystallographically controlled planes (e.g. Plate 5.3b, right). This led to progressively broader bands of pinite (Plate 5.3c).

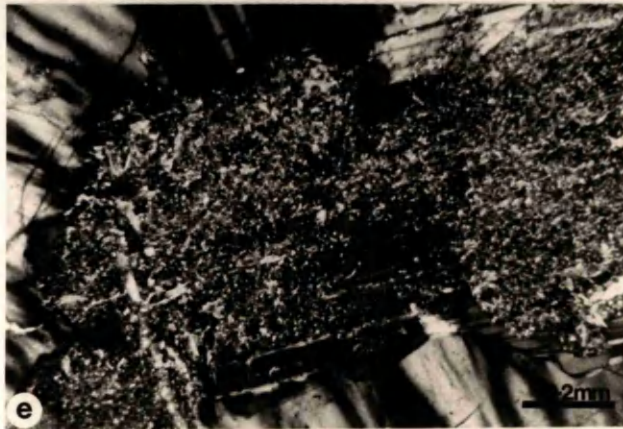
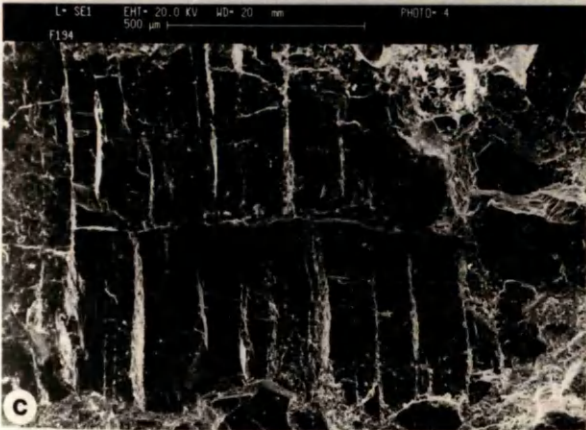
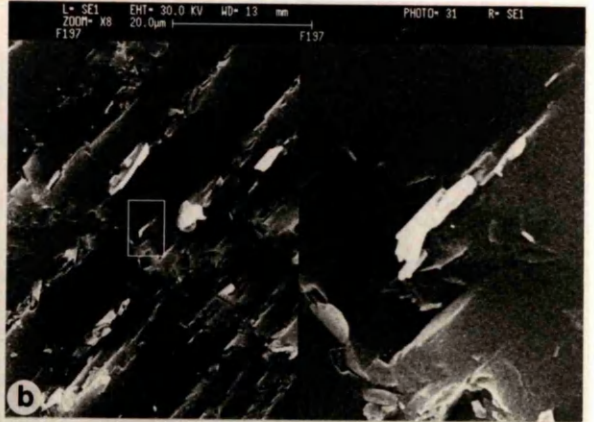
Replacement proceeded mostly from the centres of crystals outwards, with the rims of the grains remaining freshest longest (Plate 5.3d). These outermost rims were generally overgrowths which had formed during an earlier event (from cathodoluminescence (Plate 5.4)).

Plagioclase replacement continued, and often most of the crystals were consumed while the K-feldspar was still pristine (Plate 5.3e).

PLATE 5.3

Progressive replacement of plagioclase.

- Plate 5.3a Backscatter image of secondary K-rich minerals (pinite, light grey) developing at the expense of primary albite (dark grey), laterally from cracks in the crystal.
- Plate 5.3b LHS : Preferential replacement of plagioclase along cleavage planes.
RHS : Close-up of boxed area on left. Plagioclase consumed laterally from cleavage along crystallographic planes. Here cleavage is NE-SW. Pinite has started to develop at $\sim 30^\circ$ from cleavage.
- Plate 5.3c With further alteration, pinite penetrates into the crystal laterally from the cleavage, giving progressively broader bands of pinite.
- Plate 5.3d Decomposition of albite is favoured in the crystal cores.
- Plate 5.3e Albite overgrowths are the last areas of plagioclase to be replaced. Note that much of the plagioclase has been replaced before secondary minerals have even started to form at the expense of K-feldspar.



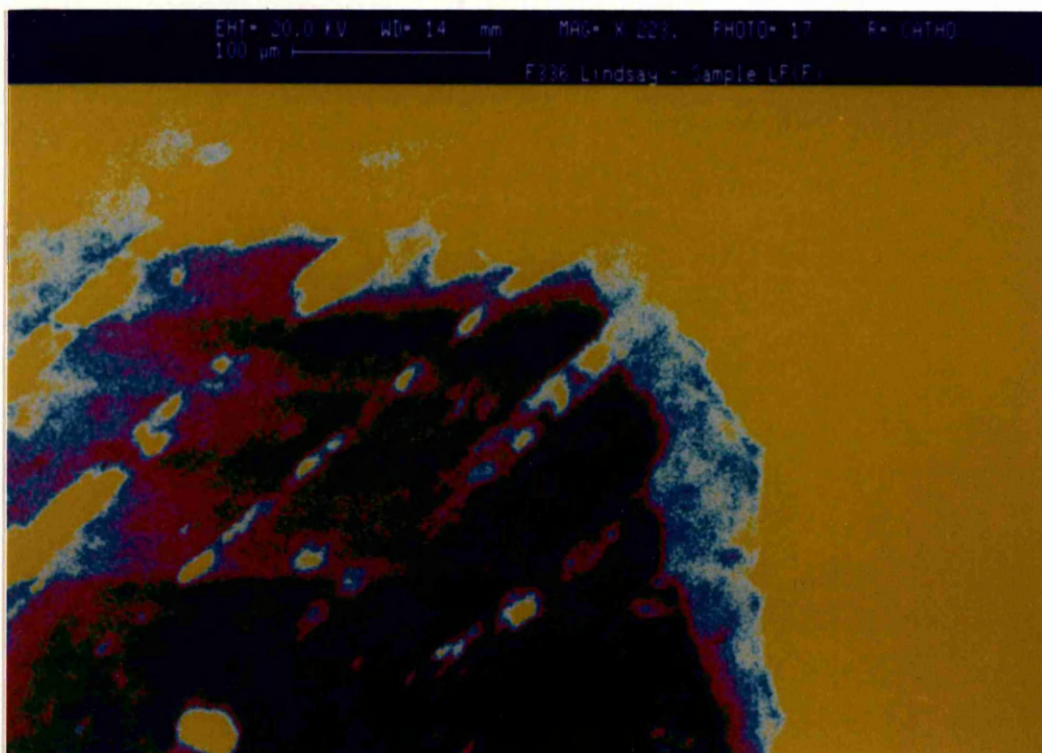


Plate 5.4

Cathodoluminescence image showing overgrowth (light blue) on plagioclase feldspar (darker blue, pinks and greens).

Note: The overgrowths were an artefact of some previous Lewisian event and were not formed due to this weathering (from their presence in fresh samples).

Chemical analysis

Quantitative electron probe analysis of the plagioclase revealed the overgrowths to be more sodic (i.e. purer albite) than the main body of the crystals (Appendix 5).

K-feldspar

In hand specimen, the K-feldspar grades from typical pale pink, translucent to transparent crystals when fresh, through salmon pink, opaque, to deep pink/reddish opaque crystals (Plate 5.5) with alteration. This occurs before the K-feldspar is consumed by pinite.

In thin section, the K-feldspar (i.e. microcline) retains its typical cross-hatched appearance despite the changes seen in hand specimen. Microcline becomes the third major mineral to be replaced by pinite (after plagioclase and biotite) and the second to be completely consumed by pinite (after plagioclase). Alteration to pinite begins between 10.7m and 14.7m beneath the unconformity in these suites.

Progressive replacement

Pinite initially develops along cracks in the microcline (Plate 5.6a). It then pervades along the cleavages and parallel to and along selected twin lamellae (Plate 5.6b), although any perthitic lamellae of more sodic composition would be replaced preferentially. Further replacement gives rise to small "islands" of remnant feldspar (Plate 5.6c). These become more mottled in appearance as they are degraded (Plate 5.6d) and decrease in size until they are indistinguishable from the pinite under ppl or xpl.



Plate 5.5
Exposure containing deep pink K-feldspar crystals.

12

PLATE 5.6

Progressive replacement of microcline.

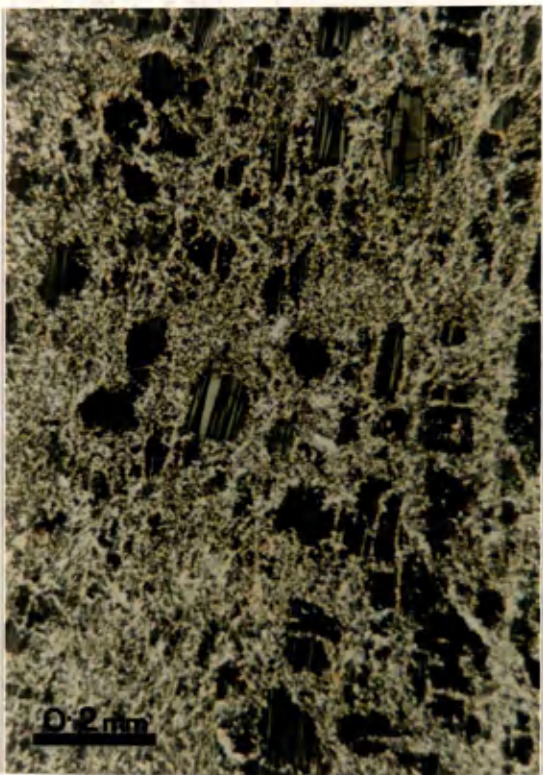
- Plate 5.6a Cracks in crystals provide zones for preferential replacement.
- Plate 5.6b Within the crystal, replacement occurs initially along cleavages with preferential consumption of selected lamellae.
- Plate 5.6c Further replacement gives rise to small 'islands' of pristine microcline surrounded by pinite.
(10.7m below unconformity).
- Plate 5.6d These 'islands' are subsequently consumed by secondary pinite. (2.0m below unconformity).



a



b



c



d

Biotite

When fresh, biotite is a black mineral with vitreous lustre in hand specimen. On alteration, it changes to creamish to pale yellow or pale yellow to pinkish and matt. While the fresh minerals appear as single crystals, gaps between the flakes are visible in the altered grains. With further alteration the remnant crystals become paler before they are completely consumed (cf. Plate 5.1b).

Biotite is the second major mineral to start altering (after plagioclase) and the third to be completely consumed by secondary minerals. Initial replacement was seen at ~15m beneath the unconformity in suites CP and CG.

Progressive alteration

Initial replacement of biotite occurs at the edges of crystals on individual flakes and penetrates inwards (Plate 5.7a). With the onset of alteration, the flakes begin to splay (Plate 5.7b) and remnant flakes in splayed areas may warp (Plate 5.7a & c). Pinite then starts to form between the cleavages (Plate 5.7c), which aggravates the amount of splaying.

The end of a zone of extensive development of pinite may be sharp and marked by a distinct kink on the basal plane (Plate 5.7d (arrows)). When viewed parallel to (001), these are seen as points of inflection, the locus of which forms a slightly irregular transition zone across the crystal (Plate 5.8a), due to further penetration of pinite into the remnant crystal. Pinite eventually forms all along the cleavage before the remnant flakes are consumed.

The secondary minerals develop laterally from the cleavage at the expense of the remnant flakes.

Pits on the surface of the flakes mark sites where secondary minerals have been dislodged (Plate 5.7d). The various shapes of these pits are indicative of the different

orientations at which the pinites developed. Unlike with other primary minerals, there is no obvious crystallographic control of the biotite flakes on the orientation of pinites.

At this stage in alteration, the areas of remnant biotite change in appearance in transmitted light. The pleochroism, which is intense when fresh, varying from lime-green to olive-green to dark brown (e.g. Plate 5.8b), becomes much weaker and changes from light brown to dark brown (Plate 5.8c). The typical mottled appearance of fresh biotite close to extinction position also disappears in the altered grains. The cleavages, sharp boundaries inside the fresh grains, appear more diffuse in the altered crystals due to the growth of secondary minerals laterally from these planes.

With further alteration, the remnant grains become yet paler brown and the zones of replacement become wider from the cleavages. At ~2.0m b.u., in suites CG and CP, pyrophyllite is found developed between biotite flakes (Plate 5.7e). The 001 plane of the pyrophyllite forms at 90° to the 001 plane of the remnant biotite (Plate 5.7f). Tourmaline also develops, usually at the ends of the altering biotites (Plate 5.8d), and tiny crystals of rutile form around the rims of the altering biotites (Plate 5.8d). With further alteration, the remnant crystals become paler brown in ppl until they are totally consumed by secondary minerals. In highly altered rocks, areas of sun tourmaline with a number of tiny rutile crystals within a few mm mark sites of precursor biotite grains, now totally consumed.

Mineral Chemistry

The chemistry of the remnant, unconsumed biotite flakes changes with alteration. Qualitative EDS analysis of biotites in almost fresh and altered rocks, from 15.0m and 2.0m beneath the unconformity respectively, were obtained under the same conditions. Comparison of results, relative to constant silica, showed that biotite had lost; especially Mg, also Fe and K on alteration (Fig. 5.2). The Al content increased and Ti remained the same. Hence if Ti is assumed to be constant, the findings would be the same as this.

However, if Al is assumed to be constant all the other elements; Mg, Fe, K, Si and Ti would have decreased.

PLATE 5.7

Progressive replacement of biotite crystals.

- Plate 5.7a Biotite replacement occurs initially at the edges of flakes.
Note - cleavage plane on left side (arrow) has started to warp. (15.0m below unconformity)
- Plate 5.7b Flakes splay at the edges after the start of alteration. (15.0m below unconformity)
- Plate 5.7c Pinite penetrates along and laterally from the cleavages. Remnant biotite flakes in splayed area may become warped. (7.8m below unconformity)
- Plate 5.7d Line of inflection on 001 face, marking limit of splaying of altering biotite flakes (arrows). Note also the pits on this surface, of sites of secondary minerals. (7.8m below unconformity)
- Plate 5.7e Pyrophyllite forming between biotite flakes (B = biotite, Py = pyrophyllite). (2.0m below unconformity)
- Plate 5.7f Pyrophyllite 001 face forms at 90° to the biotite 001 face. (2.0m below unconformity)
- | | | |
|--------------|---|--------------|
| Points 1 & 5 | - | pyrophyllite |
| Points 2 & 3 | - | biotite |
| Point 4 | - | pinite |

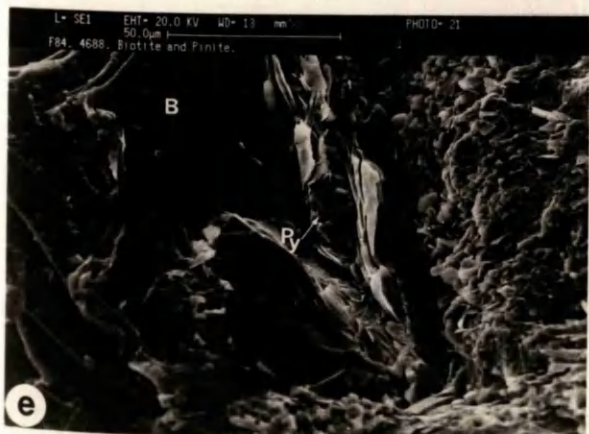
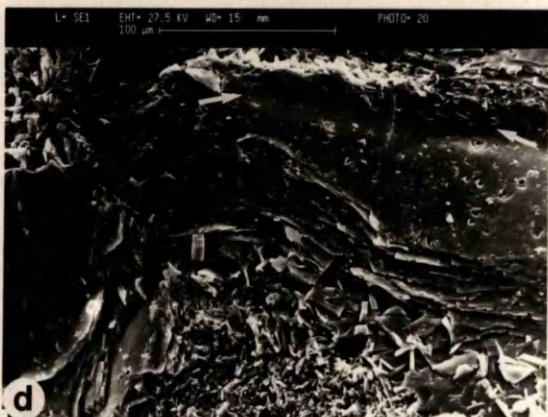
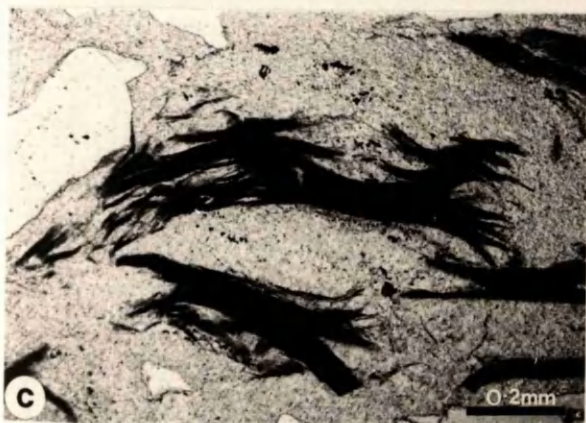
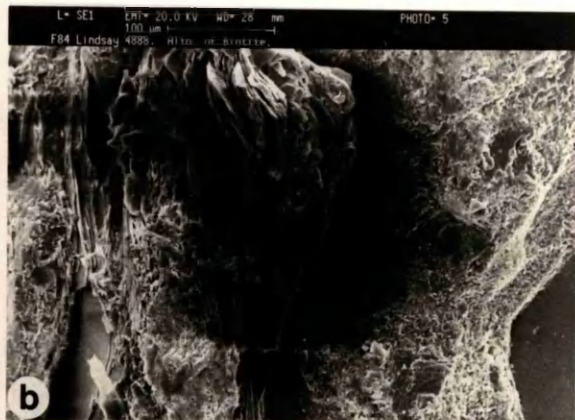


PLATE 5.8

Biotite at various stages during alteration.

- Plate 5.8a Splayed biotite crystal with pinite laths penetrating between the cleaved flakes. A pronounced, slightly irregular transition zone across the crystal marks the limit of development of secondary minerals between flakes.
- Plate 5.8b Typical fresh, cleaved biotite. (in ppl)
- Plate 5.8c Altered biotite. Replacement progresses laterally from the cleavages giving gradational zones.
- Plate 5.8d Secondary tourmaline forms at the expense of altering biotites and rutile grains develop close by.
- (T = tourmaline, B = biotite, R = rutile, P = pinite)



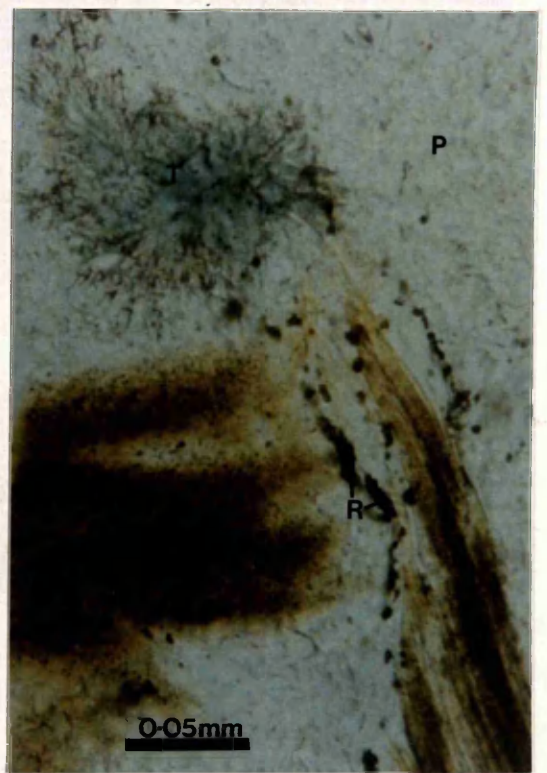
a



b



c



d

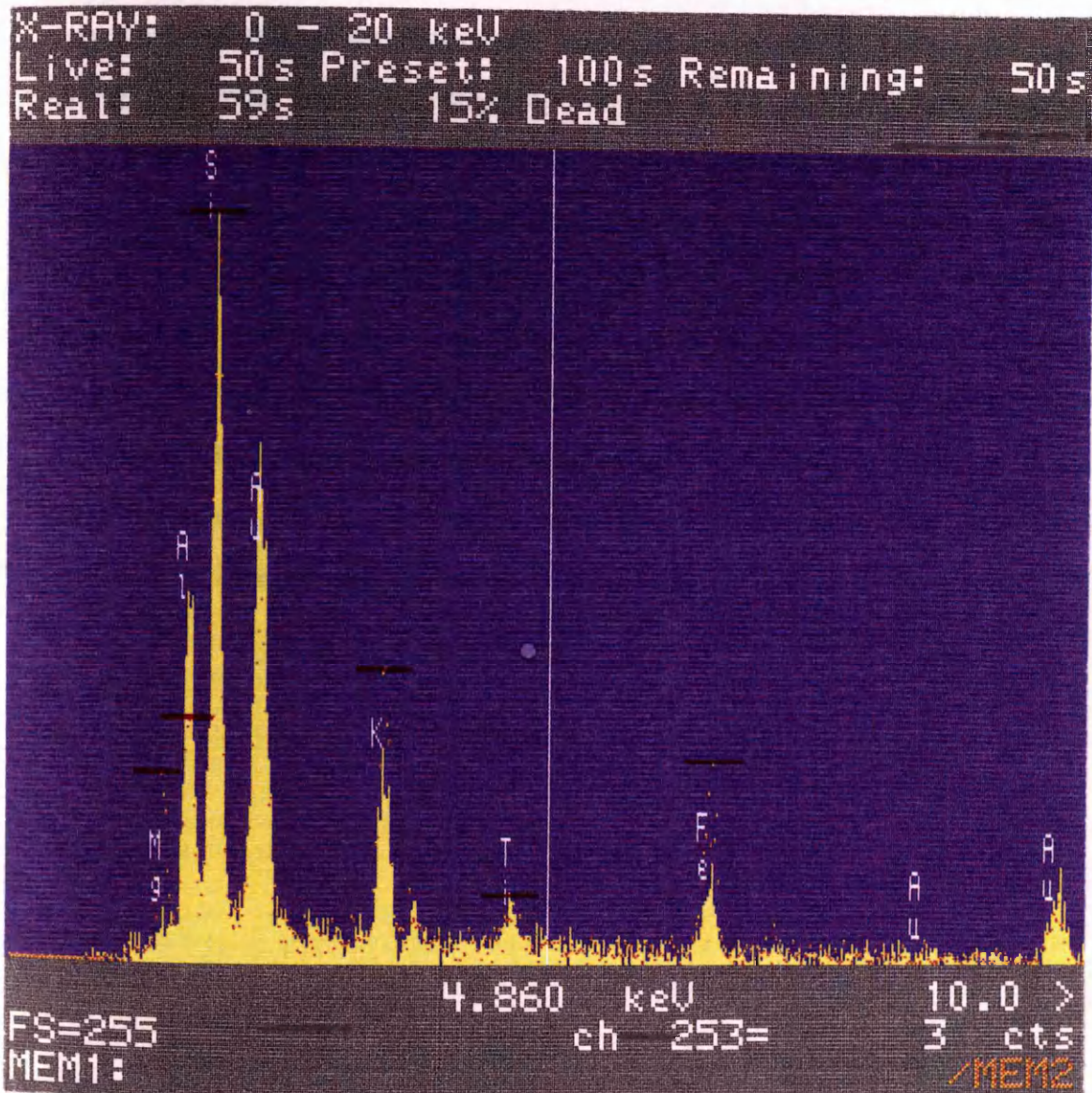


Fig. 5.2

Comparison of qualitative EDS analyses of almost fresh and altered biotite, from 15.0m and 2.0m beneath the unconformity, with respect to constant silica.

Sample from 15.0m b.u. = red dots with red bars at peaks.

Sample from 2.0m b.u. = yellow solid.

Quantitative electron probe analyses were also made on fresh and altered biotite crystals (Appendix 6). The changes in composition, with alteration, were found to be congruous with most of the changes occurring in the whole rock, as shown in the graphs in Fig. 5.3. With alteration, FeO_{tot} , MgO and MnO decrease. K_2O also decreases slightly and Al_2O_3 increases. In the case of TiO_2 , while the weight% oxide for the whole-rock does not change, the range in values obtained on analysis of biotite crystals increases with alteration, with one TiO_2 analysis even as high as 13.47%. This occurs because during the formation of biotite, titanium is involved in the formation of rutile crystals. The variation in TiO_2 content in the altered biotite analyses, coupled with the microscopically revealed presence of rutile crystals in the sites of precursor biotite, implies that even if Ti is immobile on whole-rock scale, as is often assumed or considered, it is nevertheless mobile on the crystal scale.

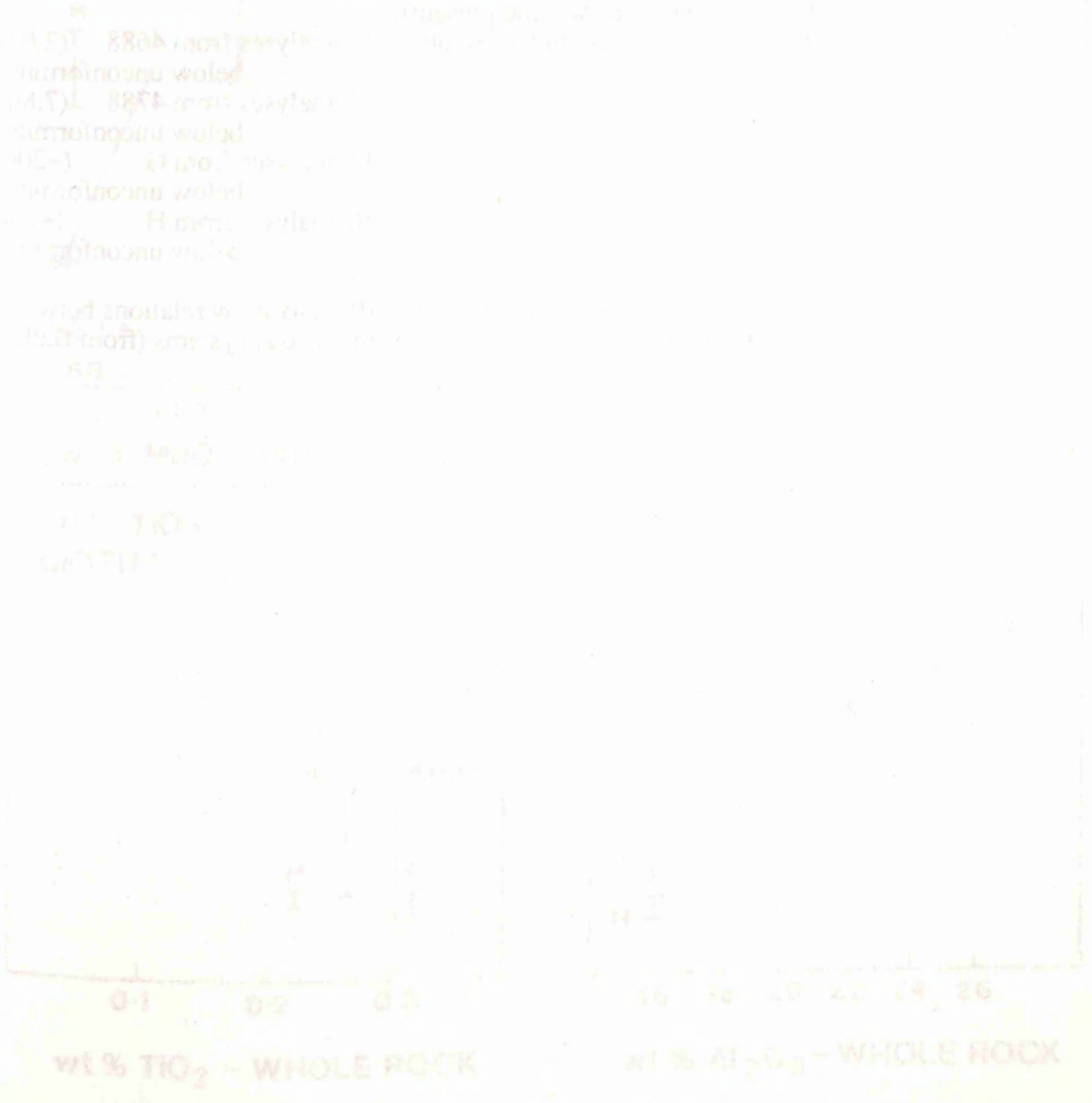


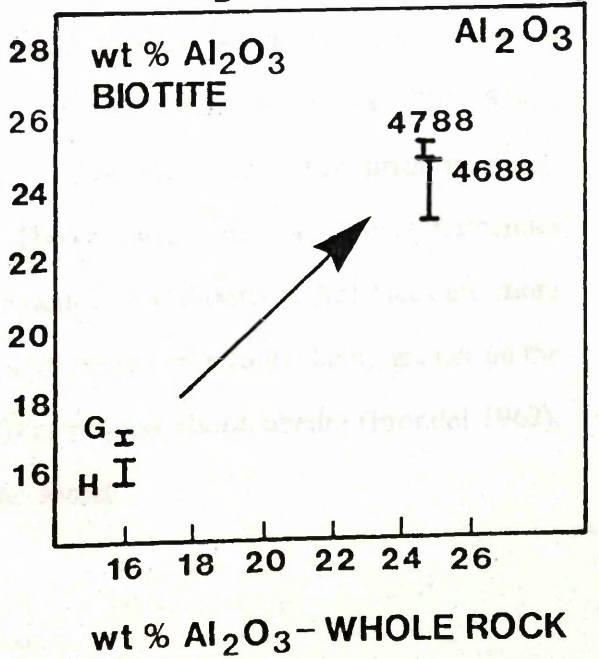
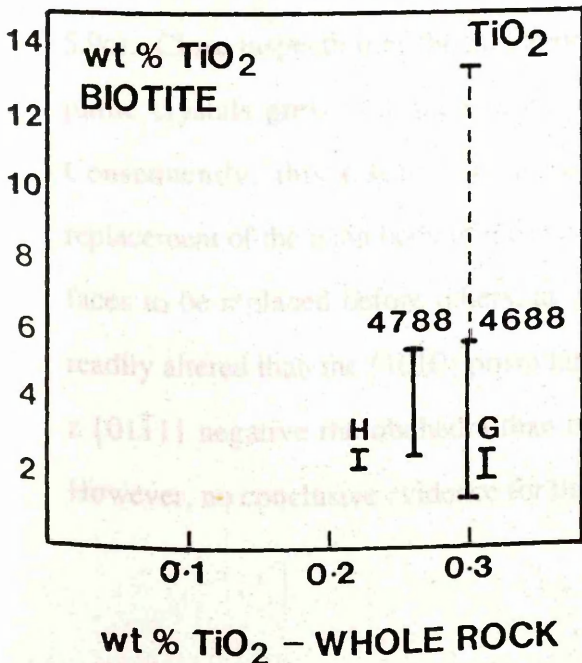
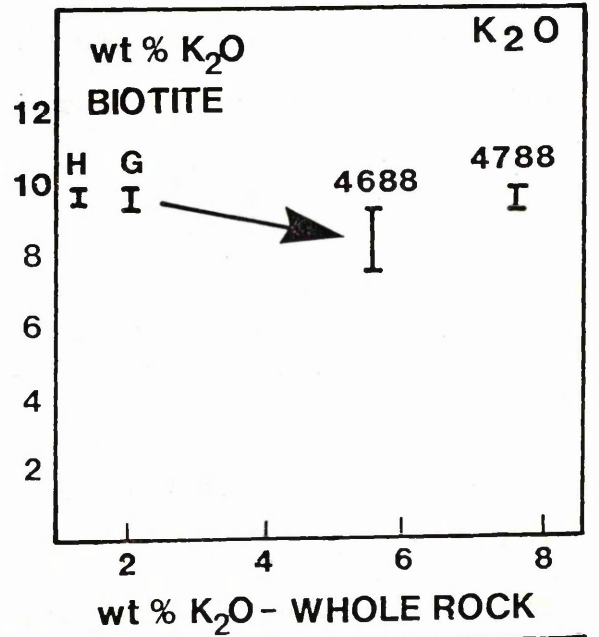
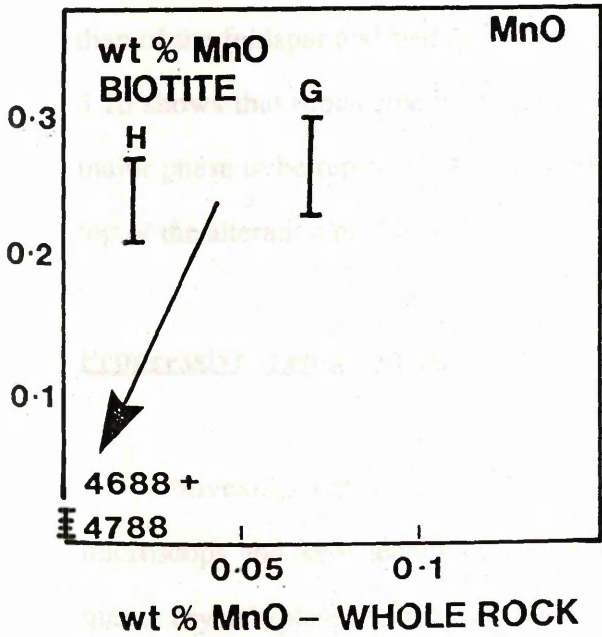
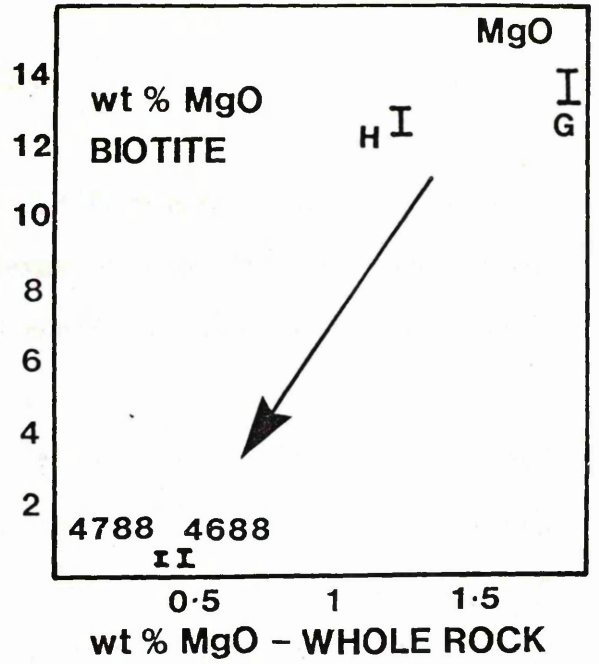
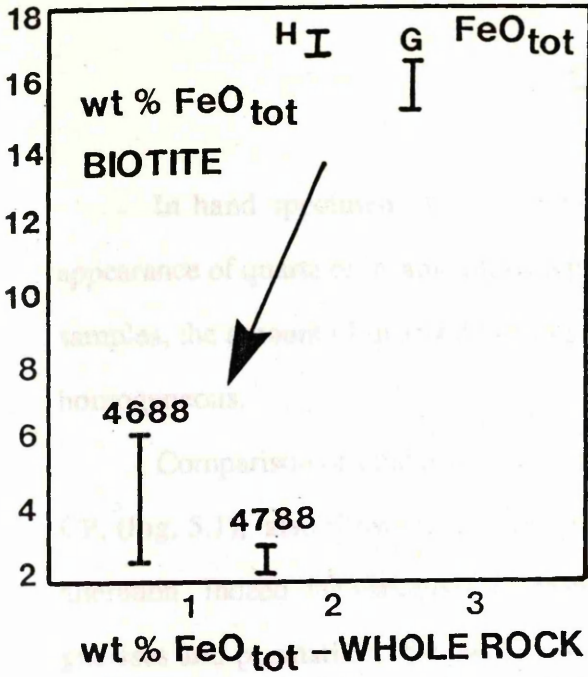
Fig. 5.3

Weight % oxide of biotite vs. whole-rock for selected major element oxides. Arrows in direction of increasing alteration. (CaO, Na₂O, P₂O₅ not shown as so little present).

The range of results plotted are of;

13 analyses from 4688	(2.0m below unconformity)
5 analyses from 4788	(7.8m below unconformity)
11 analyses from G	(~20m below unconformity)
10 analyses from H	(~25m below unconformity)

(Such plots were used by e.g. Vejnar 1971, to show relations between biotites and whole-rock compositions in igneous systems (from Bailey 1984)).



Quartz

In hand specimen, in suites CG and CP, there is no apparent change in the appearance of quartz or its amount with progressive alteration. However, in more altered samples, the amount of quartz decreases until none is visible and the rock appears more homogeneous.

Comparison of modal analyses at different stages in alteration, in suites CG and CP, (Fig. 5.1), also shows no marked trend in the percentage of quartz with increasing alteration. Indeed, the variations which do occur are within the natural variations of these gneisses and pegmatites. Hence, any replacement of the quartz is much less extensive than of the feldspar and biotite, in these suites. Close inspection of the textures in Plate 5.1b shows that replacement of quartz has indeed commenced. However, it is the last major phase to be replaced, with secondary minerals forming at its expense towards the top of the alteration profile.

Progressive replacement

Investigation of progressive replacement of quartz, using polarised light microscopy and SEM techniques, showed that replacement began along the edges of the quartz crystal (plates 5.9a & b). Later replacement occurred on the crystal faces (plate 5.9c). Close inspection of the alteration on such faces showed that the majority of the pinite crystals grew with their basal planes parallel to the quartz face (Plate 5.9d). Consequently, this resulted in decomposition of the quartz face prior to much replacement of the main body of the crystal. Theoretically, there is a tendency for certain faces to be replaced before others, as, for example, the rhombohedral faces are more readily altered than the $\{10\bar{1}0\}$ prism faces, with the rate of solution being greater on the z $\{01\bar{1}1\}$ negative rhombohedra than on r $\{10\bar{1}1\}$ positive rhombohedra (Fron del 1962). However, no conclusive evidence for this was found.

After the face was altered, the main body of the crystal itself was consumed, with pinite appearing to penetrate from the external faces into the crystal along crystallographically controlled planes. Replacement progressed in a zig-zag fashion, resulting in a serrated zone of replacement up to $\sim 10\mu\text{m}$ wide (Plate 5.9e). The boundary between each individual pinite crystal and the quartz is sharp.

There appears to be no other major crystallographic control on the way quartz is consumed by pinite. However, on a larger scale, in one small, highly altered grain, replacement had progressed to form cusped, slightly embayed areas in the quartz crystal (Plate 5.9f).

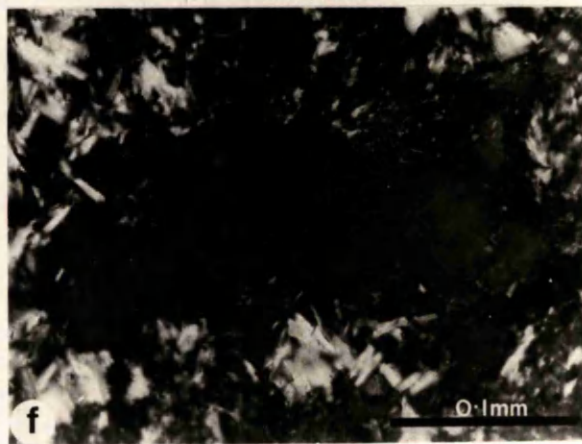
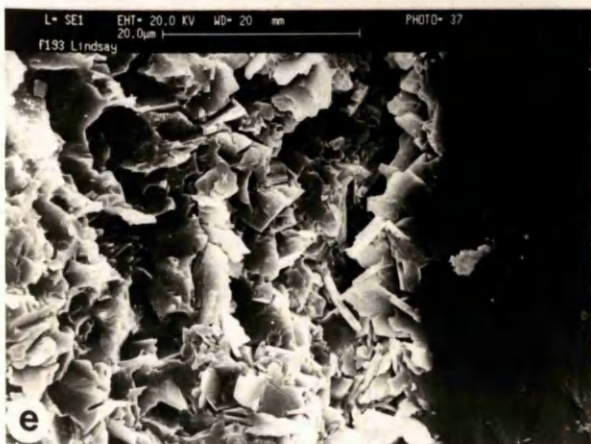
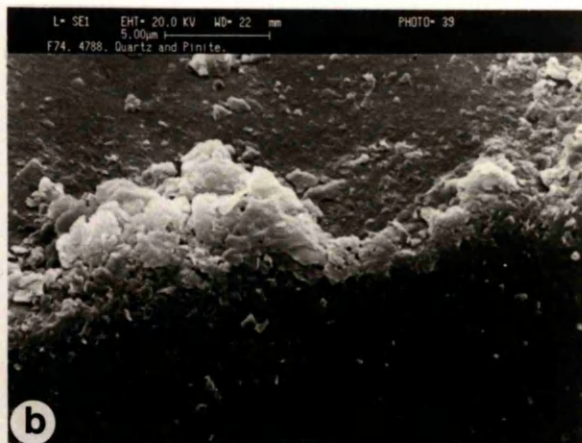
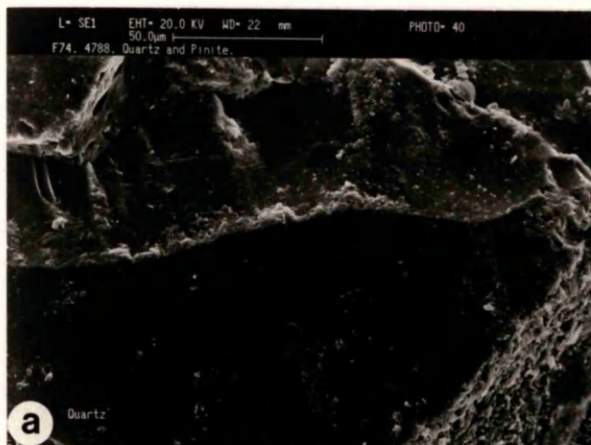
At more advanced stages of alteration, quartz crystals are replaced by what is now pyrophyllite. Replacement of quartz by pyrophyllite progresses quite differently from quartz by pinite. As with pinite, replacement begins at the outside of the crystal. However, the contact with the pyrophyllite is slightly concave (Plate 5.10a) and with progressive replacement the boundary becomes more cusped (Plate 5.10b). The consumption of quartz by pyrophyllite does not appear to be controlled by the crystal structure.

Although microscopic investigation reveals the boundary of the quartz grain to be much smoother when in contact with pyrophyllite than with pinite, SEM examination shows that the texture of the interface varies depending on the orientation of growth of the pyrophyllite. When the 001 face of the pyrophyllite is parallel to the quartz, the boundary is smooth (Plate 5.11b), but when the 001 face is perpendicular to the quartz, the contact is irregular (Plate 5.11c).

PLATE 5.9

Progressive replacement of quartz by pinite.

- Plate 5.9a Replacement is concentrated along crystal edges during early stages. (Pt1 = K, Al silicate).
(7.8m below unconformity)
- Plate 5.9b Close-up of quartz edge (Plate 5.9a) showing growth of pinite around quartz. (7.8m below unconformity)
- Plate 5.9c Secondary material has spread onto crystal faces.
(7.8m below unconformity)
- Plate 5.9d Close-up shows foliaceous habit of pinite on quartz face, with basal planes growing parallel to the quartz face.
(7.8m below unconformity)
- Plate 5.9e Zig-zag growth zone with serrated boundary as the growth of pinite is controlled by the quartz crystallographic structure. (Note sharp boundary between quartz and individual pinite laths).
(2.8m below unconformity)
- Plate 5.9f Small quartz crystal at advanced stages of replacement, showing formation of cusped scars into the body of the crystal.
(8.4m below unconformity)



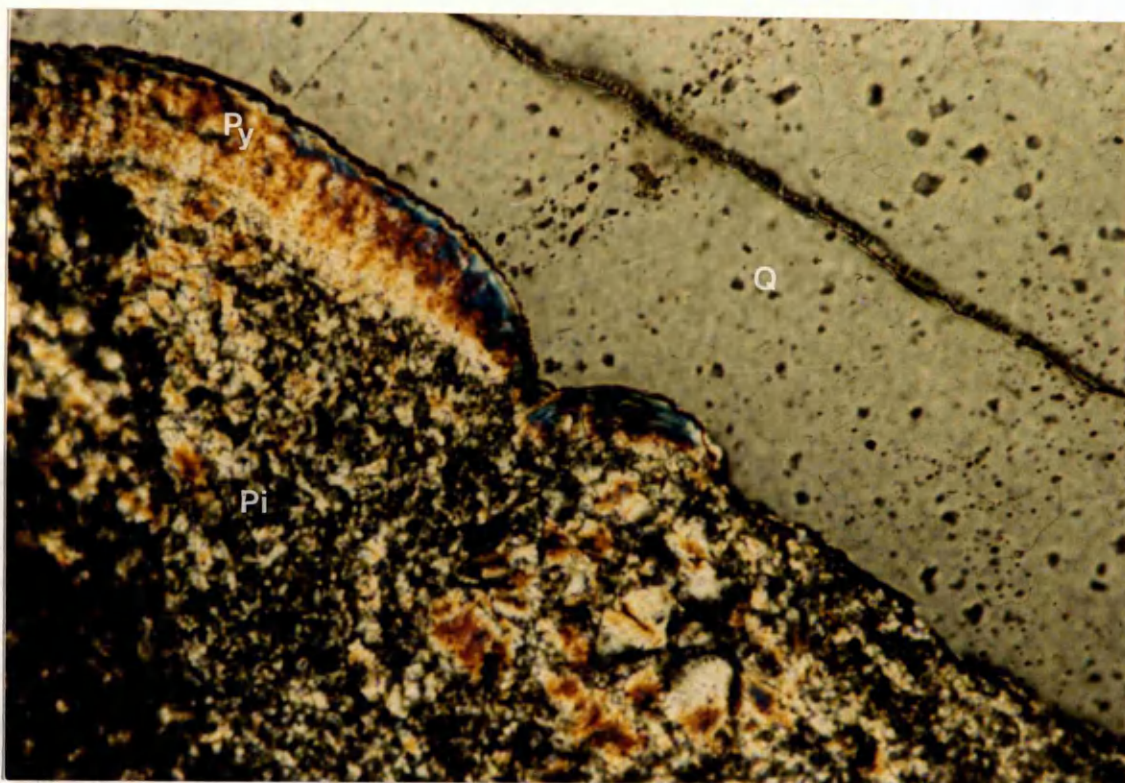


Plate 5.10a

Quartz at early stage of replacement by pyrophyllite. Slight concave scar into the quartz crystal.

(2.0m below unconformity).

Q = quartz, Py = pyrophyllite, Pi = pinite.

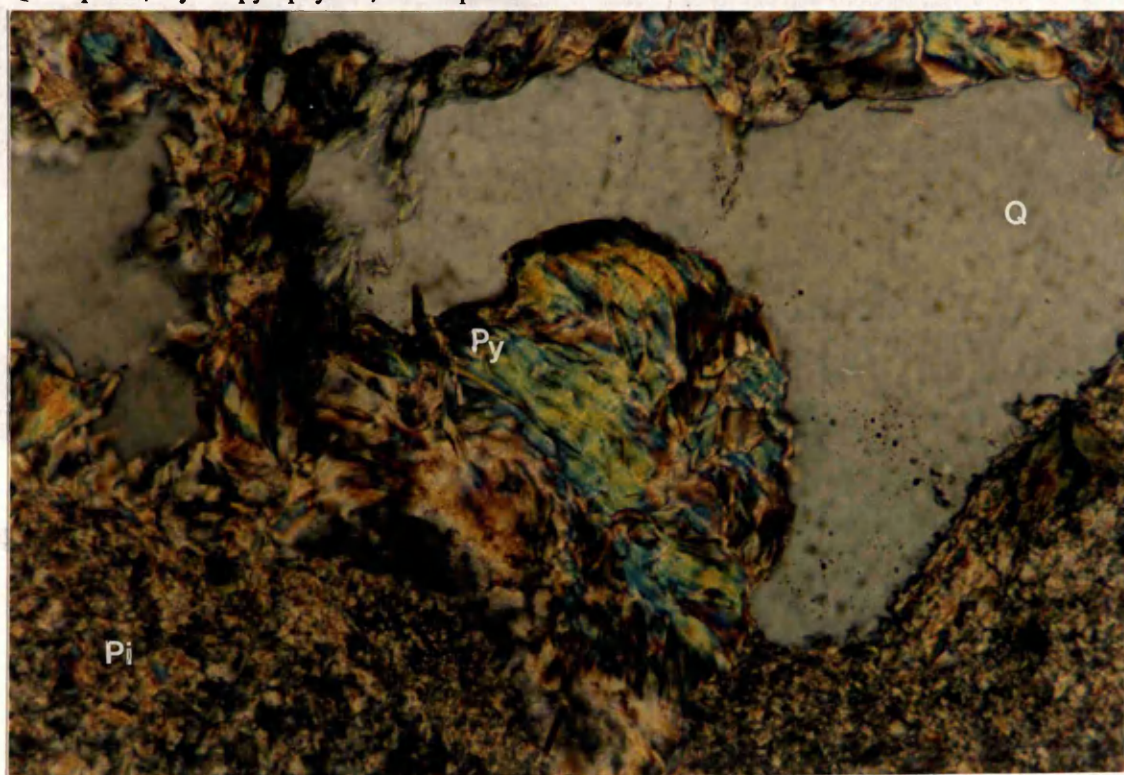


Plate 5.10b

With further replacement more quartz is consumed and the degree of curvature of the quartz/pyrophyllite contact increases.

(<2m below unconformity).

Q = quartz, Py = pyrophyllite, Pi = pinite.

SYMBOLS USED IN PLATE

Q	Quartz
Py	Pyrophyllite
Pi	Pinite

PLATE 5.11

Relationships between quartz and secondary minerals.

Plate 5.11a Pyrophyllite and pinite in degraded quartz core.

(2.0m below unconformity)

Plate 5.11b Smooth concave quartz boundary with pyrophyllite. Boundary parallel to 001 pyrophyllite face. Larger scale view of this is given in Plate 5.11a, which shows the pervasive consumption of the quartz crystal.

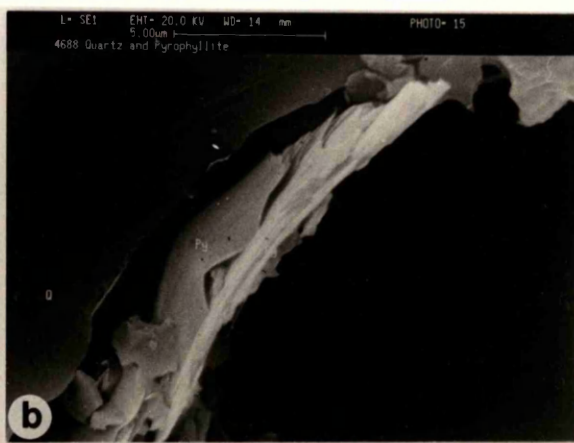
(2.0m below unconformity)

Plate 5.11c Undulatory boundary as seen perpendicular to 001 pyrophyllite face. Arrow points to platelet of remnant quartz. (Close-up of 5.11a).

(2.0m below unconformity)

Plate 5.11d Pinite size and shape scar in quartz crystal where pinite lath has been knocked out (arrow). Shows intimate relationship between quartz and pinite.

(7.8m below unconformity)



Surface Features

Quartz/secondary mineral interface textures

With replacement, the surfaces of the quartz grains develop a texture which is dependant on the mineralogy and crystallographic orientation of the secondary mineral.

Pyrophyllite may grow on either side of an area of quartz, such that interleaving plates of quartz remain and inherit an appearance very similar to that of pyrophyllite crystals (Plate 5.11c (arrow)).

Scars the size and shape of pinite crystals are visible in the quartz indicating sites previously occupied by pinite (Plate 5.11d). Other quartz textures representative of sites around which pinite grew are highlighted in plate 5.12 (arrow). These silica textures so closely resemble those of the surrounding pinite (annotated "K,Al Silicate"), that without EDS analysis, it would be very difficult to determine whether grains are quartz or pinite.

Dissolution textures

As well as textures imprinted on the quartz from secondary minerals, dissolution textures are also observed [Plate 5.12, D, 5.14c (surrounding star crystals)]. These textures have been observed only in quartz grains and may serve to distinguish quartz from pinite in SEM. One such area is highlighted in Plate 5.13. The shape of the etched area (E) conforms to trigonal-trapezohedral symmetry, produced by dissolution of quartz crystals (Fron del 1962). The distinctive shape of these etch marks affirms that they are formed on the $m \{10\bar{1}0\}$ face of the crystal (Fron del 1962). The incipient etch marks surrounding this area (e.g. highlighted area below E, Plate 5.13) indicate varying etch directions. The degree of etching varies as different faces are naturally preferentially dissolved.

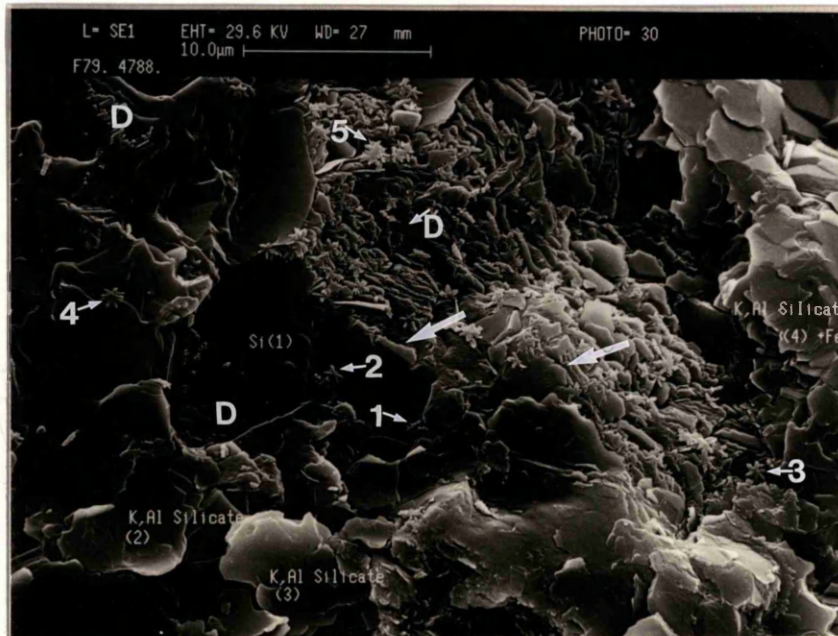


Plate 5.12

Pinite, quartz and secondary low-cristobalite.

Scalloped surface of remnant quartz reflects texture of secondary pinite (e.g. large arrows).

Remnant quartz surfaces show dissolution features (D) and secondary low-cristobalite (opal) has formed on and around the remnant quartz (Points 1-5).

Secondary Silica

Low-T cristobalite

Peculiar morphology of quartz crystals

A sample of quartz from the same area as that shown in Plate 5.12

shows the

analysis

to contrast

with the

generally

7.8-m

striking

along the

minerals

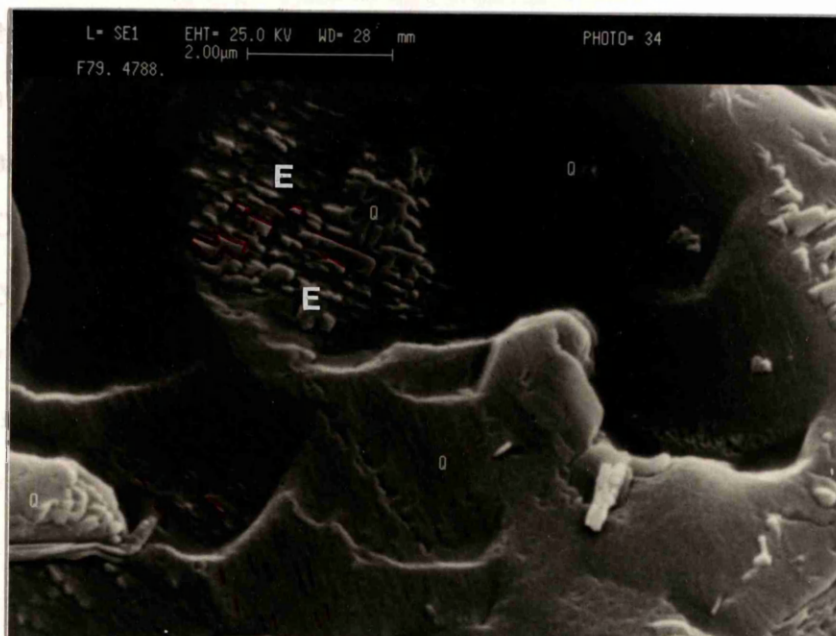


Plate 5.13 Dissolution textures on quartz crystals

Etched surface of quartz crystal.

Upper central area shows characteristic markings of $m\{10\bar{1}0\}$ crystal face.

(7.8m below unconformity)

Secondary Silica

Low-T cristobalite

Peculiar, hexagonal star-shaped crystals were discovered by SEM investigation in a sample of gneiss from 7.8m below the unconformity. Examination of this specimen shows that they appear to be concentrated around quartz-rich areas (Plate 5.12). EDS analyses of these minerals show that they contain a small but significant amount of iron in contrast to the surrounding quartz.

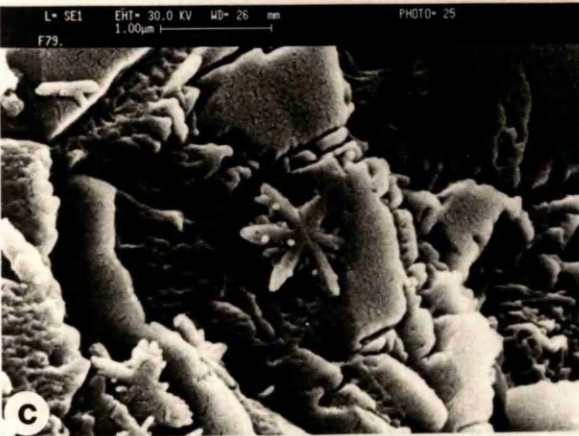
Opal (low-T cristobalite) may contain other oxides aside from SiO_2 (SiO_2 generally >90%) and H_2O ; the most abundant being Fe_2O_3 , which may range from 5 to 7% (any others <1%) (Fron del 1962). Indeed, the morphology of these crystals bears striking resemblance to the early stage cristobalite (Opal-CT) crystals of Welton (1984) from the Miocene Monterey formation, California. Hence, it may be concluded that these minerals are indeed low-temperature cristobalite, developed as a secondary form of silica.

Five stages of growth were seen (Plates 5.12 and 5.14). The crystals progress from being one-branched (Plate 5.12,1 and 5.14a (arrow)) to two-branched with $60^\circ/120^\circ$ between each limb (Plate 5.12,2 & 5.14b) and subsequently to three-branched "stars" with 60° between each limb (Plate 5.12, 3 & 5.14c). Progressive development of crystals in this fashion may be due to epitaxial growth, giving a controlled orientation on the position of branches (Fron del 1962). The stars then become stacked (Plate 5.12, 4 & 5.14d & e) and then clump together (Plate 5.12,5, & 5.14f). These provide nucleation sites for further growth which progresses to form lepispheres of opal (Welton 1984).

PLATE 5.14

Progressive stages of growth of low cristobalite (secondary silica before opal) on and around remnant quartz. (See also 5.12).

- Plate 5.14a Single blade, fully formed (central area) - second blade starting to form from the centre of the crystal?
- Plate 5.14b Twin-bladed. Two blades formed with 60°/120° between blades.
- Plate 5.14c Three-bladed "star"-shaped crystal. Note also marked dissolution textures in surrounding quartz.
- Plate 5.14d Star crystals fully formed - two stacked.
- Plate 5.14e Several stacked crystals, one on top of the other.
- Plate 5.14f Cluster of stars.



Progressive development of secondary minerals

Pinite

Pinite is the predominant secondary mineral in the alteration profile. It also constitutes the dominant mineral in most of the altered rocks immediately beneath the unconformity, where pyrophyllite is often the major phase.

In hand specimen, the pinite is predominantly olive-green (Kornerup 1967), but grades into paler greens and also pale yellow. It is white in one of the most altered rocks (at [NC 4387 6611]). Generally, with increasing alteration (i.e. towards the unconformity) the green colouration becomes paler.

Pinite is distinctively very soft (hardness ~2.5 to 3), it is waxy and is translucent to opaque.

From optical microscopy and SEM, massive pinite is found to be composed of a monomineralic aggregate of very fine-grained, well crystalline, interlocking crystals, which range in size from ~0.3 to 17 μm long and average ~8 to 10 μm (full dimensions average ~ 8x4x1 μm to 10x4x1 μm). Electron probe analysis shows these crystals are muscovite (Appendix 7).

Texture

Although at first sight pinite appears to be randomly orientated, close inspection of the textures between pinite and the minerals it is replacing suggests that the orientation of pinite laths is controlled by the crystallographic structure of the mineral being consumed. Such controlling influence is best seen in the alteration of feldspars and quartz.

With the feldspars, this is most clearly seen during early stages of alteration. Initial development of pinite crystals occurs along the cleavage planes of a plagioclase feldspar (Plate 5.15a). The crystals are lath shape to tabular and are <0.3 to ~13x1 μm .

Higher magnification reveals that the pinite grows such that its basal plane is parallel to the cleavage (Plate 5.15b). As replacement progresses, the major influence on the location and orientation of pinite continues to be the cleavages, with pinite progressively penetrating laterally into the crystal away from the cleavage planes (Plates 5.15 c & d). The basal planes of the pinite laths grow parallel to the faces along which they form. Other crystallographic features of the feldspars, e.g. compositional zoning, micro-inclusions and twinning orientations, may also influence the microtexture of the pinite aggregate.

The replacement of quartz always proceeds from the grain boundaries inwards, with pinite's basal plane once again most probably developing parallel to and along crystallographic planes, this time in a zig-zag fashion (Plate 5.15e).

Aggregates of pinite from completely altered precursor feldspars (Plates 5.15f) consist of highly crystalline, variously orientated grains, which range in size from ~0.7 to 17 μm and average ~8 to 10 μm . The grains form an interlocking texture with many grains abutting against each other. Points A, B and C (Plate 5.15f), show elongated gaps which represent sites where previously interlocking crystals have been knocked out.

When pinite is the major phase in intensely altered rocks, ghost boundaries of precursor minerals which have been completely consumed are often visible. These are best seen at low magnification under crossed polarised light and are marked by a change in the over-all interference colours. These boundaries, also visible under SEM, are due to a change in preferred orientation of the pinite laths - in turn suggested to be dependant on the crystallographic structure of the precursor minerals. For example, at least two such boundaries may be detected in Plate 5.16a. Close examination of area B relative to area A, reveals that B contains more crystals orientated ENE-WSW than A (especially seen at the left area of B). The crystals in A have different orientations, including WNW and north of NNE.

However, the type of precursor mineral may also influence the shape, as well as the orientation of the pinite grains (Plate 5.16a, area C and 5.16b). Instead of having straight edges like the crystals highlighted so far, the majority of crystals in these areas

PLATE 5.15

Pinite textures

Plate 5.15a Pinite forming parallel to NE-SW trending plagioclase cleavage.

Plate 5.15b Higher magnification of boxed area in plate a. Two pinite laths are growing together and parallel to cleavage. Pinite is also growing at an angle from the cleavage along a plagioclase face.

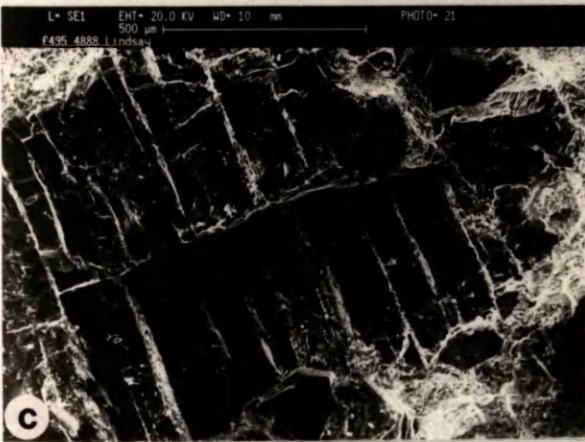
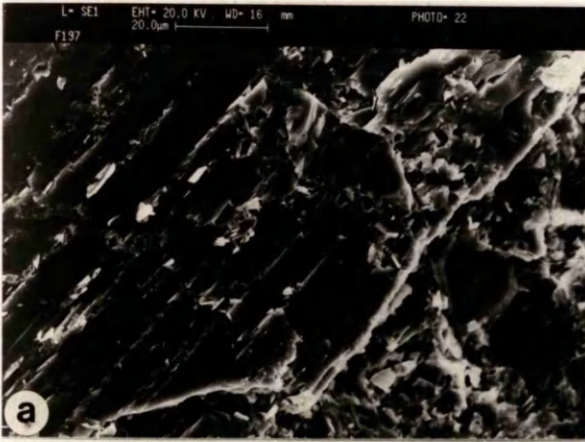
Plate 5.15c Plagioclase at more progressed stage of replacement. Cleavage exerts main control on position of pinite growth.

Plate 5.15d Close-up of plate c - Pinite formed along and laterally from cleavage planes.

Plate 5.15e Pinite growing at expense of quartz. Note again preferential growth along quartz faces.

(2.8m below unconformity).

Plate 5.15f Pinite aggregate in altered gneiss with crystals exhibiting interlocking texture. (2.0m below unconformity).



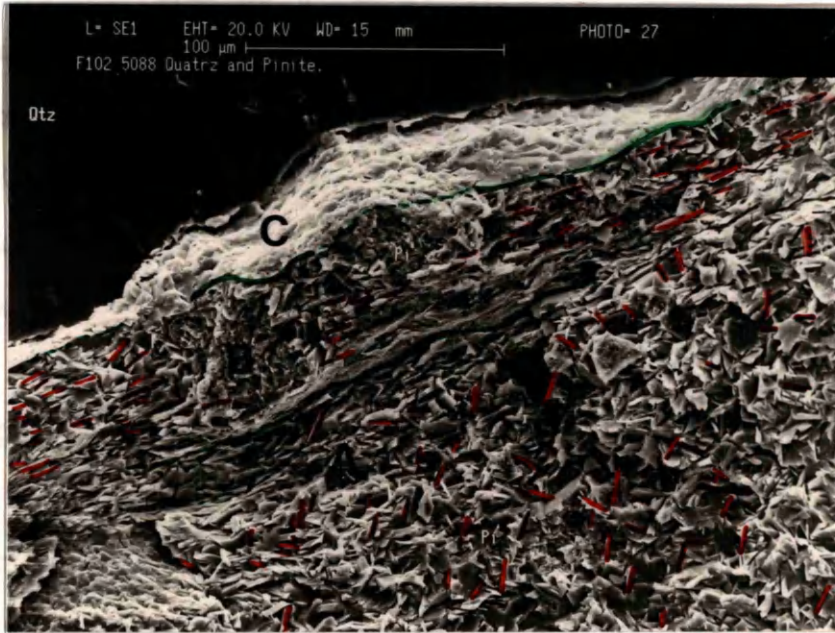


Plate 5.16a

Mass of pinite with ghost precursor mineral boundaries.

- Green lines - Ghost boundaries (probable and possible) separating areas of different precursor minerals A,B &C.
 Red dashes - highlight like orientations of pinite laths in each region.

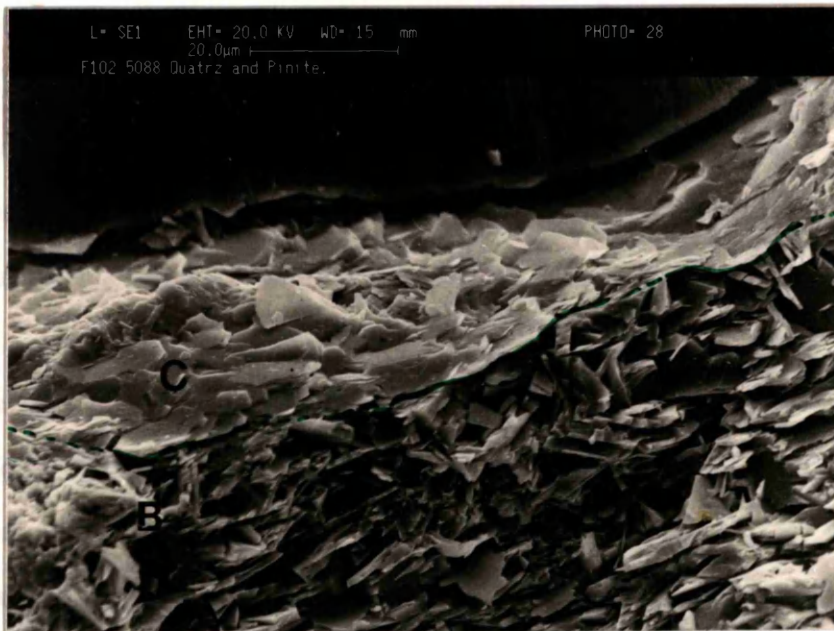


Plate 5.16b

Close-up of boundary B-C (plate 2a).

Note the different orientations and shapes of crystals in each case.

have more rounded "petal-like" edges. Such shape difference may be a consequence of the orientation. Since crystals are growing with a strong preferred orientation, they have terminated before these textures could develop. It is unlikely that the pinite structure is different in each case. It is therefore interesting to speculate that the individual crystals in area C may exhibit more of the form of uninhibited growth of single crystals of pinite, if allowed to develop into larger grains.

X-ray diffraction

From initial comparison of the x-ray diffractograms of pinite and igneous muscovite (Fig. 5.4) it is seen that the muscovite basal peaks are present in the pinite trace. The basal peaks of muscovite are characteristically enhanced, with the intensity ratio of basal : non-basal peaks high. The pinite diffractogram, in contrast, has the basal peaks relatively suppressed, while the non-basal peaks are enhanced markedly, decreasing the basal : non basal peak ratio.

The differences in diffractogram traces of these chemically equivalent minerals is due to the fact that while muscovite platelets grow parallel to each other, with perfect cleavage and a large aspect ratio, the individual pinite crystals in a massive, uncleaved pinite lump are orientated in many directions and the crystals have a much smaller aspect ratio. The muscovite crystals, therefore, have a propensity to settle on XRD glass slides with their basal planes parallel to the glass (giving intense basal reflections). However, the pinite crystals settle in a more random fashion, with only a slight preferred orientation to the basal section.

To characterise more fully the diffractograms of pinite, more detailed work was carried out to:-

- 1) investigate the reproducibility of the traces.
- 2) characterise and determine accurately:-
 - a) the d-spacings of each typical peak.
 - b) the hkl values for peaks.
 - c) the relative peak intensities (I/I_1).

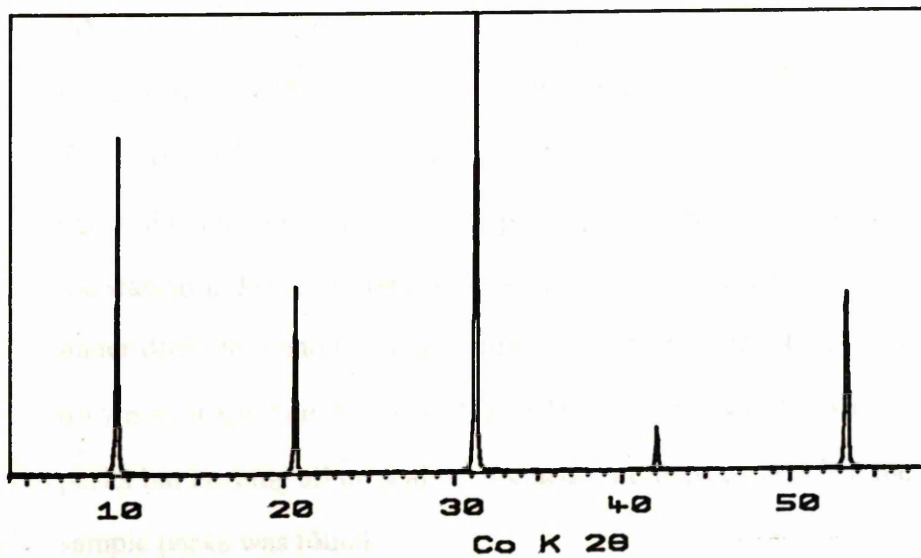
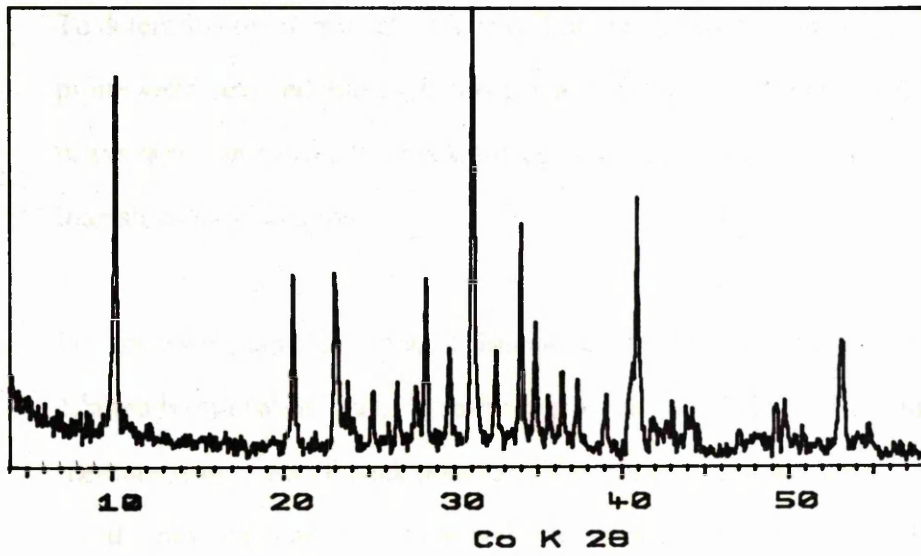


Fig. 5.4
X-ray diffractograms of pinite (above) and typical igneous muscovite (below).

Methods

- 1) To determine the reproducibility of diffractogram traces, five chips of translucent pinite were selected and each was run at $2^\circ/\text{min}$. The sample with the sharpest peaks was run twice, to check for consistency in peak positions and relative intensities in one sample.
- 2) For accurate characterisation of the traces, the sharpest sample from experiment 1, already run twice, was; 1) re-run again but at $1^\circ/\text{min}$ to allow more accurate measurement of actual peak positions. Optimum conditions were set such that all but the most intense peak were on scale, in order to enhance smaller peaks and increase measurement accuracies. The sample was run between 4° and $65^\circ 2\theta$ (~ 25.65 to 1.666\AA).
2) This sample was then spiked with a CeO_2 standard whose positions are known and recorded in JCPDS (Bayliss *et al.* 1980). CeO_2 was chosen since its major peaks do not coincide with the major peaks of pinite.
- 3) The spiked sample was scanned at $1^\circ/\text{min}$ and $T=2 \times 10^2$, between 4° and $70^\circ 2\theta$ (~ 25.65 to 1.561\AA) (large CeO_2 peaks are found between 66° and $70^\circ 2\theta$ (~ 1.644 to 1.561\AA)). The spiked sample was then re-run at $0.5^\circ 2\theta/\text{min}$ and $T=1 \times 10^2$ (TC10) between 19° and $45^\circ 2\theta$ (5.42 to 2.339\AA), i.e. in the range containing the most reliable major peaks of the sample and the principal peaks of the standard. For a further check on peak positions, the sample was again re-run under different conditions, this time between 30° and $34^\circ 2\theta$ (3.46 to 3.06\AA) at $0.5^\circ/\text{min}$, 30Kv , 16mA , $T=4 \times 10^2$ and TC4 (markedly decreasing the sizes of the peaks but keeping all on scale). A consistent distance between the standard and sample peaks was found.
- 4) d-spacings obtained for the standards were compared with JCPDS standard CeO_2 values and a correction factor was obtained, by which each peak position in

the spiked sample and subsequently the unspiked 10/min full scan were adjusted. Accurate peak positions and relative intensities were then measured by hand.

Results

1. The peak positions for various pinite samples are reproducible (Fig. 5.5).
- 2a) d Å values for each peak were compared with the JCPDS values for different muscovites. It was found that pinite is a $2M_1$ muscovite (Table 5.1).
- 2b) Now established as a $2M_1$ muscovite the diffractogram peaks of pinite were indexed by comparison with those of $2M_1$ muscovite (Table 5.1).
(Four $2M_1$ peaks were not detected in the pinite. - 2 of these, if present, would have been masked by adjacent peaks, and the other 2 small ones were undetected). A number of pinite peaks were found which are not recorded for $2M_1$ muscovite of which two or three may be found in $3T$ or $1M_1$ muscovite (see Table 5.1).
- 2c) Intensity values were measured relative to 006 (usually the most intense peak). These are also recorded. However, these intensity values can only be taken as guidelines and not considered as absolute or diagnostic, as the relative peak intensities vary from sample to sample.

The two peaks at $10.30^\circ 2\theta$ (9.95Å) and $31.10^\circ 2\theta$ (3.33Å) are consistently the most intense. After this, the order of intensity of other peaks varies between samples.

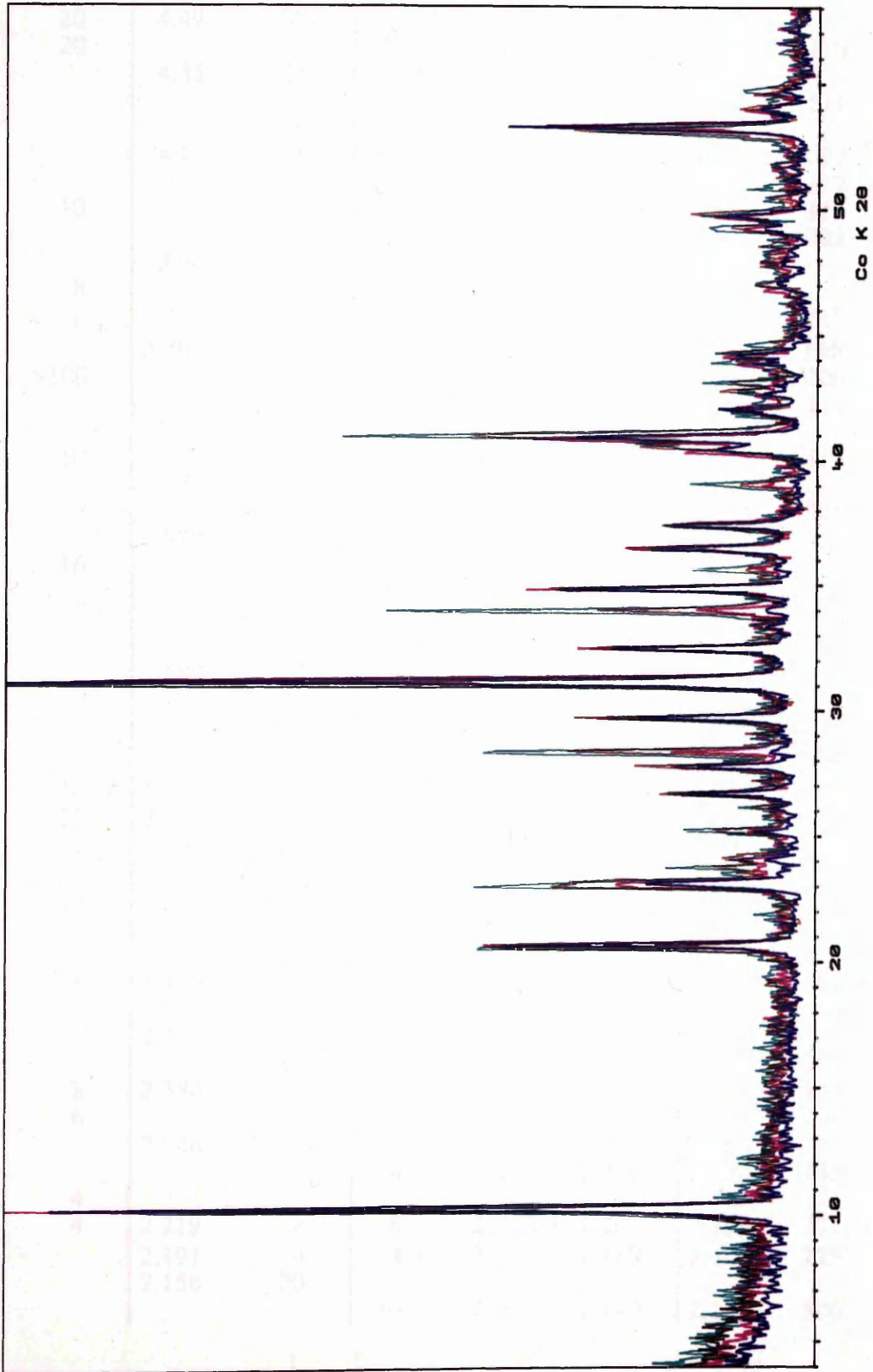
To show the scale of these fluctuations in relative intensity and in an attempt to find the most consistent peak ratios, selected peak ratios and I/I_1 values were measured (Table 5.2). The intensity ratio for one sample (re-run twice) varies up to $\pm 3\%$. Considering all five different samples, the fluctuation in ratio varies significantly from peak to peak, although each ratio shows broadly similar values. The 131/110 ratio varies least over all, ranging from 1.28 to 1.39. The I/I_1 values, related to 006, fluctuate in a

Results

Fig. 5.5

X-ray diffractograms of four pinite samples (normalised) showing consistent peak positions, but variable intensities.

N.B.	Green trace	=	Pinite - Sample 1, Table 5.2
	Brown trace	=	Pinite - Sample 5, Table 5.2
	Pink trace	=	Pinite - Sample 3, Table 5.2
	Blue trace	=	Pinite - Sample 4, Table 5.2



3T		1M		2M ₁		PINITE			
dÅ	I/I ₁	dÅ	I/I ₁	I/I ₁	hkl	dÅ	dÅ	hkl	I/I ₁
9.97	>100	10.08	>100	95	002	9.95	9.95	002	71
4.99	55	5.04	35	30	004	4.97	4.99 ^(b)	004	35
4.49	20	4.49	90						
4.46	20			20	110	4.47	4.46 ^(a)	110	38
		4.35	25	4	111	4.30	4.35	111	10
				4	111	4.30	4.30	111	10
				4	022	4.11	4.26	111	11
		4.11	16	4	022	4.11	4.10	022	8
				6	112	3.95	3.95	112	3
3.873	10			14	113	3.88	3.87	113	12
				18	023	3.73	3.71	023	14
		3.66	60				3.65		24
3.596	8			20	114	3.48	3.48 ^(5a)	114	23
		3.36	>100	25	024	3.34	<--- peak hidden-		<--->
3.331	>100			100	006	3.32	3.33	006	100
				30	114	3.19	3.19	114	21
							3.13		1
3.110	10			2	115	3.12	3.11	115	2
		3.07	50				3.06		24
				35	025	2.987	2.994	025	26
		2.929	6				2.926		5
2.884	16			25	115	2.859	2.860	115	17
				20	116	2.789	2.793	116	13
							2.748		1
		2.689	16				2.677		8
							2.628		2
					131	2.596	<--- peak hidden-		<--->
2.589	16	2.582	50						
2.546	25	2.565	90	55	202	2.566	2.578	202	22
		2.550	20				2.554		49
				8	008	2.505	2.501	008	10
2.499	12			14	132	2.491	2.478	132	5
				8	133	2.465			
2.457	8	2.450	12	8	202	2.450	2.454	202	11
							2.437		10
		2.405	4				2.409		4
				10	204	2.398	2.392	204	10
2.384	8	2.380	12	25	133	2.384	2.374	133	12
2.254	6			10	134	2.254	<-----	?-----	<--->
		2.246	8						
				4	135	2.236	2.236	135	7
2.222	4								
2.197	4	2.219	8	8	221,204	2.208	2.198	221,204	4
		2.191	4	4	223	2.189	2.178	223	5
		2.156	20						
				16	206	2.149	2.146	206	10

2.136	12			20	135	2.132	2.125	135	12
		2.109	6	4	223	2.070	2.104		3
2.056	4			6	044	2.053	2.080	223	2
		2.013	30				2.047	044	2
1.999	45			45	0010	1.993	1.999	0010	26
1.966	8			10	224,045	1.972	1.966	224,045	7
		1.957	8	6	206	1.951	1.945	206	6
				4	226	1.941	1.942	226	5
		1.900	4						
1.885	2			2	208	1.894	1.885	208	2
				4	046	1.871	1.871	046	2
							1.846	?	1
							1.828	?	2
				4		1.822	1.818		2
				4	228	1.746	1.770	?	1
				8	139	1.731	1.745	228	2
							1.728	139	4
				6	241	1.710	1.719	?	2
				6	151,150	1.704	1.714	241	2
				4	240	1.699	<-----	- ?-----	>
		1.668	18	12	0012,	1.662	1.692	240	1
					2010		1.663	0012,	7
								2010	
1.654	10								

Table 5.1

dÅ and I/I₁ values for peaks of pinite together with other muscovites from JCPDS, showing that pinite is a 2M₁ muscovite.

(hkl values of pinite were determined from comparison with 2M₁ muscovite.)

Sample No Location	1 Wheelhouse	2 NC 448 661	3 8752	4 NC4484 6614	5 Wheelhouse
Diffractogram Colour- Fig-	Green		Magenta	Cyan	Brown
002/110	1.99	4.04	3.57	4.04	1.98
004/110	0.98	1.35	0.88	1.02	1.10
006/110	2.32	4.88	3.46	2.30	2.62
131/110	1.34	1.39	1.34	1.37	1.30
006/002	1.16	1.21	0.97	1.09	1.33
I/I_1					
002	86	83	103	91	75
004	42	32	39	38	39
006	100	100	100	100	100
110	43	20	29	23	38
131	60	28	39	31	50

Table 5.2 Peak ratios and I/I_1 values for selected pinite samples.

similar fashion. With respect to the 006 peak, the 004 peak varies least with $I/I_1 = 37 \pm 5\%$.

I/I_1 values do not give absolute peak intensities. To determine how the values of pinite diffractogram peaks relate to those of the laboratory standard muscovite both pinite and muscovite were analysed under the same conditions, and are plotted together as absolute values (Fig. 5.6). Pinite, however, is plotted at 10x the scale factor of muscovite! Pinite, therefore, is much less sensitive than muscovite, with basal peaks from 0.053 to 0.029 times less intense!

Errors in measurement of peak positions and intensity

The 2θ measurements could be made to an accuracy of $\pm 0.03^\circ 2\theta$, equivalent to and varying between $\pm 2 \times 10^{-3} \text{ \AA}$ at $40^\circ 2\theta$ and $\pm 7 \times 10^{-4} \text{ \AA}$ at $65.5^\circ 2\theta$. Accuracy of manual intensity measurement = $\pm 1\%$.

Mineral Chemistry

Electron probe analysis was used to determine the chemical composition of pinite. As well as quantitative spot analyses of selected grains at different locations and positions beneath the unconformity, quantitative and qualitative analyses were made by traversing an area of massive pinite, some 30x20 mm. This was done to investigate changes in major element chemistry of pinite, and to determine its chemical consistency.

Qualitative

The graphical output of qualitative analyses shows at a glance whether the concentrations of various elements change towards/away from the centre of the large area of pinite. Counts of Na, Si, K, Fe, Mg, Al, Ca and Mn are shown in Fig. 5.7, determined from 2 traverses along the length of the pinite area.

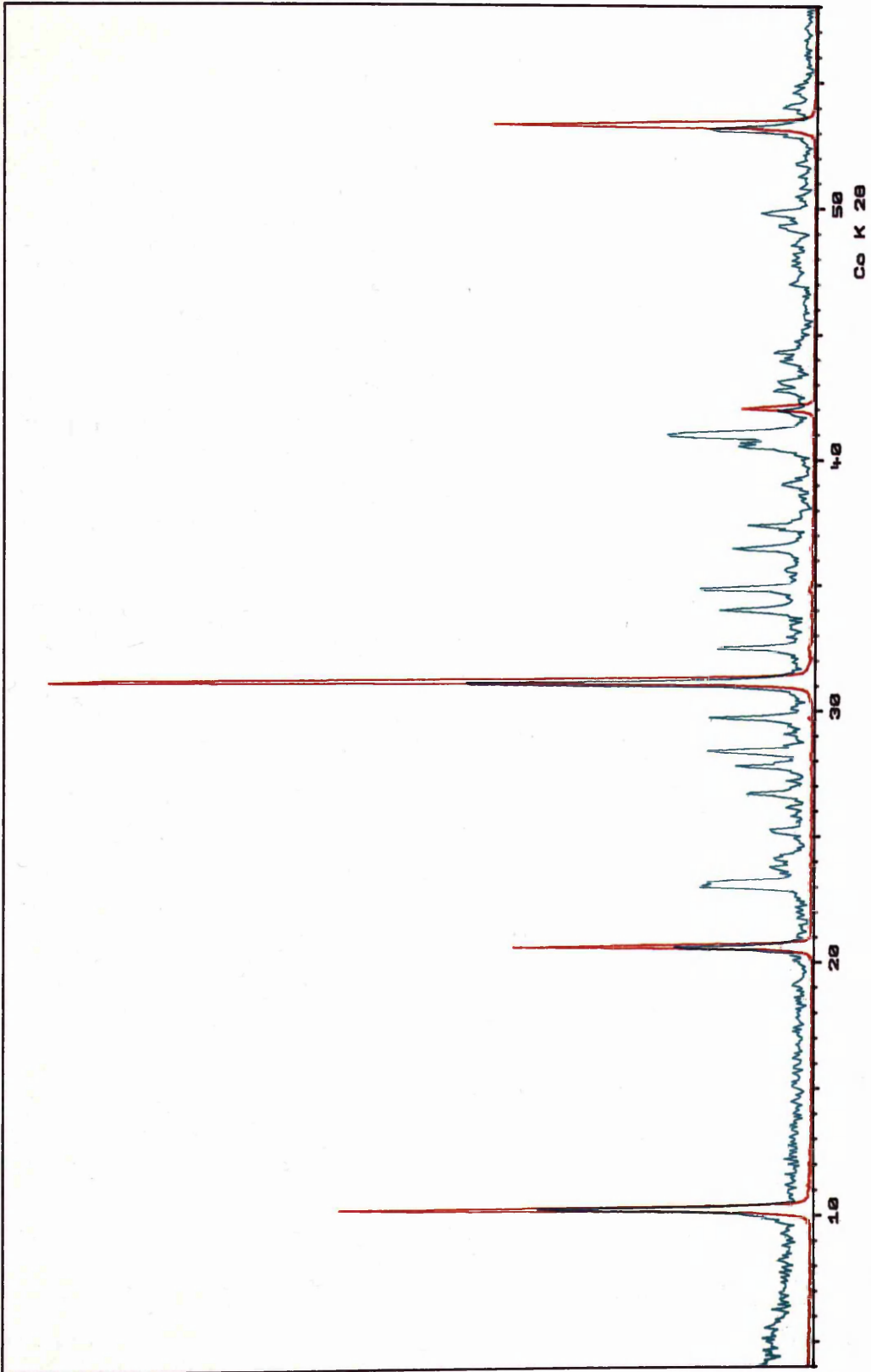


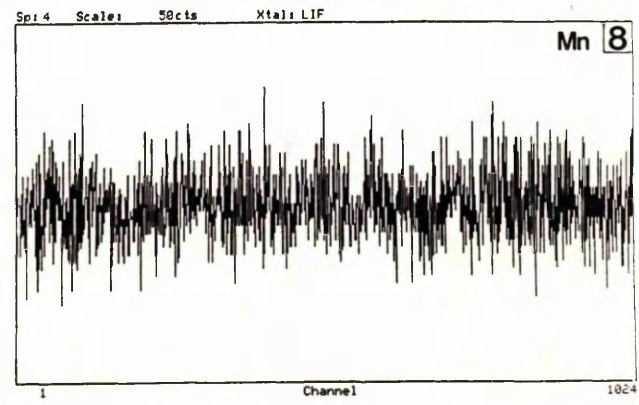
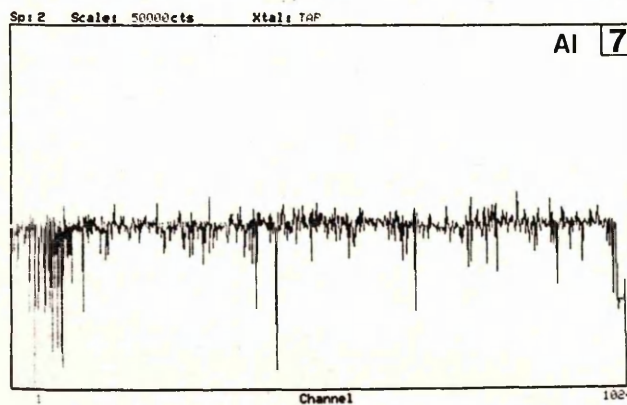
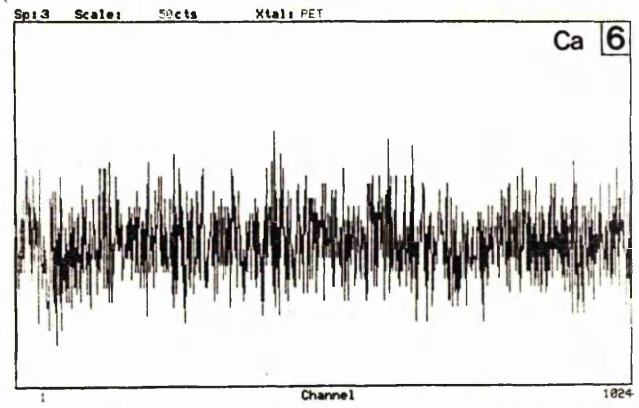
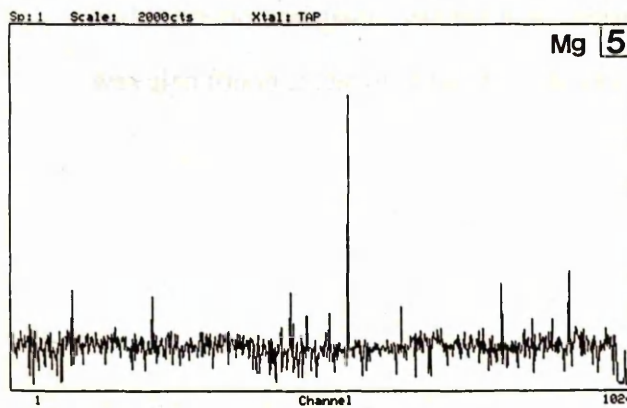
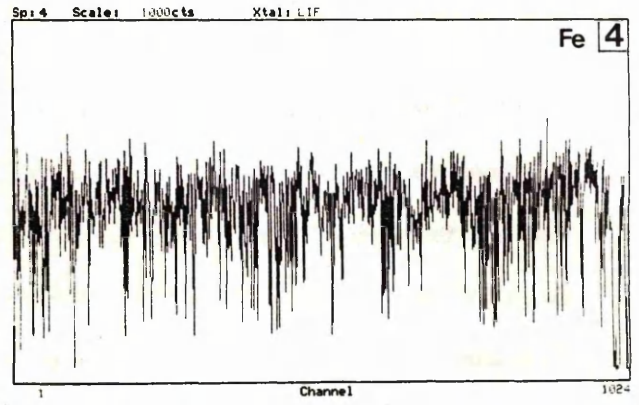
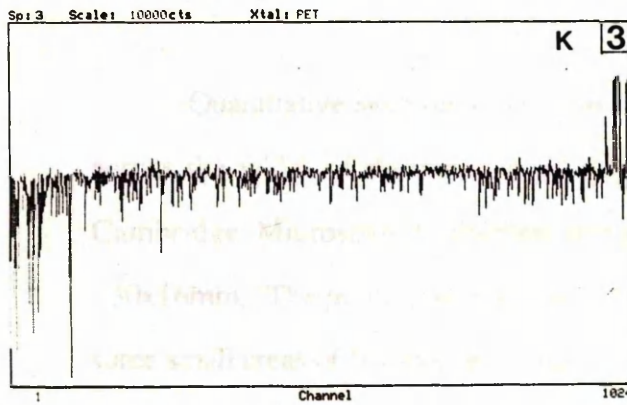
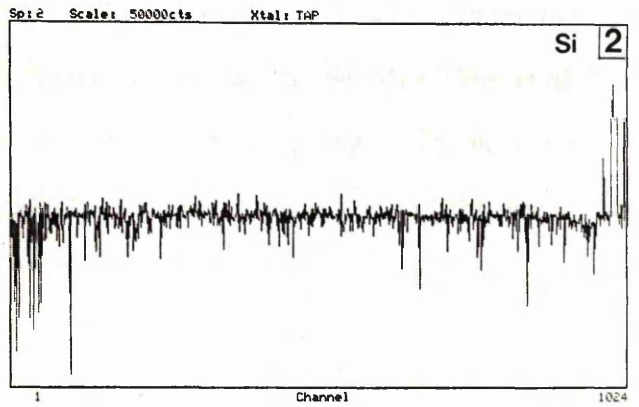
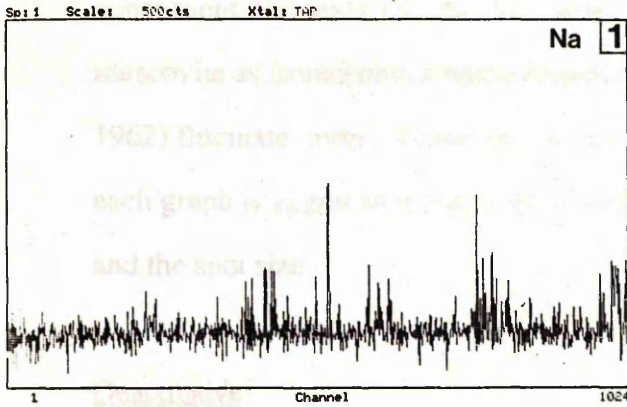
Fig. 5.6
X-ray diffractograms of pinite and muscovite analysed under the same conditions.

Fig. 5.7

Graphical output from qualitative analyses across a mass of pinite ~27mm long. Counts of Na, Si, K, Fe, Mg, Ca, Al and Mn are shown in graphs 1 to 8 respectively.

Qualitative assessment was made on Cameca Camebax electron probe. Step positions were fully automated, with linked graphical output.

Scan length	=	27,052 μ m
No. of counts per scan	=	1,024
step length	=	27,052/1,024 = <u>26.42μm</u>



The underlying trend in each graph shows no variation in concentration of each of the elements across the traverse. The graphs show that the concentrations of the main constituent elements (K, Al, Si) varies little. The other elements, which enter the muscovite as isomorphous replacements for K and Al (Na, Ca, Mg, Fe, Mn) (Deer *et al.* 1962) fluctuate more. However, the underlying trend shows no change. The noise on each graph is aggravated due to the combined effects of the fine grain size of the pinite, and the spot size.

Quantitative

Quantitative analyses were made on manually chosen grains along the length and across the width of the mass of pinite (Appendix 7) (measurements were made on Cambridge Microscan 5 electron probe). 24 analyses were made over an area ~30x16mm. The pinite crystals were consistently of muscovite composition (although some small areas of feldspar remained (differentiable with backscatter electron imaging)) and there no consistent variation in composition across the aggregate was detected (as was also found in the qualitative traverse).

Tourmaline

The presence of tourmaline in the main body of the rock is restricted to the uppermost parts of the alteration profile. It generally appears as blackish spots up to 1mm in diameter. These may be sparsely distributed, (Plate 5.1, sample 4688) or more highly concentrated throughout the whole rock, but may also be concentrated in bands (e.g. Plate 4.3 and frontispiece). Individual spots may grow into each other giving slightly larger continuous areas of tourmaline. Rocks in which tourmaline forms a major mineral are less common, but are occasionally seen within a few metres of the unconformity (e.g. Plate 5.17a & b).

Tourmaline is also present in veinlets ≤ 5 mm wide, found throughout the profile (Plate 5.17c & d). In the veinlets, tourmaline is intimately associated with quartz, the only other mineral. In hand specimen, no clear, well defined tourmaline crystal structure is obvious in this association.

In the main body of the rock, tourmaline is the second secondary mineral seen when progressing from fresh to altered rock.

Tourmaline in tourmaline/quartz veinlets

In optical microscopy, the vein tourmaline crystals are lath shape to blocky, with a much smaller aspect ratio than those in the rock body. The crystals vary in size up to ~0.6mm long, with the smaller crystals in the main part of the veinlet (Plate 5.18a). This tourmaline ranges in pleochroism from dark green to brown.

Tourmaline needles are also found in quartz crystals in the vein (Plate 5.18b). In the main zone of the veinlet, the quartz is very fine-grained and anhedral (Plate 5.18c).

Tourmaline in the rock body

Optical microscopic investigation of the most altered rocks reveals that tourmaline crystals are mostly in the form of radiating acicular aggregates, known as tourmaline 'suns' (Deer *et al.* 1986) (Plate 5.19a). These aggregates are up to $\sim_{\wedge}^{0.4}$ mm diameter. In ppl they range in pleochroism from colourless to turquoise green to light blue. They are usually isolated in the groundmass. Occasionally, individual needles of blue tourmaline ~ 0.01 mm long are seen.

Green tourmaline is also present in the rock body but is much less abundant. It was seen only in one pegmatite at [NC 4387 6611] in a sample also containing 'sun' tourmaline. The green tourmaline was localised and occurred in and around a restricted zone of brecciation. Many very fine wispy laths make up the mass of green tourmaline which frequently becomes an amorphous aggregate (Plate 5.19b). However, individual needles also penetrate into quartz crystals (Plate 5.19b).

The shape/limits of the green tourmaline most likely indicates that it formed at the expense of some precursor minerals, the limits of which are probably represented by the present limits of tourmaline. No textural evidence was found to indicate that the green tourmaline was a different generation from the blue.

Blue 'sun' tourmaline is found in association with altering biotite, although some crystals were also found in sites most likely previously occupied by feldspar.

Development of tourmaline associated with remnant biotite

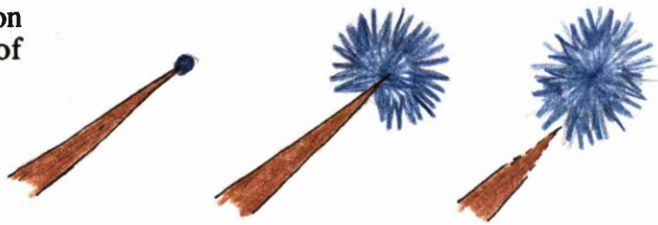
Tourmaline generally forms at the end of the remnant biotite, with acicular crystals developing radially away from the centre of growth (Plate 5.20a). With increasing alteration, tourmaline develops further at the expense of biotite. The form it takes depends on how initial growth proceeded (see sketches, Fig. 5.8, along with text). For example;

1. Thin biotite crystals (illustrated in Fig. 5.8a). Tourmaline develops initially at the end of a thin crystal of altered biotite, with needles growing radially away from this point until a spherical radiating acicular aggregate of 'sun' tourmaline remains. If the biotite crystal is sufficiently long, then the tourmaline becomes separated from the remnant biotite when the full 'sun' is formed. (Plate 5.20b).
2. Broader biotite crystals. When the initial biotite is wider and the core of the tourmaline nucleation broader, Plate 5.20c and Fig. 5.8b, then progressive alteration may be sufficient to consume the whole grain, especially if tourmaline develops at both ends of the biotite. After tourmaline forms at the end of the biotite, tourmaline crystals may also nucleate along the remnant flakes, with needles growing laterally from these planes, eg. Fig. 5.8c and Plate 5.20d. It would be reasonable to assume that all of the right side of the biotite in Plate 5.20d would be consumed if altered further. Taken to completion, the area of tourmaline would appear as merged 'suns'.

Fig. 5.8

Cartoon showing examples of tourmaline development at the expense of biotite.

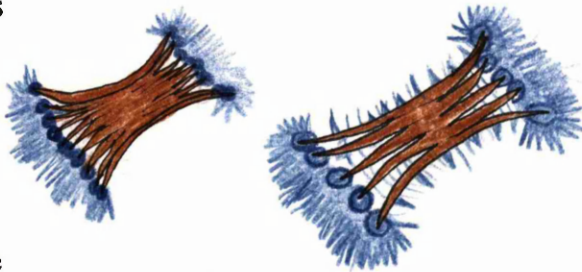
a) Biotite-narrow crystal:
tends to one point of nucleation
for subsequent growth of
tourmaline.



b) Biotite-broader at end:
many points for nucleation.



c) Progressive stages towards
consumption of whole mineral.



-nucleation may begin along the
edges of the grain and into the
remnant flakes between
cleavages.

Fig. 5.8

Cartoons showing examples of progressive development of tourmaline at the end of and at the expense of remnant biotite crystals.

Texture of tourmaline 'suns' from SEM investigation

More information is obtained about the form of 'sun' tourmaline and its association with remnant biotite from SEM investigation. The centre of the main 'sun' tourmaline in Plate 5.21a is at the centre of the photograph. Although it appears to have at least one other 'sun' intergrowing (e.g. one whose centre is $\sim 100\mu\text{m}$ to the right of the main one), higher magnification of the central area reveals that these aggregates grow in a spiral fashion about a central zone (Plate 5.21b).

Tourmaline needles which have developed radially from a remnant biotite crystal are seen in Plate 5.21c. Close examination shows the blocky termini of the crystals. However, only one convincing trigonal pyramid - typical of tourmaline (Cox *et al.* 1974) is clearly seen (arrow).

10

Plate 5.17

Tourmaline in altered pegmatite and tourmaline/quartz veinlets

- Plate 5.17a Tourmaline (dark mineral) with quartz and pinite in altered pegmatite [NC 4387 6611].
(<2 m below unconformity)
- Plate 5.17b Thick section of altered pegmatite. Tourmaline forms a major mineral along with quartz and pinite. [NC 4387 6611].
(<2 m below unconformity)
(NOTE: Plates a and b of pegmatites from pod, Plate 5.17a).
- Plate 5.17c Tourmaline/quartz veinlet insitu. The plane of the veinlet is here exposed. [NC 4357 6240].
- Plate 5.17d Group of veinlets in cross-section. [NC 4357 6240].



a



b



c

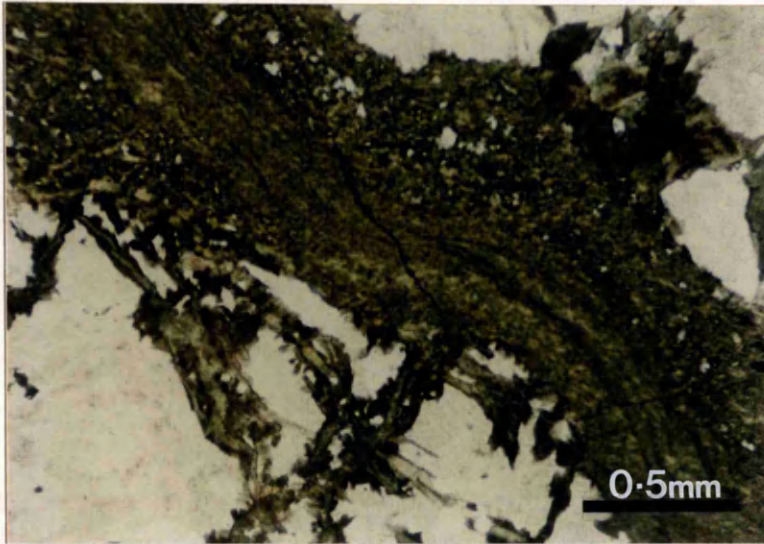
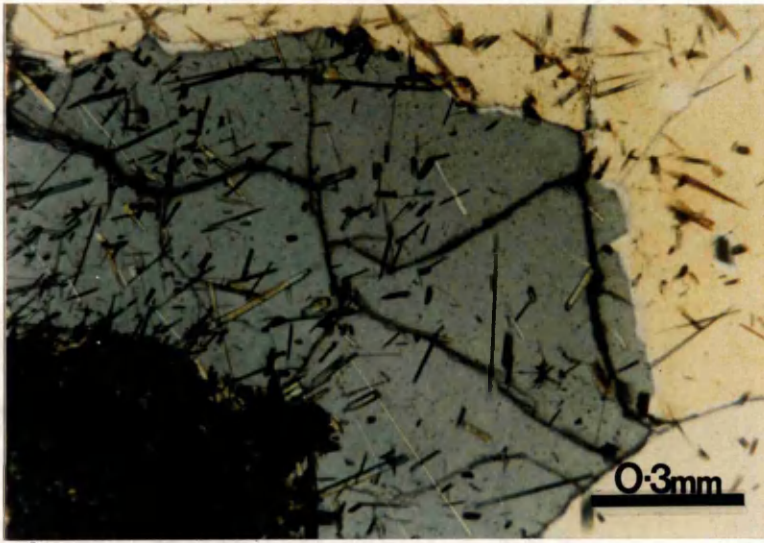
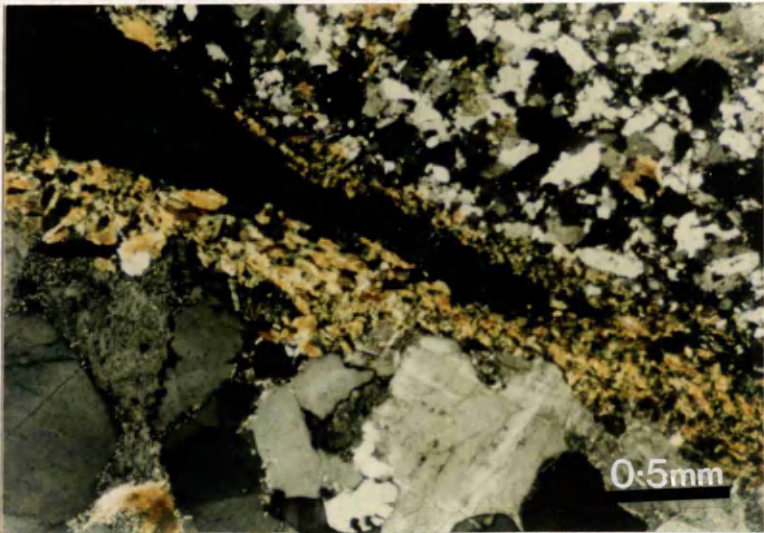


d

PLATE 5.18

Tourmaline/quartz veinlets.

- Plate 5.18a Smaller crystals of tourmaline in veinlet, with larger laths to the side. (ppl)
- Plate 5.18b Tourmaline needles are formed in quartz crystals in quartz/tourmaline veinlets. (xpl)
- Plate 5.18c Quartz in veinlets is often very fine-grained. (xpl)

**a****b****c**

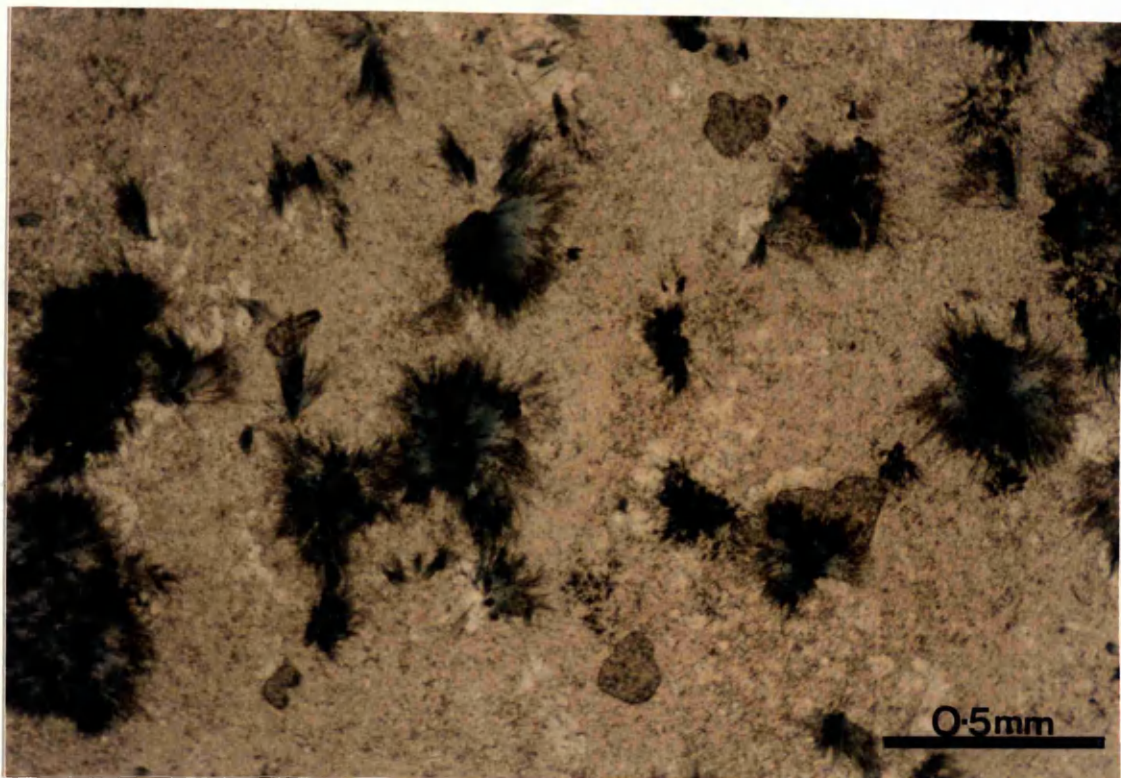


Plate 5.19a

Radiating acicular aggregates of 'sun' tourmaline. Tourmaline rosettes (suns) are surrounded by pinite.

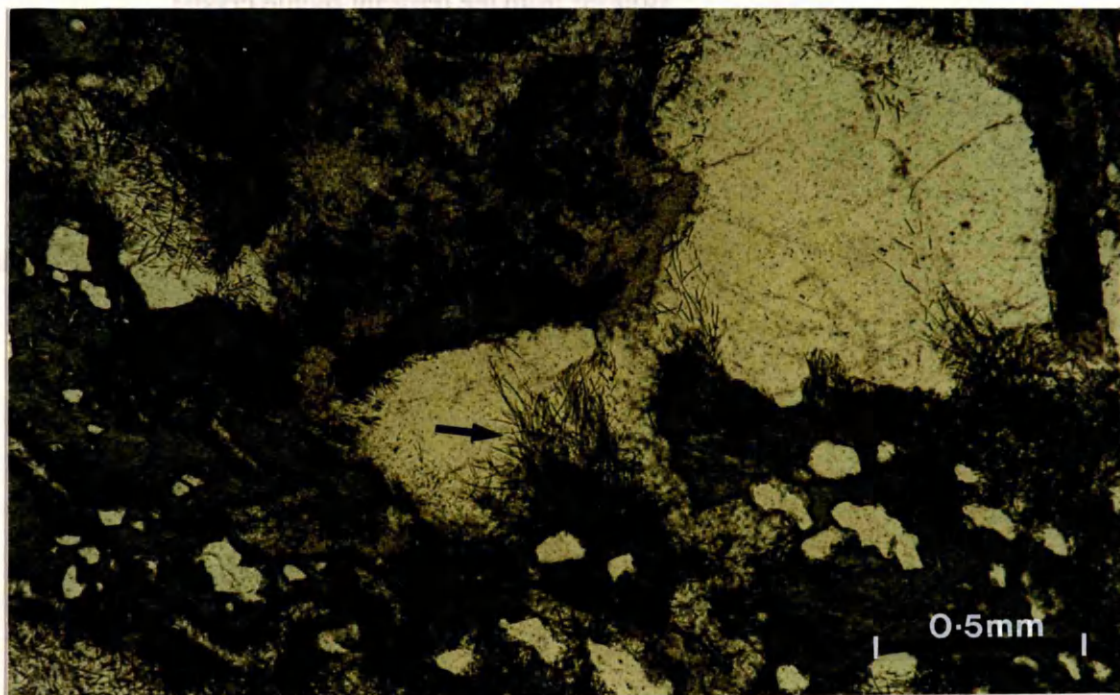


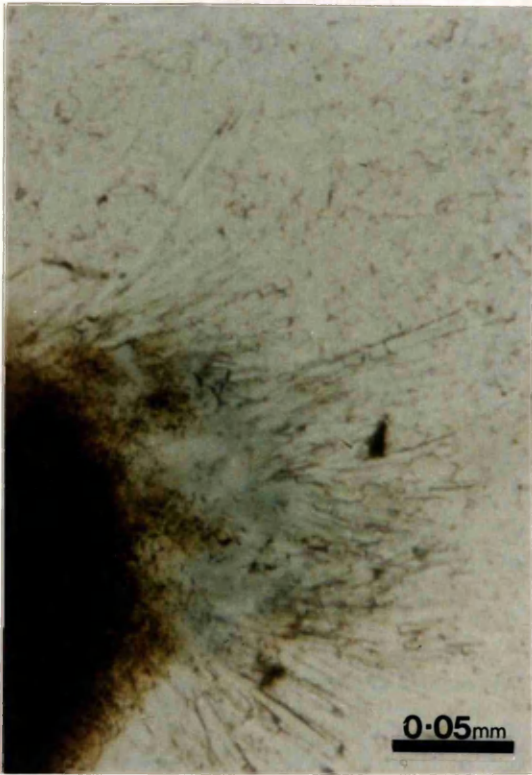
Plate 5.19b

Green tourmaline (with some blue 'suns'). Green tourmaline forms around quartz grains (bottom left) and in well defined areas surrounded by pinite. Green tourmaline laths penetrate into quartz crystals (e.g. arrow).

PLATE 5.20

Tourmaline formation associated with altering biotite.

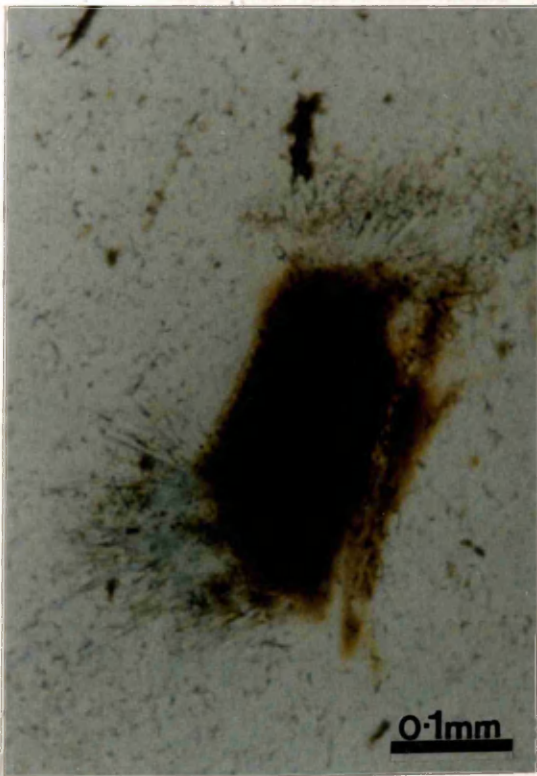
- Plate 5.20a Tourmaline formed at the end of biotite with acicular needles forming radially from the centre of growth.
(2.0m below unconformity).
- Plate 5.20b 'Sun' tourmaline formed at the end of biotite is now isolated from the remnant biotite crystal.
(2.0m below unconformity).
- Plate 5.20c Tourmaline formed at both ends of altering biotite.
(2.0m below unconformity)
- Plate 5.20d Needles of tourmaline grow around and at the expense of the remnant biotite flakes.
(2.0m below unconformity)



a



b



c



d

SYMBOLS USED IN PLATE

T	=	Tourmaline
Pi	=	Pinite
B	=	Biotite

PLATE 5.21

SEM images of 'sun' tourmaline and tourmaline associated with biotite.

Plate 5.21a Radiating acicular aggregate of 'sun' tourmaline.

(2.0m below unconformity)

Note: Smaller 'sun' intergrown ~100 μ m to right of centre.

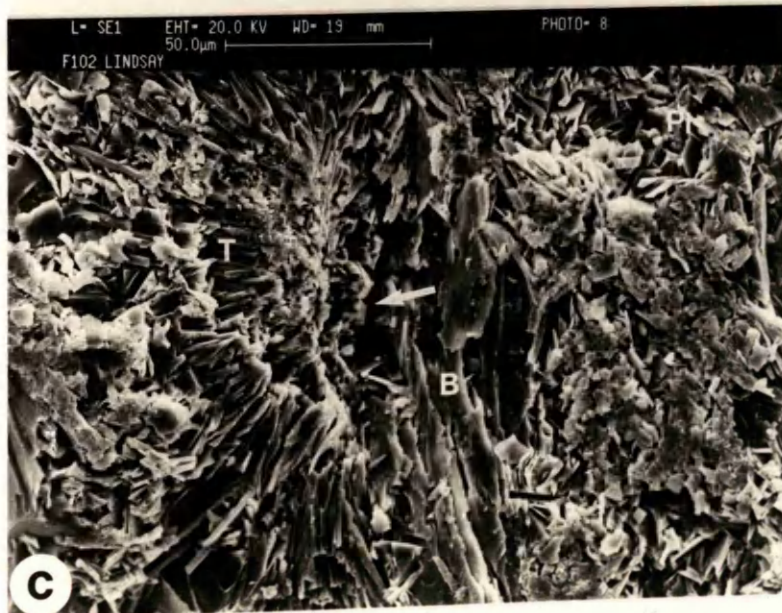
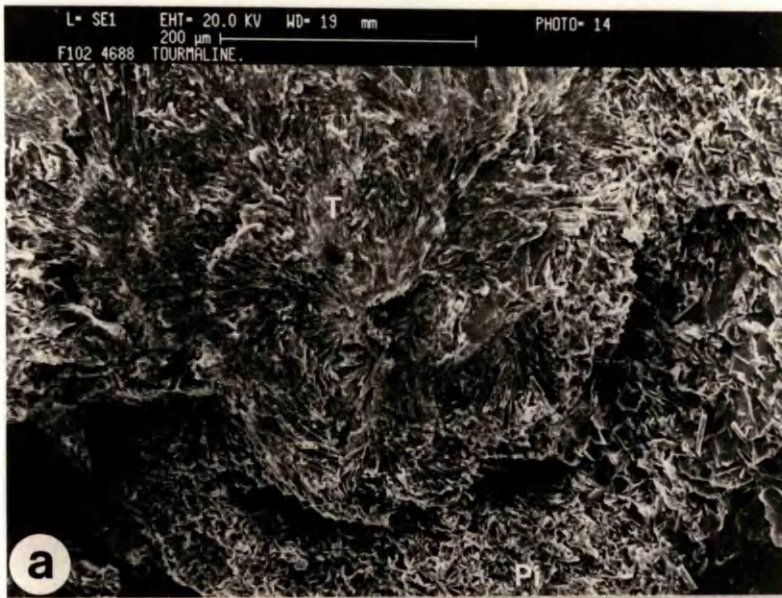
Plate 5.21b Close-up revealing spiral growth from centre - screwing anticlockwise into the page.

(2.0m below unconformity)

Plate 5.21c Tourmaline crystals radiating from altering biotite.

(2.0m below unconformity)

Blocky termini juxtapose with remnant biotite. Arrow points to trigonal pyramid form at terminus - typical of tourmaline.



Tourmaline composition

XRD analysis revealed the tourmalines in the rock at the top of the alteration profile to be schorls, and those of the veinlets, dravite.

Comparison of electron probe analyses of tourmaline (Appendix 8) with analyses given in Deer *et al.* (1986), confirmed that the 'sun' tourmaline and green tourmaline were closest to schorl in composition. However, the chemical composition of the vein tourmaline was between the schorl and dravite end member varieties. Low totals were found because the compounds ; B₂O₃, Li₂O and H₂O could not be measured on the electron probe. The values for average and maximum weight % of these oxides in schorls and dravites from Deer *et al.* (1986), are as follows:-

	<u>Schorl</u>		<u>Dravite</u>	
	<u>Mean</u>	<u>Max.</u>	<u>Mean</u>	<u>Max.</u>
B ₂ O ₃	9.96	11.00	10.13	10.80
H ₂ O ⁺	2.49	3.81	3.31	4.16
Li ₂ O	0.05	0.60	0.01	0.16
<u>TOTAL</u>	<u>12.50</u>	<u>15.41</u>	<u>13.45</u>	<u>15.12</u>

Hence, ~12.5 and 13.5 weight % on average and up to ~15.1 to 15.4 weight % maximum of the total composition in analyses of schorls and dravites respectively, would be undetected.

Blue 'sun' and green tourmaline

Relative to the schorl analyses given in Deer *et al.* (1986), these minerals are enriched in Al₂O₃ and SiO₂ and depleted in MnO, FeO_{tot}, CaO, Na₂O and TiO₂. Compared to the blue rosettes, the green schorls are all richer in Na₂O. The FeO_{tot} in the green tourmaline is at the high percentage end of the range of the blue rosettes and the Al₂O₃ content at the low end (Appendix 8).

Vein tourmaline

The composition of the vein tourmaline lies in the continuous series between the Mg end member, dravite ($\text{NaMg}_3 \text{Al}_6 \text{B}_3 \text{Si}_6 (\text{O},\text{OH})_{30} (\text{OH},\text{F})$) and the Fe, Mn end member schorl ($\text{Na} (\text{Fe}, \text{Mn})_3 \text{Al}_6 \text{B}_3 \text{Si}_6 (\text{O},\text{OH})_{30} (\text{OH},\text{F})$).

Displaying results

Problems arise in demonstrating the results of electron probe analyses of tourmalines due to

1. The limiting effects of uncertainty of B_2O_3 , H_2O , Li_2O contents.
2. Doubt over confidence in Al_2O_3 and SiO_2 contents:-

Ethier and Campbell (1977) found that specifically, their SiO_2 and Al_2O_3 contents were slightly higher than the published wet chemical analyses of Deer *et al.* (1972). The problem was also encountered by Fortier and Donnay (1975), who obtained higher values from probe analysis of particular tourmalines than Hamburger and Buerger (1948) from wet chemistry on the same minerals. That the SiO_2 and Al_2O_3 contents of the schorls from this study are higher than those of Deer *et al.* (1986) and yet similar to those of Ethier and Campbell, would either support this contention or indicate a possible error in the wet chemical analyses.

Due to the uncertainties, Ethier and Campbell used the weight % oxide ratios $\text{Na}_2\text{O}/(\text{Na}_2\text{O} + \text{CaO} + \text{K}_2\text{O})$ and $\text{FeO}/(\text{FeO} + \text{MgO} + \text{MnO})$ to evaluate differences in compositions of tourmalines. For the same reasons, these ratios were also adopted for evaluating the probe analyses of tourmalines of this project (Fig. 5.9, Appendix 8).

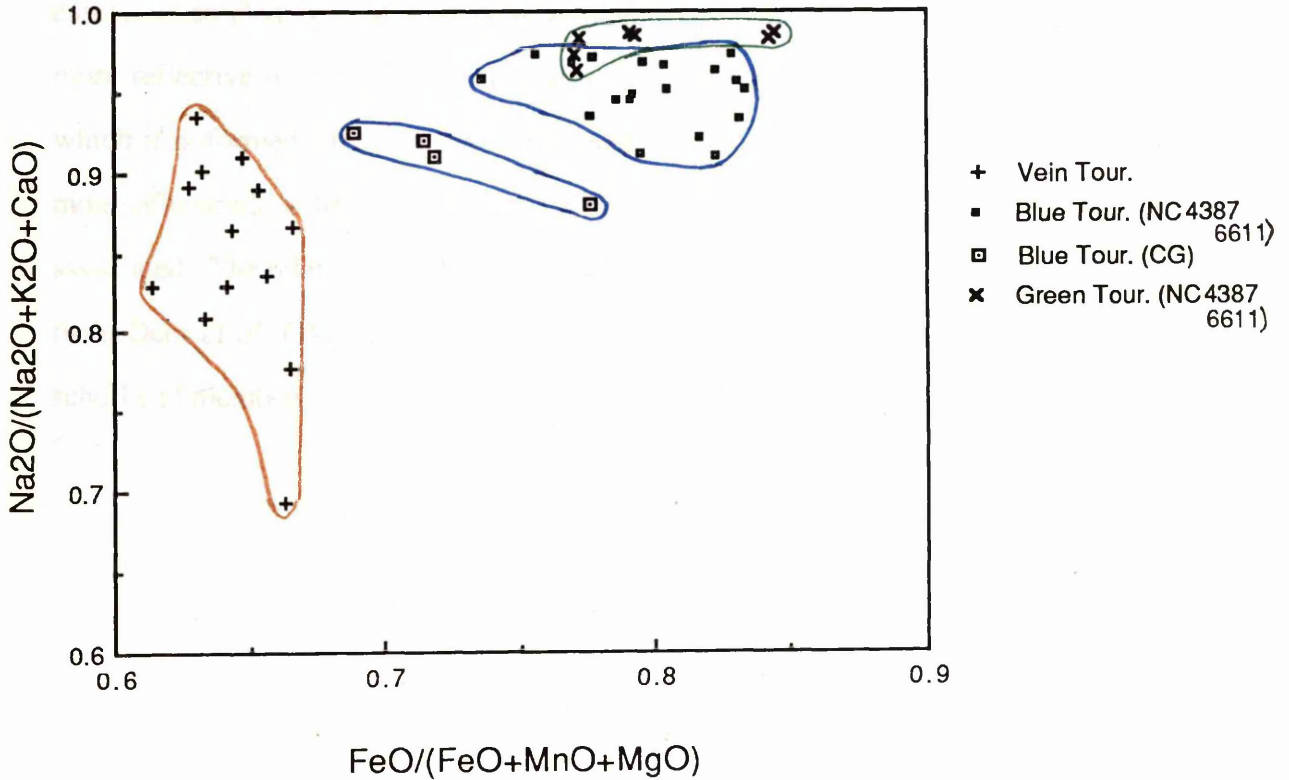


Fig. 5.9

Composition of tourmalines from the rock of the alteration profile and tourmaline/quartz veinlets.

Results and mineral interpretation

The field of results for vein tourmaline is clearly distinct from the tourmalines of the rock body. However, it is intriguing that the blue tourmalines from [NC 4387 6611] (Pod) are distinct from the blue tourmalines of suite CG and yet plot overlapping the field of green tourmalines. It would thus appear that the chemistry of the mineral is, in many cases, not so closely related to its appearance and texture as one might assume, but is more reflective of the chemistry of the rock or the fluids which affected that rock, in which it is formed. Indeed, the texture and morphology of tourmaline appears to be more influenced by the sites in which it is formed and the altering mineral with which it is associated. The relationships between these analyses and analyses of dravite and schorl from Deer *et al.* (1986), are given in Fig. 5.10, with all analyses plotting nearer the schorl end member.

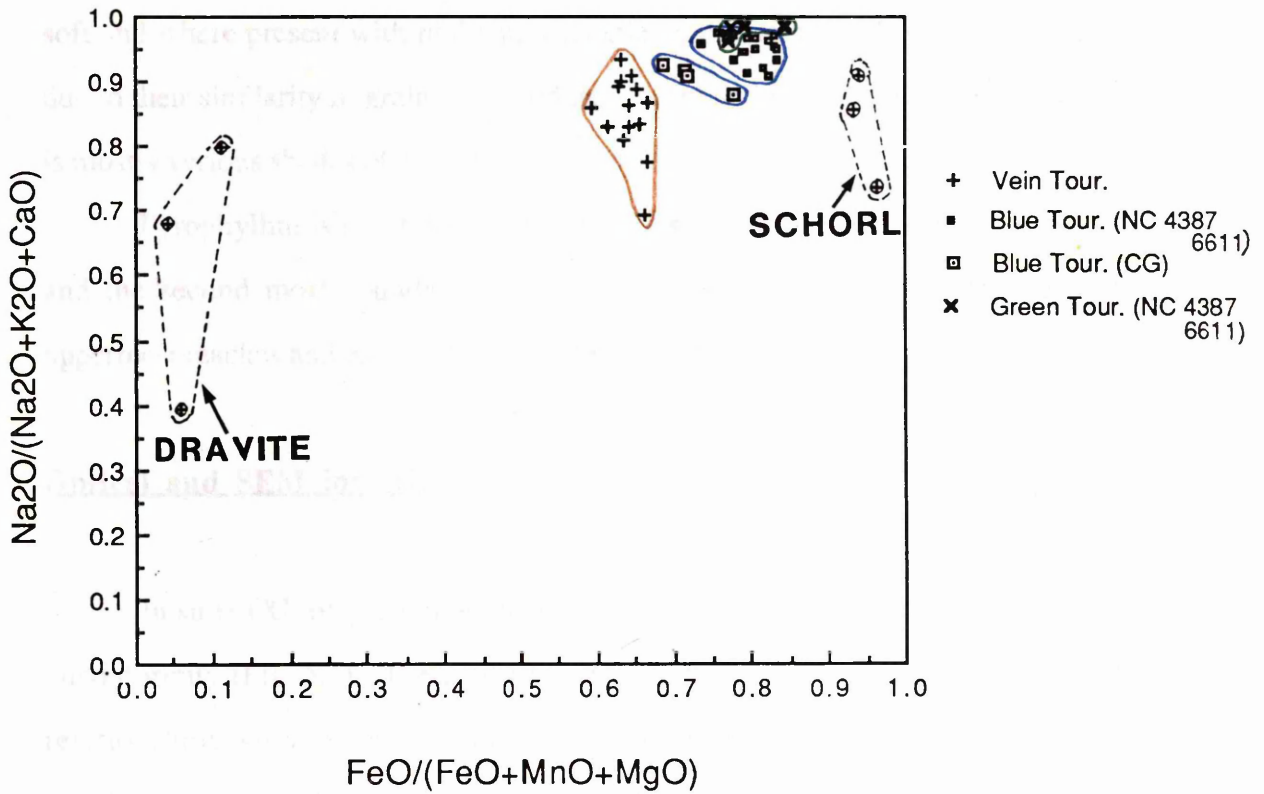


Fig. 5.10

Relationships between the analyses of tourmalines in the rock body and in the veinlet association, as compared with schorls and dravites of Deer *et al.* (1986).

Pyrophyllite

Pyrophyllite is predominantly pale yellow in hand specimen. It is cryptocrystalline and translucent to opaque, with a soapy feel and waxy lustre. It is very soft and where present with pinite in a sample, is frequently indistinguishable from it, due to their similarity in grain size, hardness, lustre and often colour. (Pinite, however, is mostly various shades of green).

Pyrophyllite is the third major or minor secondary mineral found in the profile and the second most abundant, after pinite. It does not appear until the profile's uppermost reaches and increases towards the unconformity.

Optical and SEM investigation

In suite CG, only a minor quantity of pyrophyllite is present, at 2.0m below the unconformity (Fig. 5.1). There, just the earliest stages of its development and textural relationships with other minerals are seen microscopically. More progressed development is visible in the more altered rocks at [NC 4387 6611], where pyrophyllite constitutes a major mineral and in the purple bands (see Plate 4.3), is the dominant phase.

Pyrophyllite has very similar properties to pinite in ppl and xpl and thus can be difficult to detect. However, it is most conspicuous under optical examination, when it forms at the expense of quartz (Plate 5.22). In this situation the pyrophyllite crystals are distinctly larger than the surrounding pinite.

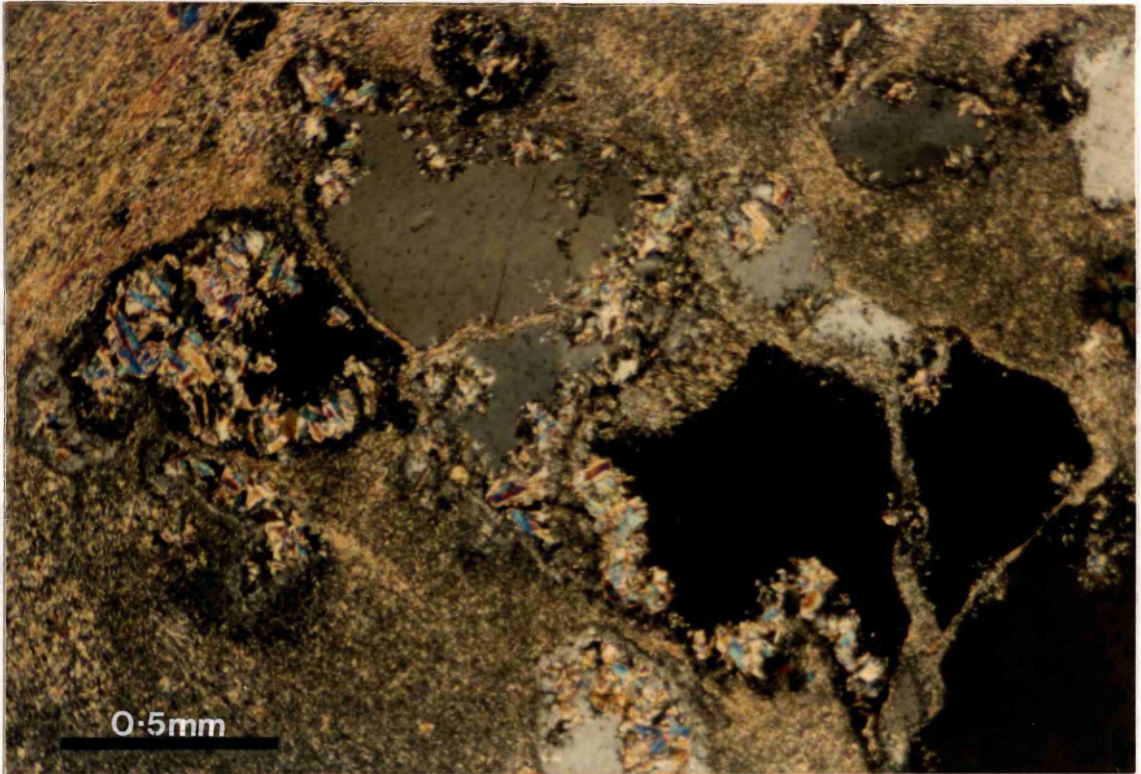
Quartz is the main mineral pyrophyllite is seen to consume. Pyrophyllite starts to develop at the edge of the quartz grain. Once this has been penetrated, pyrophyllite pervades inwards, consuming the core of the crystal (Plate 5.10). Pyrophyllite is seen to consume the centre of the grain in Plate 5.23a, whilst pinite only forms round the outside. Its deeply penetrative effects are seen in Plate 5.23b.

Pyrophyllite surrounded by pinite is shown in Plate 5.23c. The area of pyrophyllite in the centre, extending over $\sim 200\mu\text{m}$, delineates the limit of a precursor quartz crystal, largely replaced by pyrophyllite. As seen once again, pyrophyllite is generally coarser grained than pinite. The aspect ratio of the crystals is greater in pyrophyllite than pinite and the pyrophyllite crystals tend to develop with preferred orientation parallel to the basal plane (Plate 5.23d) (see also Plate 5.23b).

Pyrophyllite is also intimately associated with pinite in the degraded quartz cores and often several associated pinite laths are visible (Plates 5.23e). These pinite crystals, however, are generally larger in this association than when they form outwith this setting.

Remnant biotite flakes are other sites at which pyrophyllite develops. It forms between the cleavages at the expense of the altering biotite. There, the 001 pyrophyllite face is seen to develop perpendicular to the 001 face of the remnant biotite flake (Plates 5.7e & f). This association was only found with the aid of the SEM.

Although pyrophyllite generally only occurs as a minor phase in the profile, sufficient evidence is available to conclude that, were higher reaches of the alteration horizon preserved, it would have become a major mineral and, especially in a quartz/biotite rich precursor, a dominant phase.

**Plate 5.22**

Pyrophyllite is most readily distinguished from the pinite groundmass when it consumes precursor quartz crystals. Pyrophyllite crystals are distinctly larger than the surrounding pinite. (<1.0m below unconformity).

SYMBOLS USED IN PLATES.

Py = Pyrophyllite.

Pi = Pinite

Q/Qtz = Quartz.

PLATE 5.23

Pyrophyllite textures.

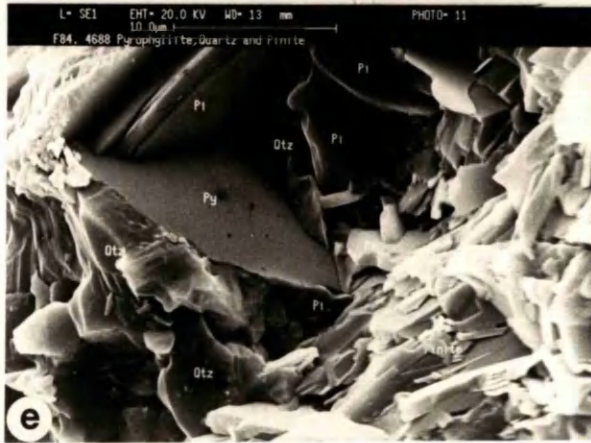
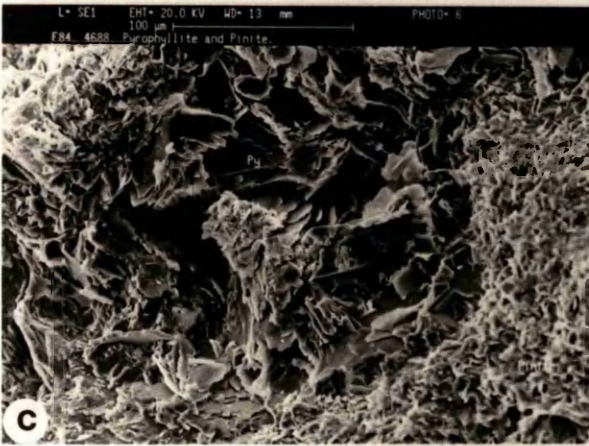
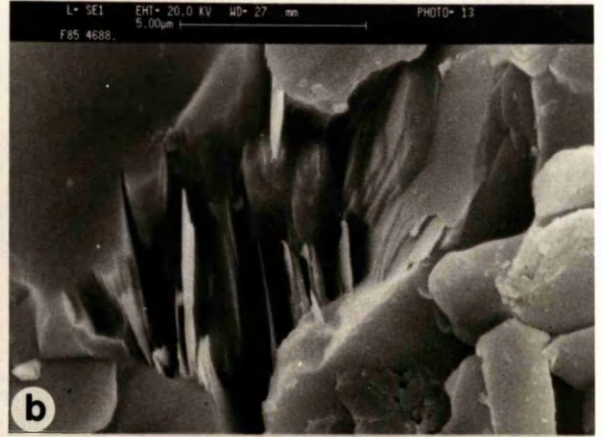
Plate 5.23a Pyrophyllite at early stages in consumption of quartz. Pyrophyllite flakes form parallel to each other and penetrate deeply into the quartz crystal. (Contrast with zig-zag development of pinite around the edge. (2.0m below unconformity).

Plate 5.23b Serrated embayment in quartz crystal, with parallel aligned pyrophyllite flakes developed at its expense. (Close-up of 5.23a). Note the very sharp boundary between the quartz and pyrophyllite. (2.0m below unconformity).

Plate 5.23c Pyrophyllite has consumed quartz crystal to a much greater extent than in Plate 5.23a. The pyrophyllite crystals are larger than the surrounding pinite laths. (2.0m below unconformity).

Plate 5.23d Pyrophyllite flakes form in a parallel fashion. (Close-up of central area, Plate 5.23c). (2.0m below unconformity).

Plate 5.23e Pyrophyllite, pinite and remnant quartz together in a degraded quartz crystal. (Close-up of right side of degraded quartz crystal, Plate 5.23c). (2.0m below unconformity).



Mineral chemistry

Backscatter imaging verified that the mineral within the corroded quartz crystal was different from the pinite. Comparison of quantitative electron probe analyses of this mineral which replaces quartz (Appendix 9), with pyrophyllite analyses of Deer *et al.* (1962), firmly established the mineral as pyrophyllite. The analyses plot consistently around the position of pyrophyllite on the graph of Garrels (1984) (Fig. 5.11).

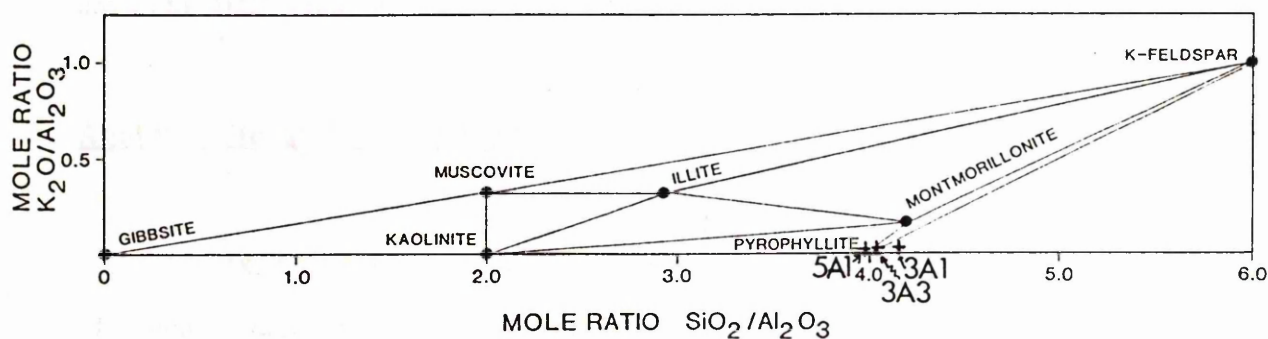


Fig. 5.11

Mole ratio plot of the major phases that occur with mixed-layer montmorillonite/illite minerals (considered as discrete phases) in the system K₂O-Al₂O₃-SiO₂-H₂O (Garrels 1984).

Analyses 3Al, 3A3 and 5Al (Appendix 9) plot around the position of pyrophyllite.

Opagues

Introduction

Opagues are found in accessory proportions throughout the profile. In the field, they are most noticeable in zones of pronounced haematite staining. They are also found within the rest of the rock body, including suite CG.

Suite CG - Rutile

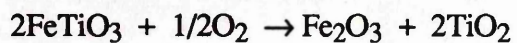
Secondary crystals of rutile are found towards the top of the alteration profile. They are generally invisible in hand specimen. The rutile crystals form in association with altering biotite and are clustered in sites previously occupied by biotite crystals. Hence, they are often found close to tourmaline 'suns' (Plate 5.8d). These rutile crystals are up to ~0.02mm long.

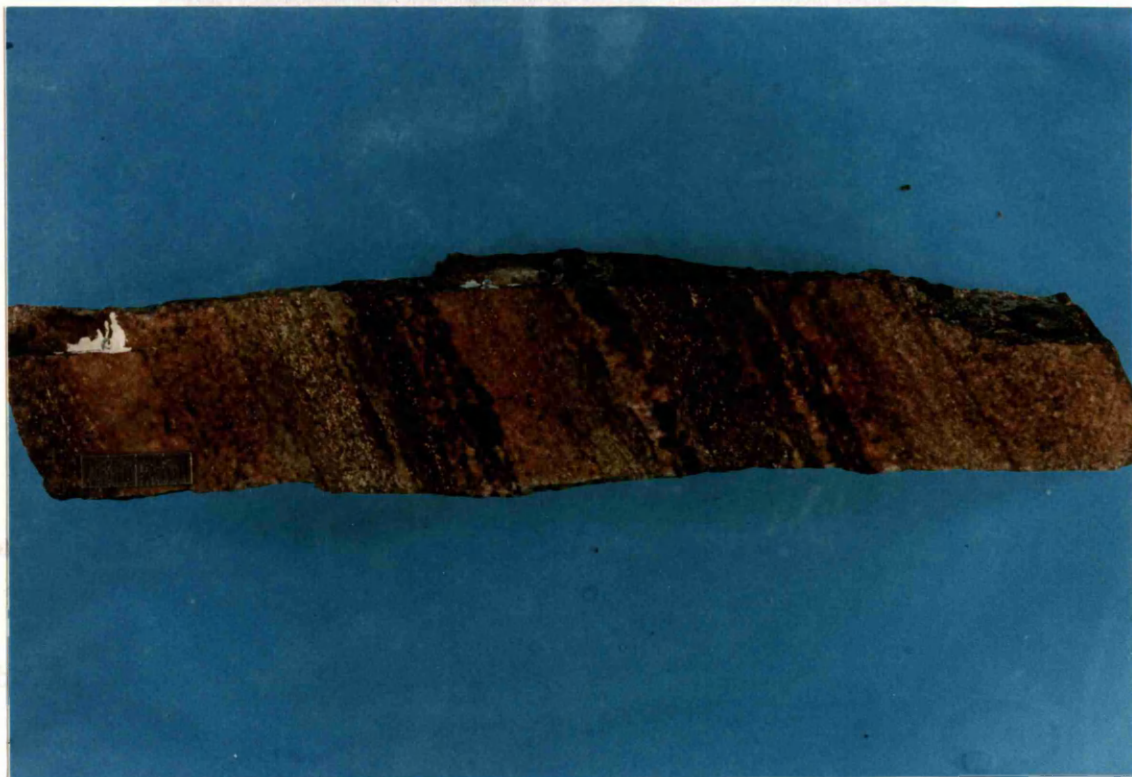
Agalmatolite at [NC 4361 6240]

An example of altered gneiss is shown in Plate 5.24. SEM backscatter imaging of typical opagues from this sample are given in Plate 5.25a, with rutile on the left and haematite in the centre. It appears as if much of the grain in the centre has been altered, with ghost lamellae and remnant haematite visible. High magnification of the haematite in the lower central area reveals a mid-grey rim to these grains (Plate 5.25b, e.g. arrow). Colour backscatter imaging shows more clearly the varying mineral compositions throughout this area (Plate 5.26). Qualitative EDS analyses (Plate 5.25c) reveals the mid-grey rim and dustings to be rich in titanium with also some iron.

Ilmenite commonly forms as exsolution intergrowths with haematite due to the solid solution between these minerals (Ramdhor 1969). This grain was most likely a haematite/ilmenite intergrowth when fresh - although it may have been of

ilmenite/magnetite, with the magnetite now oxidised to haematite. (The latter is less likely as magnetite usually only forms <10% in such intergrowths and 'magneto-ilmenites' are much rarer, (Ramdhor 1969). Whatever, when such complex grains are oxidised, the haematite remains (or develops after magnetite) while the ilmenite alters to rutile, with iron released forming haematite, i.e.



**Plate 5.24**

Altered gneiss from the profile. Gneissose banding is very prominent, but unlike fresh gneiss, this altered sample is much more purple and green with distinctive white flecks. (Sample 2889, [NC 4361 6240]) - scale bar 2cm.

901

SYMBOLS USED IN PLATE.

R = Rutile.

H = Haematite.

PLATE 5.25

Opagues from the alteration profile at [NC 4361 6240].

Plate 5.25a Opagues in sample 2839 (Plate 5.24a).

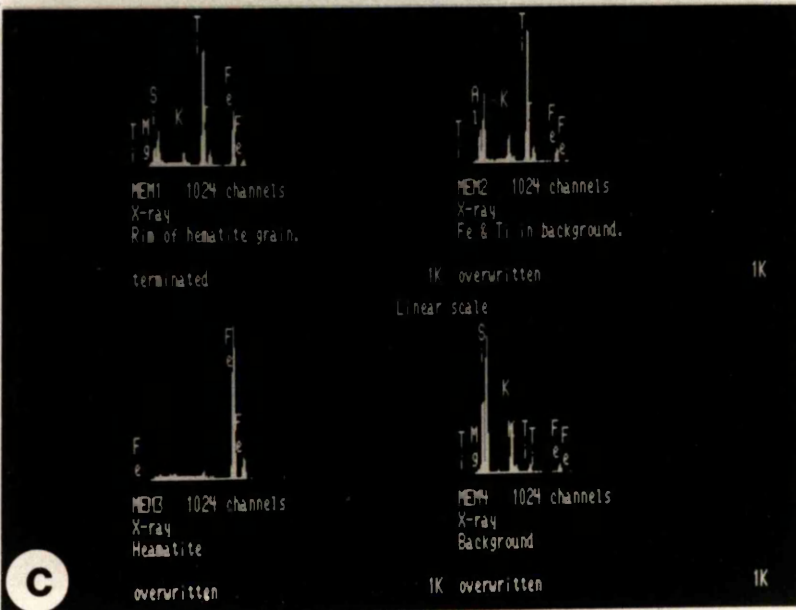
Rutile - on left and predominantly haematite in centre.

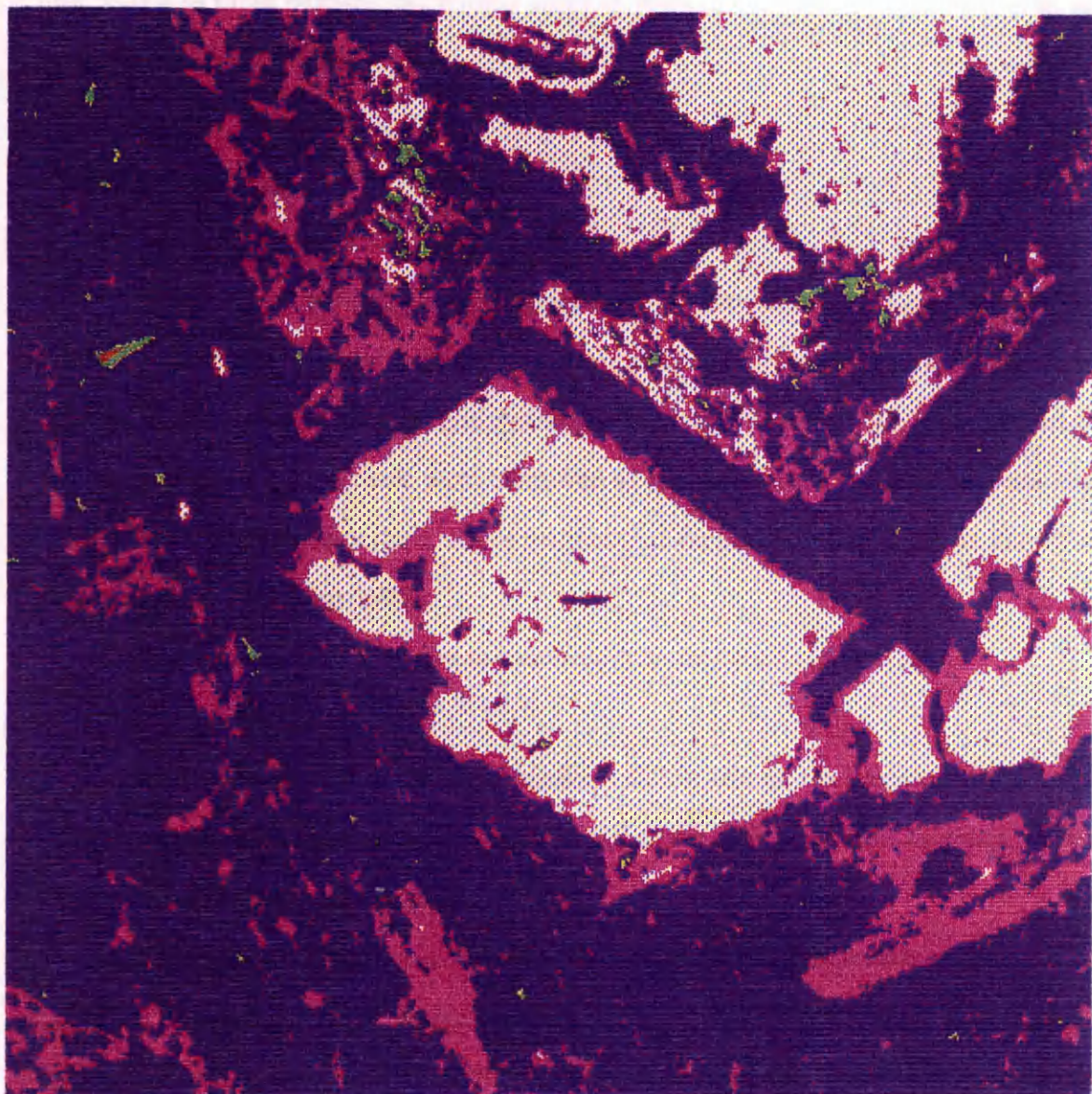
Plate 5.25b Close-up of bottom of plate 5.26a.

Note the mid-grey rim around the edge of the haematite (arrow).

Plate 5.25c Graphs of qualitative EDS analysis from points related to Plate 5.26.

- 1) Pink rim of large white grain.
- 2) Pink groundmass minerals.
- 3) Large white grain.
- 4) Purple groundmass.



**Plate 5.26**

Colour backscatter image of lower central section of Plate 5.25a.
EDS analysis (Plate 5.25c) reveals the pink minerals to be rich in Ti and Fe.
(Note - green = holes in slide).

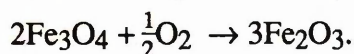
Zones of deep red staining

Patches of steely-grey opaque minerals up to several cm long are found clustered in and around zones where the rock is deep red from haematite staining (Plate 5.27a & b). Close to these patches, occasional areas of pronounced creamy-white material are also present (Plate 5.27b).

Steely grey minerals

Under reflected light, the metallic areas are predominantly light grey and brightly reflective, but also contain regular, parallel aligned parallelogram to triangular shape inclusions of a darker grey (slightly pinkish) mineral (Plate 5.27c). With the aid of electron probe analyses, these were identified as haematite and magnetite respectively. The process giving this texture, where magnetite is replaced by haematite, is known as 'martitisation' (Ramdhor 1969).

The alteration of magnetite to haematite is an oxidation process, i.e.



However, there is so much haematite staining around the opaques in this zone, that haematite also appears to have been added to the system as well as being present solely due to oxidation of magnetite.

Martitisation may occur during incipient weathering (Ramdhor 1969). Thin platelets of haematite are typically formed along the octahedral planes of the magnetite (Ramdhor 1969 after Gruner 1929) with most roughly the same thickness in all directions. However, often one direction is favoured, especially when martitisation occurs at high temperature. Such is not obvious in these samples.

White material

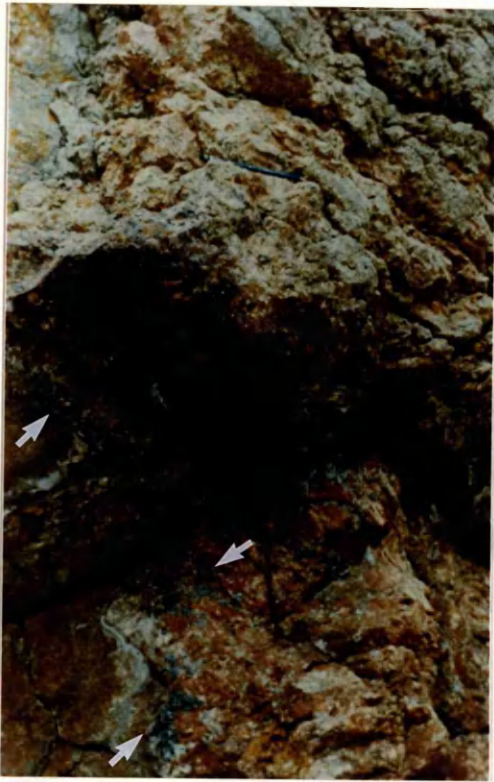
Reflected light examination coupled with electron probe analysis, reveals the white material to be a very fine-grained meshwork of brightly reflective rutile laths (Plate 5.27d), pinite groundmass and peculiar small amorphous masses. Such may be called a 'rutile nest' and may have originated from an ilmenite grain, which was first altered to an aggregate of anatase (Ramdhor 1969).

Anatase (TiO_2) is very common in epimetamorphic and weathered rocks, being able to form at very low temperature and pressure (although conditions favouring the formation of anatase over rutile are unknown) (Ramdhor 1969). As in the alteration of ilmenite to rutile (p.108), ilmenite to anatase is also an oxidation process.

PLATE 5.27

Opagues from haematite-rich zone.

- Plate 5.27a Band of opaques (arrows) in a haematite rich zone at [NC 4385 6614] (cave) (~12-14m below unconformity).
(Note the red feldspars in the purple groundmass in the centre of the picture).
- Plate 5.27b Slice of a sample taken from this zone, containing steely grey and white patches.
(Polished thin section made of delineated area - sample 2489a)
- Plate 5.27c Martite from haematite-rich zone (metallic area in 2489a).
Haematite replaces magnetite along octahedral planes.
- Plate 5.27d Laths of rutile in a 'rutile nest' (white area in 2489a).
Rutile may have originated from an ilmenite grain, first altered to an anatase aggregate.



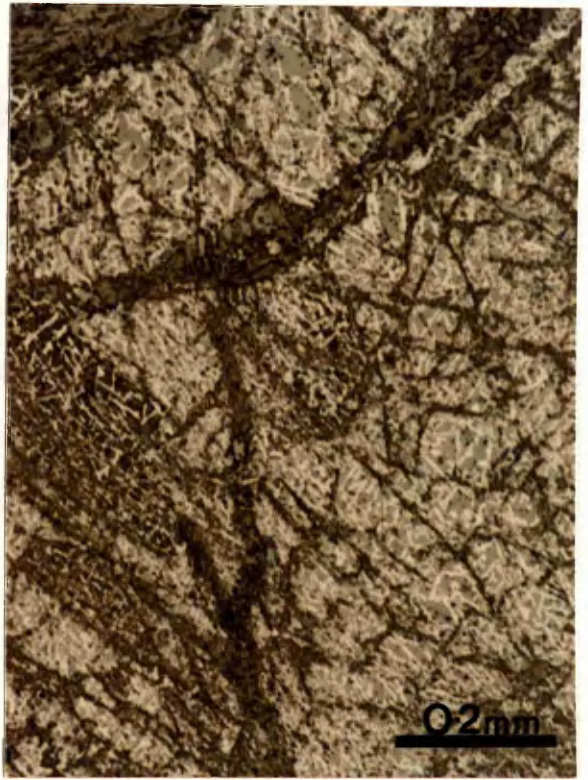
a



b



c



d

CHAPTER 6**GEOCHEMISTRY****INTRODUCTION**

Major and trace element compositions of rocks throughout the profile were determined, with the primary aim of discerning gains and losses of elements due to alteration. Samples were collected at known depths beneath the unconformity, and wherever possible, from the same gneissic layer or pegmatite vein. Six suites from various places along strike of the unconformity were examined. The major element oxides determined were; SiO_2 , TiO_2 , Al_2O_3 , Fe_2O_3 , FeO , MnO , MgO , CaO , Na_2O , K_2O , P_2O_5 , H_2O and CO_2 , with results expressed in weight %. The trace elements determined were; Ba, Ce, Co, Cr, Cu, Ga, La, Ni, Pb, Rb, Sr, Th, U, Y, Zn and Zr, and these results are expressed as ppm. The analytical methods and accuracy of results are outlined in Appendix 10.

RESULTS

The major and trace element compositions of samples at various depths below the unconformity in different suites are given in Appendix 11. Variation diagrams showing the chemical trends in the gneiss, pegmatite and amphibolite suites from the cave at [NC 4385 6614] are given in Fig. 6.1 and from other locations in Appendix 12. The main changes in the abundance of major elements towards the unconformity are summarised below in Table 6.1.

SUITE	INCREASE		DECREASE	
	DISTINCT	SLIGHT	DISTINCT	SLIGHT
Gneiss	Al ₂ O ₃	H ₂ O	CaO Na ₂ O	MgO MnO FeO
Pegmatite	Al ₂ O ₃	H ₂ O CO ₂	CaO Na ₂ O	
Amphibolite	Al ₂ O ₃ K ₂ O	Fe ₂ O ₃ H ₂ O	CaO Na ₂ O	MgO FeO CO ₂

Table 6.1

General variations in weight % of major element oxides with increasing alteration at [NC 4385 6614].

The most consistent and distinctive changes are the increase in Al₂O₃ and H₂O and decrease in CaO and Na₂O with progressive alteration. After this, there appears to be a decrease in MgO and possibly MnO and FeO with alteration in each case. However, the findings from the gneiss suite ought to be taken with most confidence as there should be least primary variation in the gneiss suite due to the fine grain size of the constituent minerals. It should also be most representative of what happens throughout the whole area affected since gneisses represent >80% of the Lewisian rocks (Sutton and Watson 1951).

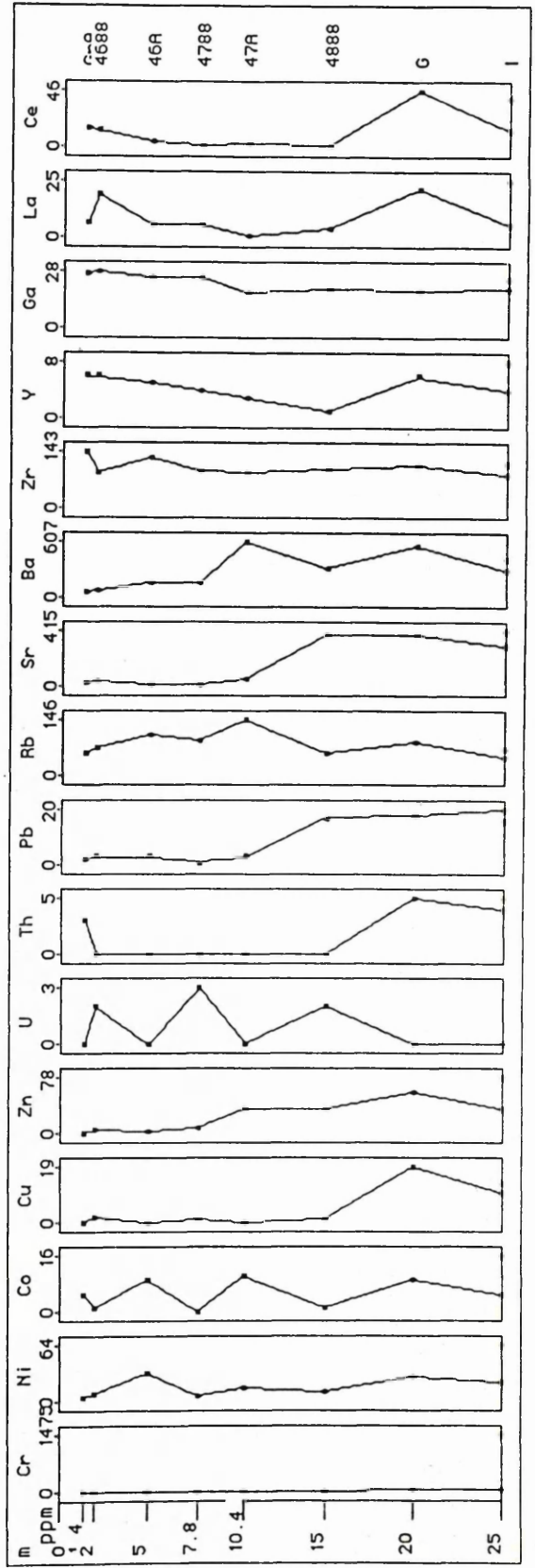
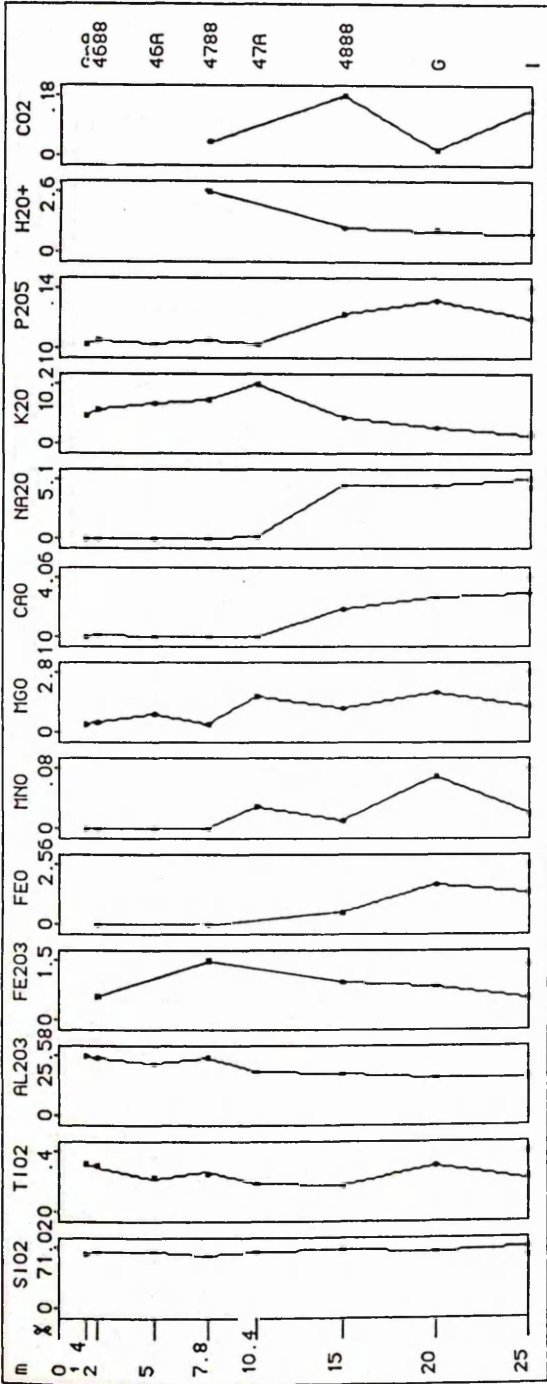
SITE		DEPTH (m)	
NC 4385 6614	≤15m	110	100
NC 4390 6609	~20-25m	110	100
NC 4390 6609	~20-25m	110	100
NC 4390 6609	~20-25m	110	100
NC 4390 6609	~20-25m	110	100

Fig. 6.1 a.b & c.

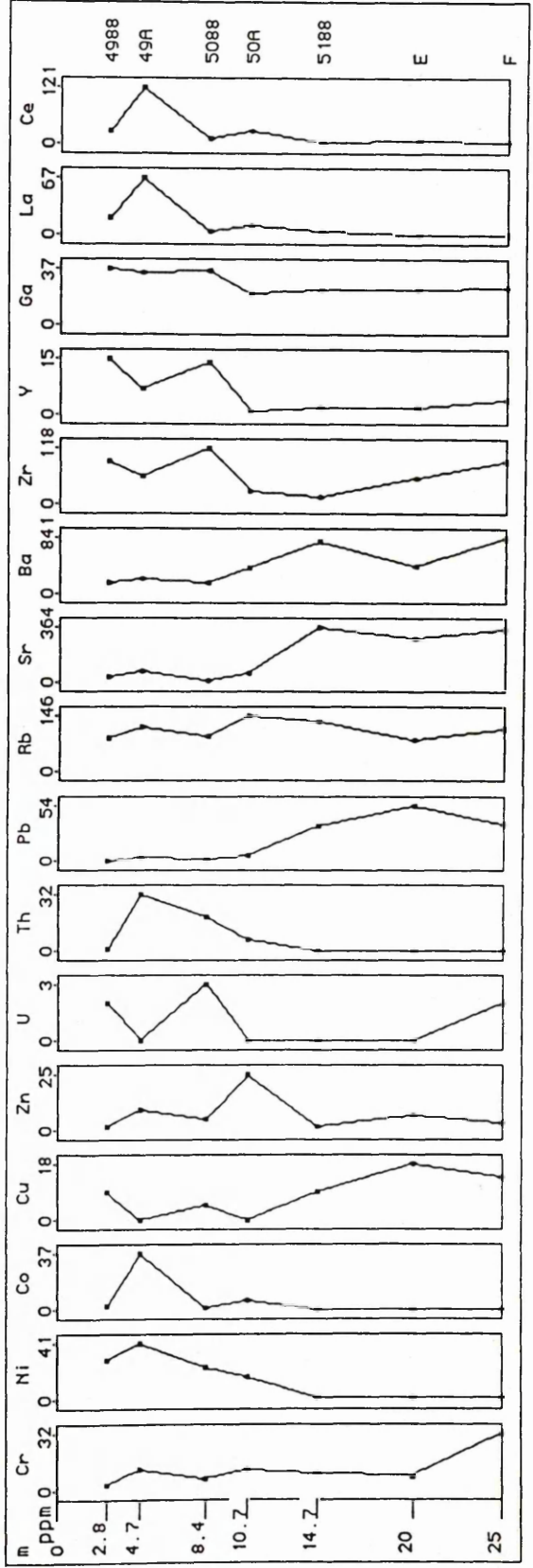
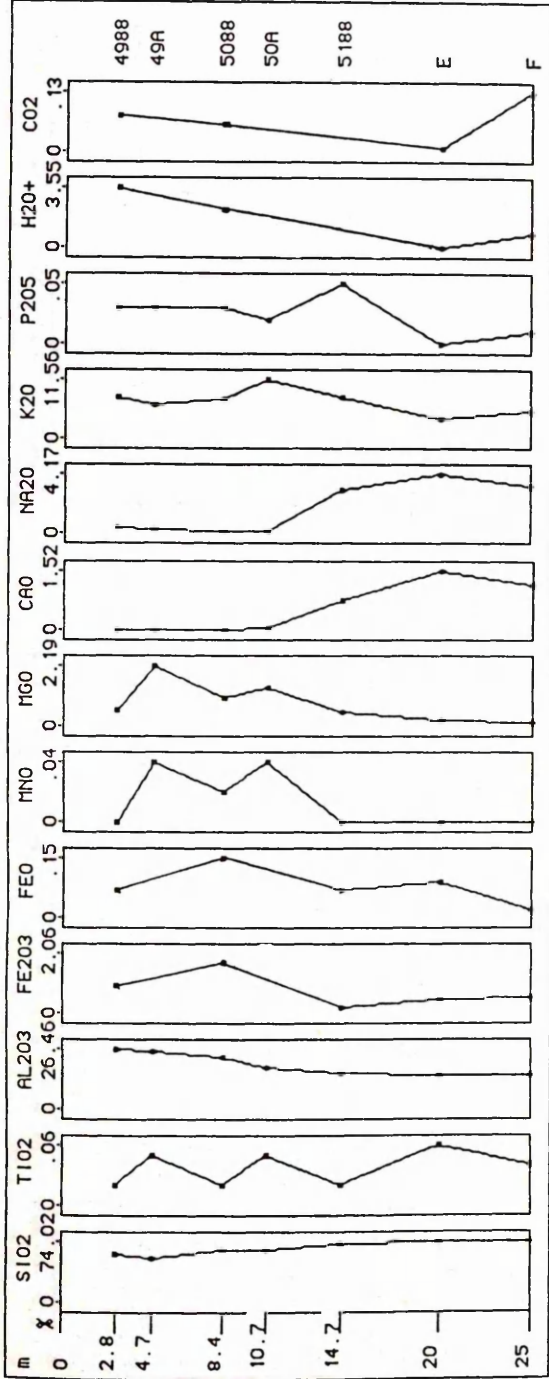
Variation diagrams for major element oxides and trace elements with depth below unconformity at the cave; at [NC 4385 6614] (≤15m) and [NC 4390 6609] (~20-25m).

Note. Samples ~≥20m below unconformity do not belong to the same layer or vein as the others and hence there may be a variation introduced at ≥20m due to comparison with a different protolith.

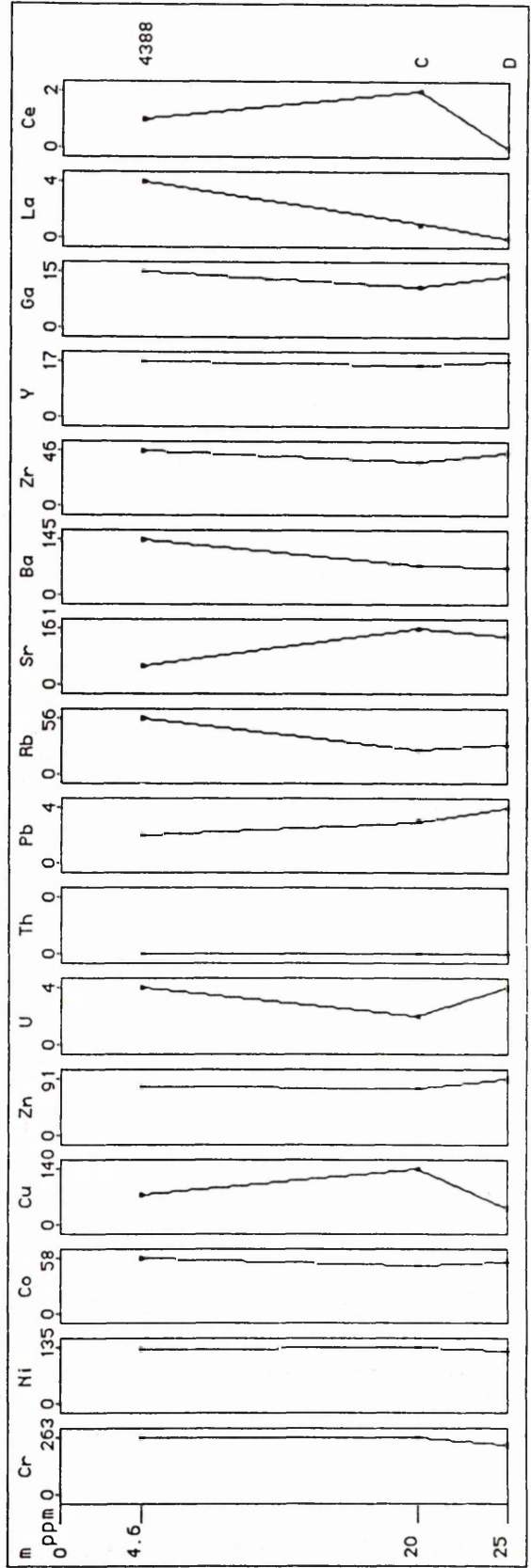
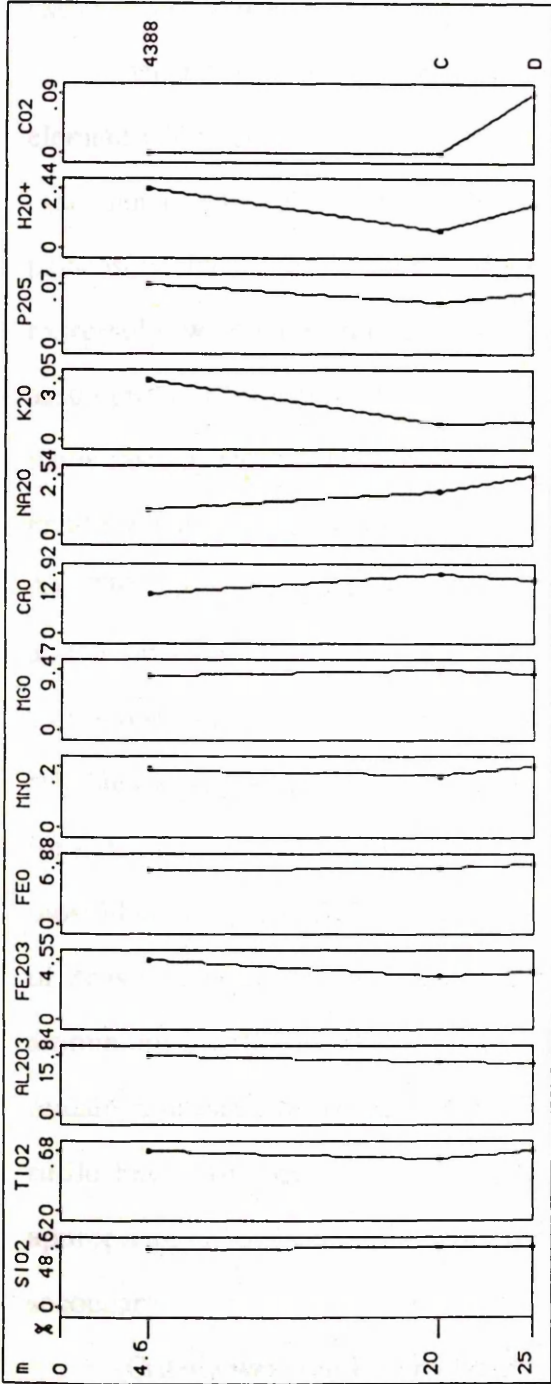
a) GNEISS (NC 4385 6614)



b) PEGMATITE (NC 4385 6614)



c) AMPHIBOLITE (NC 4385 6614)



INDEXING WEATHERING

The changes in chemistry undergone by rocks due to weathering have been used by a number of researchers to define an index which records the degree of weathering. Weathering indices have been devised mainly to compare the degree of weathering of rocks in and between weathering profiles. (Nesbitt and Young 1982, however, have also used a chemical weathering index to infer palaeoclimates and plate motions!)

Most chemical weathering indices assume that aluminium is immobile. It is the element which generally shows the most consistent increase in absolute concentration (and hence least relative decrease) with progressive weathering, in most soils and palaeosols. Indeed, aluminium oxides and hydroxides form the dominant phases in most extremely weathered rocks. However, some researchers do not advocate this assumption. Chittleborough (1991) argues against assuming aluminium immobility in many cases as movement of aluminium between the A and B horizons leads to inaccurate results when using the assumption (even to the point of B appearing more altered than A). This should not present a problem with indexing this profile as these uppermost A and B horizons have been removed by erosion. The index that was proposed by Chittleborough (1991) is based on zircon as a resistant mineral and uses ZrO_2 as a reliable measure of zircon (with >95% Zr in zircon). But this could not form the basis for indexing this profile as the total Zr content is so small that primary variations would most likely over-ride the variations detected for weathering (and, indeed, the behaviour of Zr is inconsistent with progressive alteration). Other indices which do not assume aluminium immobility also use particular minerals on the assumption that they have remained resistant to weathering and immobile - e.g. quartz, tourmaline (primary) and rutile have also been used (see Chittleborough 1991). None of these would be appropriate either in this profile as quartz is consumed and tourmaline and rutile are secondary.

Criteria were outlined by Harnois (1988) for an index to be applied to a particular profile, i.e. the index should:-

- (1) include only elements with consistent geochemical behaviour during weathering.
- (2) be independent of the degree of oxidation of the weathered material.
- (3) be simple and easy to use.
- (4) involve elements commonly reported from soil analyses.

One index which satisfies these criteria is the Chemical Index of Alteration of Nesbitt and Young (1982). This index was used in this investigation.

Chemical Index of Alteration

The Chemical Index of Alteration (CIA) was devised on the basis that the dominant process during chemical weathering of the crust is the degradation of feldspars to clay minerals. The consequent removal of calcium, sodium and potassium, which generally accompanies weathering, results in an increase in the proportion of alumina to alkalis in the resultant soil. Thus Nesbitt and Young (1982) propose the index:-

$$\text{CIA} = [\text{Al}_2\text{O}_3 / (\text{Al}_2\text{O}_3 + \text{CaO}^* + \text{Na}_2\text{O} + \text{K}_2\text{O})] \times 100$$

where CaO* is the amount of CaO in the silicate fraction of the rock. Concentrations of element oxides are in molecular proportions. With progressive weathering, the value of CIA increases.

Results

With increasing proximity to the unconformity, the value of CIA in the altered profiles increases (Fig. 6.2 and Appendix 13). In the cave suites the freshest samples of gneiss and pegmatite (below 15m b.u., Fig. 6.2a(1) and (2)) have values between 50 and 60, with values increasing to around 75 in the pegmatite suite and over 80 in the gneiss suite. Similar values are seen in the gneiss suite at [NC 434 662] (Fig. 6.2b(1)). The same trend is found in the amphibolite suite, although CIA values are lower (Fig. 6.2a(3)). The trend is less consistent in the altered pegmatites at the Telegraph Hut [NC

4435 6394]. This can be related to the coarse-grained nature of pegmatites and thus the variations in proportions of minerals between hand samples. Also, the restricted depth range from which samples were taken in this suite would exacerbate any sampling variations. In the pegmatites and gneisses from Cranstackie, Fig. 6.2b(3), there is no trend with increasing proximity to the unconformity.

Interpretation

Nesbitt and Young report values between 45 and 55 for fresh granites and granodiorites. The CIA values of the freshest gneisses and pegmatites from the gneiss and pegmatite suites in Figs. a(1) and a(2) are compatible with this, considering that they are only slightly altered. Lower values from the amphibolites are to be expected. CIA values around 75 of the pinitic-rich samples between 10m and 2.0m b.u. in the gneiss and pegmatite suites (Figs. a(1), a(2), b(1)) are also consistent with the idealised muscovite value of 75 (Nesbitt and Young 1982). The higher values above 2.0m b.u. in the gneiss suite (Fig. 6.2a(1)) are interpreted as due to the presence of pyrophyllite, as the introduction of an aluminosilicate phase would increase the proportion of alumina to alkalis in the whole rock.

In the Cranstackie suite (Fig. 6.2b(3)), the scatter of values around the restricted CIA of ~53 to 58 for all samples (pegmatites and gneisses) from 0.35m to 460m b.u. substantiates the field and microscopic observations that the rocks below the unconformity at Cranstackie are unaltered.

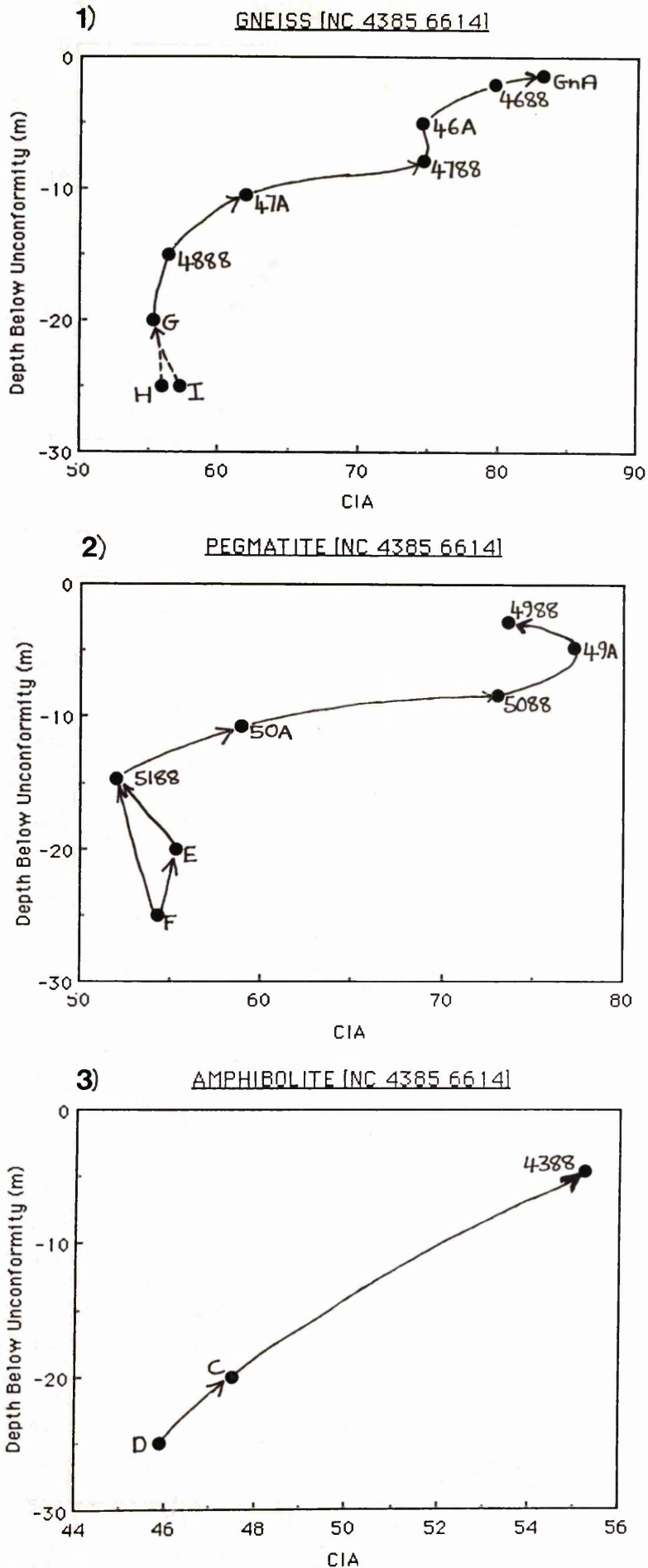


Fig. 6.2a

Variation in Chemical Index of Alteration (CIA) with depth in the profile on gneiss, pegmatite and amphibolite suites from the cave [NC 4385 6614].

NOTE: Scales on both axes vary from one diagram to another.

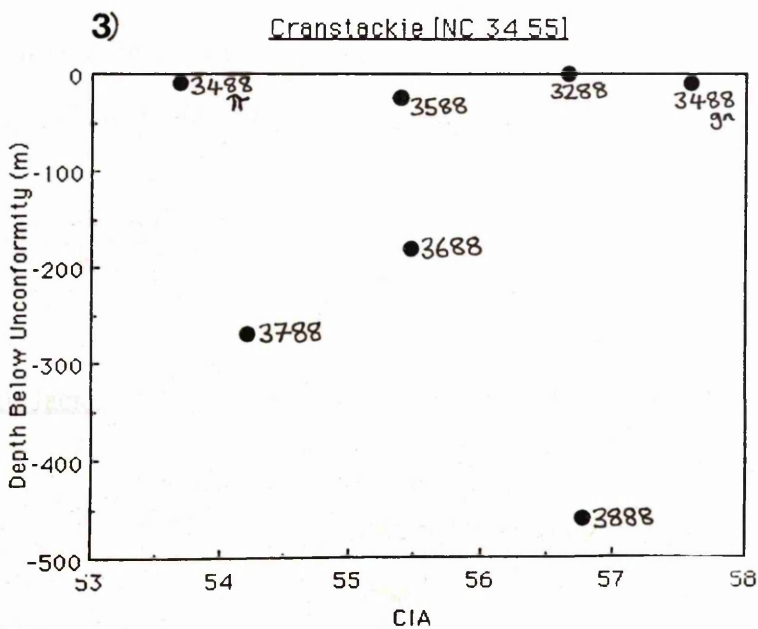
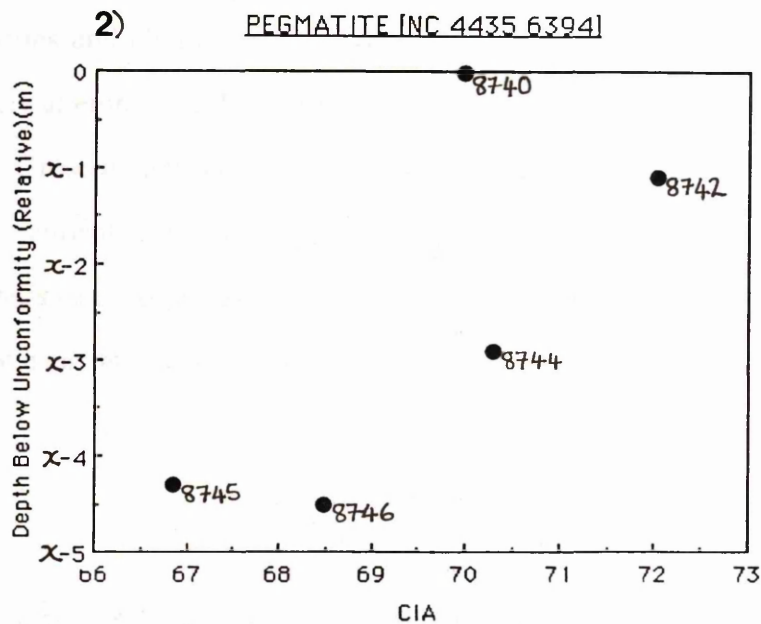
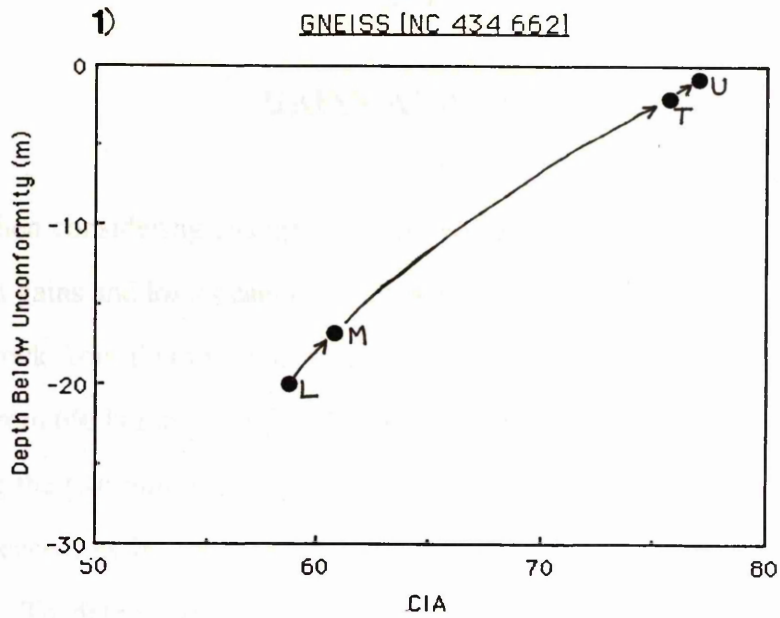


Fig. 6.2b

Chemical Index of Alteration (CIA) against depth for suites from other locations.

NOTE: Depths from samples in Fig. b(2) are relative with x between 5m and 8m. (See Appendix 2a(1)).

GAINS AND LOSSES

When considering changes in any element or oxide with alteration, an accurate estimate of gains and losses cannot be made by merely subtracting the weight % oxide in the fresh rock from that in the altered rock. For example, if the K_2O content of a rock changed from 6% before alteration to 8% afterwards, it cannot be ascertained simply by comparing the two numbers, whether K_2O has in fact, a) increased, b) had no change, or c) decreased, as its concentration is influenced by changes in the other oxides or elements. To determine the gains and losses between rocks, both the changes in concentrations and changes in volume require to be known. Two applications of a method were attempted in this project to investigate the gains and losses with alteration. These are Gresens' analysis (after Gresens 1967) and Grant's (1986) more recent graphical treatment of Gresens' equations. Gresens' method has been used by a number of researchers (e.g. Appleyard and Woolley 1979, Kresten 1988, Dipple *et al.* 1990) in the study of element mobility.

1. Gresens' analysis

Gresens (1967) devised a general set of equations which allows the calculation of gains and losses in terms of chemical analyses and specific gravities between metasomatic and unaltered rocks. The equations may be generalised as:-

$$100 \left[f_v \left(\frac{g_B}{g_A} \right) C_n^B - C_n^A \right] = x_n$$

where

$f_v =$ Volume factor

i.e. the amount by which the volume of solids on the left side of the equation is multiplied in order to obtain the volume of solids on the right side

-when

$f_v = 1$ replacement is volume for volume.

$f_v > 1$ replacement with volume gain.

$f_v < 1$ replacement with volume loss.

g_A and g_B = Specific Gravity of rocks A and B - rock A = parent rock.

rock B = altered rock.

C_n = Weight fraction of component n.

X_n = Loss/gain of component n during alteration.

Results expressed as grams per 100g of rock.

The unknowns in this equation are f_v and X_n .

In order to solve this equation, an assumption must be made; either a volume factor is chosen, e.g. $f_v = 1$ if a volume-for-volume replacement is suspected on textural grounds, or the assumption of a gain, loss or no change in one or more of the components must be made. Since at this stage it is not wished to assume immobility of any element, an estimate of f_v therefore has to be made. This is done using composition - volume diagrams.

Composition - volume diagrams

Composition-volume diagrams show the volume factor (f_v) (along the abscissa) vs the gains and losses (ordinate) (e.g. Figs. 6.3a and b). To construct a composition-volume diagram a series of f_v values is initially assumed. These are substituted into the above equation for each element oxide in turn, to give the data points and hence the line for each oxide. Where the lines for several components cross the gain-loss zero line together, this value is regarded as the most likely volume factor for the alteration reaction.

Application and Results

Composition-volume diagrams for gneiss and pegmatite samples from the cave suites [NC 438 661] are shown in Figs. 6.3a and b. These diagrams illustrate the changes in weight % of major element oxides for different volume factors. The approximately horizontal, sub-zero lines for CaO and Na₂O, for example, indicate that no matter what the volume change was (realistically), CaO and Na₂O have been lost from the system.

The changes found between the 'freshest' gneisses (G and H at ~20 to 25m below unconformity) and the most altered considered (4688 ~2.0m below unconformity) are, as expected, very similar (compare Fig. 6.3 a(1) and 6.3a(2)). The changes between 4888 (~15m below unconformity) and 4688 (Fig. 6.3a(3)) are also similar, although some are less pronounced (e.g. at $f_v = 1$, the increase in K₂O is only 1 to 2% between 4888 and 4688 whereas it is 3.5 to 4.5% between G and H and 4688). The graph of changes between 4888 and 4788 (~7.8m below unconformity) (Fig. 6.3a(4)) also has a similar shape as there is a significant change in degree of alteration between 4888 and 4788 (cf. plate 5.1). In any of these graphs, there is no one point at which a number of lines crosses the gain-loss zero line. However, weathering typically involves volume loss, so it is most likely that the volume factor is <1 although its value is unknown. In each of the graphs a(1) → (4), at all values of f_v , where $0.6 \leq f_v \leq 1$, CaO, Na₂O and SiO₂ have been lost from the system and at most values, Al₂O₃ and K₂O have been added. However, if aluminium is considered immobile, in most cases all other elements would have been lost.

The graph changes shape in comparison between the altered rocks 4788 and 4688 (Fig. 6.3a(5)), showing that with progressive alteration, the initial variations change. Below $f_v = 0.92$, all major element oxides have been lost. Between 0.92 and 1.0, SiO₂ shows the greatest increase with Al₂O₃ increasing only when $f_v > 0.98$. Al₂O₃ is constant at $f_v = 0.98$. Significantly, K₂O has decreased at all values below $f_v =$

1.3, indicating that it has probably been lost from the system. (Na_2O and CaO curves are hidden around the gain-loss zero line as neither was present in either 4788 or 4688).

In the rocks from the pegmatite suite, similar changes are seen (Fig. 6.3b). However, between the most altered samples 5088 and 4988 (8.4m and 2.8m below unconformity) e.g. there is no change in K_2O at $f_v = 1$ (Fig. 6.3b(3)). The greater percentage of pinitite (and significantly the lack of pyrophyllite) in 4988 as compared with the more altered gneiss at similar depth (4688) would explain the difference. The significant decrease in SiO_2 in Fig. 6.3b(3) must be treated with caution, as the primary variation in quartz content fluctuates more in the pegmatite.

Although much information can be gained from these diagrams, they have limited use in solving the problem addressed, as there is no obvious single or restricted range of f_v defined in this system.

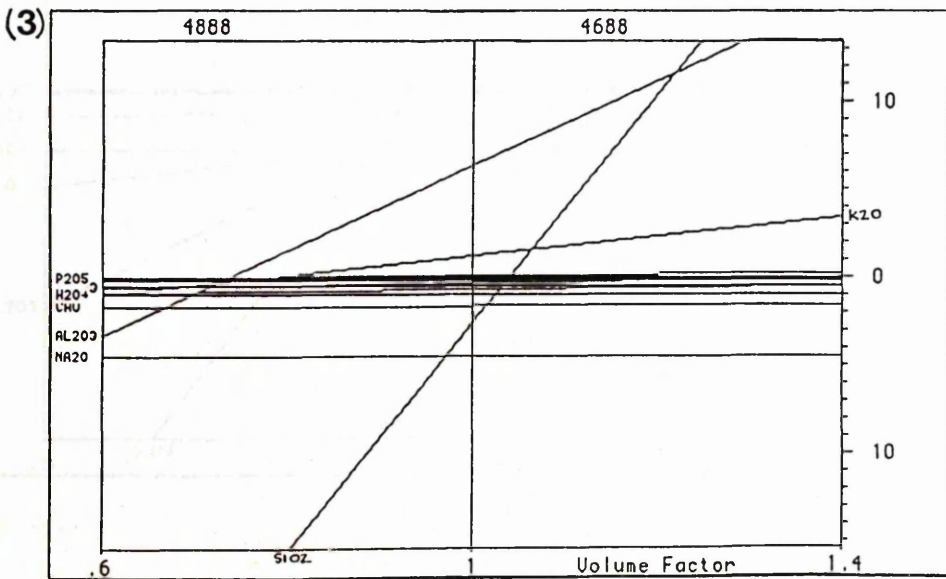
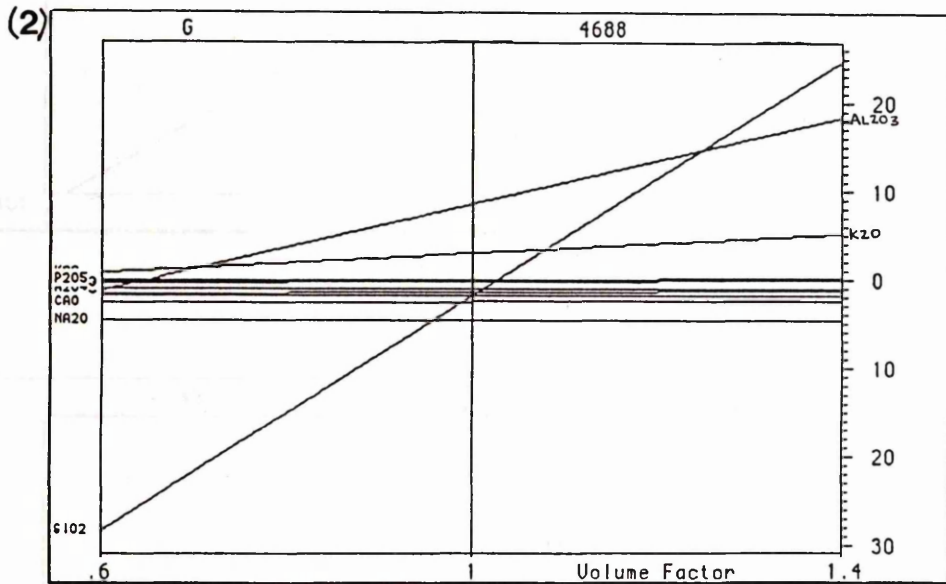
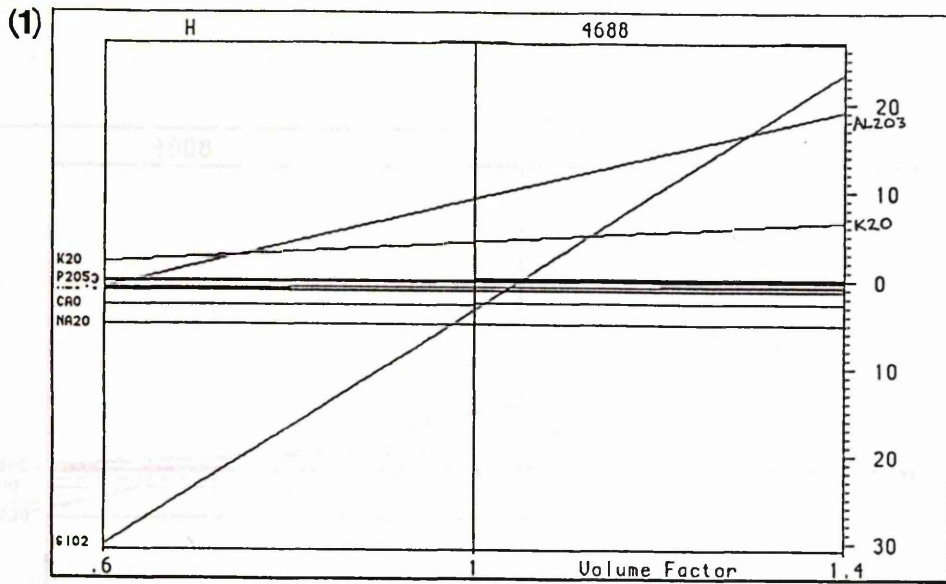


Fig. 6.3(a) cont'd.
 Samples from cave gneiss suite [NC 4385 6614].

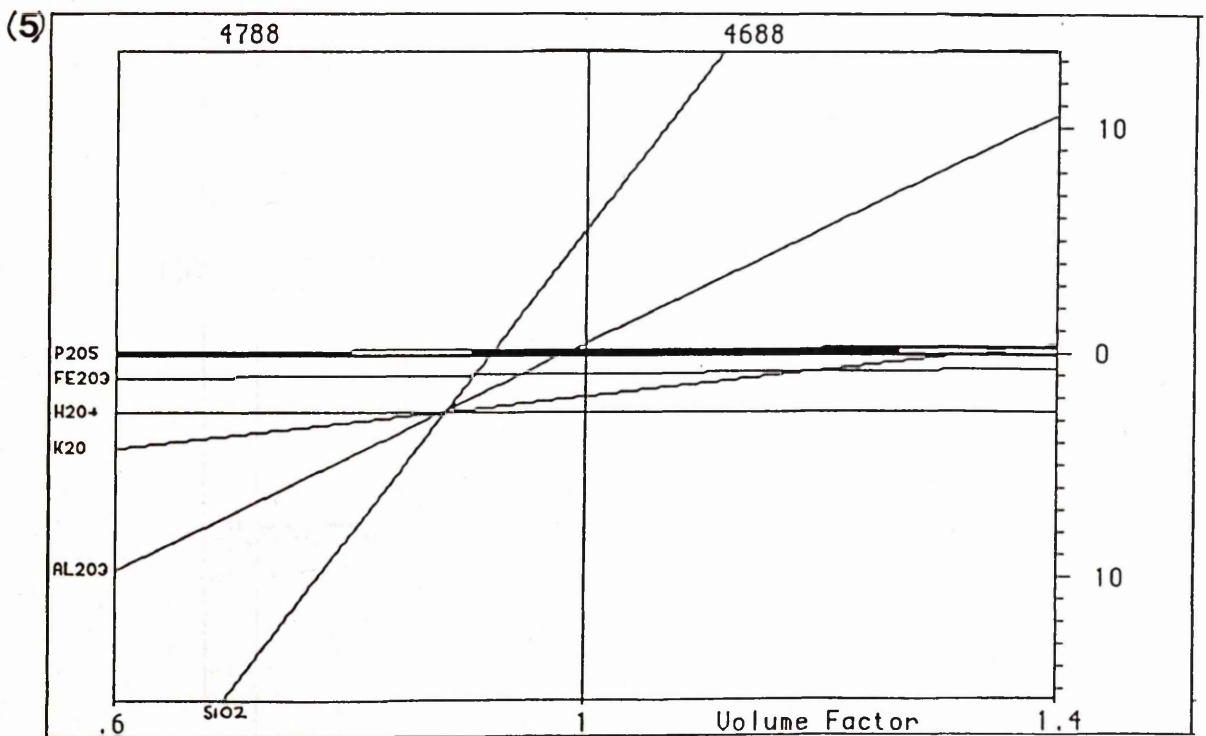
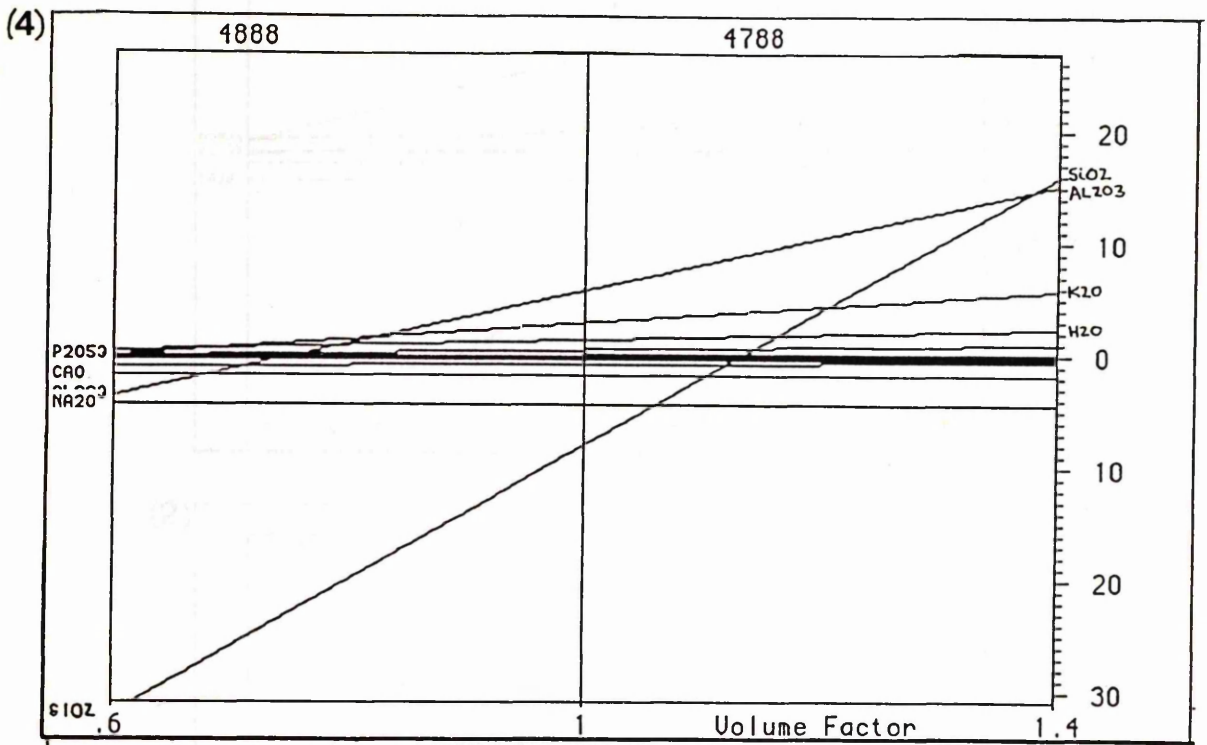


Fig. 6.3(a) cont'd...

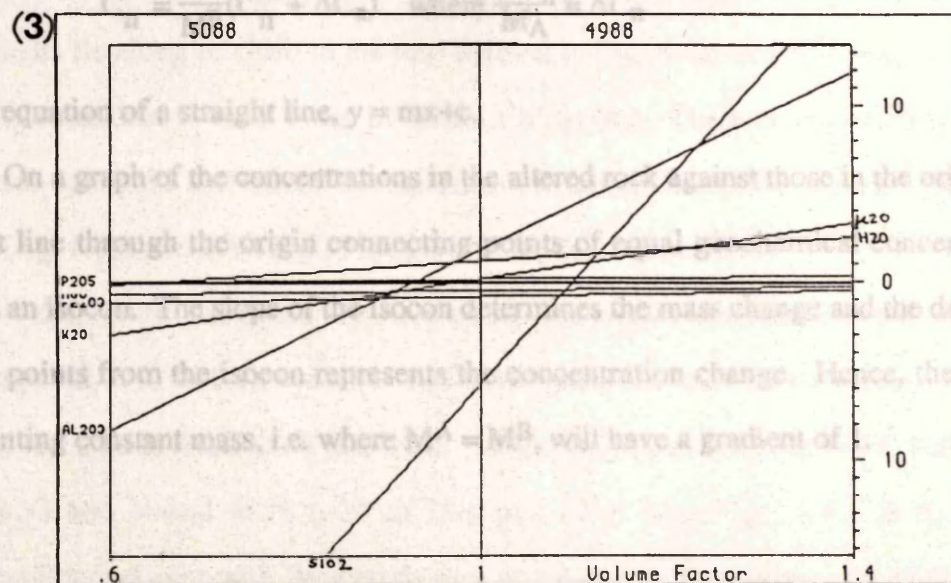
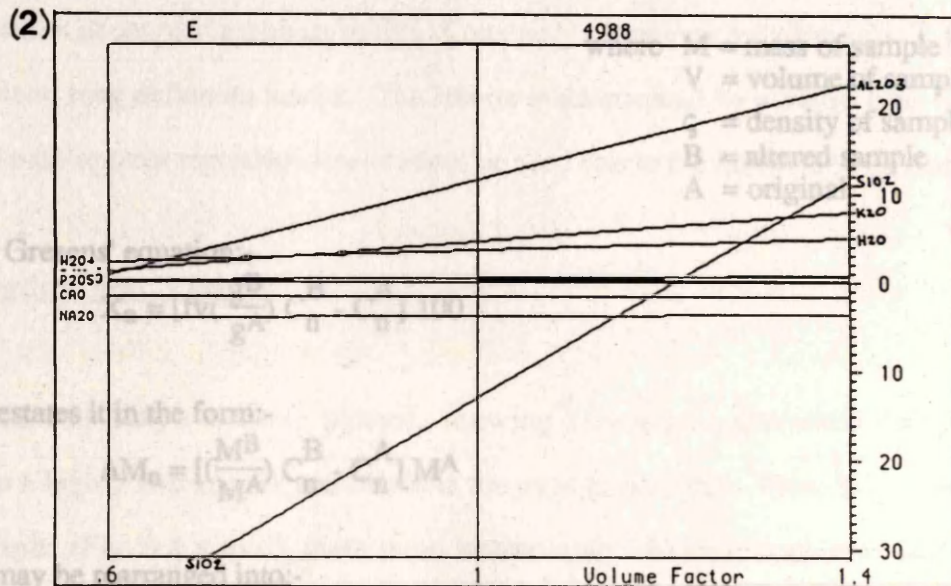
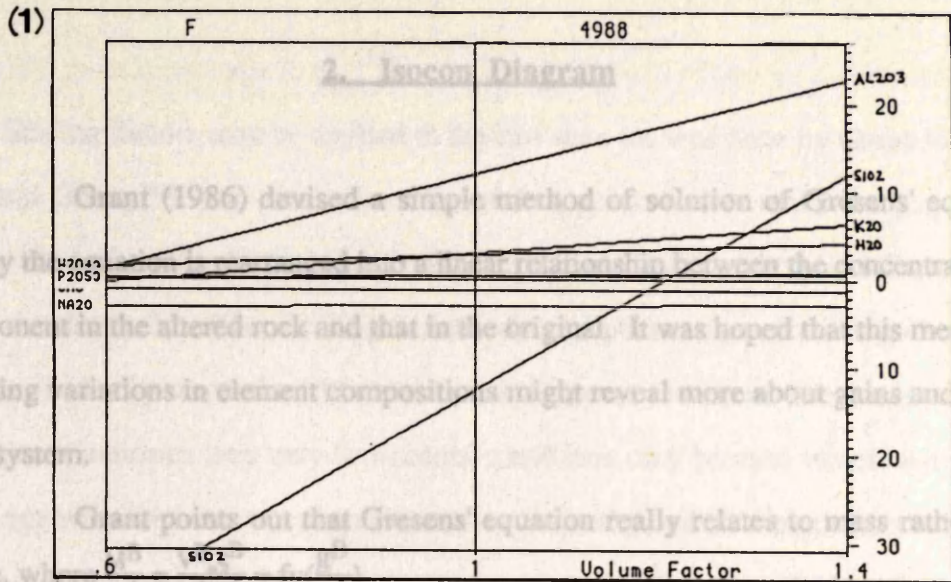


Fig. 6.3(b)

Samples from cave pegmatite suite [NC 4385 6614].

2. Isocon Diagram

Grant (1986) devised a simple method of solution of Gresens' equation whereby the equation is rearranged into a linear relationship between the concentration of a component in the altered rock and that in the original. It was hoped that this method of displaying variations in element compositions might reveal more about gains and losses in this system.

Grant points out that Gresens' equation really relates to mass rather than volume, where $\frac{M^B}{M^A} = \frac{V^B \cdot \zeta^B}{V^A \cdot \zeta^A} = fv \left(\frac{g^B}{g^A} \right)$

where M = mass of sample
V = volume of sample
 ζ = density of sample
B = altered sample
A = original "

Taking Gresens' equation:-

$$X_n = [fv \left(\frac{g^B}{g^A} \right) C_n^B - C_n^A] 100$$

Grant restates it in the form:-

$$\Delta M_n = \left[\left(\frac{M^B}{M^A} \right) C_n^B - C_n^A \right] M^A$$

which may be rearranged into:-

$$C_n^B = \frac{M^A}{M^B} (C_n^A + \Delta C_n) \quad \text{where} \quad \frac{\Delta M_n}{M^A} = \Delta C_n$$

i.e. the equation of a straight line, $y = mx+c$.

On a graph of the concentrations in the altered rock against those in the original, a straight line through the origin connecting points of equal geochemical concentration defines an isocon. The slope of the isocon determines the mass change and the deviation of data points from the isocon represents the concentration change. Hence, the isocon representing constant mass, i.e. where $M^A = M^B$, will have a gradient of 1.

Plotting the diagram

Scaling factors may be applied to the raw data (as was done by Grant 1986 and Olsen and Grant 1991) to prevent overlap of data points and to make the graph more legible. Since the same factor is applied to a species in both the fresh and altered rock, neither the slope of the line nor the gain/loss of a component changes with scaling. The isocon is chosen by inspection. If a number of components forms a linear array through the origin, it indicates they may be immobile and thus may be used to define a best-fit isocon against which other components may be compared (although geochemically dissimilar components should be chosen, as similar components may have changed but have just not decoupled geochemically). Constancy of mass or volume, as well as some component, may define an isocon. The isocon is determined by a visual best-fit to the data. (Least-squares regression lines cannot be used due to the different scale factors).

Application and Results

Isocon diagrams were plotted, showing changes in elemental composition between a highly altered rock and others in the cave gneiss suite. From inspection of all four graphs (Fig. 6.4 a to d), there is no immediately obvious, consistent isocon line along which a number of geochemically dissimilar components lie. However, many components lie along or close to the line defined in Fig. 6.4a, and Al_2O_3 and TiO_2 lie along the same line in most cases in the four diagrams. These components are often considered immobile and indeed aluminium is considered immobile in most weathering indices (e.g. Nesbitt and Young 1982 and see Chittleborough 1991).

If aluminium is assumed to be immobile, then almost all other elements have been lost compared to it, and the rock has suffered a mass decrease on alteration, of ~30% between the almost fresh 4888 and 4688 (15.0m and 2.0m b.u., Fig. 6.4b) and ~37% between G and H and 4688 (~20 to 25m and 2.0m b.u., Figs. 6.4 c & d). Such depletion is consistent with the weathering process which involves loss of chemical components. However, between the two most altered rocks, 4788 and 4688 (7.8m and

2.0m b.u.), there is no mass loss. This is understandable as both are highly altered and contain predominantly pinite, with very little primary crystalline minerals (apart from quartz) remaining.

K_2O initially increases, but ultimately decreases with alteration. Between the freshest rocks (G and H) and the most altered (4688), the increase is 180% (H to 4688), Fig. 6.4d, and 40% (G to 4688), Fig. 6.4c. Such large values are to be expected as secondary K-rich minerals form initially at the expense of plagioclase. In the almost fresh to highly altered rocks from the same gneissic layer, (which has less primary variation), there is an over-all decrease in K_2O of ~8% between 4888 and 4688, Fig. 6.4b. The K_2O content initially increases (again due to the formation of pinite at the expense of plagioclase) and decreases most towards the top of the profile; ~26% decrease between 4788 and 4688, Fig.6.4a.

A notable exception to the trend is the increase in the REE, La and Ce, and also Y, with alteration in the same gneissic layer, between 4888 and 4688, Fig. 6.4b. (This is also found between 4788 and 4688 (not shown)). These changes shall be discussed at the end of the chapter.

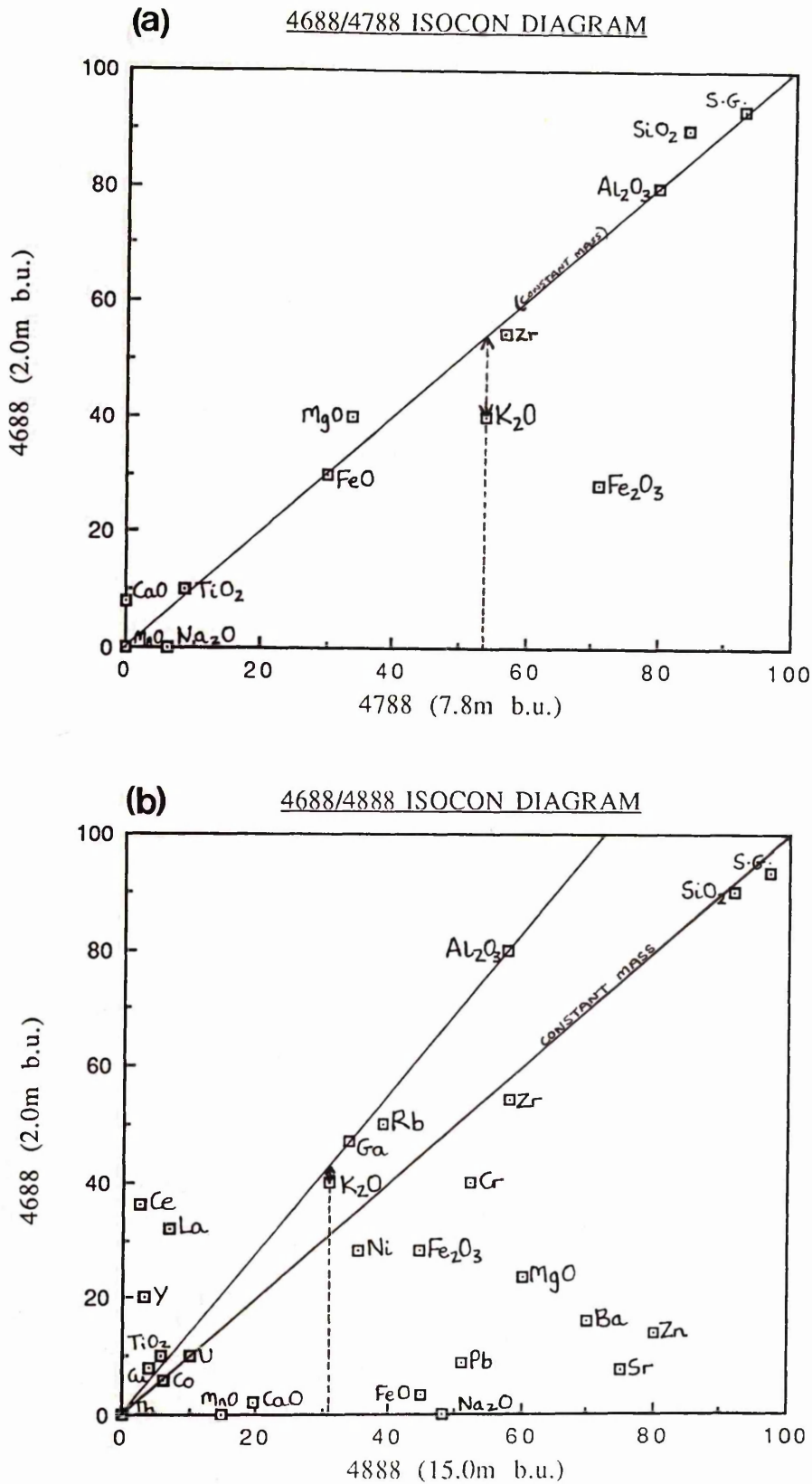


Fig. 6.4

Isocon diagrams comparing rocks from the cave gneiss suite [NC 438 661].

N.B. Samples 4688, 4788, 4888 (9a & b) are from the same gneissic layer [NC 4385 6614].

Samples G and H are from a different layer from the others [NC 4390 6609].

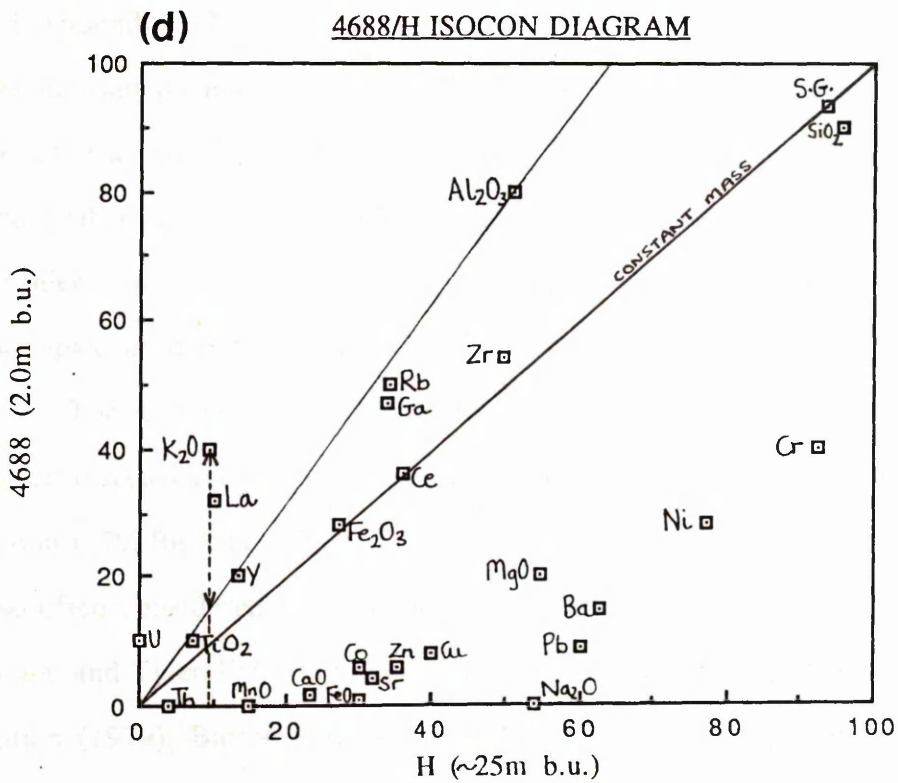
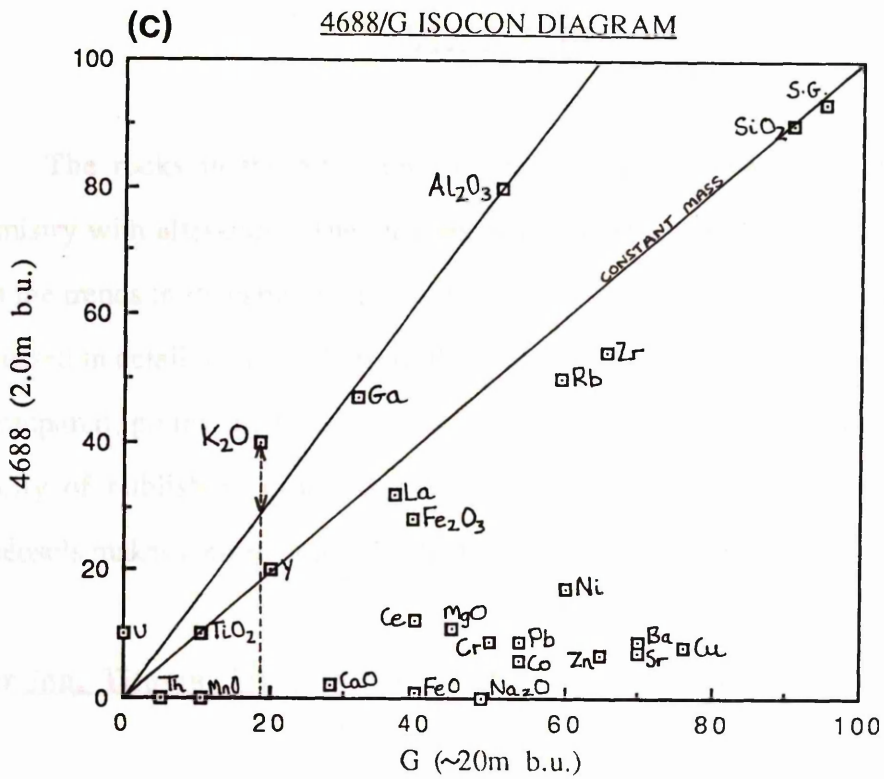


Fig. 6.4 cont'd...

DISCUSSION

The rocks in the alteration profile have undergone significant changes in chemistry with alteration. The changes observed and how they compare and contrast with the trends in Precambrian palaeosols and modern day weathering profiles, shall be discussed in detail in turn. (A list of the Precambrian palaeosols with which this profile is compared, giving their age, protolith and location, is found in Appendix 14). The paucity of published information on a number of trace elements in Precambrian palaeosols makes comparison difficult in some cases.

Alumina, Titania, Silica and their implications concerning pH

The absolute Al_2O_3 content increases greatly with progressive alteration (Fig. 6.1 and Appendix 12). Increasing uncorrected alumina content is typical of most Precambrian palaeosols. Al_2O_3 is frequently considered to be conserved during Precambrian weathering (e.g. Hoeve and Sibbald 1978, Gay and Grandstaff 1980, Grandstaff *et al.* 1986, Reimer 1986) and thus the variations in other elements are often considered using the assumption of constant alumina. Increasing absolute alumina is also typical of modern soils and most chemical weathering indices assume it is immobile.

The absolute TiO_2 content is very low in each suite and fluctuates with alteration. The uncorrected TiO_2 content increases in most Precambrian palaeosols investigated (e.g. Button 1979, Button and Tyler 1979, Grandstaff *et al.* 1986, Williams 1968) and TiO_2 is also often considered to be immobile (e.g. Hoeve and Sibbald 1978, Button 1979, Button and Tyler 1979, Grandstaff *et al.* 1986, Retallack 1986) with researchers e.g. Button (1979), Button and Tyler (1979), Retallack (1986) recalculating elemental concentrations to uniform TiO_2 content. TiO_2 may also be considered relatively immobile in modern soils (Taylor and McLennan 1985). Although Button and Tyler (1979) recalculated to constant TiO_2 in a palaeosol on a granitic protolith (with low TiO_2 content) as well as basic protoliths, it is considered unwise in these suites as the TiO_2

content is so low and variations would be strongly influenced by primary fluctuations. However, that it generally lies close to or on the Al_2O_3 isocon in Figs. 6.4a to d, supports the contention that it is immobile - certainly on whole rock scale.

The absolute silica content remains approximately constant with alteration. Assuming constant alumina, SiO_2 decreases between the fresh and altered rocks (Figs. 6.4b,c,&d). However, this decrease is reduced with further alteration and between the most altered pair examined, 4788 and 4688, the silica content increases (Fig. 6.4a). This behaviour is different from that in most Precambrian palaeosols described in the literature. The absolute silica content decreases, and any corrected values even more so, in palaeosols on basic and acidic protoliths examined by Williams (1968), Kalliokoski (1975), Button (1979), and Button and Tyler (1979). Indeed Retallack (1986) commented that "ancient weathering appears to have caused significant loss of SiO_2 ". Slight loss in silica, and more so when compared to constant alumina, is recorded in modern day profiles (e.g. in an intensely altered soil in Brazil (although silica increases at the top) (Kronberg *et al.* 1979), and in a weathered rind on a syenite protolith also in Brazil (Kronberg *et al.* 1987b).

The bearing of silica and alumina mobility on pH has been discussed by a number of authors. Button (1979) argued that silica dissolution near the surface and concentration deeper in the profile indicated a pH of 9 to 10. A pH ~9 was also advocated by Kalliokoski (1975) for the groundwater, to explain the large amounts of SiO_2 and Al_2O_3 lost from a Precambrian profile developed on a granodiorite. Alumina is dissolved in strongly acid conditions (Fig. 6.5, after Mason 1966). (This is demonstrated in SE Australia, where kaolinite in a deeply weathered profile is dissolved by very acidic waters, pH 2.8 (McArthur *et al.* 1991)). The lack of strong depletion in silica and alumina in this profile would restrict the pH to moderate values. The greater similarity to modern soils, which generally have a pH ~4 to 5, might suggest that the fluids affecting the rocks in NW Scotland were slightly acidic.

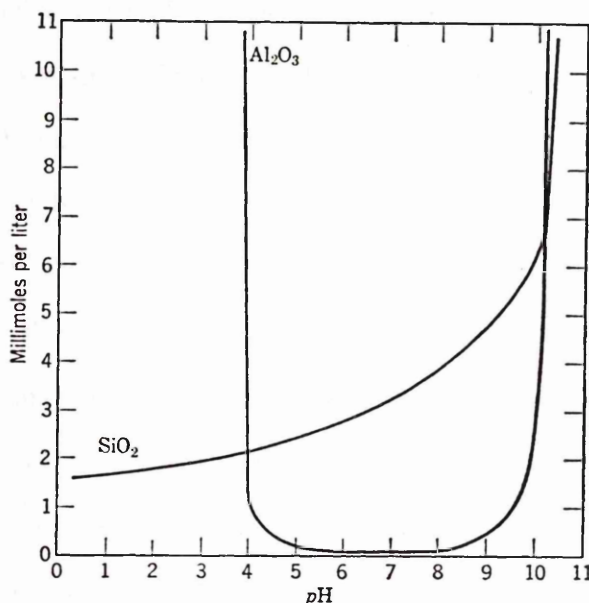


Figure 6.5

The solubility of silica and alumina as a function of pH (Mason 1966).

Alkalis

A distinct feature is the consistent loss of Na_2O with increasing alteration (Fig. 6.1, Appendix 12). The heavier alkali, K, does not show such a pronounced trend and the K/Na ratio increases markedly towards the top of the alteration profile (Fig. 6.6(1), Appendix 11). The Rb value decreases above the sample at 10.4m beneath the unconformity in the gneisses and about the same level (above the sample at 10.7m beneath the unconformity) in the pegmatites. (Below this depth the Rb content is variable, being higher in the pegmatite than in the gneiss suite. However, this reflects the initial K-feldspar content, which is higher in the pegmatites than in the gneisses). The K/Rb content also increases greatly towards the top of the profile (Fig. 6.6(2), Appendix 11).

The general behaviour of K is difficult to ascertain directly from the absolute results, but it decreases less than the other alkalis. In the gneiss suite it increases to

10.4m b.u. then decreases progressively upwards. This gneiss suite is plagioclase-rich and poor in K-feldspar (Fig. 5.1) so as K-rich secondary minerals increase in concentration initially, the K_2O content consequently rises. The rise in K_2O content of the amphibolites is also explained by the paucity of K-bearing phases in the fresh amphibolite. An initial rise in K_2O is also seen in the pegmatites. Although these are more K-feldspar rich, K-rich secondary minerals form firstly at the expense of plagioclase minerals, thus explaining the initial rise.

However, K_2O is actually lost from the system during the later stages of alteration, when considering the composition - volume diagrams and isocon plots (e.g. Fig. 6.4a). Hence, all the alkalis analysed (Na, K, Rb) decrease with alteration.

A "pronounced loss of sodium is the most consistent feature of palaeosols of all ages" (Kimberly and Grandstaff 1986). Also, remarkably large ratios of K/Na are commonly found in Precambrian palaeosols (e.g. Kimberley *et al.* 1980, Kimberley and Grandstaff 1986). However, unlike this profile, most Precambrian (Archaean) palaeosols do not show the upward decrease in K_2O and Rb. However, loss of Na, K and Rb is typical of modern profiles, especially those formed in humid, tropical conditions (Kimberly and Grandstaff 1986). Hence, the trend of behaviour of alkalis in the sub-Cambrian alteration profile, NW Scotland, is more akin to that in modern soils than in Precambrian (Archaean) palaeosols.

Alkaline Earths

CaO, MgO, Sr and Ba all decrease in the gneiss suite and all but MgO, which fluctuates more, in the pegmatite. (However, the MgO content is low and is very sensitive to fluctuations in the amount of biotite, so little can be concluded from this).

Sr decreases in most palaeosols and modern soils. Nesbitt *et al.* (1980) state that Sr is generally transported in solution from the weathering site. G-Farrow and Mossman (1988) discovered that although Sr decreased in all three Precambrian palaeosols from acid to basic protoliths, Sr decreased much more dramatically in one palaeosol than in the

others. This they attributed to palaeotopographic differences. Rb/Sr, although variable, increased in the altered rocks from fresh (Appendix 11), indicating preferential loss of Sr. The isocon diagram (Fig. 6.4b) also shows a greater decrease of Sr than Rb with alteration. Coupled with the marked decrease in CaO and Na₂O, this is consistent with the observation of Nesbitt *et al.* (1980) that Ca, Sr and Na (smaller cations) are most rapidly removed (as dissolved species) during weathering of fresh continental rocks.

Ba behaviour is more variable in Precambrian palaeosols. G-Farrow and Mossman (1988) reported an increase in the middle and top of their alteration profiles, while Button (1979) also saw an increase at the top. Although Ba decreases generally in this case, a large value is recorded at 10.4m below the unconformity in the gneiss suite. According to Nesbitt *et al.* (1980), Ba may increase or decrease in weathering profiles, demonstrating that "relative to K, both types of behaviour can occur even in the same profile".

CaO and MgO show various degrees of depletion in most Precambrian palaeosols (e.g. Button 1979, Button and Tyler 1979 (all South African Precambrian palaeosols), G-Farrow and Mossman 1988 and Reimer 1986). Decreasing CaO and MgO is also found in a profile on the pre 900 Ma to 1100 Ma peridotite, N. Michigan, apart from in a dolomite-rich zone, interpreted as veiniform palaeocaliche features (Kalliokoski 1975). The large losses of CaO, MgO (and indeed Na₂O) indicate the presence of sufficiently mobile porewaters to allow their removal (Reimer 1986), indicating a humid environment (Reimer 1986). The profile of Kalliokoski (1975) containing the CaO and MgO enriched horizons is interpreted as having formed in a semi-arid to arid environment. Certainly, the loss of all alkali earths (CaO, MgO, Sr and Ba) as is found in the sub-Cambrian profile in NW Scotland, is typical of modern day humid weathering environments.

CO₂, H₂O

The behaviour of CO₂ is difficult to ascertain as the results are so low that analytical errors could have greatly influenced their values. However, the H₂O content

increases towards the unconformity in the suites investigated (see Fig. 6.1 and Appendix 12). This reflects the mineralogy, as there is an increase in the proportion of hydrous phases with alteration. This trend is typical of chemical weathering, which principally involves hydration and hydrolysis reactions, with the most weathered modern soils containing minerals in the system $\text{Al}_2\text{O}_3\text{-SiO}_2\text{-Fe}_2\text{O}_3\text{-H}_2\text{O}$.

P₂O₅

P_2O_5 is depleted with increasing alteration in all the suites analysed (except for the amphibolite suite whose values are extremely low). Such depletion is also seen in the three Precambrian palaeosols analysed by G-Farrow and Mossman (1988). However, this, as expected, contrasts with the behaviour in modern soils, where phosphate is retained in the upper parts of a soil by vascular land plants.

Iron

The total iron content in the gneiss suites decreases with alteration, but varies in the other suites (Fig. 6.1 and Appendix 12). However, iron enrichment is found in haematite-rich zones which generally occur along and laterally from joints (see Chapter 5, Plate 5.27a and p.112).

A general decrease in Fe, as found in the gneisses, is consistent with that seen in many Precambrian palaeosols, both pre and post 2.0 Ga old (Williams 1968, Kalliokoski 1975, Button 1979, Button and Tyler 1979, Kimberley and Grandstaff 1986). Its decrease in both pre and post 2.0 Ga profiles is compatible with Clemmey and Badham's (1982) observation that Fe loss from a palaeosol is not necessarily indicative of an O_2 -deficient atmosphere. Indeed, according to G-Farrow and Mossman (1988), the exact relationship between the total iron behaviour and atmospheric pO_2 is as yet uncertain.

Fe³⁺/Fe²⁺

The Fe³⁺/Fe²⁺ ratio increases with alteration (Fig. 6.6(3)). The Fe³⁺/Fe²⁺ ratio of a weathering profile can be affected by subsequent diagenetic/low-T metamorphism (Grandstaff *et al.* 1986). However, as such fluids are mostly reducing, this will usually decrease the ratio (Grandstaff *et al.* 1986). Hence the Fe³⁺/Fe²⁺ ratio as a result of weathering would probably have been at least as high.

Most authors conclude that an increase in Fe³⁺/Fe²⁺ indicates that a profile has formed in an oxidising environment (e.g. Rankama 1955, Retallack *et al.* 1984, Retallack 1986). However, caution is required as the presence of Fe₂O₃ is not necessarily indicative of an oxygenic atmosphere, since Fe²⁺ is oxidised to Fe³⁺ at very low O₂ activities (Schau and Henderson 1983). Nevertheless, the independent and corroborative evidence of e.g. Twist and Cheney (1986) and Baker and Fallick (1989), indicates that the atmosphere changed from reducing to oxidising by around 2.0 Ga. Furthermore, the pO₂ rose after this and is considered to have been at least 0.1 PAL (present atmospheric level) at the beginning of the Cambrian to permit the evolution of shell-forming organisms (Kasting 1987). Hence an oxidising environment of formation is most likely.

Mn

In most suites the Mn content fluctuates and little is concluded about its behaviour as the concentrations in each suite are so small. However, Mn decreases in the cave gneiss suite (Fig. 6.1(a)) and compared to constant alumina there is a large decrease. The behaviour of Mn is reported to follow that of iron in the Precambrian palaeosols described by Button (1979) and Grandstaff *et al.* (1986), decreasing with alteration. Kimberley and Grandstaff (1986) report a correlative (with Fe) but greater loss of Mn. In the complex clay-rich modern soil of Bahia, Brazil, the Mn content is also low and fluctuates greatly, with little being concluded from the variations there. Similarly, the behaviour of Mn follows that of iron in this profile.

Co, Cr, Ni

There is no distinct trend in the absolute values of Co and Cr with alteration. Ni shows no pronounced trend either, although it increases in the cave pegmatite suite. Compared to aluminium, Co, Cr and Ni are all depleted (apart from in the cave pegmatite where Ni is enriched).

Little information is available about the behaviour of all three elements in Precambrian palaeosols. Most information was found about Ni, which generally decreases (e.g. Kalliokoski 1975, Button 1979, Kimberley and Grandstaff 1986 and G-Farrow and Mossman 1986), and Co and Cr decrease also (Button 1979, Kimberley and Grandstaff 1986). Ni increased in one suite on a pre-2100 Ma granodiorite protolith studied by G-Farrow and Mossman (1988). They attributed this contrasting behaviour of Ni to the adsorption of this element upon ferric hydroxides.

In recently weathered alkaline rocks, Kronberg *et al.* (1987b) report no significant variation in these signatures in the initial stages of weathering. However, Cr and Co are enriched in the complex clay-rich rocks of Bahia, Brazil and Cr in the more weathered kaolinitic material from the Amazon region. Their concentration is believed to be due to their importance as biological elements (Kronberg *et al.* 1979). Ni may show little change in more recently weathered rocks (e.g. Rose *et al.* 1979). However, Ni and Ni-Co enrichments are known in laterites on ultramafic complex protoliths (e.g. serpentinised dunite (e.g. late Cretaceous to early Tertiary, Elias *et al.* 1981 and Nahon *et al.* 1982)). Ni enrichment was also found 23m below the surface in a profile on massive and disseminated sulphides, in takovite, a green hydrocarbonate of Ni and Al (Nickel *et al.* 1977). These protoliths, however, are quite different from the sub-Cambrian protoliths investigated.

Ga

The absolute concentration of Ga increases in each of the suites at the cave, increasing above 10.4m and 10.7m in the gneiss and pegmatite suites respectively (Fig. 6.1). However, from the isocon diagrams, it stays approximately constant, assuming aluminium immobility. The absolute concentrations also increase in the gneiss suite [NC 434 662] (Bay 1, Appendix 12) but fluctuate more over the more restricted depth range in the pegmatites at [NC 4435 6394] (Telegraph Hut, Appendix 12). In each profile, gallium behaves in a similar fashion to aluminium with alteration (cf. Fig. 6.6(4)). Below aluminium in the periodic table and with similar ionic potential, this behaviour should be expected. Nevertheless, differences in behaviour have been recorded (e.g. oceanic behaviour, Orians and Bruland 1988) and it is not known if sympathetic behaviour with respect to Al is typical of weathering profiles or palaeosols. However, G-Farrow and Mossman (1988) recorded that Ga registered "a possible slight increase upwards in each palaeosol in the 20-40 ppm range" in the three sub-Huronian Precambrian palaeosols they investigated. They also recorded an increase in Al content although neither Ga/Al ratios nor XRF data is given. Also, in recent weathering, bauxites often show a concentration of gallium (Mason 1966) "with gallium extracted as a bi-product from the production of aluminium". And in the kaolinite-rich modern soils of the Amazon, Kronberg *et al.* (1979) consider that Ga could be substituting for Al. In the complex clay-rich soil of Bahia, Brazil, the Ga concentration (Kronberg *et al.* 1979) may also be due to this substitution.

Lanthanides: La,Ce

The light Rare Earth Elements (REE) La and Ce increase with alteration in each of the suites of altered rocks (e.g. see Fig. 6.4b). It is not known how these elements have fractionated with respect to the other REE. (REE are strongly fractionated under modern tropical weathering conditions which produce bauxite (Kimberley and Grandstaff 1986)).

However, concentration in these light Rare Earth Elements is seen in a modern aluminous soil in Surinam, at 3-4m below the surface of the Earth (Kimberley and Grandstaff 1986). In the five chemical profiles from the four Precambrian palaeosols investigated by Kimberley and Grandstaff (1986), (all ≥ 2.3 Ga old on both granitic and basaltic basement), none showed the trends observed in the modern Surinam soil with "specifically no concentration of La, Ce independent of Eu". Kimberley and Grandstaff considered it possible that erosion prior to burial removed concentrations of light REE.

Closer comparison between this sub-Cambrian profile and the Surinam soil is hindered as the degree of weathering in the Surinam soil is not given - only that it is a modern aluminous soil and the analyses were made from 3-4m below the surface. Nevertheless, the concentration seen in this profile is akin to that seen towards the top of the modern soil profile of Surinam.

Actinides: U, Th

The concentrations of U and Th are low in most samples with values close to and below detection limit. U and Th vary independently and their concentrations, especially that of U, fluctuate with alteration. Hence little can be concluded from these changes.

Y and Zr

The absolute values of the refractory metals Y and Zr increase with alteration, with Y increasing monotonically in the cave gneiss suite. Increase in these elements was also seen in the Precambrian palaeosols analysed by G-Farrow and Mossman (1988). Relative to constant alumina, Y is still enriched above 15m below the unconformity (Fig. 6.4 b), but Zr decreases (although only slightly, between 4788 and 4688 (Fig. 6.4a)). Whether this is influenced most by primary variation (as the absolute Zr value fluctuates more) or is due to weathering is uncertain. The absolute value of Zr also

increased in the palaeosol on the 2200 My Hekpoort basalt and was reported to follow the same pattern as TiO_2 and Al_2O_3 (Button 1979). Constancy of ZrO_2 has been used by Chittleborough (1991) as an assumption in his recently proposed weathering index. Zr and Y are also reported to increase in the recent complex (intermediate to advanced) weathering horizons of Bahia, Brazil (Kronberg *et al.* 1979). According to Kronberg *et al.* (1979) the least soluble refractory oxides are enriched in even highly leached soils.

Zn, Cu, Pb

Zn, Cu and Pb absolute values all decrease in the suites from the cave and Bay 1 (Appendix 12). The results corrected also indicate a decrease (see Fig. 6.4). The data set is very poor for these elements in Precambrian palaeosols. Indeed, little is concluded about the behaviour of lead. It is understood to be depleted in sub-Cambrian altered granitic rocks, Illinois (Duffin *et al.* 1989), but this has been attributed to leaching by later hydrothermal fluids (Duffin *et al.* 1989, but see Chapter 7). In the three palaeosols analysed by G-Farrow and Mossman (1988), lead behaviour varies but they conclude a possible slight increase with alteration. Lead is enriched in the recent Bahia soils of Brazil as it may be exhibiting biological affinity (Kronberg *et al.* 1979). As in NW Scotland, depletions in Zn and Cu are also found in other Precambrian palaeosols (e.g. Button 1979, G-Farrow and Mossman 1988). However, in the modern intermediate to advanced weathered Bahia soils, Cu and Zn, which are bio-important elements, are concentrated (Kronberg *et al.* 1979). Clearly any bio-effects would have been much less in the Precambrian than in the present tropics of Brazil and hence this may account for the difference in behaviour of Cu and Zn and indeed Pb between Precambrian and modern soils.

Au

Gneissic samples from the cave at 2.0m, 7.8m and 15.0m below the unconformity were analysed for their gold content and all contained 0(ppb) (Analyses by aqua regia digestion, followed by atomic absorption spectrophotometry (detection limit 20ppb) , courtesy of Navan Resources plc.). Since the almost fresh sample from 15.0m contained no gold, these results give no indication of what would happen to Au-bearing rocks in this environment.

CONCLUSION

The behaviour of the major and trace elements examined strongly supports the findings from the field evidence that the alteration profile formed as a result of weathering. The trends indicate that the profile formed under humid, tropical weathering conditions, in an oxidising environment (up to 0.1 PAL) at moderate pH. The variations imply the profile is geochemically more akin to a modern day pedalfer than to most Precambrian palaeosols described (most of which are formed on pre-2000 My protoliths, and are generally believed to have formed under alkaline reducing conditions). However, as expected, the behaviour of many bio-important elements is at variance with that found in modern day soils.

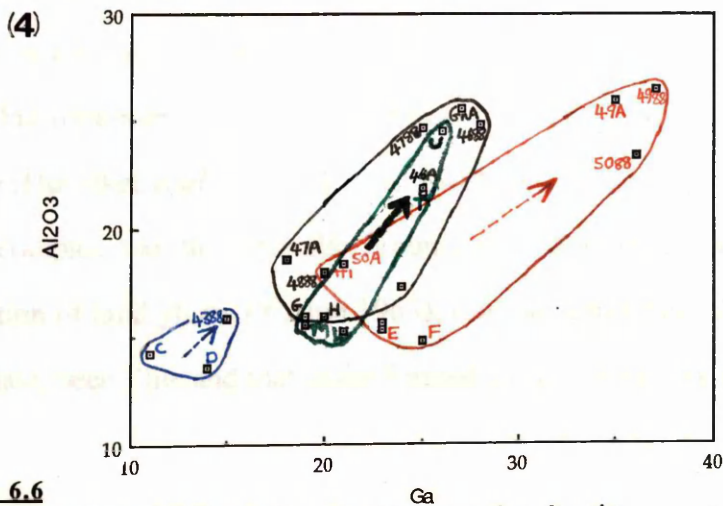
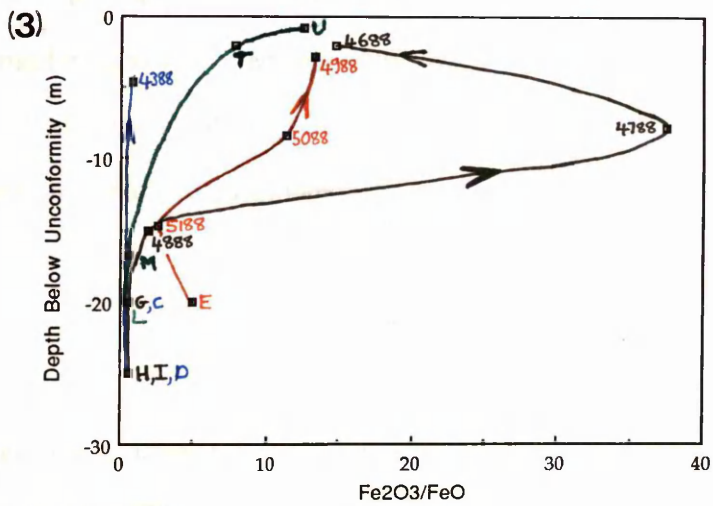
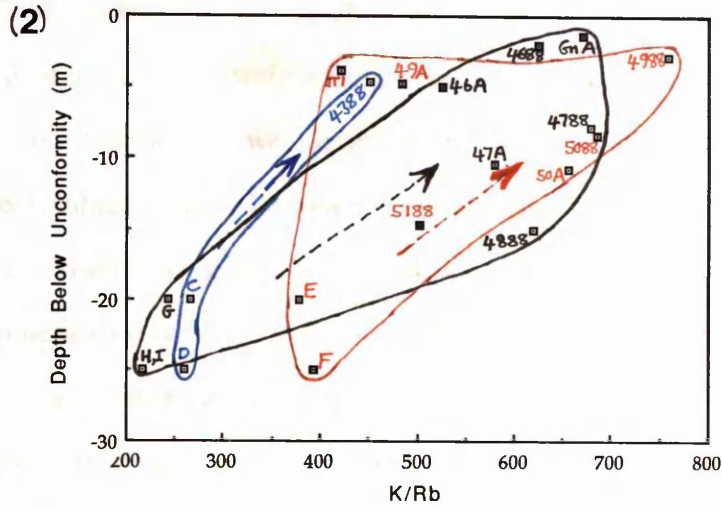
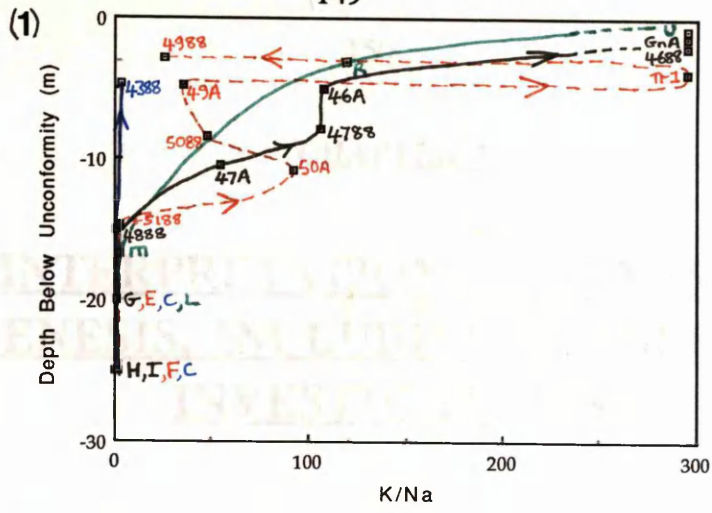


Fig. 6.6

Relative behaviour of different elements with progressive alteration.

Arrows in direction of increasing alteration.

Black = gneiss, Red = pegmatite, blue = amphibolite..from [NC4385 6614]. Green = gneiss from [NC 434 662]

CHAPTER 7

INTERPRETATION OF MINERAL PARAGENESIS. INCLUDING STABLE ISOTOPE INVESTIGATIONS

The field relationships and geochemical changes with alteration strongly support the hypothesis of a weathering origin for the rocks of this profile. However, the present mineralogy is not typical of a weathering profile, which would be expected since the profile has been subject to burial beneath the overlying Cambrian strata and an unknown thickness of Caledonian nappes. The chemistry of the saprolite, as well as the presence of primary minerals in most of the profile and its limited thickness in places, indicates that much of the original weathering profile was eroded prior to deposition of the overlying strata. It is therefore the 'C' horizon that is preserved. Hence, most of the clays which predated the present minerals should have been complex clays (see Chapter 3), which in modern soils are predominantly smectites, illites and chlorites (Kronberg *et al.* 1987a). The genesis of the major secondary minerals and the alteration of the primary phases shall each be considered.

PINITE

Petrographic evidence of a remnant precursor to pinite was not found using XRD and SEM. Cardenas (1986) suggests that the precursor was mixed layer K-beidellite and illite. Pinite is a very fine-grained form of $2M_1$ muscovite (see Chapter 5, p.78 and Table 5.1). 1Md illite may evolve to $2M_1$ muscovite by means of a continuous structural modification (Hunziker *et al.* 1986). Coupled with this, since the pinite precursor would have been a complex clay and since illite is considered to be the major complex clay prior to the evolution of land plants (Yaalon 1963), it is suggested here that the precursor to pinite may have been illite and that pinite formed by the above process. This process is

completed around the anchizone/epizone boundary (Hunziker *et al.* 1986). These rocks are understood to have reached 250°C (to 275 ± 30°C) (Downie 1982, Johnson *et al.* 1985, Ferguson 1987) during the Caledonian orogeny, thus enabling this transformation to take place. The K₂O content of the pinite in NW Scotland ranges from 9.8 to 11.4 wt. %. Hunziker *et al.* (1986) stated that anchimetamorphic illites had K₂O = 8.6 to 10.2 wt. %, while epimetamorphic illites to muscovites had K₂O = 9.9 to 11.4 wt. %. Hence, the pinite analyses from the profile correspond to epimetamorphic muscovites.

PYROPHYLLITE

Pyrophyllite is found at the top of the profile and forms initially mainly at the pinite-quartz boundary and predominantly at the expense of quartz as it consumes this mineral with progressive alteration (e.g. Plate 5.10).

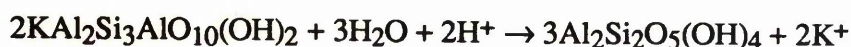
There are two possible reactions for its formation:-

1. Pyrophyllite may have formed due to reaction between pinite or its precursor muscovite and quartz, i.e.



The consumption of muscovite and silica appears consistent with the initial textural information (Plate 5.10a). During this reaction, the rock will become more hydrous and less potash-rich. This is consistent with what is found geochemically and with the trend in modern day weathering environments.

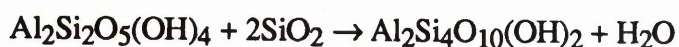
2. Since pyrophyllite is only found at the top of the alteration profile, it is possible that it may have formed after kaolinite. Kaolin phases form after dissolution of complex clays (e.g. Kronberg and Melfi 1987) as weathering reaches an advanced stage. The reaction from muscovite to pyrophyllite (i.e. assuming an illite precursor to pinite) is in this case a two stage process.

First stage

muscovite

water

kaolinite

Second stage

kaolinite

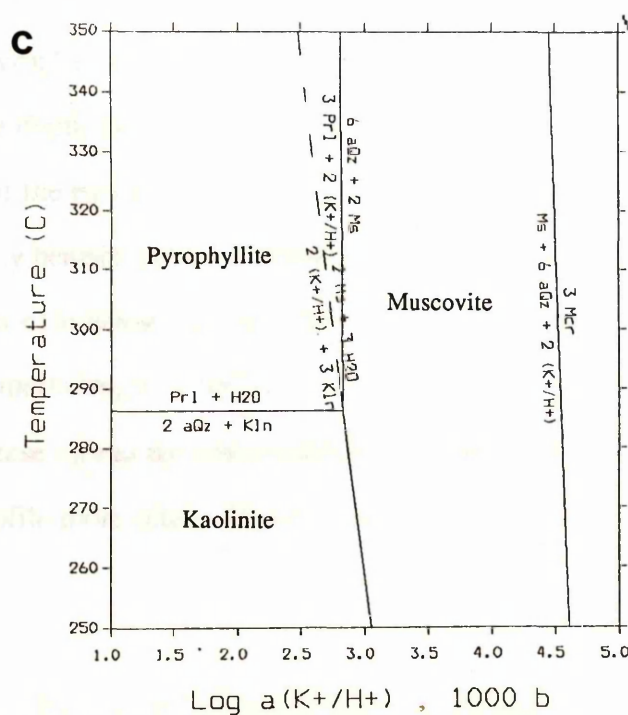
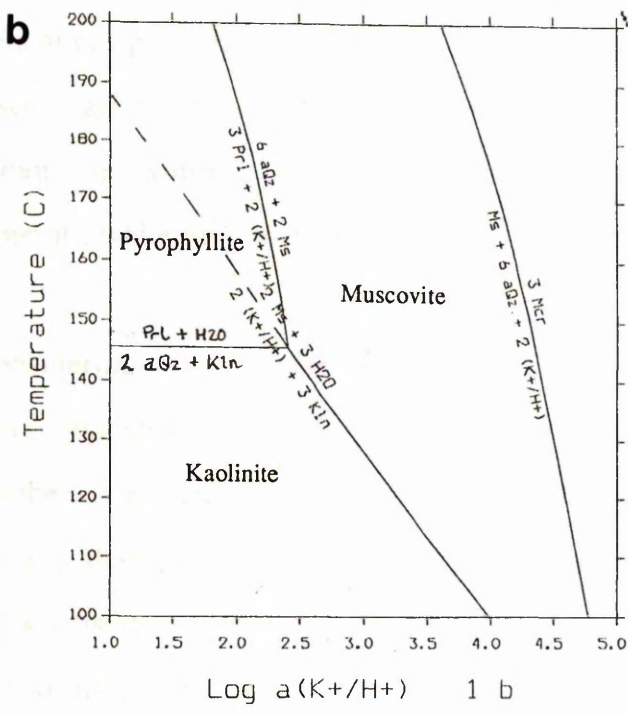
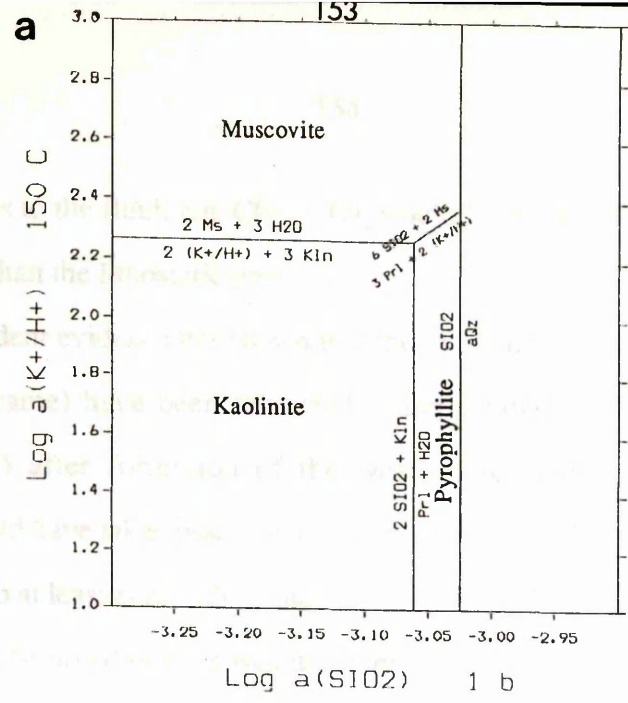
silica

pyrophyllite

water

Pyrophyllite is generally considered a metamorphic mineral. Theoretically it can form at 25°C, but only in water-absent regions (Chesworth 1983). However, this is unrealistic for near surface environments (even in very arid regions) and pyrophyllite has not been found as an authigenic phase in soils (Chesworth 1983). Much work has been carried out on the lower stability limit of pyrophyllite, represented by the reaction, kaolinite + 2 quartz → pyrophyllite and water. Thompson (1970) concluded that the lower limit should be 345 ± 10°C at 2kb. However, other workers (e.g. Day 1976) have considered this too high. Tsusuki (1967) stated that kaolinite transformed into pyrophyllite at 270°C and Velde (1977) suggested the precise value of 250°C for the transformation at 2kb.

Using the GEO-CALC:PTA-SYSTEM for calculation of phase diagrams (Brown *et al.* 1988), which permits the user to specify pressure, temperature and activity variables, phase diagrams were produced which show transformation of kaolinite into pyrophyllite as low as 146°C at 1 bar (Fig. 7.1b). The other proposed reaction, i.e. muscovite → pyrophyllite, is also shown occurring at, or above, the temperature of transformation of kaolinite to pyrophyllite over a more restricted and higher $a(\text{K}^+/\text{H}^+)$ range (Fig. 7.1a to c). Increasing the pressure increases the reaction temperature (Fig. 7.1c), although in this case the temperature is higher than that which other researchers have found. (Brown *et al.* 1988, used data of Helgeson *et al.* 1981, Berman *et al.* 1985 and Berman 1988). It should be noted that the pressure given in Fig. 7.1c is $P_{\text{H}_2\text{O}}$ and therefore these conditions would probably be achieved under higher lithostatic pressure



(as any additions to the fluid, e.g. CO_2 , CH_4 , would lower its activity, producing a $P_{\text{H}_2\text{O}}$ which is lower than the lithostatic pressure).

Independent evidence has shown that the rocks around Loch Eriboll (from where these samples came) have been subjected to temperatures of 250°C (Downie 1982, Ferguson 1987) after formation of the weathering profile and the formation of pyrophyllite could have taken place under these conditions. This temperature would have required burial to at least 8km ($\sim 2\text{kb}$) and this is geologically acceptable.

It should be noted that the minimum temperature of transformation of muscovite to pyrophyllite occurs at the temperature of the reaction of kaolinite to pyrophyllite (hence, apart from at this point, the muscovite to pyrophyllite reaction occurs at higher temperatures) (see Fig.7.1b&c). Furthermore, the transformation from kaolinite to pyrophyllite can be simply an up-temperature reaction (progressive metamorphism/burial), while muscovite to pyrophyllite requires a change in chemical activity.

When considering which of the two above cases was more likely for the transformation to pyrophyllite, textural information and field relationships as well as information from the phase diagrams must be considered. With progressive alteration it is obvious texturally that quartz is the main phase consumed in the formation of pyrophyllite. This satisfies the requirements in both cases. Although pyrophyllite is always restricted to the upper reaches of the profile, it occasionally constitutes the predominant mineral within 1(to 2?)m of the unconformity. These instances may be localised, with pyrophyllite constituting only a minor phase in pinite (muscovite) - quartz rocks at the same depth even less than a metre away, with no apparent structural control on the location of the pyrophyllite-rich rocks. Indeed in some places no pyrophyllite is found immediately beneath the unconformity. Since pyrophyllite-pinite-quartz and pinite-quartz rocks from $<1\text{m}$ below the unconformity in the Eriboll area were both subjected to the elevated temperature, it is unlikely that the muscovite + quartz \rightarrow pyrophyllite transformation (case 1) was the main reaction, as pyrophyllite would then be expected at the top of the profile more often. However, a variable extent of weathering, around the

transition from intermediate to advanced weathering, with kaolinite forming a more dominant phase in places, is much more likely. Therefore it is concluded that pyrophyllite most probably formed due to reaction between kaolinite and quartz.

PLAGIOCLASE

In plagioclase, the preferential alteration of the more calcic cores, with the more sodic overgrowths being last to be altered (Chapter 5, p.49), is consistent with Goldich's (1938) stability series (see Chapter 3, p.9) and with Loughan's (1969) order $\text{CaO} > \text{Na}_2\text{O} > \text{K}_2\text{O} > \text{SiO}_2 \gg \text{Al}_2\text{O}_3$, based on the work on electro dialysis of feldspars by Armstrong (1940).

The weathering of plagioclase (predominantly albite in this case) to muscovite is a hydrolysis reaction and may be represented by:-

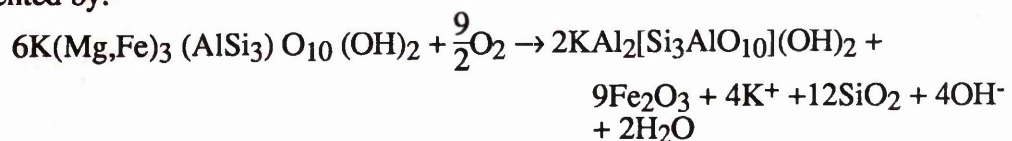


(of Nordstrom and Munoz 1986).

Hence, at this initial stage of weathering, there is an uptake of K^+ and loss of Na^+ and Ca^{2+} from the system.

BIOTITE

An overall reaction for the consumption of biotite by muscovite may be represented by:-



...where Fe^{2+} ($\rightarrow \text{Fe}^{3+}$), Mg^{2+} , K^+ and Si^{4+} are mobilized. As shown in Fig. 5.3 (and p.59) the change in the mineral chemistry of biotite is congruous with the change in whole rock chemistry with alteration. As biotite is the major phase bearing Fe, Mg and

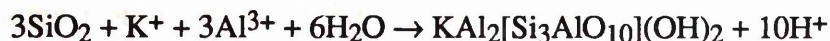
Mn, its behaviour strongly influences the geochemical trends of these elements in the whole rock. Hence, these changes indicate that the system loses MgO, FeO_{tot} and MnO with alteration (which is not clear in some suites when there is a significant primary variation in biotite content, especially when the weight % of an oxide is low).

QUARTZ

Primary:

Quartz is the last of the major primary phases to be consumed. Dissolution of quartz during weathering is a common phenomenon even in modern soils (with pH ~ 4 to 5), and should not be considered to be restricted to profiles formed under alkaline conditions, in which there is pronounced silica depletion (Taylor and McLennan 1985).

Quartz is seen to be initially consumed by pinite (see Plate 5.9). The reaction.....



.....consumes K⁺ and Al³⁺ ions, releasing only H⁺ and thus increasing the acidity of the water. The dominant consumption of quartz, however, is thought to have occurred later, during the formation of pyrophyllite.

Secondary:

Secondary silica is found 1) in veinlets, most noticeably tourmaline-quartz veinlets, which penetrate the profile, and also 2) as low-T cristobalite stars, aggregates of which form opal.

Silica formed at or near the Earth's surface is generally in the form of opal (Fron del 1962), formed "by the chemical weathering of silicates". Hence, the cristobalite stars were probably a weathering product.

Opal is also formed at or near the Earth's surface biochemically and it is interesting to speculate about a possible relationship to late Precambrian micro organisms, despite its depth in the present profile. If organic in origin, more opal would be expected above 7.8m beneath the unconformity.

K-FELDSPAR

The alteration of K-feldspar proceeds after that of plagioclase and before quartz. The hydrolysis reaction.....



(of Nordstrom and Munoz 1986)

.....indicates that K^+ (as well as Si^{4+}) is lost to solution during this reaction, and thus contributes to the loss of potassium from the system in the mid to upper reaches of the profile.

Prior to complete consumption, however, the remnant primary K-feldspars change in hand specimen from fresh, typical pale pink translucent crystals, through salmon pink, to deep pink opaque crystals. Interpretation of X-ray diffractograms shows a transition from pure high-T igneous K-feldspar, to low-T authigenic respectively. Although K-feldspar had not been replaced by different secondary minerals at this stage, some process had caused this change. There was good likelihood, therefore, that the $\delta^{18}\text{O}$ isotopic signature of the feldspars had been affected as a result of this. $\delta^{18}\text{O}$ isotopic investigation was, therefore, carried out;.....

- to determine if the signatures had been affected, and,
- to see if a wider investigation might help determine the processes which caused the change in these rocks.

Oxygen isotope investigation of K-feldspar (separates)

K-feldspar samples were separated by hand picking under microscope and heavy liquid separation. Purity was checked by XRD before analysis. Oxygen isotope values were determined at the SURRC using standard techniques described e.g. in Halliday *et al.* (1983).

Samples

K-feldspar samples analysed included:-

-4 suites of 2 to 6 samples from different depths beneath the unconformity, from; the Cave [NC 438 661]; Small Bay [NC 43 66]; Telegraph Hut [NC 4435 6394] and Cranstackie [NC 34 55].

-Individual samples from other locations at known depths below the unconformity.

-a typical Laxfordian pegmatite K-feldspar separate.

Results

The results (Table 7.1 and Fig. 7.2) show that the $\delta^{18}\text{O}$ value increases with progressive alteration towards the unconformity.

In Table 7.1, the final two columns give the general appearance of analysed feldspars and indications of the degree of alteration of the rocks from which these separates were taken. The degree of alteration indicated is subjective and based on % pinitite in the samples and colour of the feldspars. Comparison of degree of alteration of each sample with its K-feldspar $\delta^{18}\text{O}$ shows that, apart from one sample, the $\delta^{18}\text{O}$ values are consistent with degree of alteration throughout the whole investigated area (samples up to ~30km apart) in every case, i.e.....

	Degree of alteration.	$\delta^{18}\text{O}$
Fresh	---	7.1 to 9.2
Least altered	*	9.9
	**	10.3 to 12.4
Most altered	***	13.7 to 13.8

When all results are considered together (especially those within 15m of the unconformity) (Fig. 7.2, Table 7.1) it is seen that the $\delta^{18}\text{O}$ value of a sample is obviously not dependent only on its depth below the unconformity. However, it is clear that in any one suite of samples (apart from Cranstackie) the $\delta^{18}\text{O}$ value increases with proximity to the unconformity - and indeed in each case, with increasing weathering. In the Cranstackie suite, no signs of weathering are visible.

Name and Location	Sample	Depth below unconformity (m)	$\delta^{18}O$	Degree of alteration of whole rocks	Appearance of K-feldspar.
Cave [NC 438 661]	50A	10.70	13.7	* * *	Deep pink - opaque Pale pink-translucent Pale pink-translucent Deep red, haematite stained
	5188	14.72	9.9	*	
	LF(E)	~20	7.8	-----	
	2489/A	12.5	13.5		
Small bay [NC 4348 6619]	8749	0.3	12.4	* *	Salmon pink-opaque Pale pink-translucent
	8752	~17	9.2	-----	
Telegraph Hut [NC 4435 6394]	0690	5.7 to 8.6	13.8	* * *	Salmon pink-opaque
	0590	6.2.to 9.1	12.8	* *	Salmon pink-opaque
	0490	8.3 to 11.2	13.5	* *	Salmon pink-opaque
	0390	8.9 to 11.8	12.3	* *	Salmon pink-opaque
	8746	9.4 to 12.3	12.1	* *	Salmon pink-opaque
Cranstackie [NC 34 55]	3288	0.4	7.8	-----	Pale pink-translucent
	3488	10.0	8.5	-----	Pale pink-translucent
	3688	182	7.1	-----	Pale pink-translucent
	3788	270	8.0	-----	Pale pink-translucent
VF [NC 4357 6240]	VF	<4.0	12.0	* *	Salmon pink-opaque
Wheelhouse [NC 4047 6111]	LF whse	0.05 to 0.10	11.8	* *	Salmon pink-opaque
Arkle [NC 3035 4444]	3088	<2.0	9.2	* *	Salmon pink-opaque
	3188	<1.0	10.3	* *	Salmon pink-opaque
Laxford Brae [NC 232 485]	1090	Deep! (Fresh-typical Laxfordian K-feldspar)	7.2	-----	Pale pink-translucent

Table 7.1

$\delta^{18}O$ isotopic values for K-feldspar separates from sub-unconformity and other basement rocks. Degree of alteration:- ----- : Fresh
* * * : Most altered

Interpretation

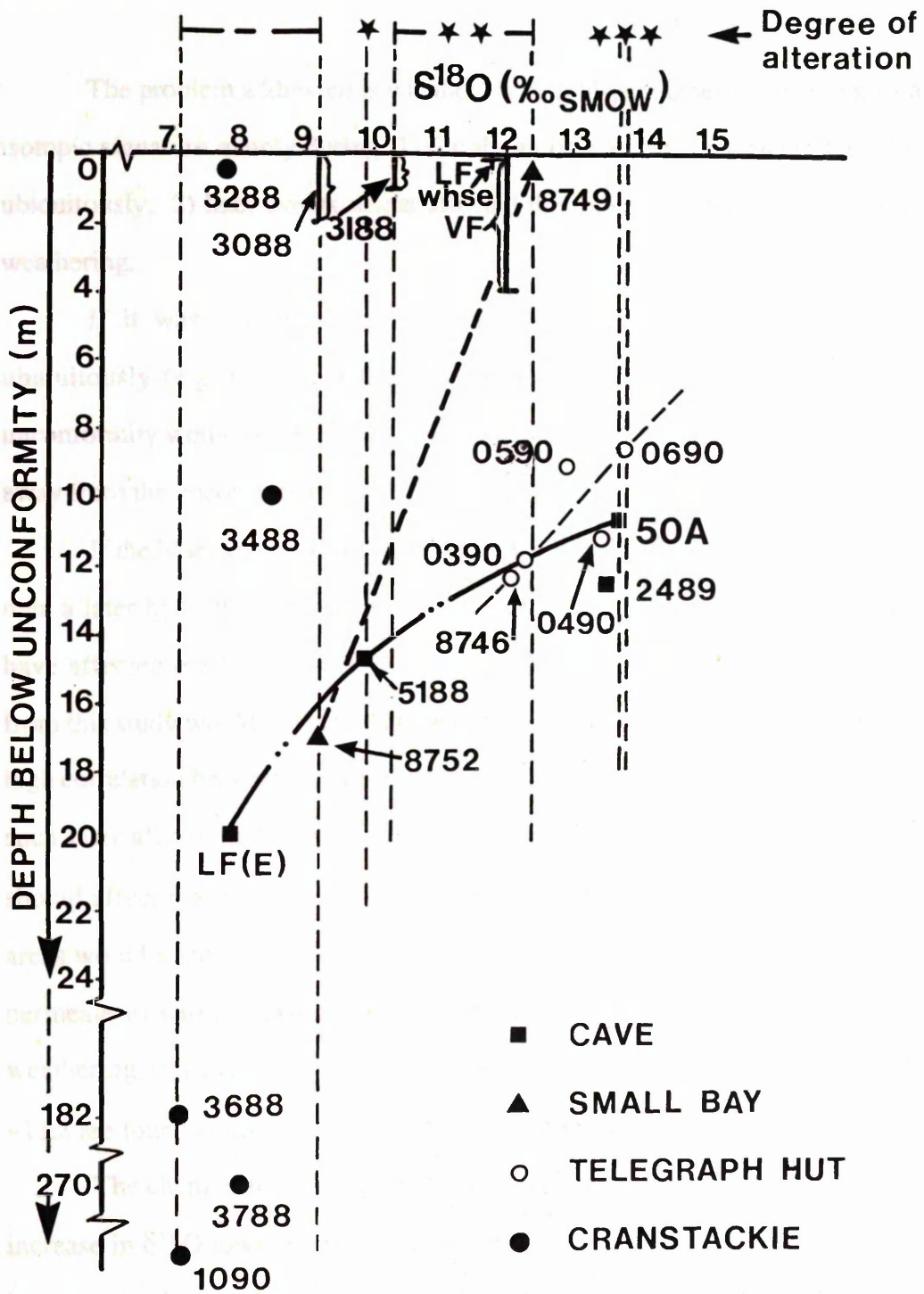


Fig. 7.2

Variation in $\delta^{18}\text{O}$ of K-feldspar separates, with depth below the unconformity.

Interpretation

The problem addressed is whether the K-feldspars inherited their appearance and isotopic signature mainly during; 1) Cambrian or later events which affected the rocks ubiquitously, 2) later events which affected the rocks to varying extents, or 3) during weathering.

If it was a single later event which affected the sub-unconformity rocks ubiquitously (e.g. Cambrian marine transgression), then the values just below the unconformity would be expected to be the same at all points and decrease monotonically away from the unconformity.

If the basement rocks were completely unaltered after deposition of the Cambrian, then a later hydrothermal event which affected the rocks to different extents may also have affected the K-feldspars to differing extents. However, the weight of evidence from this study would indicate that the rocks were previously weathered. Since there is a high correlation between degree of weathering and $\delta^{18}\text{O}$ value, it is then unlikely that any such later alteration caused these variations in $\delta^{18}\text{O}$. That later hydrothermal fluids should affect the feldspars more in the more weathered and less in the less weathered areas would appear to be too coincidental. A further argument, that later fluids could permeate to varying extents beneath the unconformity due to the varying degree of weathering and thus affect the $\delta^{18}\text{O}$ isotopic signature, loses ground when values of ~ 11.8 are found within centimetres of the unconformity.

The changes in $\delta^{18}\text{O}$ are best interpreted as due to weathering. The progressive increase in $\delta^{18}\text{O}$ towards the unconformity in any one suite and the direct relationship between the degree of weathering and the $\delta^{18}\text{O}$ values are consistent with a weathering effect.

TOURMALINE

The presence of tourmaline in the sub-Cambrian alteration profile was intriguing due to the paucity of this mineral in the Lewisian basement (Peach *et al.* 1907). Field and petrological criteria showed that the tourmaline was secondary and peculiarly associated with the alteration profile. Hence, it must have formed either during weathering or later in the profile's history.

To understand more about the fluid and temperature conditions under which tourmaline formed, $\delta^{18}\text{O}$ and δD data were acquired on tourmaline separates and $\delta^{18}\text{O}$ on quartz separates.

Stable isotope investigation

Tourmaline and quartz were separated from a tourmaline/quartz veinlet from near the top of the profile at [NC 4357 6240], Plate 5.17 c & d, and an altered pegmatite vein from ~<2m below the unconformity at [NC 4387 6611], Plate 5.17 a & b, by hand picking under a microscope and heavy liquid separation.

Results

$\delta^{18}\text{O}$ and δD data from the separates are shown in Table 7.2.

SAMPLE	$\delta^{18}\text{O}$ ‰ (SMOW)	$\Delta\text{OTZ-TOUR}$ = $\delta^{18}\text{O}(\text{quartz})-\delta^{18}\text{O}(\text{tour})$	δD ‰ (SMOW)	H_2O (μ moles mg^{-1})
Veinlet quartz-1 (VQ)	15.38 } 15.47±	+3.25	-22	1.44
Veinlet quartz-1 (VQ)	15.56 } 0.09			
Veinlet tourmaline (VT)	12.22			
Pegmatitic quartz (PQ)	10.27	-3.31	-38	1.75
Pegmatite tourmaline (PT)	13.58			
1 σ	±0.1		± 2	

Table 7.2

$\delta^{18}\text{O}$ smow ‰ and δD results from tourmaline and quartz mineral separates. (Sample VQ repeated to check results reproducible).

Although the two tourmalines have reasonably similar $\delta^{18}\text{O}$ values, the quartz values are widely different. The quartz and tourmaline data for the veinlet plot firmly on the line of Appalachian-Caledonian tourmalines and quartzes from Taylor and Slack (1984) (Fig. 7.3). Taylor and Slack (1984) have suggested that the general linear correspondence indicates that the "tourmaline and quartz exhibit similar oxygen isotope exchange kinetics". Hence, the position of the veinlet data on this line would suggest that these minerals are co-genetic. The data for the pegmatite (with $\Delta_{\text{Q-T}} = -3.31$) plot off this line, illustrating that they are not co-genetic and are grossly out of oxygen isotopic equilibrium. This is consistent with the field and microscopic evidence; quartz and tourmaline are intimately related in the veinlet but, in the altered pegmatite, the large quartz grains are primary, while the tourmaline is secondary. The position of the veinlet data towards the high positive value end of the line indicates that they more resemble massive sulphide deposit, than igneous pegmatite tourmalines. Indeed, values of 14-16‰ are often considered typical of hydrothermal quartz (Fisk 1986 after Levitian *et al.* 1975).

Combining the δD and $\delta^{18}\text{O}$ data for the tourmalines from this project with data from Taylor and Slack (1988) (Fig. 7.4), the pegmatite data plot in the range of massive sulphide deposit tourmalines, while the vein data is yet heavier.

Fig. 7.4
Oxygen and deuterium
(filled circles) and
fields. (Data also from
close to the field
higher on the

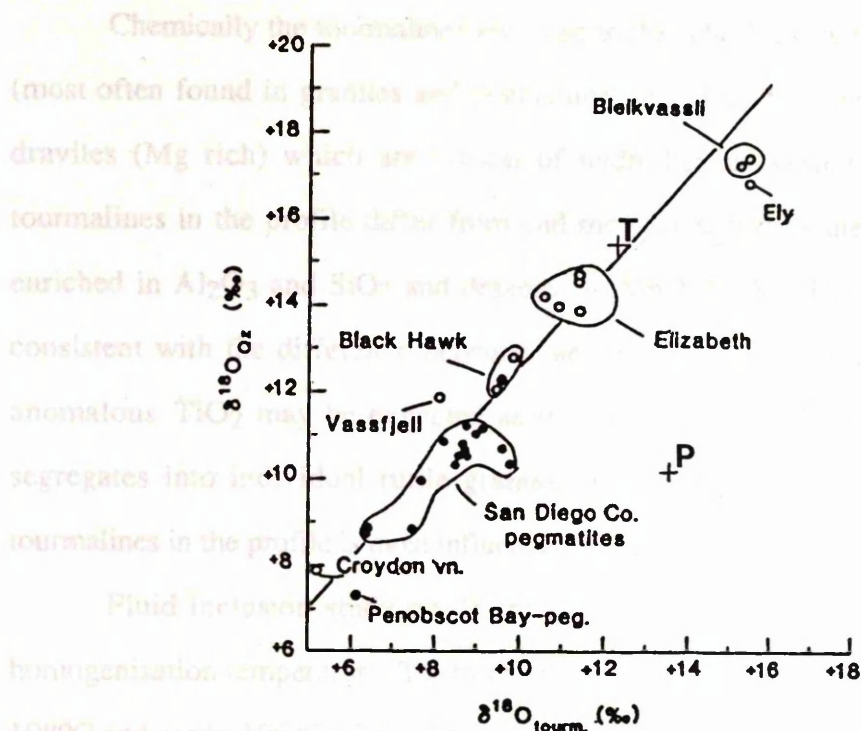


Fig. 7.3

A general linear correspondence between the oxygen isotope compositions of quartz and tourmaline from pegmatites (filled circles) and massive sulphide deposits (open circles) suggesting that tourmaline and quartz exhibit similar oxygen isotope exchange kinetics. (After Taylor and Slack 1984).

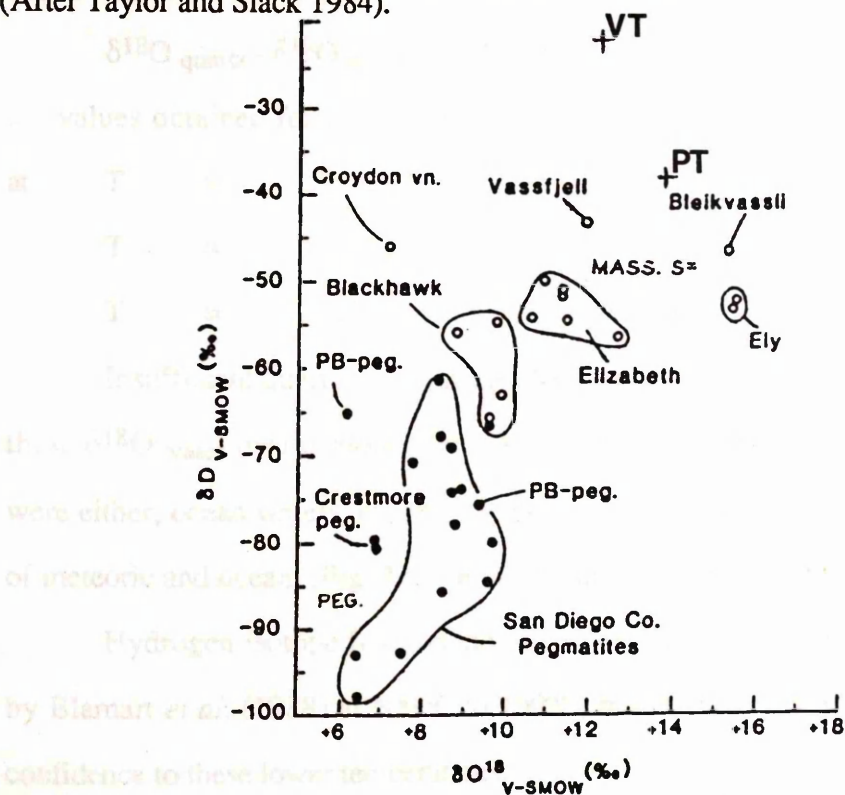


Fig. 7.4

Oxygen and hydrogen isotope compositions of tourmaline from igneous pegmatites (filled circles) and massive sulphide deposits (open circles). The data plot in distinct fields. (Data after Taylor and Slack 1984). The pegmatite data from this project plot close to the field for massive sulphide deposit tourmalines, while the veinlet data are higher on the graph.

Chemically the tourmalines are close to the schorl (Fe rich) end member variety (most often found in granites and pegmatites) (e.g. Fig. 5.10) and are therefore unlike dravites (Mg rich) which are typical of hydrothermal systems. Furthermore, the tourmalines in the profile differ from end member schorl as they are relatively more enriched in Al_2O_3 and SiO_2 and depleted in MnO , FeO_{tot} , CaO , Na_2O (and TiO_2) - consistent with the difference between the fresh and altered rocks. (The apparently anomalous TiO_2 may be expected as the TiO_2 released during biotite breakdown segregates into individual rutile grains). Hence, the chemical composition of the tourmalines in the profile is most influenced by the chemistry of the profile itself.

Fluid inclusion study on 38 inclusions in the veinlet quartz gave a range in homogenisation temperature, T_h , from $\sim 82^\circ\text{C}$ to 131°C , with a mean of 107°C , median 108°C and mode 106°C (Fig. 7.5).

Using the oxygen isotope quartz-water fractionation equation of Matsuhisa *et al.* (1979):.....

$$\delta^{18}\text{O}_{\text{quartz}} - \delta^{18}\text{O}_{\text{water}} = 3.34 \times 10^6 T^{-2} - 3.31 \quad (\text{T in Kelvin}).$$

.....values obtained for $\delta^{18}\text{O}_{\text{water}}$ are

at	T	=	82°C ,	$\delta^{18}\text{O}_{\text{water}}$	=	-7.72
	T	=	107°C ,	$\delta^{18}\text{O}_{\text{water}}$	=	-4.35
	T	=	131°C ,	$\delta^{18}\text{O}_{\text{water}}$	=	-1.68

Insufficient quartz was available for investigation of fluid inclusion δD , but from these $\delta^{18}\text{O}_{\text{water}}$ results alone, the most likely fluids involved in the quartz formation were either; ocean waters, ocean crust pore waters, meteoric or probably a combination of meteoric and ocean, (Fig. 7.6), certainly surface-derived fluids.

Hydrogen isotope fractionation between tourmaline and water was investigated by Blamart *et al.* (1988) at 500°C to 700°C , but their results cannot be projected with confidence to these lower temperatures.

Fig. 7.5

$\delta^{18}\text{O}_{\text{water}}$ vs T_h

(From data of Blamart *et al.*)

Interpretation

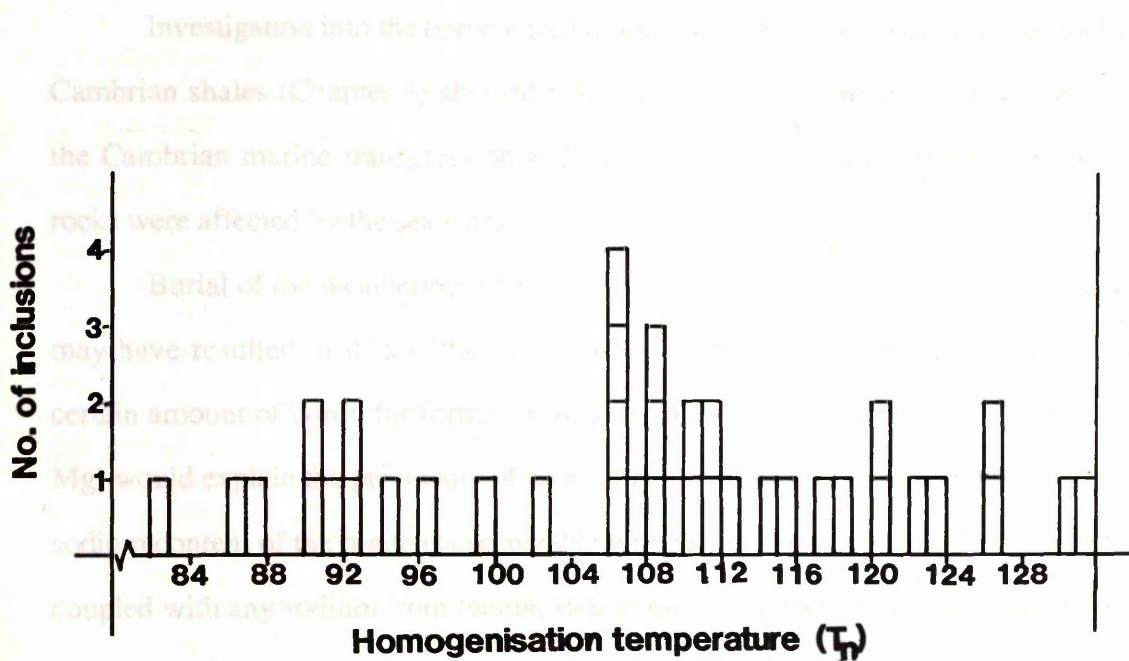


Fig. 7.5

Homogenisation temperature (T_h) for fluid inclusions in the veinlet quartz.

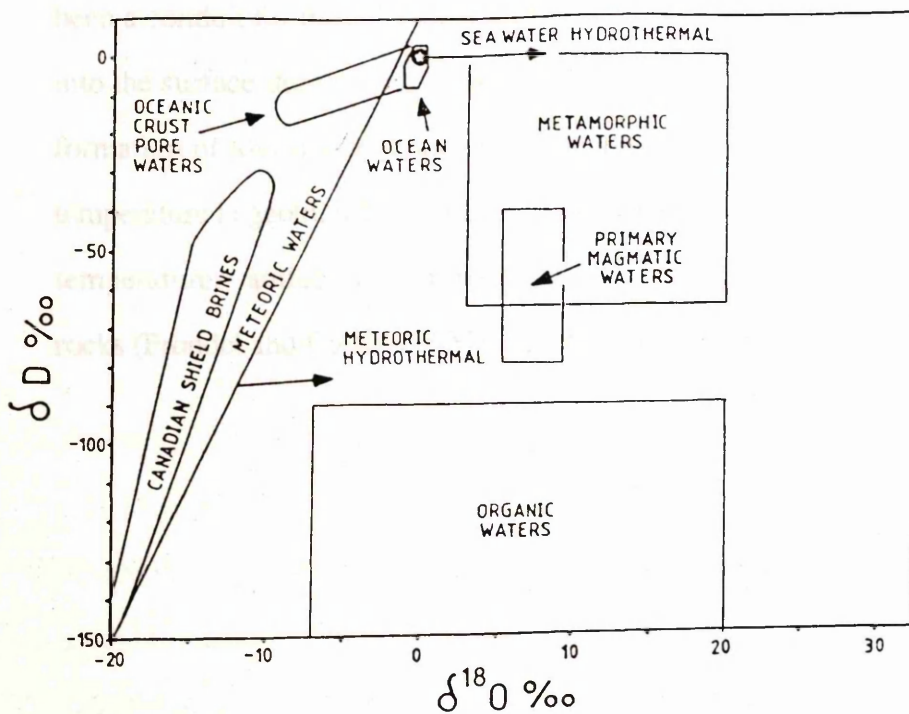


Fig. 7.6

$\delta^{18}\text{O}_{(\text{SMOW})}$ and $\delta\text{D}_{(\text{SMOW})}$ fields for naturally occurring waters. (From data of Sheppard 1986).

Interpretation

Investigation into the boron concentration of altered and fresh Lewisian rocks and Cambrian shales (Chapter 8) showed that boron was most probably introduced during the Cambrian marine transgression and hence tourmaline must have formed after the rocks were affected by the seawater.

Burial of the weathering profile under the progressively thicker sedimentary pile may have resulted in illites (the main host of boron (see Chapter 8, p 194)) losing a certain amount of boron for formation of tourmaline. The requirement of Fe (and some Mg) would explain the propensity of tourmaline to form adjacent to altering biotites. The sodium content of the pinites is comparable with that of the tourmaline and this, certainly coupled with any sodium from biotite, should satisfy the sodium requirement of the blue sun tourmaline, although absorption of sodium onto the clays during the marine transgression need not be discounted. The green tourmalines are slightly more Na-rich and may have formed in the sites of more sodic remnant primary phases. However, most of the green tourmaline occurred in a restricted zone of brecciation, which may have been a conduit for more Na-bearing fluids. Local expulsion of boron towards cracks or into the surface-derived fluids passing through the system could have brought about the formation of tourmaline in the veinlets, along with quartz at about 100 to 110°C. This temperature is geologically reasonable as tourmaline can crystallise over a wide range of temperatures; authigenic tourmaline occurs widely in unmetamorphosed sedimentary rocks (Fronde! and Collette 1957) and tourmaline is also a primary igneous mineral.

DISCUSSION

Mineral paragenesis of the alteration profile:

The sequence of alteration of the major primary phases; plagioclase, biotite, K-feldspar then quartz, is consistent with the stability series of Goldich (1938) for such phases during weathering.

The mineralogy and mineralogical sequence is also very similar to that found in other Precambrian palaeosols throughout the world (See Appendix 14). "Sericite" is generally the dominant phase (often equivalent to pinite, Allison *et al.*, in press) occurring in most, if not all, Precambrian palaeosols. Pyrophyllite and rutile also form secondary phases in these profiles and quartz is often present. Tourmaline, however, has not been recorded in any of the literature surveyed and appears to be peculiar to this profile. However, its presence is considered to be related to the combined effects of weathering, marine transgression and subsequent burial and not formed only due to weathering or weathering with later metasomatism. Like this profile, most Precambrian palaeosols are various shades of green and some authors report also yellows and greys. Maroons are reported in younger Precambrian, haematite-rich profiles (e.g. Holland *et al.* 1989). Little information on textural relationships of Precambrian palaeosols is given in the literature (and none in most papers), even although they are important when considering the alteration of primary minerals to the various secondary phases. However, in the early Proterozoic NAN palaeosol developed on a granodiorite protolith in Canada, G-Farrow and Mossman (1988) report that sericitization of the feldspars occurs mainly at crystal boundaries and twin planes and that rutile grains are clustered around areas of biotite alteration. They also show the slightly concave grain boundaries of quartz where it is being replaced by sericite, giving a scalloped edge to the quartz grain. Such textures are typical of the profile in NW Scotland. Certain textures of the opaque minerals (martitisation and rutile 'nests') in the profile in NW Scotland are found in both weathering and higher temperature environments. However, in either case they are indicative of formation in an oxidising environment.

The transformations from primary silicates to secondary clays involve mainly hydrolysis reactions, explaining the increase in H₂O content with weathering. The uptake of K⁺ into muscovite during weathering of plagioclase explains the initial increase in K₂O content, especially in plagioclase-rich precursors. However, K⁺ is lost during weathering of K-feldspars to muscovite so the trend is later reversed. Hence, in any precursor pegmatite or gneiss where K-feldspar is the only feldspar present and the dominant mineral, only a decrease in K₂O content would be observed. The loss in K₂O is greater higher up in the weathering profile, when kaolin became the major secondary phase during weathering.

The precursor weathering minerals proposed for this profile are illite and kaolinite. Although kaolinite is a common phase in modern soils, smectite, rather than illite, generally forms the dominant complex clay phase. However, Button (1979) considered illite to be the dominant complex clay in the profile on an Archean basalt, due to the alkaline conditions prevalent at that time, and Yaalon (1963) has suggested that prior to the appearance of land plants, K became fixed in illite, which was the dominant clay mineral. This would imply that illite may have been the main complex clay until the Devonian. Interestingly, however, kaolinite and illite are the major secondary phases in the "deep and highly leached" modern soil of Bahia, Brazil (Kronberg *et al.* 1979). Indeed, according to Grim *et al.* (1953), both kaolinite and illite may occur in pedalfers, while in pedocals, illite and montmorillonite are dominant. And the Bahia soil is a pedalfer. Hence, this suggests that the precursor weathering profile in NW Scotland may have been a pedalfer. This is consistent with the suggestion from the geochemical changes that it was a pedalfer.

The increase in K₂O content of illite with temperature during the illite to 2M₁ muscovite transformation recorded by Hunziker *et al.* (1986) and the similarity between pinite and Hunziker's epimetamorphic illites (p.151) suggest that prior to heating, the K₂O content of precursor illite was lower. Hunziker (1986) argued that many authors found a similar increase in potassium in illites/muscovites with increasing burial, better crystallinity or increasing temperature. However, he also cited Gavish and Reynolds

(1970) who did not find such a correlation. Hunziker *et al.* (1986) reasoned that this was because of growth in K-poor host rocks. Such an argument implies that the K-content of the muscovite/illite is dependent on the chemistry of the rock itself.

If a pinite precursor was poorer in K, then during the transformation to pinite, either: 1) K^+ ($\sim 2\%K_2O$) was added to the system from e.g. a fluid passing through, or 2) K^+ was provided for the muscovite by other reactions within the system which released K^+ , or a combination of both.

If a significant K-bearing fluid passed through the system during burial in the Caledonian, then the $\delta^{18}O$ of the feldspars in the basement should have been homogenised, and this has not occurred.

For the second option, the only viable possibility could be the release of K during formation of pyrophyllite. This is unlikely to have supplied the required K, as the amount of pyrophyllite is very small compared to the amount of pinite in the system, and as discussed in the pyrophyllite section (p.154), there are many places where pyrophyllite does not exist in pinite-rich rocks. However, although I would still advocate the kaolinite + quartz \rightarrow pyrophyllite reaction (p.152) for the formation of pyrophyllite from the reasoning given, it is possible that the muscovite \rightarrow pyrophyllite reaction may also have occurred at elevated temperatures and contributed some K^+ to the system.

The intimate textural relationships between pinite and the primary minerals suggest that during the formation of pinite, there was further decomposition of the original minerals. However, since both plagioclase and K-feldspar show this relationship (as well as quartz and biotite), it is not known if more K_2O would be released to (as in K-feldspar \rightarrow muscovite) or taken up from the system (as in plagioclase \rightarrow muscovite).

Seawater prior to the development of land plants had a high a $[K^+/(K^+ + Na^+)]$ (Buyce and Friedman 1975). The possibility that K^+ ions from the seawater were adsorbed onto the clays during the marine transgression and later incorporated into the illite/muscovite structure during heating may also be considered.

Comparison of authigenic K-feldspar from the sub-Cambrian profile in NW Scotland with that from profiles in the N. American mid-continent:

The reddening of alkali feldspars in sub-Cambrian basement rocks has been reported from a large area in North America (e.g. Doe *et al.* 1983, Mensing and Faure 1983, Sheih 1983, Duffin 1989, Harper *et al.* 1991). Hypotheses for the origin of these feldspars and other authigenic feldspars found in the basement will be discussed, in light of the $\delta^{18}\text{O}$ isotopic investigation of sub-Cambrian uppermost basement K-feldspar of NW Scotland in this project.

Authigenic K-feldspar in sub-Cambrian alteration profiles has been identified in six different states of the mid-continent of the U.S.A. with occurrences up to 1200km apart (Duffin 1989). It has also been recorded in Ontario, Canada (e.g. Harper *et al.* 1991) and a genetic link has been suggested due to their widespread occurrence (Duffin 1989). The profile below the Cambrian unconformity is \sim <1 to 8m thick (Duffin 1989) and formed on basement igneous and metamorphic protoliths. Authigenic feldspar occurs throughout the profiles and is in the form of wholly authigenic rhombs, overgrowths, vein fillings etc., but also in the form of replacement of primary phases, including K-feldspar, where haematite inclusions may give a red colour to the feldspar (e.g. Sheih 1983).

Mensing and Faure (1983) report Rb/Sr ages of 599 ± 69 Ma for "salmon pink" authigenic feldspar after primary K-feldspar from Scioto County, Ohio, while Duffin (1989) reports whole rock Rb/Sr ages from immediately beneath the unconformity of 554 ± 45 Ma from Lake County, Illinois. Duffin (1989) also reports K/Ar ages of 549 ± 18 Ma for wholly authigenic K-feldspar (in various forms) from Illinois. Both this feldspar and wholly authigenic feldspar from Lake County, Ohio gave $\delta^{18}\text{O}$ of 17.5. Harper *et al.* (1991) also report high values from Ontario, Canada with $\delta^{18}\text{O}$ of K-feldspar from 18.4 to 21.4‰. However, Sheih (1983) determined $\delta^{18}\text{O}$ of 8.8‰ from 1.8m below the unconformity in Stephenson County, Illinois. Sheih (1983) and Mensing and Faure

(1983) consider that the authigenic feldspar formed by low-T hydrothermal alteration from fluids emanating from the Cambro-Ordovician sedimentary sequence above.

During Mensing and Faure (1983) dated 14 alkali feldspar concentrates from various depths in one drill hole. The well intersected 11.3m of Precambrian granitic gneisses. Samples in the upper 6.4m of basement core were reported as severely altered, containing: 60% salmon-coloured K-feldspar, biotite, magnetite, apatite, chlorite, haematite and limonite and no plagioclase, with calcite and dolomite in fracture-filling veinlets. Below 7.7m the rocks were relatively fresh, with the major minerals including alkali feldspar, plagioclase, quartz, hornblende and biotite.

In fact Mensing and Faure (1983) report Rb/Sr ages of 1162 ± 11 Ma for the fresh basement material and 599 ± 69 Ma for the salmon pink adularia. They concluded that the salmon pink adularia formed by reconstitution of primary clays (after weathering), with this K-feldspar forming under low-temperature hydrothermal conditions by the reaction of the clays with brines derived from the overlying upper Cambrian Mount Simon formation.

Conclusion This interpretation is clearly contrary to the weathering hypothesis for the change in the feldspars in NW Scotland. Mensing and Faure (1983) knew from petrological evidence (e.g. purity of K-feldspars and cathodoluminescence) that the feldspar was authigenic. They subsequently arrived at the hydrothermal interpretation, based on these age determinations, all from one well. There are two reasons why I would doubt this interpretation. Firstly, this age is not Cambrian (let alone upper Cambrian) but Precambrian according to the most recently published time scales (e.g. Harland *et al.* 1988, where the Precambrian/Cambrian boundary is at 570 Ma, and even younger, ~525 Ma if the preliminary results of Compston 1990 are substantiated). Secondly, in light of the results of this study, I suggest it may be very significant that interpretation was made from only one well core. Conclusions based on results from one core preclude any inter-suite comparison, which was fundamental to the hypothesis proposed as a result of this project. This project notably involved no age determination of the red feldspars but highlighted the direct relationship between the reddening/alteration of the K-feldspar and

the degree of weathering (a Precambrian event). Hence, it could be suggested that the salmon pink feldspars in Ohio studied by Mensing and Faure inherited their appearance during weathering. The Rb/Sr ages of Mensing and Faure (1983) would certainly support this hypothesis.

Doubts about this antithesis could be raised in light of the large error bar associated with the 599 Ma age (i.e. ± 69 Ma) and the possibility that the age of the authigenic K-feldspar could be younger (due to possible mixing of authigenic K-feldspar with remnant primary phases, as mentioned by Mensing and Faure 1983). However, in view of the ages and similarity with K-feldspar from NW Scotland, a weathering influence on their origin is still considered most likely.

The monotonic increase in $\delta^{18}\text{O}$ of alkali feldspars from $\delta^{18}\text{O} = 7.1$ at 70m below the unconformity to 8.8 at ~ 1.8 m below the unconformity in Stephenson County, Illinois (Sheih 1983) is interpreted by Sheih (1983) as due to the effect of similarly low-T hydrothermal fluids at the same time and from the same source as those described by Mensing and Faure (1983). However, I would suggest this is unlikely. The $\delta^{18}\text{O}$ is expected to have been higher if it was due to the same widespread event "that affected much of mid continent North America", Duffin (1989), which caused the $\delta^{18}\text{O} = 17.5$ of authigenic feldspar from rocks in both Illinois and Ohio, (Duffin 1989). The increase in $\delta^{18}\text{O}$ would also be expected to have occurred over a shorter depth range, as the other profiles described by Duffin (1989) and Mensing and Faure (1983) were all less than 12m deep. The variation over such a large depth would also militate against a weathering origin similar to that in NW Scotland.

The 549 ± 18 Ma age of Duffin (1989) for the wholly authigenic K-feldspar from Illinois is younger than the 599 ± 69 Ma age of Mensing and Faure (1983). However, the 549 Ma age is for all authigenic K-feldspar including overgrowths, rhombs etc., while the 599 Ma age of Mensing and Faure (1983) is restricted to salmon pink replacement primary K-feldspar indicating that the reddening of the feldspar may have been earlier than the formation of overgrowths, rhombs etc.. Whether the 549 Ma age is young enough to represent the effects of waters associated with the upper Cambrian Mount

Simon sandstone, however, I do not know, as there is much contention over the lower limit to the Cambrian era (see e.g. Harland *et al.* 1990).

Such abundant K-feldspar in the form of rhombs, overgrowths etc., as described from Ohio (e.g. Duffin 1989), was not observed in NW Scotland. However, the reddening of the primary K-feldspars was. Considering this, the differences in authigenic K-feldspars and the age differences (above), I propose that the reddening of the primary K-feldspars in the sub-Cambrian profiles of the North American mid-continent occurred or was influenced during weathering. The widespread development of the K-feldspar overgrowths, rhombs etc. was probably due to a later event, the effects of which were either a) patchy, b) varied from place to place or c) both (from $\delta^{18}\text{O}$ values discussed).

CHAPTER 8**GEOCHEMICAL LINKS BETWEEN THE
ALTERATION PROFILE AND CAMBRIAN
SHALES OF NW SCOTLAND****INTRODUCTION**

In this chapter, the proposed link between the genesis of authigenic feldspar found concentrated in dark grey argillites in the overlying Cambrian succession, and the alteration profile, as proposed by Russell and Allison (1985) is investigated.

The black shales of the Cambrian clastic succession are concentrated in part of the Fucoïd Beds member of the An t-Sron formation ~175m to 200m above the unconformity (Fig. 8.1). This member consists mainly of interleaving layers of dolomite, argillaceous dolomite and argillite. The shales are up to ~7m thick (from McKie 1988), and are composed predominantly of authigenic K-feldspar. Occasional detrital K-feldspar and quartz clasts (~20 to 50µm diameter) and rarely mica flakes are also present. The authigenic feldspar occurs as overgrowths on K-feldspar clasts (Plate 8.1a) and as a replacement of the mud, surrounding detrital grains (Plate 8.1b).

The K-feldspar rich shales contain ~10 to 12wt.% K₂O (average 11.5wt.%, Bowie *et al.* 1966). This is grossly different from the world average shale, with a clark of only 3.24wt.% K₂O, but similar to other shales of this age. This K₂O enrichment makes these rocks a significant potash source and they are currently being quarried on a small scale near Loch Assynt (at [NC 250 157]) for use as a slow-release source of K in fertiliser (see Bowie *et al.* 1966). The most recent research has shown that a stimulatory effect on growth is observed when adularia is added in addition to standard fertiliser (i.e. K₈SO₄) (Erstad 1990).

Black, authigenic feldspar-rich shales and green illitic shales are also found as thin <10cm thick layers between the massive quartz-cemented quartz arenite beds of the

Lower Member and Pipe Rock of the Eriboll Sandstone Formation. These layers are very much thinner and are laterally discontinuous.

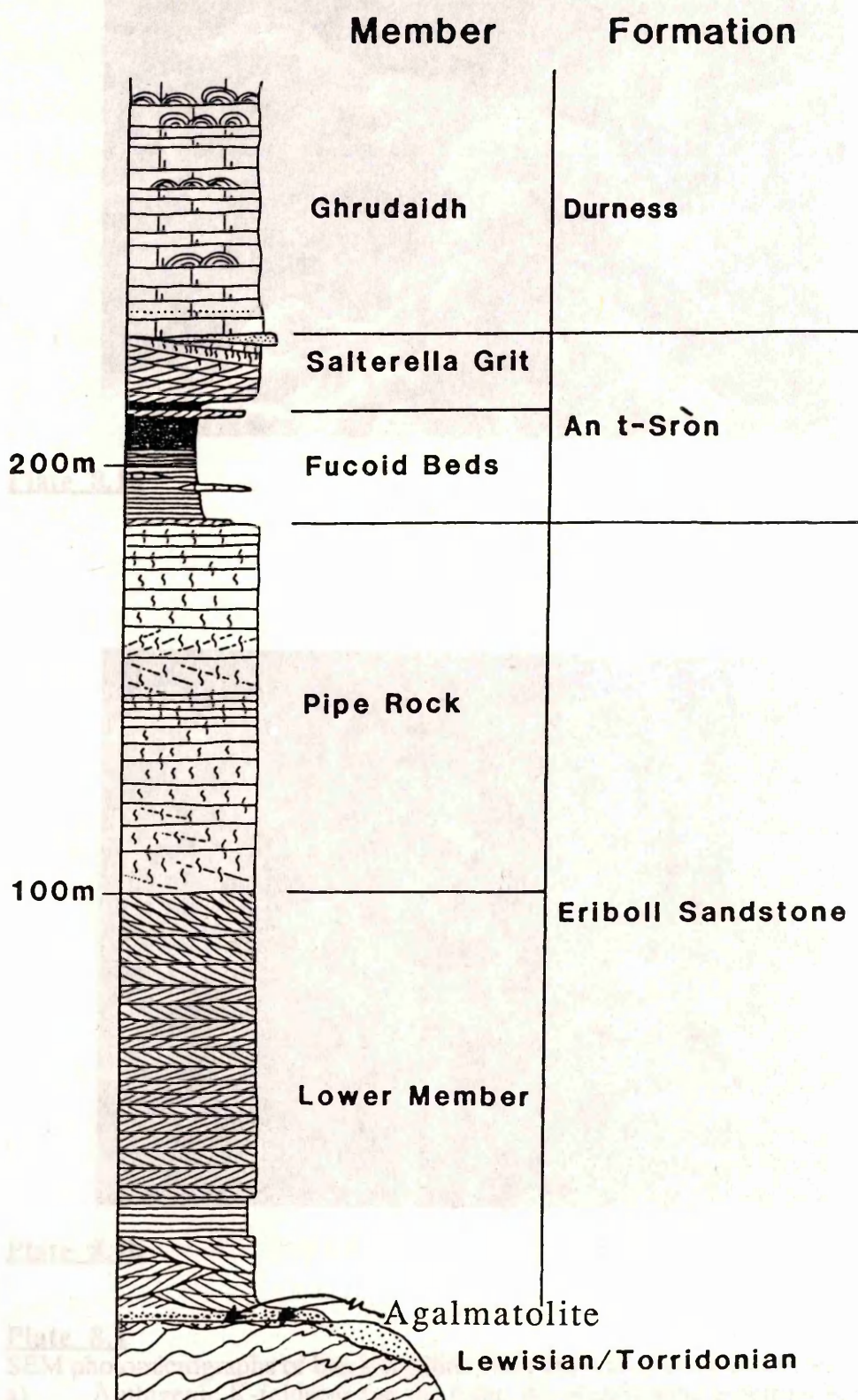


Fig. 8.1 Stratigraphic log of Cambrian clastic sediments (after McKie 1988).

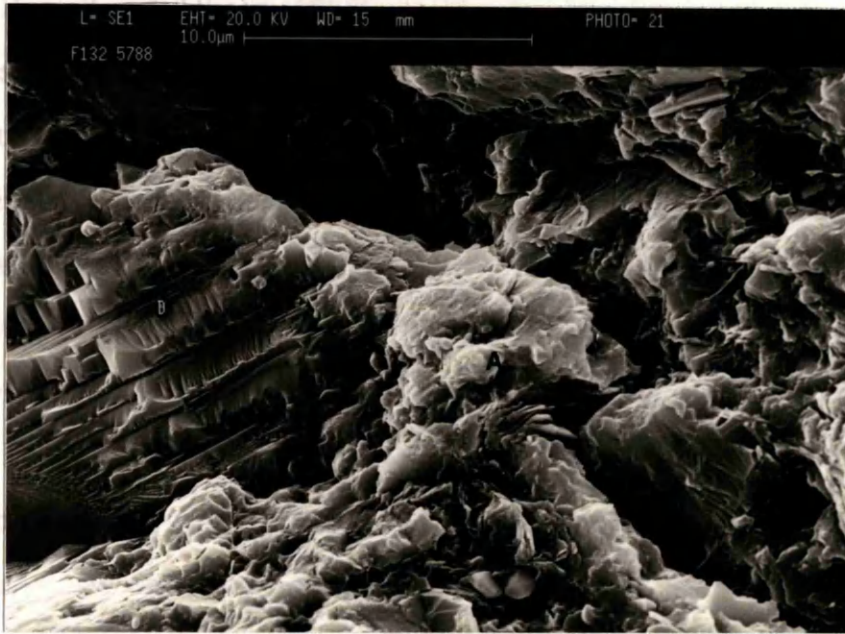


Plate 8.1a

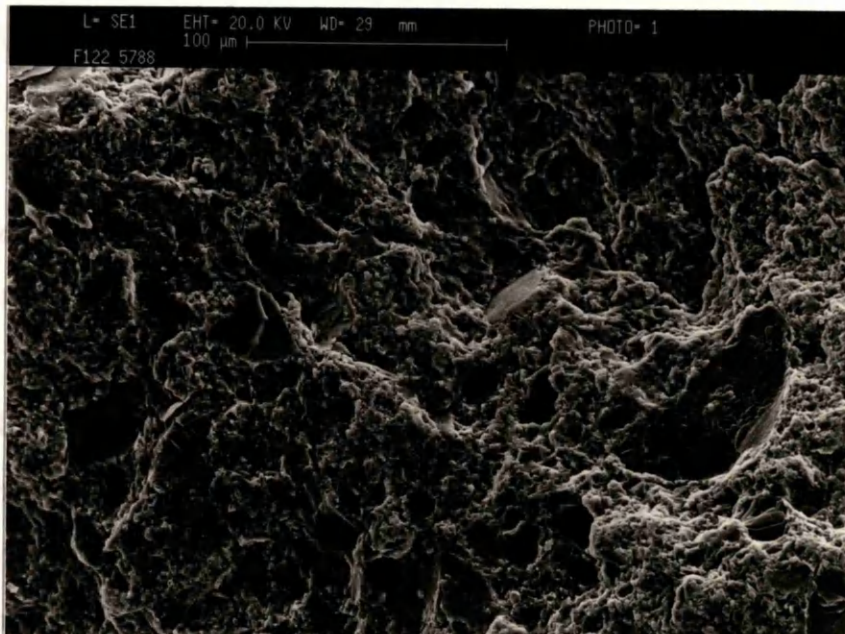


Plate 8.1b

Plate 8.1

SEM photomicrographs of black argillitic shale from the Fucoïd Beds member.

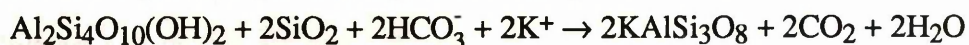
- a) Authigenic K-feldspar (on the right, A) overgrowing a detrital K-feldspar clast (on the left, D).
- b) General view of fine grained authigenic feldspar, the dominant phase, surrounding detrital grains.

Mica: Russell and Allison (1985) consider that the deeply weathered Precambrian landmass was the source of ions for the authigenic K-feldspar of the Fucoïd Beds. They suggest that ground and river waters carried "ionic potassium, ionic or colloidal aluminium as well as silica sufficient to produce chemical precipitates of feldspar in the evaporating, alkaline lagoonal waters in Fucoïd Beds times". They propose that the intermittent green shaly layers in the Eriboll Sandstone were derived from green muscovite or illite of the soil developed on a land surface of Lewisian Gneiss Complex.

Sigillite: McKie (1988) considers that both the authigenic K-feldspar of the black shales of the Eriboll Sandstone and Fucoïd Beds formed due to "reverse weathering" (Mackenzie and Garrels, 1966) of "detrital muscovite early in the depositional history". While he favours formation of muds of the Eriboll Sandstone in back-barrier lagoons, he argues that those in the Fucoïd Beds were transported to and deposited on the shelf on which the Fucoïd Beds member formed. The green muscovite-rich units were unaffected by this process of reverse weathering. McKie (1988) considers the reaction (of Kastner and Seiver 1979):



for the conversion of mica to potassium feldspar, which is chiefly dependant on the dissolved silica and K^+/H^+ ratio of the pore water. Russell (1985), however, proposes "smectite" reacting to authigenic feldspar, advocating the reaction:



A weathering source of ions for formation of Lower Paleozoic authigenic K-feldspar-rich shales has also been proposed by Buyce and Friedman (1975).

Feldspar: In the previous chapters, it was shown that the alteration profile is a palaeosaprolite. In this chapter, the mineralogical and field evidence are outlined and chemical criteria are presented which support the proposed link between this palaeosol and the Cambrian shales. Work on age determination of Cambrian shales, given in Chapter 9, provides further supporting evidence.

Mineralogical and Field Evidence

The green muscovite/illite material, most highly concentrated in interleaving green shales, is also present in the matrix in the quartz-rich sandstones. Clasts of this material have been found in the basal conglomerate of the Lower Member, immediately above the unconformity (e.g. [NC 4426 6387], Map 1 and [NC 4055 6110], Map 2). The green colour is very similar to some pinite in the agalmatolite beneath the unconformity. Significantly, some XRD traces of the green shaly layers are identical to that of pinite. In others, the subordinate peaks are more suppressed (see McKie 1988, p.199). This information, together with the close proximity of the palaeosaprolite, which field evidence has shown to be an extensively developed horizon, is supporting evidence to link the provenance of the minerals of the green shales to the soil profile (as concluded by McKie 1988). Further evidence for the link with the green shales is in the geochemistry.

K⁺ supply

Results of the geochemical investigation (recorded in Chapter 6) indicate that K⁺ ions have been lost towards the top of the alteration profile. The trend indicated that such loss would have been even greater in the now eroded top of the profile, giving rise to groundwaters enriched in K⁺ and Al³⁺ ions. Erosion of the upper horizons would also result in significant alumina being transported in ground and river waters. Hence the weathered Lewisian could well have supplied the K⁺ and alumina for the authigenic feldspar precipitation as was proposed by Russell and Allison (1985).

K/Rb RATIOS IN CAMBRIAN SHALES, AGALMATOLITE AND PRECAMBRIAN ROCK UNITS

K/Rb ratios for different groups of Scottish Precambrian rock units are all consistently low (Figs. 8.2 and 8.3), with results from various authors (Fig. 8.3) and from this study (Fig. 8.2) corroborating. Indeed, the average crustal abundance of K/Rb is also very low (i.e. 230, see Beeson *et al.* 1989). However, rocks from the alteration profile and shales from various members of the Cambrian succession all group together in a quite separate and distinct area (Fig. 8.2 and Appendix 15).

Hearn *et al.* (1987) state that igneous feldspars generally have K/Rb ratios below 440, while authigenic feldspars almost always have values above this. However, Hearn *et al.* (1987) obtained K/Rb values around 1300 for their authigenic feldspars - clearly much higher (see Figs. 8.2 and 8.3). The K/Rb values of modern soils also differ from those of the agalmatolite and Cambrian shales. Of the analyses reported by Kronberg *et al.* (1987b) from three weathered regions in Brazil, all nine soil samples from the intermediate to advanced weathered Bahia region and the twelve from the advanced weathered Amazon region, none gave K/Rb ratios in the same range as the agalmatolite and Cambrian shales (i.e. $440 < \text{K/Rb} < 860$). Ten of the sixteen extremely weathered Goias samples also gave K/Rb values outwith this range. And of the six within, three gave Rb values of 1ppm - leaving much room for error.

The modern sand, silt and clay sized sediments listed by Taylor and McLennan (1985), from the Barents Sea and Gulf of Paria, also have low K/Rb ratios (between 144 and 296). Hence the rocks of the palaeosol and the Cambrian shales have distinctive K/Rb values.

The agalmatolite samples lie mostly within the field of K/Rb of the green shales (Fig. 8.2). The greater variation in K/Rb values of the green shales is most likely due to varying amounts of detrital K-feldspar in the green shales. Indeed, these green Cambrian rocks vary from shales to shaly sandstones (wackes, Pettijohn 1975). Together with the evidence cited on p.180, this close relationship between the K/Rb of the green shales and

agalmatolite, highlighted by their significant difference from all other Precambrian rock units investigated, recent sediments noted and the authigenic K-feldspar of Hearn (1989), indicates the provenance of the green shales as the soil profile.

The K/Rb of the black shales from the Lower Member, Furoid Beds and Salterella Grit also lie within this field for the green shales (see p184). Hence, they too have a close link with the agalmatolite. With this information and again considering the widespread development of the illitic saprolite and furthermore the lack of primary muscovite in Lewisian gneisses (Sutton & Watson 1951), I propose that the "detrital muscovites" of McKie (1988) in the reaction of Kastner and Seiver (1979) (p.179) were illitic clays from the soil zone. This indicates a clastic, as well as chemical link between the soil and the Furoid Beds.

Fig. 8.2

$K_2O(\%)$ vs Rb (ppm) of Scottish Precambrian rocks and Cambrian sediments determined in this project.

p183 -Includes individual data with summary overlay showing fields for different rock units.

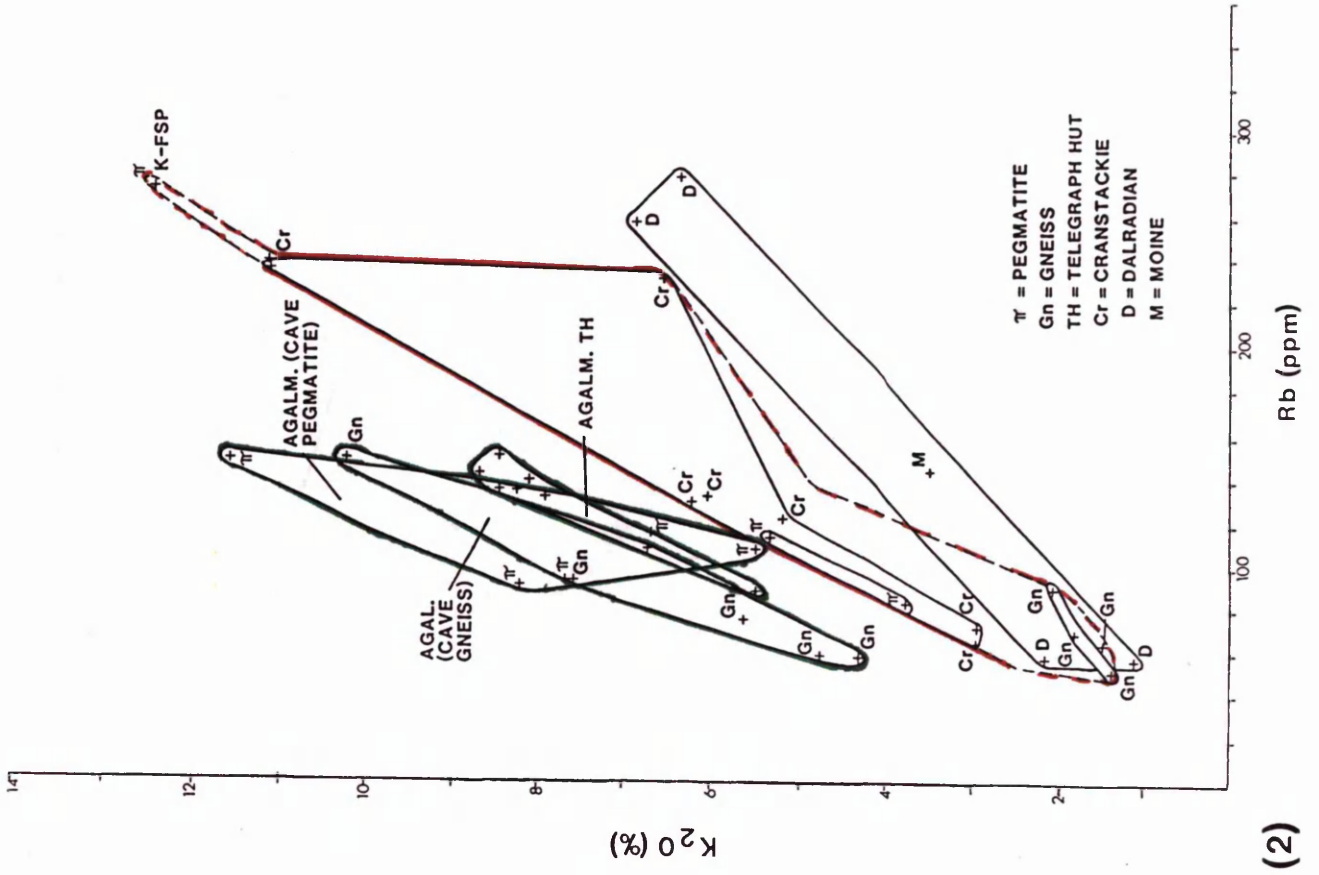
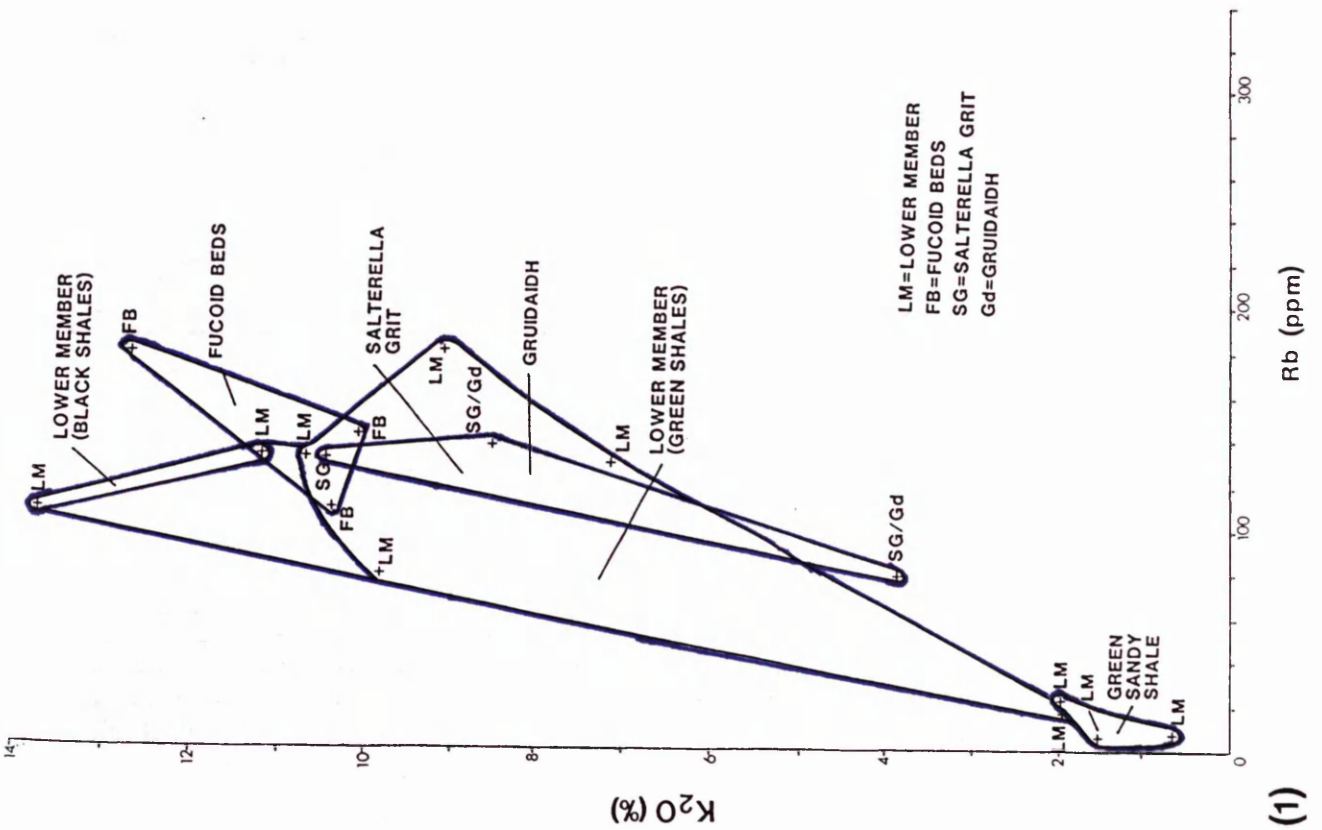
p184 -Graphs highlighting data points given on p183: 1) from various members of the Cambrian succession and 2) agalmatolite, unaltered Lewisian and Dalradian and Moine results.

Blue lines - surrounding Cambrian sediment values

Green lines - surrounding agalmatolite values

Red lines - surrounding unaltered Lewisian values

Black lines - surrounding Dalradian and Moine values.



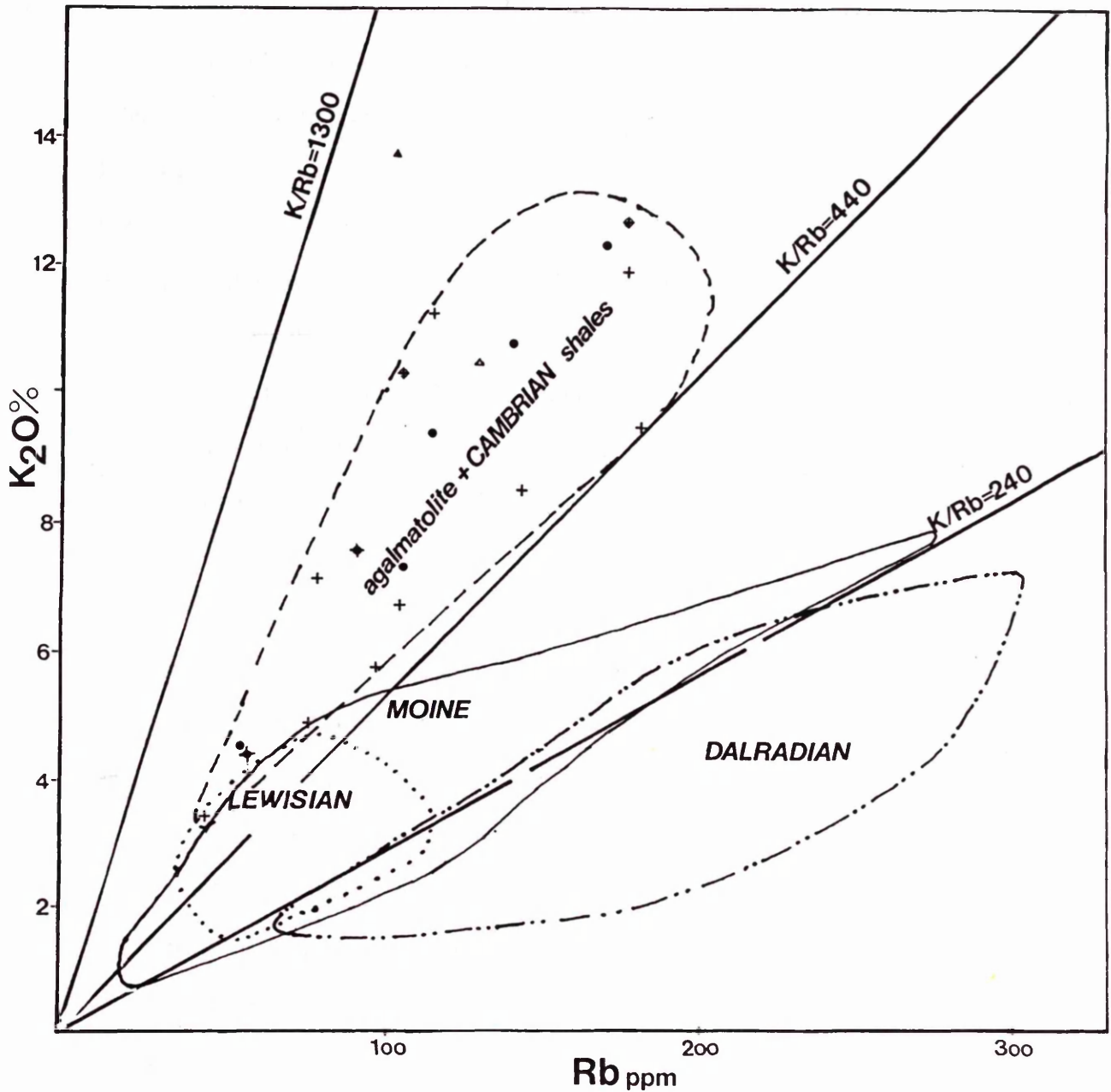


Fig. 8.3

K_2O (%) vs Rb (ppm) of Scottish Precambrian rocks and Cambrian sediments. (Lewisian, Moine and Dalradian data from Holland and Winchester 1983 and Rock *et al.* 1986. Cambrian shales and agalmatolite data include values from Bowie 1966 and Cardenas 1986 respectively).

BORON

Introduction

The boron content of the Lewisian is very low (cf. Plate 8.2). Indeed, no reference is made to tourmaline, the major boron bearing phase of metamorphic rocks, in Lewisian rocks from the whole area of interest in the NW Highlands 1907 memoir (Peach *et al.* 1907); the only references to Lewisian tourmaline being in rocks associated with the Letterewe limestone, NE of Loch Maree, much farther (~50km) south. Hence, the peculiar development of secondary tourmaline at the top of the alteration profile, together with the tourmaline/quartz veinlets which penetrate the profile, is of great interest. It suggests that the boron content of the altered profile is anomalously high, with this element playing a significant role during the alteration of these rocks to their present state. However, boron is also enriched in the Cambrian succession (Plate 8.2 and cf. IGS 1982). In light of the link between the soil and overlying shales, the fact that both are enriched is intriguing.

The boron concentrations of both rocks of the alteration profile and Cambrian shales were determined, with the 3-fold purpose of ascertaining; 1) if there is an enrichment at the top of the alteration profile, 2) if there is any similarity in boron concentration between the altered profile and the Cambrian shales, and 3) with the hope of elucidating the provenance of the boron ions. The results show just how similar the concentrations of boron are between these two rock groups.

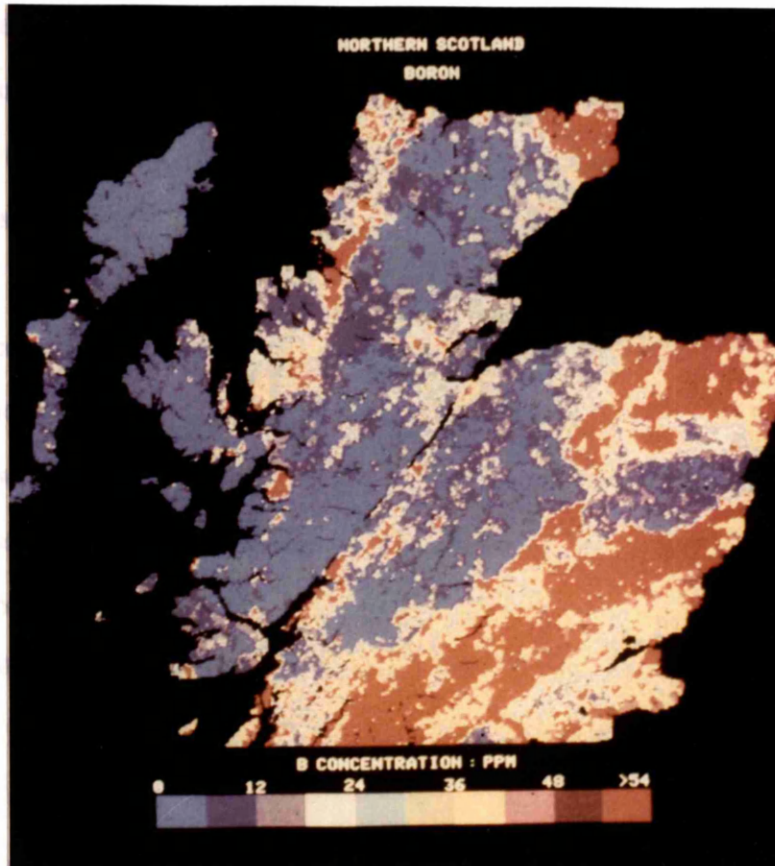


Plate 8.2

Boron concentrations over Scotland. (Stream sediments sampled at a density of 1 per 1km²).

Map by IGS (1982).

Methodology

The approach used to determine the boron content of the rocks was that of Walsh (1985) based on fusion with potassium carbonate and measurement by inductively coupled plasma (ICP) spectrometry. His technique is essentially a slight modification of the "traditional" fusion method using sodium carbonate. Walsh argues that potassium carbonate is as effective as a flux for boron minerals, with tests confirming no evidence of a significant boron loss during fusion. Indeed, experimental results of Walsh (1985) demonstrate that even when boron occurs in a refractory phase there is no substantial loss. The fusate is leached with warm water since boron is soluble in the warm water. Many of the major constituents of silicate rocks do not dissolve and are removed by filtration or centrifusion. The main advantage of using potassium carbonate flux is that the bulk of the flux is easily removed by adding perchloric acid. Potassium perchlorate is relatively insoluble in cold water and can be removed after centrifusion. The boron remains in solution and is then determined by ICPS. The full sample preparation procedure, based on that from Walsh (1985), together with the ICPS operating conditions (Walsh 1985) are given in Appendices 16a & b. Walsh (1985) quotes a sensitivity of $1-2\mu\text{gg}^{-1}$ as a realistic working detection limit.

Analyses and determination of Bppm from intensity values determined by ICP

Reproducibility of results was tested by comparing analyses of distilled water and blanks (Appendix 16c). Two standards were analysed at both 4 and 40ppm B and subsequently the 4ppm sample of the most reproducible standard was analysed periodically throughout and at the end of the run. Four blanks and four known standards were analysed at the beginning and an individual standard after every three samples run, to check for accuracy and precision of results. A blank was also run at the end (Appendix 16c).

With the given intensities (Appendix 16c) the values of Bppm (Appendices 16c & e) were determined using the equation given in Appendix 16d.

Samples

Samples whose boron concentrations were determined include:-

- (1) fresh and altered rocks from the cave suite [NC 438 661].
- (2) typical Lewisian gneisses and pegmatite K-feldspar separate, and,
- (3) shales and shaly sandstones from each of the Cambrian members.

Results

The whole rock concentrations of boron increase towards the unconformity with samples from $\geq 14.7\text{m}$ below the unconformity showing no enrichment over unaltered Lewisian rocks or K-feldspar separates (Fig. 8.4). In the gneiss suite, 4688 was duplicated twice and H once. The t-test (Appendix 3) was applied and 4688 can be considered different from 4788 at 95% confidence level and G from H with 90% confidence. The Cambrian samples; 1589, 1189 and 0689 have less boron as they are quartz rich. However, the other shales have boron concentrations within the range of marine mud (measured in this experiment and standard, Walsh 1985) and pelagic clay (Taylor and McLennan 1985). Indeed, all the results above 14.7m below the unconformity and excepting 0689 lie within the wide range of boron concentrations of deep sea sediments given by Kronberg *et al.* 1986 (Fig. 8.4). The most enriched shales have similar concentrations to the most altered pegmatites and gneisses.

There appears to be a close relationship between B and Al_2O_3 in the rocks (Fig. 8.5), with both increasing towards the unconformity and with decreasing Al/B in this direction (Figs. 8.5 & 8.6). However, the fresh K-feldspar separates have the same B concentration as the Lewisian whole rocks, even though they have higher Al contents.

In the Cambrian shales there is also an increase in boron content with aluminium. The Cambrian shale analyses, apart from 0689 and 0289u (carbonaceous), plot between $Al/B = 485$ and $Al/B = 687$ (Fig. 8.5). Interestingly, the most altered gneisses and pegmatites also plot in this range. Considering the black (more authigenic K-feldspar rich) and green (more illite/muscovite rich) shales separately, it is seen that the black shales all have higher B/Al than the green shales (Fig. 8.6). The agalmatolite results straddle these two groups.

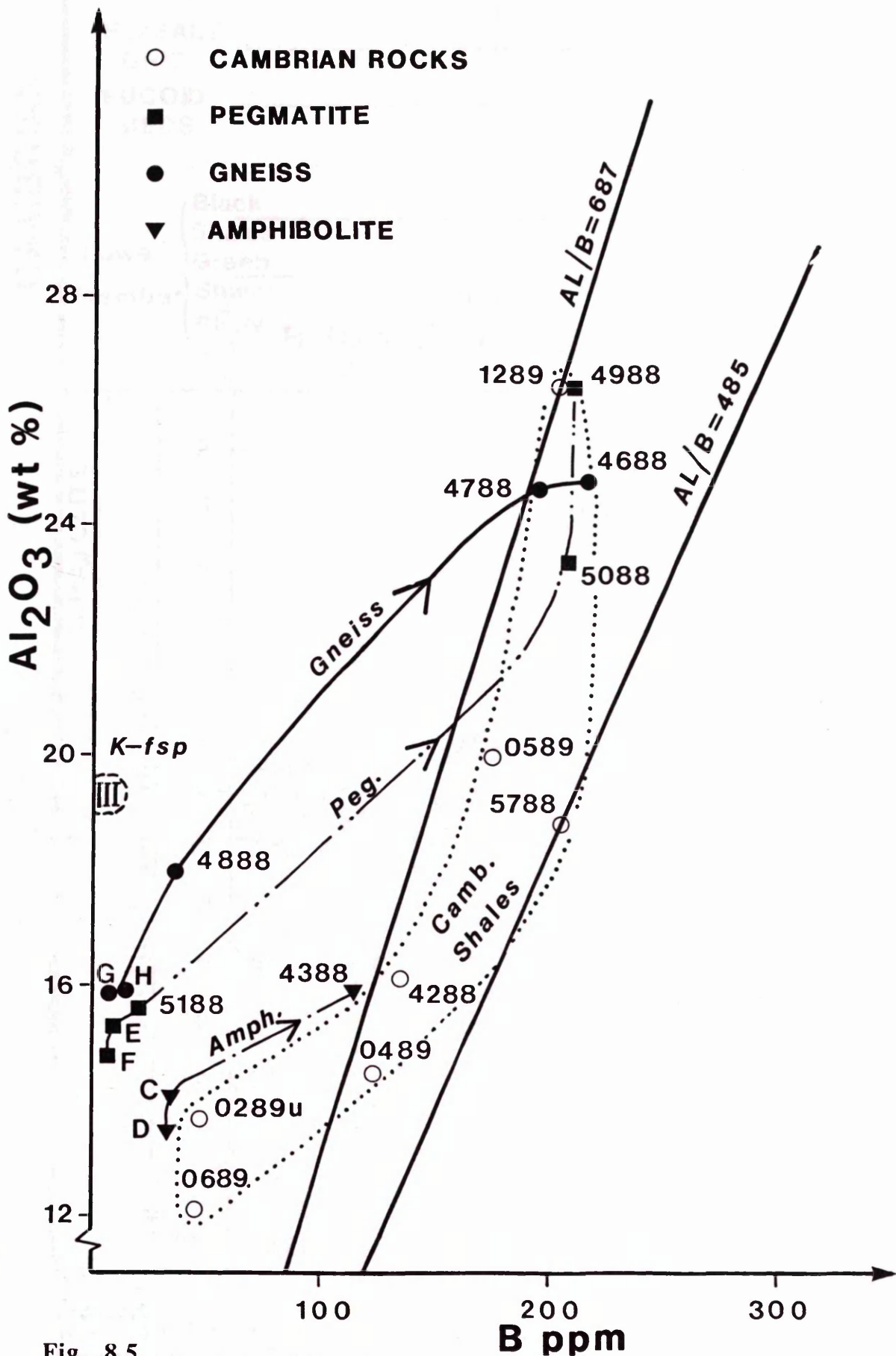


Fig. 8.5

Boron (ppm) vs Al_2O_3 (wt%) for altered and fresh sub-unconformity rocks and Cambrian shales.

Lines join samples from individual suites and arrows point in the direction of increasing alteration.

Interpretation

In all the samples analysed, only one contained visible tourmaline (4688). Hence, boron must also be concentrated in another phase or other phases in these rocks. Boron may be absorbed by illites formed from weathering due to later absorption from seawater (or by simultaneous incorporation of boron into the illite/mica lattice during its formation) (Harder 1961). Boron is absorbed onto the clay then taken into the tetrahedral sites (Wedepohl 1974). Indeed, Ethier and Campbell (1977) report that "the maximum boron concentration in a secondary mineral occurs in illite". Hence secondary illitic clays after weathering (before pinite) would have provided appropriate sites for boron ions to concentrate. Also, authigenic K-feldspar from saline, alkaline lakes may contain large concentrations of boron (>1000ppm and up to 5000ppm) (Sheppard and Gude 1973).

Towards the unconformity the proportion of the whole-rock Al content contained in pinite (illite) to primary feldspar increases, thus explaining the concomitant rise in boron concentration. The K-feldspar separates, although containing more Al_2O_3 than the other fresh Lewisian samples, have the same B content as the aluminium is associated with primary feldspar in both cases.

In the Cambrian rocks, the green shale (1289) contains as much boron as the most boron-rich black shale (5788) (Fig. 8.4). However, the black shales have higher B:Al ratio than the green rocks (Fig. 8.6). This is most likely because of a greater proportion of detrital feldspars in the green shale (1289). It is also possible that the different phases accommodated significantly different boron concentrations, although this is less likely due to the similarity in B:Al ratio in the black shales and the sub-unconformity rocks.

Comparing the analyses of agalmatolite and Cambrian shales, the very similar Al/B ratio between the most altered gneisses and pegmatites (<9m below unconformity) and most of the shales (Fig. 8.5) would imply the same source for boron in both these rock groups. Boron may have been introduced; 1) during the weathering process, 2) during a later B metasomatic event, 3) from the seawater.

As boron is not known to be enriched in weathering profiles especially of intermediate to advanced stages, and as tourmaline or other boron minerals are not characteristic features of weathering profiles, either modern or Precambrian, it is unlikely that boron was included in the clay structure during weathering. Indeed, from nine analyses of intermediate to advanced weathered rocks containing mostly kaolinite and illite from Bahia, Brazil, (Kronberg *et al.* 1979), none yielded as high boron concentrations and all had Al/B ratios >1000.

Although a hydrothermal/boron metasomatic event cannot be ruled out on the grounds of the boron analyses, the evidence from other investigations on tourmaline etc. would weigh heavily against it. Nevertheless, the boron source was almost certainly the same for both the weathered profile and the shales, due to the remarkably similar Al/B ratios. (Indeed in all 37 analyses from intermediate to advanced, advanced and extremely weathered rocks of modern soils from three areas in Brazil (Kronberg *et al.* 1979) none had Al/B between 485 and 687 ppm; 32 ranged from 765 to 76,537 (mean 17,649) and five from 362 to 483 (mean 427)).

However, both the sub-unconformity rocks and the Cambrian shales were affected by seawater. Boron in illites and dioctahedral micas may be attributed to incorporation of boron from seawater (Harder 1961) (and indeed, most of Harder's (1961) experiments were on illites as weathered relics). Also Reynolds (1965) reported anomalously high boron levels for illites affected by Proterozoic seawater. Hence, it is likely that the boron may have been incorporated from the seawater. As the boron concentrations in the most altered rocks and shales lie within the range of "marine" and "pelagic" mud (Fig. 8.4), and since the Al/B ratio for the pelagic mud is smaller than for the altered rocks and shales, the seawater obviously has the capacity to provide the boron requirement. (Even the boron concentration of the pinite sample 1889 (with two analyses giving 994ppm and 1004ppm) lies within the range of deep sea sediments).

The rocks in the present alteration profile have not, however, been directly exposed to deep sea conditions, as the regolith was covered by overlying near-shore sediments. However, around the shoreline and near-shore, the perpetual mixing of the

seawater would continually replenish any boron absorbed by illite, thus providing an essentially infinite reservoir. Using a simplistic mass balance, an ~1300m to 1900m column of seawater would be required to produce the concentrations of boron in the alteration profile (Appendix 16e). Considering a point at the shore covered by 1m of seawater during every tide, then with 365 days in one year and 2 tides in one day, it would take $\sim 1300/(365 \times 2)$ to $1900/(365 \times 2)$, i.e. ~ 1.8 to 2.6 years to cover that one point with 1300m-1900m of seawater. Consequently, if all the boron in the 1m column was absorbed by the illite during each tide, it would require 1.8 to 2.6 years for sufficient boron to be added to the underlying regolith. If only 1% of the boron, then 180-260 years, 0.1%, 1800-2600 years and so on. Hence it would be reasonable to assume that the boron requirement could have been met this way. Therefore, the seawater is proposed as the source of boron ions in these rocks.

The high concentration of boron in the Cambrian seen in the geochemical map (Plate 8.2) has been attributed by the British Geological Survey to possible detrital tourmaline or volcanic glass fractions. Since no tourmaline was observed in any of the shales analysed and considering the paucity of tourmaline in the Lewisian (except as a later mineral in this alteration profile), it is unlikely that detrital tourmaline would have been the source. As the shales in the Cambrian succession contained high B:Al ratios, it seems more likely that the boron enrichment found in the sediments over the Cambrian units was contained in the illitic/muscovite and authigenic feldspar phases in the Cambrian rocks.

DISCUSSION

Weathering and erosion of the Proterozoic landmass in late Precambrian times could have provided the K^+ and Al^{3+} ions to the ground and river waters as proposed by Russell and Allison (1985) and detrital clays to the lagoons and near-shore environments, thus resulting in a clastic as well as ionic and colloidal link between the weathered profile and the overlying shales. B^{3+} ions would then have been incorporated into the illitic

muds from the seawater and also into the alteration profile from the seawater during the marine transgression.

Ages of ~500 Ma were determined for growth of authigenic K-feldspar by $^{40}\text{Ar}/^{39}\text{Ar}$ laser probe analysis (detailed account in Chapter 9). Such ages are compatible with the above hypothesis and imply that the authigenic K-feldspar formed in its present state some 25 to 70 Ma after deposition in the sedimentary succession in Cambro-Ordovician times.

Although once considered rare, authigenic K-feldspar-rich rocks are now known to be abundant in Lower Palaeozoic strata. They crop out from the mid-continent of North America to the Appalachians and in other localities including Newfoundland, Greenland, Scotland and Norway around the edge of the proto-Atlantic Ocean (Buyce and Friedman 1975).

Authigenic feldspar may develop in different rocks in different ways depending on "the supply of dissolved silica... and the supply of alkali metals" (Kastner and Seiver 1979) and a number of models have been proposed for its formation (see Kastner and Seiver 1979). Various hypotheses have been suggested concerning its formation in the Lower Palaeozoic.

Tephra derivation.

Although authigenic K-feldspar-rich horizons are much less abundant in post-Ordovician strata, they have been reported in Cenozoic alkaline lake deposits (e.g. Sheppard and Gude 1973, see Buyce and Friedman 1975 and Kastner and Seiver 1979). These authigenic K-feldspar deposits "are known to have formed from tephra by replacement of an intermediate zeolite stage" (Buyce and Friedman 1975). It has subsequently been suggested that the Lower Palaeozoic authigenic K-feldspar-rich horizons could represent such altered tephra horizons (Boles, pers. comm., Buyce and Friedman 1975). These are proposed to have originated from a zone of island arcs along the western margin of the Lower Palaeozoic proto-Atlantic Ocean (see Buyce and

Friedman 1975). However, Buyce and Friedman (1975) note that the Lower Palaeozoic and Cenozoic rocks are not strictly analagous, as detrital feldspar is not present in the Cenozoic tephra-derived deposits. Furthermore, the thorium and uranium contents in the Fucoïd Beds of NW Scotland were considered too low to be consistent with a volcanic origin (Bowie *et al.* 1966). There is also no textural evidence reported to suggest that the shales of the Fucoïd Beds were once tuffs. Furthermore, the close similarity between the K/Rb values and B/Al values of the alteration profile and black shales are inconsistent with this hypothesis.

Genesis related to later mineralising events.

Hearn *et al.* (1989) report Late Carboniferous to Early Permian ages (278-322 Ma) for the authigenic K-feldspar in Cambrian carbonate rocks of the central and southern Appalachians, determined by $^{40}\text{Ar}/^{39}\text{Ar}$ laser probe analysis. Hearn *et al.* (1989) suggest a possible genetic link between the regional occurrences of authigenic K-feldspar and nearby Mississippi Valley-type (MVT) mineralisation, with their hypothesis being supported by the discovery of authigenic K-feldspar intergrown with sphalerite in the region. Indeed, ore deposits are often hosted by black shales (e.g. lead-zinc deposits of Mid-Proterozoic age, northern Australia (Beeson *et al.* 1989), polyelement-rich Lower Cambrian black shales, southern China (Dalian 1983). In the shales of the Fucoïd Beds, however, there is no known Pb-Zn enrichment. Trace element determination (Appendix 15 and that of Bowie 1966) gave Pb values \leq average shales values (20ppm) and Zn values significantly lower than average (95 ppm). The authigenic K-feldspar in the Fucoïd Beds is also much older (Cambro-Ordovician, ~500 Ma) than the ages given by Hearn *et al.* (1989) for that in the Appalachians. Hence, the genesis of the authigenic feldspar in NW Scotland was clearly not the same as that proposed by Hearn *et al.* (1989) for its formation in the Appalachians.

In N. America, the altered basement is considered as one of the sources of Pb for the MVT deposits (evidence e.g. from lead isotope data, Doe *et al.* 1983). Duffin *et al.* (1989) suggested that the relatively very permeable palaeosols "would permit fluid/rock

interaction that could likely dissolve significant quantities of Pb and Zn". Doe *et al.* (1983) also consider the considerable Pb loss in the uppermost Precambrian granite as probably due to the disturbance associated with MVT mineralisation. I suggest that all the Pb depletion may not have been solely due to this event if the altered horizon was a palaeosol. Although the behaviour of lead in Precambrian palaeosols appears to vary (see Chapter 6, p.147), it is depleted in the sub-Cambrian profile of NW Scotland. Hence, some Pb in these sub-Cambrian rocks of North America may have been lost during weathering prior to events associated with MVT mineralisation. Indeed, in NW Scotland, the sub-Cambrian basement palaeosol is depleted in Pb (and Zn), without any enrichment of these metals in the overlying shales.

CHAPTER 9**AGE DETERMINATION OF CAMBRIAN
SHALES AND PINITE FROM THE PALAEO SOL** **$^{40}\text{Ar}/^{39}\text{Ar}$ LASER PROBE INVESTIGATION OF AGES OF CAMBRIAN
SHALES****Introduction**

The geological history of the palaeosaprolite from its formation at the Earth's surface through burial under the sedimentary pile and deeper during orogenesis in the middle Palaeozoic, followed by later uplift, is long and complex. The present minerals may have developed at various times during this long history. Determination of mineral ages of feldspar and mica in Lower Cambrian shales overlying the palaeosaprolite would constrain the models proposed for the shales' development and may indicate the time of growth of the minerals in the palaeosaprolite. These results can then be compared with the ages of similar feldspar-rich horizons in the Cambro-Ordovician successions and uppermost Proterozoic alteration horizons in central U.S.A.

Material studied

The shales and shaly sandstone in the Cambrian succession are subdivided into two groups, based on their colour and mineralogy:-

- 1) Black shales - consisting predominantly of authigenic K-feldspar and varying amounts of detrital biotite.
- 2) Green shales - containing authigenic K-feldspar and illite/muscovite.

Shales and shaly sandstone samples analysed by laser probe are given in table 9.1. Details of the experimental procedure for the $^{40}\text{Ar}/^{39}\text{Ar}$ laser probe analysis and age determination are given in Appendix 17.

Table 9.1 - Samples investigated in this project

<u>Sample</u>	<u>Rock formation</u>	<u>Type</u>	<u>Location</u>	<u>Grid Ref</u>
1. 0988	Eriboll sandstone (Lower member)	Green shaly sandstone	W. of L. Eriboll	NC 4395 6374
2. 0100	An t-Sron (Fucoïd beds)	Black shale	Assynt(Knockan Cliff)	NC 19 09
3. 0589	Eriboll sandstone (Lower member)	Black shale	Ullapool	NH 13 94

1. Green Shale (Eriboll Sandstone (Lower Member)) (0988)

Sample description

This greenish-buff rock is a faintly laminated, matrix-supported feldspathic wacke (Pettijohn 1975) (Plate 9.1a). It consists of small feldspar and quartz clasts in a matrix of very fine-grained, microscopically unidentifiable material. Accessory minerals include opaques (rutile and haematite), generally concentrated in laminations, and biotite and zircon. The clasts range in size from ~0.01 to 0.44 mm, with most ~0.22mm (Plate 9.1b). Modal analysis by point counting (500 points) shows the rock to contain 60.0% clasts and 40.0% matrix.

XRD analysis revealed that the rock contains a small percentage mica, as well as the K-feldspar (argillite) and detrital quartz which constitute the bulk of the rock. However, SEM backscatter imaging and quantitative EDS analysis on a polished thin section gave most information about the compositions and textures of different minerals. Backscatter imaging (plate 9.2a) shows the matrix to be a darker grey than the feldspars, indicating immediately that their compositions are different, with the matrix of higher mean atomic number. At higher magnification (plate 9.2b) the matrix is seen to contain lath-shape crystals up to ~20 x 4 μm , with a mica-like shape. There appears to be no difference in composition between the laths and the more platy crystals (e.g. plate 9.2b, pt. 1).

On comparing the quantitative analyses of matrix and feldspar clasts, it is found that the matrix contains relatively more Al, Fe and Mg and less Si and K than the K-

feldspar (plate 9.3) (analyses results in Appendix 18). The matrix is closest to muscovite in composition. Comparison of the quantitative EDS analyses of the matrix (Appendix 18) with the values for muscovite in Deer *et al.* (1962), shows the matrix to be richer in Si than most muscovites, and depleted in Al. Thus the analyses will plot between the muscovite and K-feldspar end members in Fig. 5.11 (after Garrels 1984), but much nearer the muscovite end.

Results

When the ages determined are plotted on the histogram shown in Fig. 9.1 (values also given in Appendix 19), the results fall into 5 distinct populations (including those between 1.4 and 1.5Ga). Applying the t-test (Appendix 4), these 5 populations are all statistically different at greater than 99.5% confidence level .

(1) Two biotites yielded the oldest ages, i.e. 1427 ± 13 Ma and 1471 ± 10 Ma.

(2) The single value of 587 ± 5 Ma is of a mineral much lighter brown than biotite in irradiated thick section, yet with cleavage still visible. This probably represents either the age of a mixture of the edge of a biotite flake and underlying material, or an altered biotite flake.

(3) Two feldspar clasts form a small population at 553 ± 2 Ma and 558 ± 3 Ma.

(4) The most intriguing results show that the bulk of the feldspar clasts and matrix form two distinct populations, with the matrix population older than the main feldspar clast population. And this despite the potential analytical difficulties in correlating colour and composition! The matrix yielded ages of 510 to 478 Ma, whilst the bulk of the feldspars 458 to 434 Ma. The two oldest ages of the youngest population were lighter brown than the matrix and therefore, as the ages testify, probably represent a degree of mixing of the feldspar with the matrix.

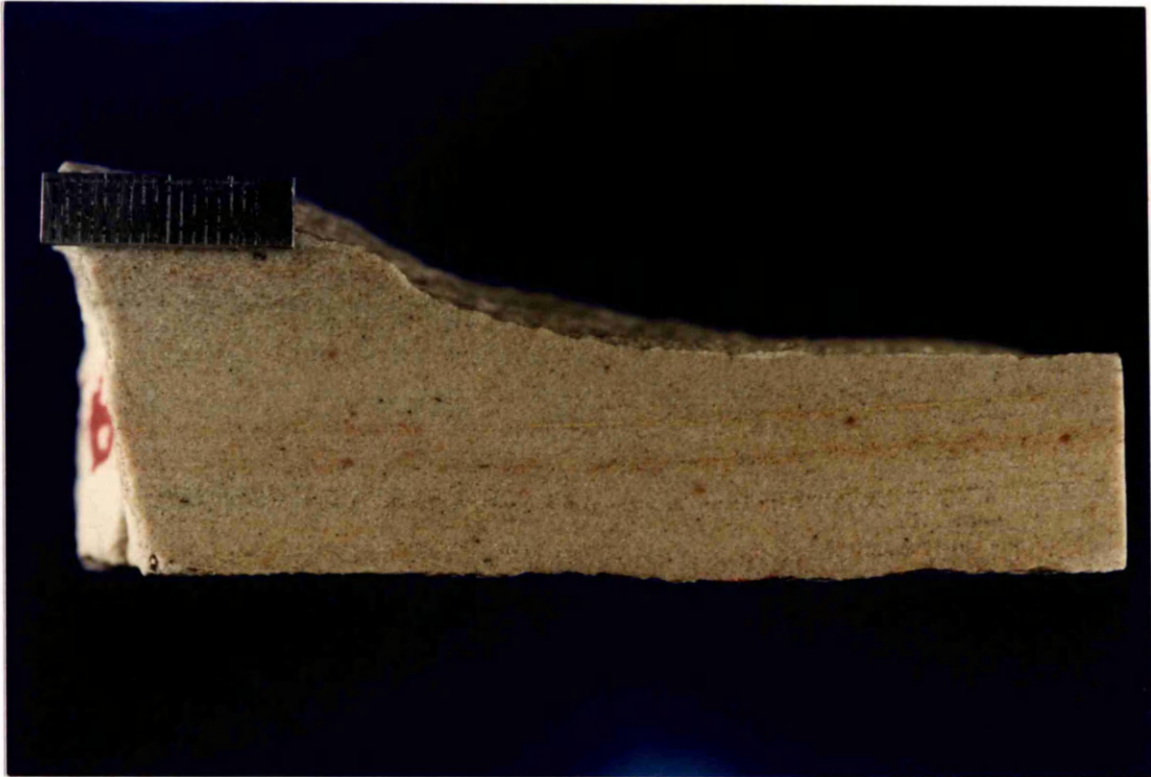


Plate 9.1a
Sample 0988.

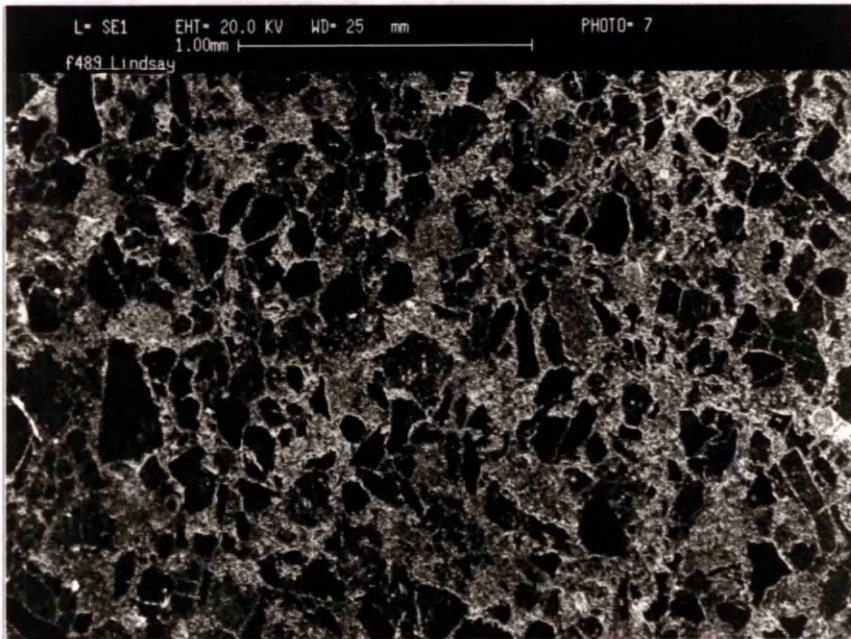


Plate 9.1b
SEM secondary electron image of a polished thin section of 0988.

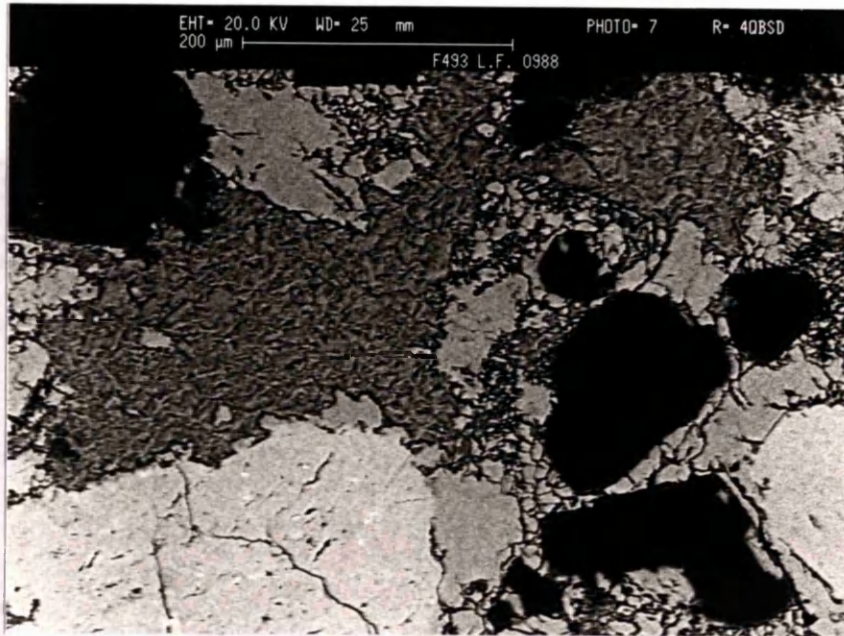


Plate 9.2a

Backscatter electron image of 0988.

NOTE: Quartz = Dark grey.
 K-feldspar clasts = Light grey.
 Matrix = Medium grey.

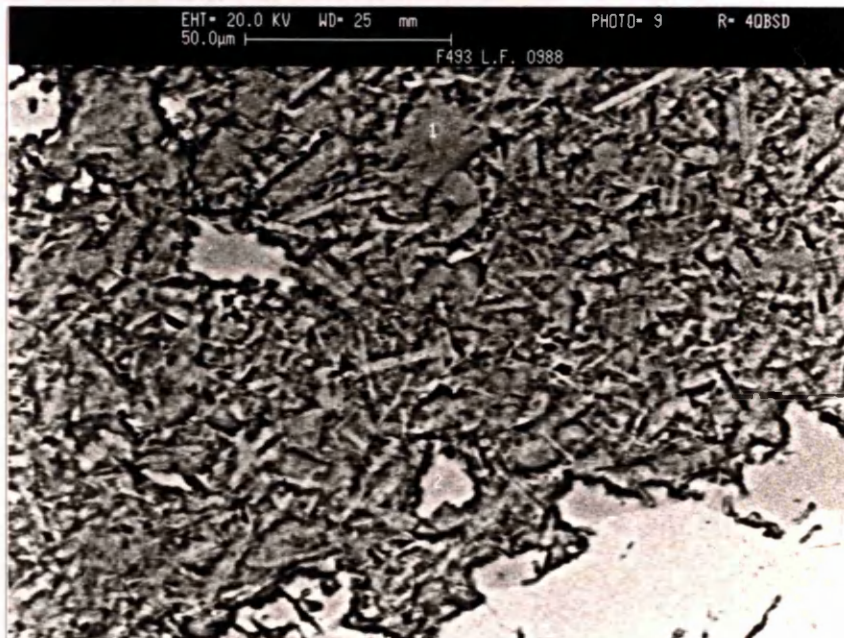


Plate 9.2b

Close-up of matrix : 1 = Mica, 2 = K-feldspar.

Note size and shape of grains and inclusions of K-feldspar within the matrix.

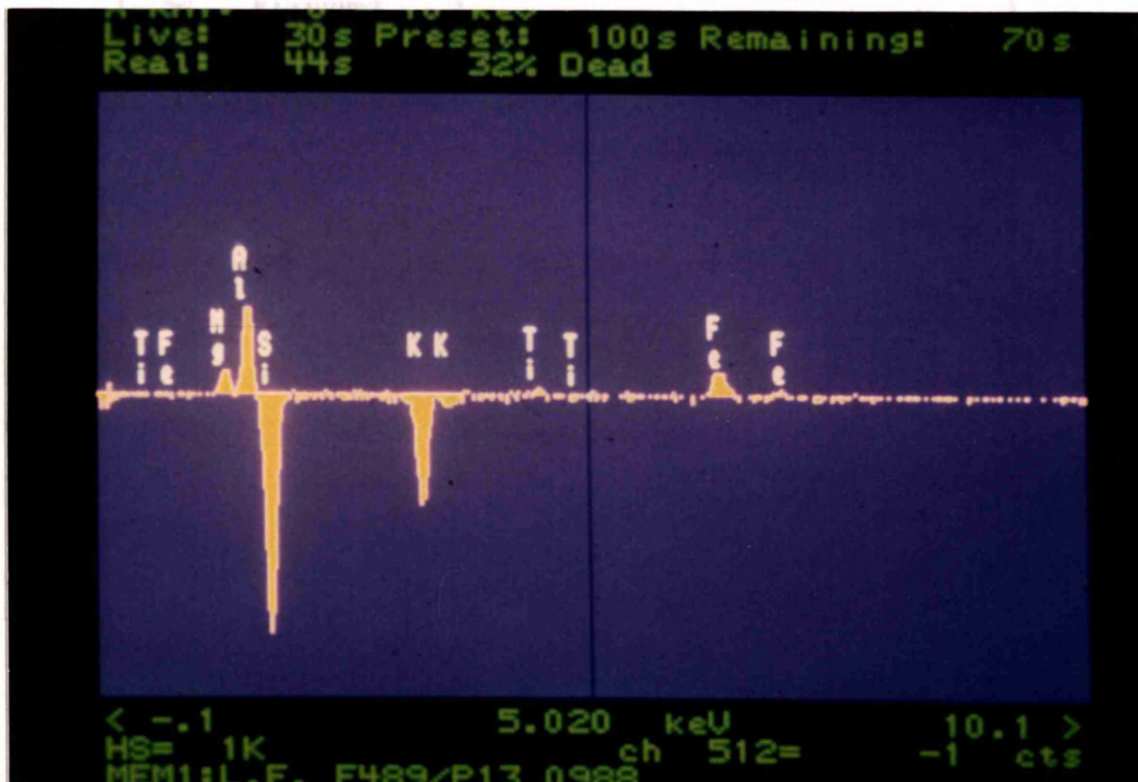


Plate 9.3

Composition of matrix as compared with feldspar clasts. (Above centre line = more of a given element : Below centre line = less). Matrix contains relatively more Al, Mg and Fe and less Si and K than feldspar.

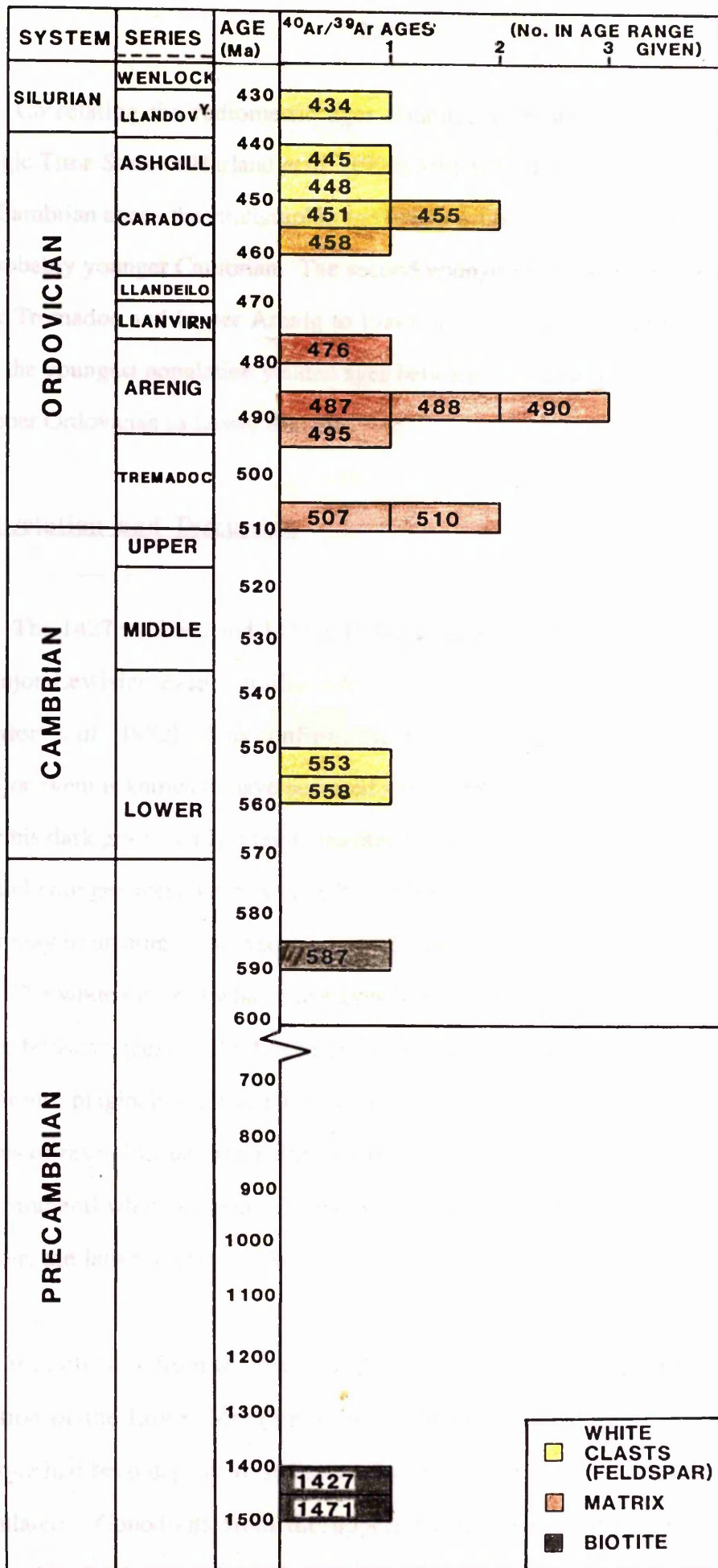


Fig. 9.1

$^{40}\text{Ar}/^{39}\text{Ar}$ ages for minerals from green shaly sand, 0988.

System and Ordovician and Silurian Series limits based on the Geologic time scale of Harland *et al.* (1990).

Correlating the radiometric ages obtained with stratigraphic ages using the Geologic Time Scale of Harland *et al.* (1990), (Fig 9.1), it is seen that only two analyses yield Cambrian ages - the stratigraphic age of deposition of the Basal Quartzite, although it is probably younger Cambrian. The second youngest population formed between the Lower Tremadoc and Upper Arenig to Llanvirn, i.e. during Lower Ordovician times, whilst the youngest population yielded ages between the Caradoc and Llandovery, i.e. in the Upper Ordovician to Lower Silurian.

Interpretation and Discussion

The 1427 ± 13 Ma and 1471 ± 10 Ma ages obtained from the biotites record the last major Lewisian event (uplift), which occurred between 1700 and 1400 Ma ago (Anderton *et al.* 1982). This confirms these biotites to be detrital Lewisian minerals. No major event is known to have occurred around 587 Ma which would explain the next age in this dark grain. Only a faint cleavage is visible and it may represent a mixture of older and younger ages, but may have been inherited during some localised event at this time or may be an artefact of Precambrian weathering.

The white material which gave ages between 553 Ma and 558 Ma are unlikely to be pure feldspar ages, as the feldspars in this sample have been reset above both K-feldspar and plagioclase closure temperatures (see below). Hence, they could also be mixtures of reset feldspar and older material underneath, or they may be some other K-bearing mineral which inherited its age or formed at that time, but which has not reset. However, the latter is very unlikely considering the mineralogical composition of the rock.

It is obvious from the results that the minerals in the matrix formed after the deposition of the Lower Member in the sedimentary succession. After the Eriboll Sandstone had been deposited, sedimentation continued until ~1.5km of sediments had accumulated. Conodonts from the uppermost member of the Cambro-Ordovician sequence (the Durine member) give the youngest known age for the deposition of this

whole sedimentary succession in NW Scotland as early Llanvirn or more probably late Arenig (Higgins 1967, Lindstrom 1971 and Higgins and Austin 1985). As seen from Fig. 9.1, this is consistent with the youngest age of the matrix. Hence, the matrix formed during the latter stages of Cambro-Ordovician sedimentation, probably when the temperature of the lowermost units had increased sufficiently for these minerals to form. The spread of results is most likely due to overlap with other minerals. The diameter of the clasts and the size of the areas of matrix are similar to the diameter of the laser pit ($\sim 100 \mu\text{m}$). Also, small detrital grains may be seen in the matrix (Plate 9.2b). It is therefore difficult to ensure that single grains are being analysed. Hence, the oldest ages, 507 and 510 Ma, may be purest matrix and may most accurately represent the age of neof ormation. With more and more overlap with feldspars, the ages progressively decrease. (It is also possible that growth may have been incremental or progressive over a long period giving varying mixtures of slightly different ages on analysis). In either case, the matrix formed after deposition while the overlying Ordovician sediments were being deposited.

After deposition of the sedimentary succession, no major event is known to have affected these rocks until the Caledonian orogeny. Soper (1971) reported that the earliest deformation of the Caledonian orogeny affected the fossiliferous Cambro-Ordovician shelf sediments. The Caledonian deformation is dated as younger than Arenig (to Llanvirn (Higgins 1967), i.e. c. 478Ma) and older than the age of intrusion of the Ross of Mull granite, i.e. 414 ± 4 Ma (Johnson *et al.* 1985, after Halliday *et al.* 1979). Peak Caledonian metamorphic activity is considered to be at c. 450Ma (Kelley and Powell 1985). As seen in the results, ages from the youngest population, i.e. 458 to 434 Ma, all occur entirely within the period of Caledonian orogenesis, and most around the period of peak metamorphic activity. However, the rocks around Eriboll reached their highest temperatures ~ 245 to 275°C between 408 and 429 Ma (Johnson *et al.* 1985 and below) and therefore these feldspars should have reset to slightly younger ages. Furthermore, the peak metamorphism at 450 Ma occurred prior to the main thrust emplacement - up to 80 km away! Hence the synchronicity of the results with peak Caledonian

metamorphism appears coincidental. These K-feldspar ages are most likely to represent mixtures of feldspars which have reset to ~408 to 422 Ma, and the older matrix, thus decreasing the apparent age. This is most clearly evidenced in the oldest ages of the population which had a brownish appearance. The youngest age, 434 Ma, is likely to be of the feldspar with the least matrix overlap and thus closest to the actual ages of the K-feldspar.

Reason for resetting of clasts and not matrix

The differences in composition of the feldspars and matrix and their respective blocking temperatures must be taken into account to understand why, during the Caledonian Orogeny, the events which caused the clasts to reset clearly did not affect the matrix.

The clasts are of K-feldspar while the matrix is closest to muscovite in composition. The closure temperature for Ar in unmixed alkali feldspars is ~150°C (Foland 1974, Harrison and McDougall 1982) (for plagioclase it is 200 to 250°C (McDougall and Harrison 1988)), while muscovites do not reset until ~350°C (McDougall and Harrison 1988). In order to reset the feldspar but not the matrix, therefore, the temperature needed to have exceeded 150°C and been less than 350°C in Eriboll during the Caledonian. Downie (1972), in a study of Lower Cambrian acritarchs along the Moine Thrust Zone, found their degree of carbonization varied along strike. He found that palaeotemperatures ranged from approximately 150°C at Ord (~170 km farther south) to ~250°C at Eriboll. X-ray diffraction analysis of illite crystallinity in the Furoid Beds shales was used by the author (1987) to determine variations in diagenesis/low grade metamorphism in the Moine Thrust Zone. Results corroborated Downie's findings of range in temperatures from ~150°C at Ord to ~250°C at Eriboll and were compatible with similar findings of Johnson *et al.* (1985) who suggested $275 \pm 50^\circ\text{C}$ as the highest temperature reached by rocks directly under the Moine Thrust.

These temperatures are much lower than the blocking temperature for muscovite, which explains why the matrix has not been reset.

2) Banded Black Shaly Rock (Furoid Beds Member 0100)

$^{40}\text{Ar}/^{39}\text{Ar}$ laser probe analyses on a banded black feldspathic shale from the Furoid Beds member were made by S. Kelley at the SURRC and the results are presented here. Analyses were made at 1mm step intervals across the sample. One traverse of 16 analyses, and a shorter traverse of 7 analyses, gave the ages shown in Fig. 9.2.

Results and Interpretation

The age of neof ormation of authigenic feldspar is most likely to be between ~490 Ma and 510 Ma, i.e. early Ordovician (Tremadoc to Arenig) from the pronounced plateau of 5 analyses in the centre of the graph (Fig. 9.2).

On the left side of the graph all except 2 results from the first 6 or 7 analyses in both traverses yield Precambrian ages, and therefore represent detrital minerals or mixtures of minerals.

From the plateau of youngest ages around 500 Ma, the dates increase towards the right side of the graph. These ages on the right may represent mixtures of authigenic feldspar and detrital minerals. Some could also be detrital minerals which inherited younger ages during late Precambrian events - such as weathering or localised hydrothermal alteration. It is unlikely that these represent solely ages of development of authigenic feldspar, since these rocks were deposited in the Lower Cambrian (\Rightarrow <570 Ma, Harland *et al.* 1990) and possibly <525 Ma! (Compston *et al.* 1990). Also, the large spread of dates on the right would suggest that these ages are not representative of a single period of growth.

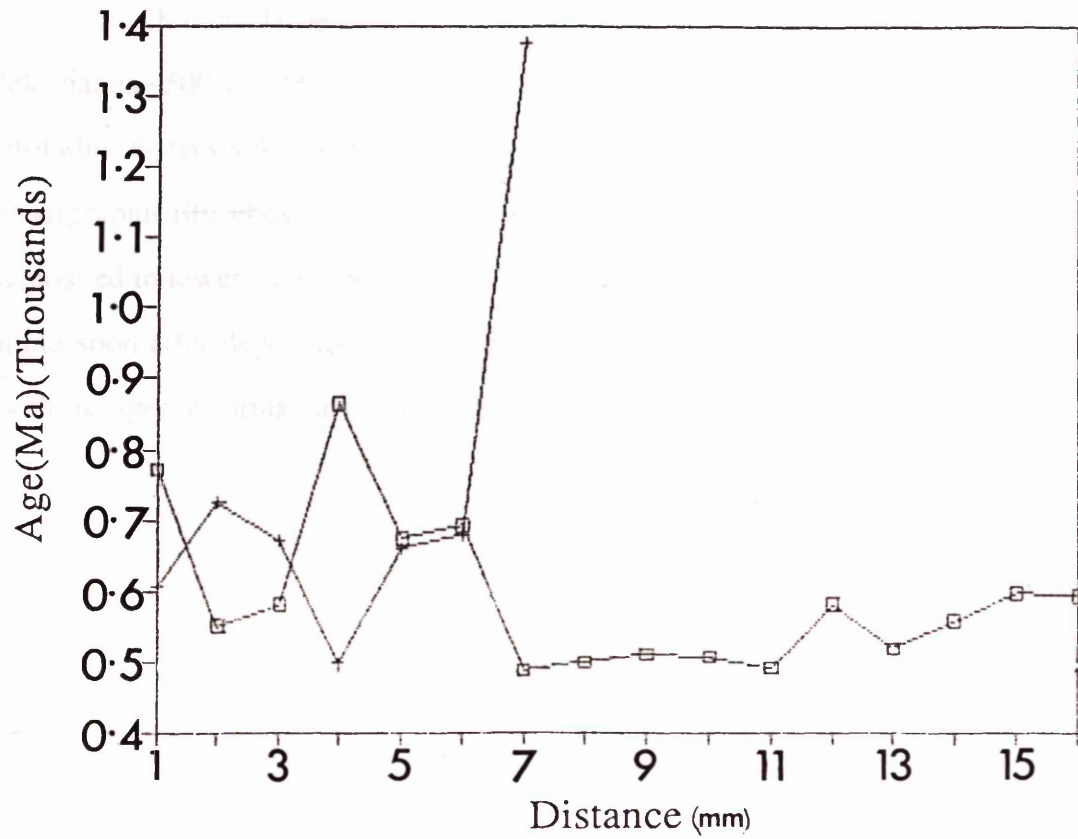


Fig. 9.2

$^{40}\text{Ar}/^{39}\text{Ar}$ laser probe ages from traverses in Furoid Beds sample (0100). Traverse across detrital mineral-rich zone (LHS) and authigenic feldspar-rich area (centre).

Discussion

It is obvious that the feldspar in this sample has not been reset to Caledonian ages, indicating that temperatures in Assynt were not as high as farther north in Eriboll. This is consistent with the findings of Downie (1972), Johnson *et al.* (1985) and Ferguson (1987).

Much confidence can be placed in the age of neoformation of the authigenic feldspar as $\sim 500 \pm 10$ Ma, due to the good reproducibility of ages in the central area (and probably analysis 4, traverse 2). The Furoid Beds member, some 150m to 200m stratigraphically above the positions of 0988 and 0589 in the Lower Member, was deposited in lower Cambrian times. Hence, the authigenic feldspar would have formed quite soon after deposition in the sedimentary succession. These ages are congruous with the ages of formation of the matrix in 0988.

3). Black Shale (Eriboll Sandstone (Lower Member) 0589)

Sample description

The black shaly laminations at [NH 137 938] (Ullapool) are in units up to 0.3m thick and are interleaved between the much thicker, white, quartz-cemented quartzarenite beds of the Lower Member, (plate 9.4a). The rock is a dark grey, very fine-grained, finely laminated shale (laminations 0.1 to 1mm thick), (Plate 9.4b). The laminations are accentuated by colour banding, from white in the quartz and feldspar-rich areas to grey and black in the authigenic feldspar-rich bands. Fine-grained detrital biotite flakes found along with the authigenic feldspar are aligned along bedding surfaces.

XRD analysis shows the darker laminations to contain ~75 to 77% argillitic K-feldspar, ~10% biotite and 12 to 15% quartz.

Analyses and analytical problems

Laser probe analyses were made of the black shaly areas, the white feldspar clasts and also one analysis of brown matrix material, like that in 0988. However, problems were encountered on analysis of this black shale. Due to the very fine grain size of the black biotite and authigenic K-feldspar mixture, it was very difficult to distinguish areas solely of biotite or feldspar on the scale of an analysed spot (~100µm). Hence, any analysis would contain either feldspar or biotite or more probably a mixture of the two.



Plate 9.4a

0589 is from the black shale horizons found interleaving between thicker quartz-cemented quartzarenite beds in the Lower Member [NH 13 94].

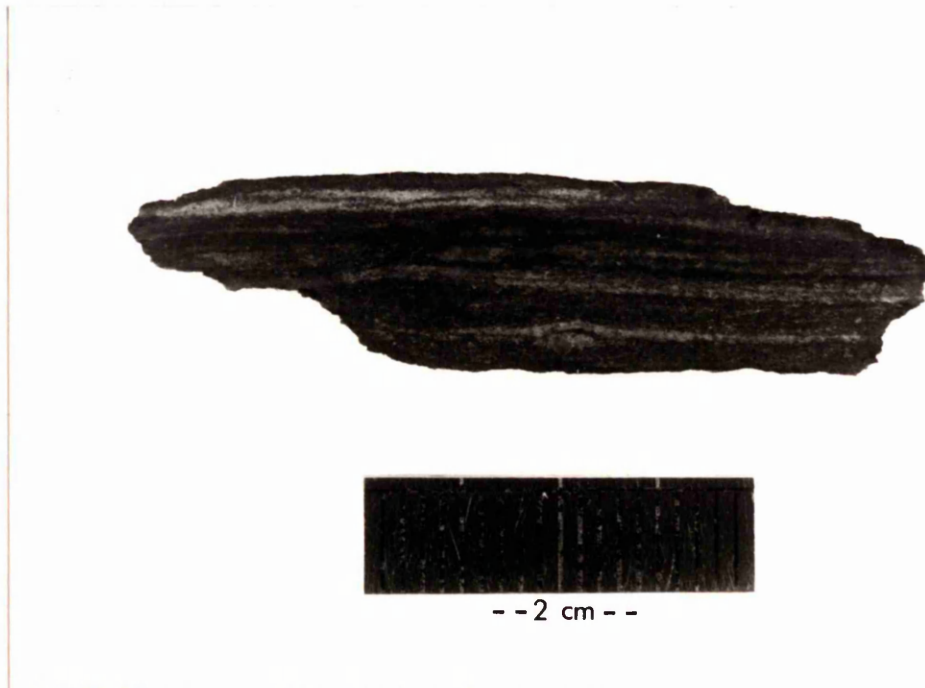


Plate 9.4b

Thick section of black shale, 0589.

Results

Feldspars:

The detrital feldspars analysed in 0589 have ages which plot in 3 distinct areas (Fig. 9.3) (results also in Appendix 19); of 1141 ± 15 Ma, 917 ± 6 Ma and 641 to 672 Ma - all of which are older than those in the green rock (0988) (Fig. 9.1).

Black Shale:

A large spread of results was found for the black shales due to the heterogeneity of the material (Fig. 9.3 and Appendix 19). These ages are most likely to fall between the two end members for biotite and authigenic K-feldspar. Assuming each grew during a single period of growth and assuming detrital biotite is older, the detrital biotite must have been formed at ≥ 953 Ma and the authigenic feldspar ≤ 580 Ma.

If the age of the detrital biotite is assumed to be 1450 Ma (from analyses of green shales and Anderton *et al.* 1982), and an analysed point is assumed to have the same ratio of biotite to authigenic K-feldspar as the whole-rock determined by XRD analyses, (i.e. ~12% biotite to 88% authigenic feldspar), then for authigenic feldspar to be ≤ 580 Ma, the analysed spot would have to be ≤ 682 Ma.

i.e.

XRD 10% biotite and 75% authigenic K-feldspar in whole-rock.

\Rightarrow biotite : authigenic feldspar ~ 12:88 (normalising)

$$\frac{12}{100} \times 1450 \text{ Ma} + \frac{88}{100} \times 580 \text{ Ma} \leq X \text{ Ma}$$

Age of biotite
Age of authigenic feldspar
Age of analysed spot.

\Rightarrow X (analysed spot) < 682 Ma.

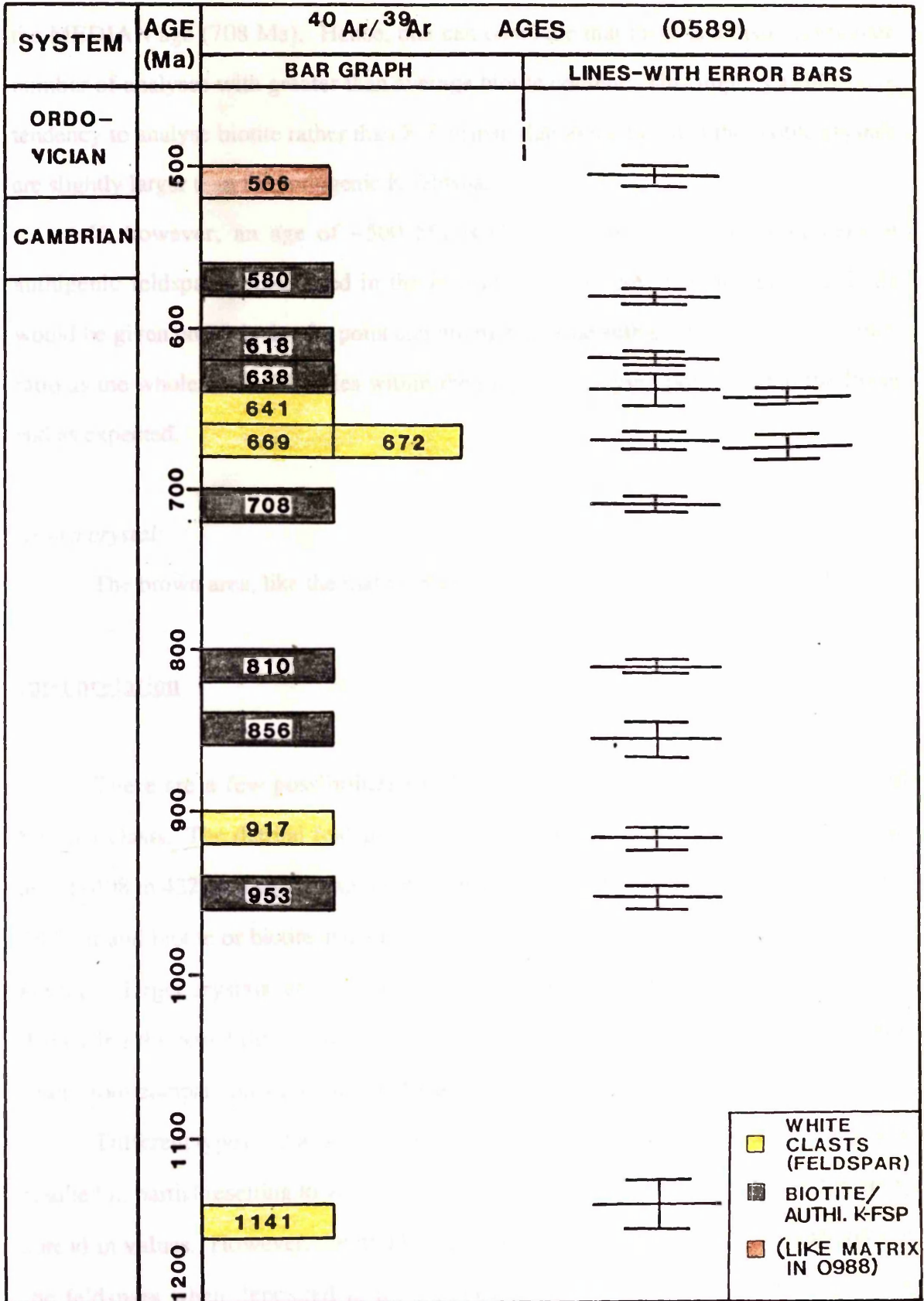


Fig. 9.3

$^{40}\text{Ar}/^{39}\text{Ar}$ ages for minerals from black shale, 0589.

Clearly this is younger than both the MEAN age of the black shale (738 Ma) and the MEDIAN age (708 Ma). Hence, one can conclude that there is a disproportionate number of analyses with greater than average biotite content. This implies a subjective tendency to analyse biotite rather than K-feldspar due to the fact that the biotite crystals are slightly larger than the authigenic K-feldspar.

If, however, an age of ~500 Ma is chosen as the age of development of authigenic feldspar as measured in the Fucoïd Beds sample, then an age of 612 Ma would be given on analysis of a point containing the same authigenic K-feldspar : biotite ratio as the whole rock. This lies within the range of analysed points and at the lower end as expected.

Brown crystal:

The brown area, like the matrix in 0988, yielded the youngest age at 506 ± 6 Ma.

Interpretation

There are a few possibilities for the differences in ages of the white, detrital feldspar clasts. The detrital feldspar clasts could have been totally reset to Caledonian ages (~408 to 422 Ma) and the ages determined could represent mixtures of detrital, reset feldspar and biotite or biotite and authigenic feldspar. This is unlikely as these feldspars are much larger crystals, and are in more quartz and detrital feldspar-rich laminations, decreasing the possibility of overlap. It is also unlikely that these feldspars were totally reset, from comparison with other feldspar ages in this sample and 0100.

Different types and amounts of perthitic laminae in the detrital feldspars may have resulted in partial resetting to varying extents. This is also doubtful because of the broad spread in values. However, the numbers are most likely to represent the actual ages of the feldspars when deposited in the Lower member. All ages are Precambrian but especially the younger ages were possibly inherited during weathering of the basement

rocks and represent mixtures of fresh Lewisian feldspar and authigenic K-feldspar (see Discussion).

The examples above of ages for mixtures of biotite and authigenic feldspar in whole rock proportions do not prove that the authigenic feldspar formed at ~500 Ma. However, it does support this contention and certainly supports the ages of around 500 Ma obtained for neof ormation of the authigenic feldspar of the Fuco id Beds (sample 0100).

The 506 ± 6 Ma age for growth of the brown material is consistent with the age of the matrix in 0988, the authigenic K-feldspar in 0100 and, most likely, with the authigenic K-feldspar in this sample.

Discussion

That the detrital and authigenic feldspars in 0100 and this sample have not been reset, indicates that temperatures in these rocks did not reach 200°C maximum in Assynt and Ullapool. The lack of resetting found in these samples is consistent with the decrease in temperature from Eriboll southwards, found from illite crystallinity (Johnson *et al.* 1985, Ferguson 1987) and colour indexing of Cambrian achritarchs (Downie 1982). The temperature, however, would have been greater than 150°C as measured at Ord, ~110 to 130 km further south (Downie 1982, Ferguson 1987).

In the case of the feldspar clasts from this sample (0589), the oldest and youngest ages overlap with Rb/Sr ages of adularia from lower to intermediate and upper zones respectively of sub-unconformity basement rock from Ohio, U.S.A (Mensing and Faure 1983), (Fig.9.4). The Rb/Sr ages from the lower and intermediate zone (>6.4m b.u.) were 1162 ± 11 Ma and from the upper zone (<6.4m b.u.), 599 ± 60 Ma. Mensing and Faure (1983) suggested that this adularia could have formed from low-temperature hydrothermal alteration of weathering products during the deposition of overlying Cambrian sandstone. However, the K/Ar ages of those feldspars give younger ages; from 750 to 850 Ma, to ca. 370 Ma, (Macintyre 1986). Later circulating fluids,

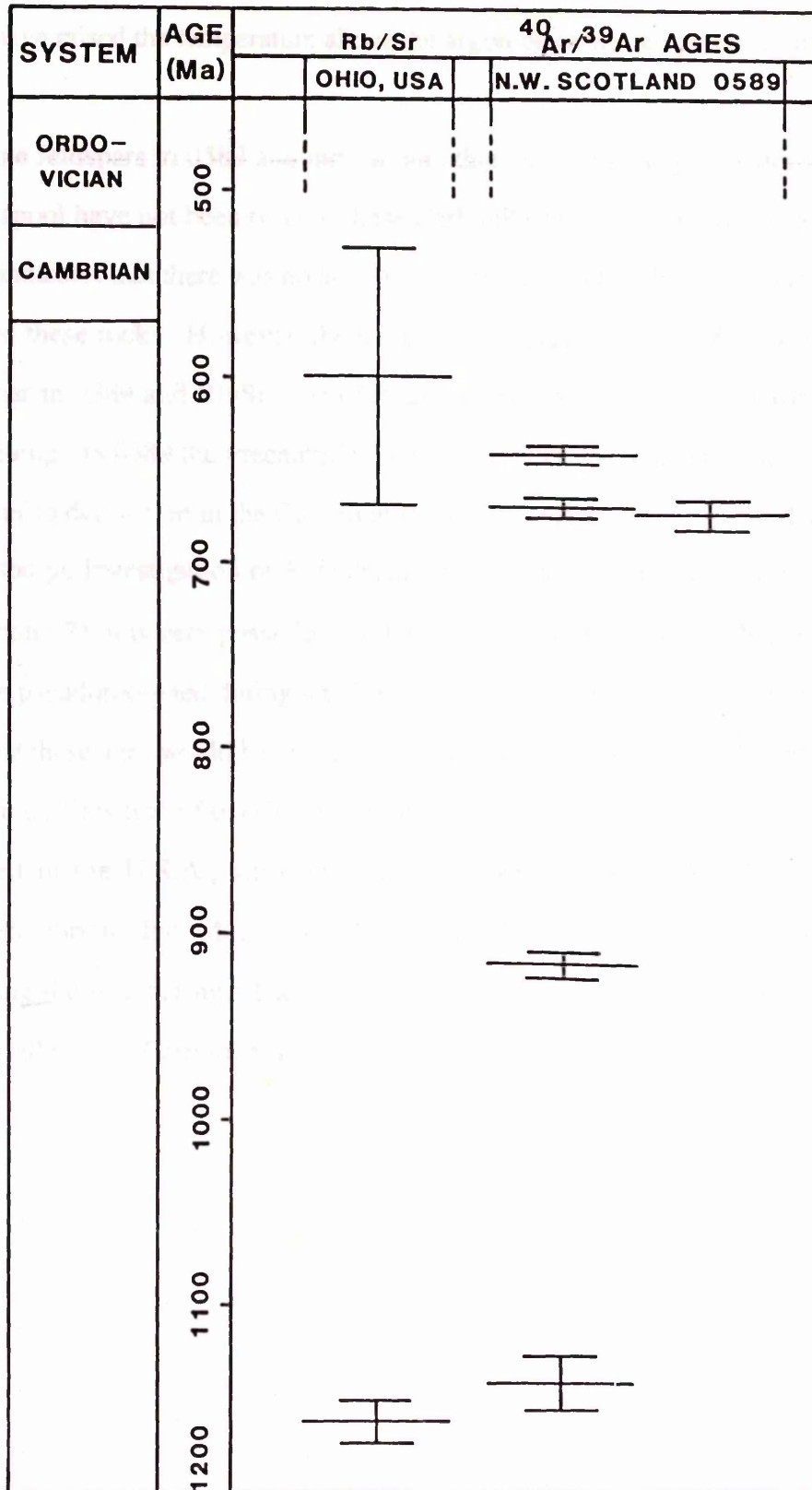


Fig. 9.4

$^{40}\text{Ar}/^{39}\text{Ar}$ ages of detrital feldspars from 0589, NW Scotland, and Rb/Sr ages of 5 adularia or adularia - K-feldspar mixes (younger) and 7 primary feldspar (older), from lower to intermediate and upper zones respectively, of altered, sub-unconformity rocks, Ohio, U.S.A.

associated with the widespread Mississippi Valley Type mineralising event, are suggested to have raised the temperature above the argon blocking-temperature, and reset the ages.

That the feldspars in 0589 and indeed the other shales or shaly sandstones from Eriboll to Ullapool have not been reset to these Carboniferous ages, or indeed any other younger age, indicates that there was no later hydrothermal event with such temperatures, which affected these rocks. However, the similarity in spread of $^{40}\text{Ar}/^{39}\text{Ar}$ ages of the detrital feldspar in 0589 and Rb/Sr ages of feldspar from beneath the unconformity in Ohio, is intriguing. In 0589 the Precambrian dates imply that the feldspars had inherited these ages prior to deposition in the Cambrian shales. However, from results discussed in the $\delta^{18}\text{O}$ isotope investigation of K-feldspar from beneath the unconformity in NW Scotland (Chapter 7), it is very possible that these ages in Scotland were inherited when feldspars were pseudomorphed during late Precambrian weathering. Moreover, it is very improbable that these ages would have been acquired from low-temperature hydrothermal alteration during deposition of overlying Cambrian sandstones (or other later sediments) as is proposed in the U.S.A., since the youngest age in 0589 is 641 ± 4 Ma, i.e. definitely Precambrian. Indeed, it is possible that the Rb/Sr ages in Ohio, U.S.A. were inherited during the weathering. The youngest age from Ohio of 599 Ma (± 69) is also Precambrian, rather than Cambrian (after Harland *et al.* 1990 and considering Compston 1990).

Table 3.2

$^{40}\text{Ar}/^{39}\text{Ar}$ ages for feldspar from 0589

All successive error bars are 1 σ . The error bars for the first two ages are 1 σ considering the range in ^{39}Ar yields. The error bars for the last two ages may have been due to incomplete gas extraction.

K/Ar DETERMINATION OF THE AGE OF PINITE FORMATION

Introduction

The age of pinite was determined in a preliminary investigation by conventional radiogenic K/Ar dating. All samples were collected from beneath the unconformity to the west of Loch Eriboll, <4 km from the North coast. Separated chips of pure pinite aggregates were analysed. The K/Ar ages were determined at the SURRC by R.M. Macintyre and J. Imlach, using the techniques described in Macintyre and Hamilton (1984).

Results

The results (Table 9.2) show a range in values from 403 to 429 Ma, with a mean age of 414 Ma and a median of 408 Ma.

Sample No.	Grid Ref. and Location	Age (Ma)
8714	NC 4462 6394 Knoll	406 ± 8
0788	NC 4361 6240 Clachaidh	403 ± 8
1889 - (10)p	NC 438 637 Hill-slope	429 ± 9
1889 - (10)c	NC 438 637 Hill-slope	408 ± 8
I(A) 1		425 ± 9

Table 9.2

K/Ar ages for pinite samples from west of Loch Eriboll.

All successive error bars of the results overlap. Indeed, the ages are very similar, considering the range in results for one sample (1889 - (10)), although the older ages may have been due to incorporation of tiny amounts of remnant K-feldspar.

Interpretation and Discussion

These K/Ar ages suggest that pinite formed during the closing stages of the Caledonian orogeny. The Moine Thrust is considered by Johnson *et al.* (1985) to have ceased movement before 414 ± 4 Ma, from a recent date for the Ross of Mull granite intrusion. The main emplacement of the thrust sheets is thought to have taken place at ~ 432 Ma (Johnson *et al.* 1985). A consequent rise in footwall temperature to $\sim 245^\circ\text{C}$ would, therefore, have been reached (using the model of Oxburgh and Turcotte 1974 given in Johnson *et al.* 1985) by ~ 422 Ma and a temperature of 275°C (considered to be the maximum footwall temperature) is stated to have occurred at about 408 Ma.

The ages determined for pinite (= $2M_1$ muscovite) are clearly remarkably consistent with the above spread in ages for the temperature rise from 245°C to 275°C , a range which covers the required temperature for the transformation of illite to $2M_1$ muscovite (i.e. 250°C and possibly up to 275°C , Hunziker *et al.* 1986). This implies that pinite formed after the main emplacement of the thrust sheets, when the footwall temperature had risen sufficiently to permit this transformation.

CONCLUSIONS

The K/Ar and $^{40}\text{Ar}/^{39}\text{Ar}$ results are mutually supportive with the K/Ar data for pinite elucidating the events which affected the ages of the Cambrian shales.

$^{40}\text{Ar}/^{39}\text{Ar}$ results show that the authigenic feldspar and illitic/muscovite matrix of the green and black shales in the Lower Member and Furoid Beds from Eriboll to Ullapool developed at $\sim 500 \pm 10$ Ma in the earliest Ordovician as sedimentation continued. Detrital feldspars north of Assynt have been reset to Caledonian ages, while those in Assynt and farther south at Ullapool have not, indicating that the temperatures during the Caledonian did not exceed a maximum of 200°C in Assynt and Ullapool, but were higher farther north. That the muscovite/illitic matrix and detrital biotite in the north was not reset, limits this temperature in the north to $<350^\circ\text{C}$. This is consistent with the findings of Downie (1982), Johnson *et al.* (1985) and Ferguson (1987), who all consider a temperature increase northwards on the Moine Thrust, reaching a maximum of 245 to 275°C in Eriboll. The different ages of detrital K-feldspar in the shales from Assynt and Ullapool, ranging from Lewisian to Late Proterozoic ages, may have been adopted during weathering of the exposed Lewisian landsurface.

Pinite from the palaeosol at Eriboll in the north yields ages between 403 Ma and 429 Ma, consistent with the age proposed by Johnson *et al.* (1985) for when these rocks reached the maximum footwall temperature considered to be 245 to 275°C after the main Caledonian thrust emplacement. This temperature increase permitted the formation of pinite which is also consistent with the temperature of transformation of illite to 2M_1 muscovite (i.e. c. 250°C) as proposed by Hunziker *et al.* (1986).

CHAPTER 10**IMPLICATIONS OF THIS STUDY AND
FURTHER WORK****SUMMARY OF THE GEOLOGICAL HISTORY**

The exposed Lewisian basement of NW Scotland was weathered during late Precambrian times. At that time these rocks were situated in equatorial regions (Piper 1987, Moores 1991, Dalziel 1991, Davidson 1992) and prolonged weathering occurred under humid, tropical conditions in an oxidising environment (up to 0.1 PAL) and at moderate pH. Thus a weathering profile akin to a modern day pedalfers was formed.

The major complex clay phase of the soil, formed during initial to intermediate weathering, was illite, with kaolinite forming the dominant phase under advanced weathering conditions higher up in the profile. The order of alteration and consumption of primary phases is consistent with that of modern weathering conditions and the feldspars altered to a deep red colour before consumption.

Chemical weathering resulted in a loss of most major and trace elements from the profile although Al_2O_3 , TiO_2 and possibly ZrO_2 were retained. In the absence of vascular land plants the clay-rich soil would have been easily eroded by surface waters which would carry, among other things, ionic K^+ , ionic and colloidal Al^{3+} , silica and detrital clays to marginal lagoons and the open sea.

Late Precambrian faulting, probably in association with the breakup of the Precambrian supercontinent and the formation of the Iapetus Ocean to the SE of the study area (e.g. Piper 1987, Davidson 1992), resulted in differential movement of the basement rocks. After this the sea encroached over the Lewisian land surface during the Cambrian marine transgression. The perpetual winnowing by the sea gave rise to a well sorted quartz sand and coastal erosion resulted in a regionally smooth peneplaned land surface. Erosion removed any remaining loose soil from the weathered horizon leaving only the

lowermost 'C' horizon, i.e. the altered rock, on which the Cambrian basal conglomerate and quartz-rich sandstones were deposited. Rarely, rip-up clasts from the saprolite were incorporated into the basal conglomerate of the Eriboll Sandstone. Thus a saprolite, consisting predominantly of illite with varying amounts of kaolinite in the uppermost reaches, was preserved underneath the Cambrian sandstones. The variation in amount and type of clay minerals preserved from place to place was due to natural variation in degree of alteration, influenced by jointing etc. and differential movement of Precambrian faults. During the marine transgression, illites in the exposed saprolite absorbed boron ions from the seawater into their structure. Clays eroded from the weathered profile were redeposited off-shore in shaly layers between the quartz arenite beds and also as matrix in the sandstones. These too were repositories for boron absorbed from the seawater. The Cambrian sedimentation is considered to have commenced around 570 Ma (after Harland *et al.* 1990) although possibly as recently as ~525 Ma! (Compston 1991).

Clays deposited in saline, alkaline lagoons were "reverse weathered" and thus authigenic K-feldspar was formed "soon after deposition" (McKie 1988). However, the interleaving green muscovite/illitic shales were unaffected by this process. The authigenic K-feldspar of the Lower Member and Fucooid Beds and the illite/muscovite of the shales and shaly sandstones in the Lower Member all developed at $\sim 500 \pm 10$ Ma, i.e. during early Ordovician times (Tremadoc to Arenig). Cambro-Ordovician sedimentation continued with ~ 1.5 km of sediments accumulating.

Following burial beneath the sedimentary succession, no major event is known to have affected these rocks until Caledonian orogenesis. Main emplacement of the thrust sheets occurred at ~ 432 Ma (Johnson *et al.* 1985) when the foreland in the north was buried to a deeper level than farther south. Consequently, the temperature in the footwall of the thrust belt increased, reaching its maximum of ~ 245 to 275°C in the northern area from ~ 422 to 408 Ma ago (Johnson *et al.* 1985). This increase in temperature caused the K-feldspar in the north to reset, but the K-feldspar in the cooler rocks in Assynt and farther south were unaffected. This temperature increase also resulted in the formation of pinite and pyrophyllite, which replaced the original

weathering products of illite and kaolinite respectively in the palaeosaprolite. Tourmaline probably developed around this time also. Thus the rocks of the palaeosaprolite adopted their present mineralogy at this time during the late Silurian in response to the effects of Caledonian tectonism.

WIDER IMPLICATIONS

With the increase in the study of Precambrian palaeosols through the 1980's there has been a consequent increase in the amount of information in the literature describing their mineralogy and geochemistry. However, little attention has been paid in their interpretation to relating the rocks of the palaeosols (so often more correctly palaeosaprolites) to the degree of weathering they have undergone. To relate the behaviour of elements to degree of weathering is crucial when making interpretations of geochemical results.

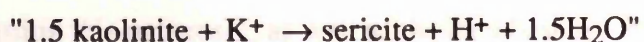
The behaviour of elements and the secondary minerals that are formed in a weathering profile vary with the degree of weathering. While significant weathering may be found in very shallow profiles "weathering rinds" (e.g. Ilha de Sao Sebastiao, Brazil (0.08m), Kronberg *et al.* 1987), likewise it is equally possible to have only a limited degree of weathering preserved in much deeper profiles. Furthermore, as subsequent erosion may occur to any depth in the profile prior to deposition of the overlying rocks, it is neither sufficient to say how deep the palaeosol is nor at what depth the sample was taken from beneath the unconformity in the interpretation of results. This gives no idea of the degree of weathering.

For example, in the gneiss suite at [NC 4385 6614] in NW Scotland, there is an overall increase in K_2O between the freshest and most altered rock (cf. Figs. 6.1 and 6.4c & d). However, in reality K_2O increases markedly in the initial stages, then decreases towards the top (see Figs. 6.4a & b). This initial increase is due to the formation of secondary K-rich minerals at the expense of albite. It decreases further up, however, as weathering progressed to an advanced stage and kaolinite rather than illite

became dominant. Hence, if a suite containing a greater percentage K-feldspar and less plagioclase than this one was analysed, or if more of the profile had been preserved, then the opposite trend (i.e. an overall decrease in K₂O) might be observed! Therefore, taking into account: 1) the change in behaviour of K₂O at each stage, 2) the mineralogy at each stage and 3) the degree of weathering of the rock, it is clear that the trend would be for continuing decrease in K₂O in higher parts of the now eroded profile, with weathering resulting in an overall decrease in K₂O.

Grandstaff *et al.* (1986) report an increase in K₂O relative to Al and Ti with alteration on the Dominion profile in South Africa. Sericite is the first and major secondary phase to form and no pyrophyllite is reported. This palaeosol developed on an originally plagioclase-rich granodiorite and from their graphs of modal minerals, sericite has formed predominantly and initially at the expense of plagioclase and at the expense of microcline higher in the profile. Hence this situation is very similar to that seen at the bottom of the profile in NW Scotland, below the level of pyrophyllite (see e.g. Fig. 5.1). Grandstaff *et al.* (1986) argue that an increase of K₂O relative to Al and Ti is "fairly common in Precambrian palaeosols (Gay and Grandstaff 1980). However, in modern soils of humid climate, K is lost". Indeed, other authors report 'dramatic' increases in K₂O in the Archean. While this may be the case for other Precambrian palaeosols, I suggest, from the information given, that it is entirely possible that the increase in K₂O observed in the Dominion profile could be primarily a weathering phenomena, influenced by their position in the weathering profile. This allows the possibility that K₂O may have decreased higher up if more of the palaeosol was preserved.

Another concern I have with Grandstaff *et al.*'s. (1986) interpretations is that, while they consider that sericite was formed due to diagenetic/metamorphic processes, they suggest the reaction....



...for its formation. With this reaction they are consequently obliged to consider a source for potassium. Indeed they say "it appears that sericite was formed during low-T diagenetic/metamorphism due to K-metasomatism of earlier clays which is revealed by a

major increase in K-content". My suggestion, however, is that illite was the initial clay. As in NW Scotland, sericite is the first (and their only) major secondary phase. However, kaolinite is NOT a typical first secondary weathered phase, but complex clays are e.g. smectite or illite (see Chapter 3, p.9). Assuming illite was the major complex clay at this time (e.g. Yaalon 1963) then it seems much more likely that sericite would have formed due to later restructuring of the already K-bearing illite. Hence, having to conclude such a significant influence from later K-metasomatism is therefore not necessary.

FURTHER WORK

Age determination, (using K/Ar and Ar/Ar techniques) of fresh pale pink primary K-feldspar to deep red authigenic K-feldspar from different depths beneath the unconformity in one suite from the palaeosaprolite, would further constrain the time of this alteration. Results could be compared or contrasted with those of Mensing and Faure (1983) and Macintyre (1986) from the North American mid-continent. K-feldspar at different depths from various suites would be most appropriate to analyse, but would probably have to come from Assynt or further south as the K-feldspar further north should have been reset (cf. $^{40}\text{Ar}/^{39}\text{Ar}$ for sample 0988 - reset feldspar).

Rare earth element behaviour in the palaeosaprolite could be investigated for comparison with their behaviour in modern soils and other palaeosols. The study of REE in such rocks appears to be increasing. Little information is recorded in the literature on REE in Precambrian palaeosols, so rigorous comparison with these cannot be made at present. However, an investigation of REE would add to the data base of information concerning this palaeosol, as well as the data base for Precambrian palaeosols in general, allowing for comparison to be made in the future.

When the tourmaline in the profile developed is unknown, therefore age determination of this mineral would be informative. Dating tourmaline by the K/Ar method could be attempted, although it may prove difficult as tourmaline frequently contains excess ^{40}Ar (Faure 1986).

1. *Agalmatolite is developed on Laurentian palaeosols in the Laurentian craton.*

With the aid of oxygen isotopes there may be a possibility of quantifying the degree of weathering with the oxygen isotopic value of the K-feldspar separates, using e.g. the Chemical Index of Alteration (Nesbitt and Young 1982) or some other index. This could then be applied for comparison with such feldspars from other profiles and could be a method of determining the degree of weathering of rocks from elsewhere.

2. *Field evidence suggests that the equivalent profile in the Laurentian craton is a palaeosol.*

Research could spread to a broader scale. Detailed investigation could be made of the equivalent unconformity around the margin of the Laurentian craton and elsewhere in the world and comparison made with the palaeosaprolite in NW Scotland. Comparison might help determine if the profiles formed under the same/similar conditions. Investigation of the sub-Cambrian profile from another location not affected by later temperature increase might also give more insight into the mineralogy and textural relationships of the profile after weathering. On a global scale, further investigation of palaeosols might help with palaeo-reconstruction models.

satisfied while more is known about the Laurentian craton.

The behaviour of many elements, especially many trace elements, needs to be more rigorously categorised in Precambrian palaeosols, especially as there is a dearth of information about behaviour of some. More understanding of their behaviour caused by weathering would diminish any confusion with other later processes.

the extent of the sub-Cambrian palaeosol in the Laurentian craton.

beneath the equivalent of the Laurentian palaeosol in the Laurentian craton.

then ~120km away, and in relation to the Laurentian craton.

a similar soil profile may have been developed in the Laurentian craton.

CHAPTER 11**CONCLUSIONS**

1. Agalmatolite is developed on Lewisian basement immediately beneath the Cambrian unconformity over a wide area of NW Scotland. Alteration increases towards the unconformity and penetrates the $\geq 20\text{m}$ beneath this boundary. Pinite is the major secondary mineral in most of the rocks exposed immediately beneath the unconformity, although occasionally pyrophyllite is the dominant phase.
2. Field evidence suggests that the alteration profile had formed in late Precambrian times prior to the deposition of overlying Cambrian strata.
3. The similarity in colour, mineralogy, vertical thickness and geological setting of agalmatolite compared to other Precambrian palaeosaprolites suggests it is a palaeosaprolite.
4. Of the criteria for identification of palaeosols of Grandstaff *et al.* (1986), seven of their nine points are satisfied. Of the other two, one (point 5, p.12) partly satisfied while there is no evidence for the other (point 8, p.13), though this may be due to poor exposure and since only the lowermost 'C' horizon of the soil profile has been preserved.
5. Field evidence suggests that the original soil profile was developed throughout the extent of the sub-unconformity rocks over an area $\geq 80 \times 65\text{km}^2$. (Alteration beneath the equivalent Proterozoic/Phanerozoic unconformity in Newfoundland, then $\sim 1200\text{km}$ away, and indeed in the North American mid-continent, suggests a similar soil profile may have been developed over thousands of km^2).

6. Differential movement from late Precambrian faulting along with possible variations in depth of weathering affected the degree of alteration preserved.
7. Thrusts may have used the soft soil profile as an easy-slip horizon in the central area, leading to the (apparently) poor development of agalmatolite there.
8. The orientation of sheared agalmatolite at [NC 3154 3241] is consistent with a Caledonian sense of movement, indicating that agalmatolite had formed by the end of the Caledonian orogeny and was affected by these movements.
9. The order of alteration of the major primary Lewisian minerals; plagioclase first, then biotite, K-feldspar and finally quartz, is consistent with Goldich's (1938) stability series for these phases during weathering.
10. The major secondary minerals in the profile are pinite, pyrophyllite, tourmaline, rutile and haematite.
11. Pinite is a $2M_1$ muscovite. The orientation of the crystals in the very fine-grained monomineralic aggregate is influenced by the crystallographic structure of the phase it is replacing.
12. Pyrophyllite occurs in varying amounts at the top of the profile but generally as a minor phase. However, sufficient evidence is available to conclude that were higher reaches of the alteration horizon preserved, it would have become a dominant phase.
13. The precursor weathering clays to the present pinite and pyrophyllite are considered to be illite and kaolinite respectively, indicating that the part of the profile preserved had suffered up to intermediate to advanced stage weathering.

14. The tourmalines are schorls and their chemistry is strongly influenced by the composition of the altered gneisses. Fluid inclusion data on quartz in quartz/tourmaline veinlets indicate that these minerals formed at $\sim 110^{\circ}\text{C}$ from surface-derived fluids.
15. The reddening of K-feldspar prior to replacement by pinitite occurred due to weathering.
16. From the results of the oxygen isotopic investigation of K-feldspars in the palaeosaprolite of NW Scotland, I propose that the reddening of primary K-feldspars in the sub-Cambrian profiles in North America described by Doe *et al.* (1983), Mensing and Faure (1983), Duffin (1989) and Harper (1991) occurred or was influenced during weathering, rather than being solely due to a later hydrothermal event.
17. The martitization of magnetite, the alteration of ilmenite to rutile and the concentration of haematite in certain layers indicates that alteration occurred under oxidising conditions.
18. The trend in Chemical Index of Alteration (CIA) of the rocks of the profile is consistent with that found in modern weathering profiles.
19. It is insufficient to compare absolute values of geochemical data in order to ascertain gains or losses of components. A method such as Gresens' (1967) should be used. Grant's (1986) graphical isocon method for the solution of Gresens' equations is considered to be more useful for indicating the behaviour of elements than Gresens' composition-volume diagrams.

20. Geochemical behaviour varies through a weathering profile and hence it is important to relate elemental variations to position in the profile when making interpretation of the data.
21. The behaviour of the major and trace elements is very similar to that found in other Precambrian palaeosaprolites as well as recently weathered rocks and is further support that the alteration profile formed as a result of weathering. The geochemical trends indicate that the profile formed under humid, tropical weathering conditions in an oxidising environment (up to 0.1 PAL) and at moderate pH. The variations imply that the weathering profile was more like a modern day pedalfer than most Precambrian palaeosols (most of which are Archean and considered to have formed under alkaline conditions). This supports the hypothesis of Kalliokoski (1975) that "by about 1000 Ma the soil-forming environment was capable of producing a soil that resembles a modern type", although, as expected, the behaviour of many bio-important elements differs from that of modern soils.
22. K^+ ions were lost during weathering. Weathering could thus have supplied K^+ as well as the "ionic or colloidal aluminium" and silica which were also transported from the weathering profile and which were constituents in the K-feldspar-rich horizons in the overlying strata as proposed by Russell and Allison (1985).
23. It is furthermore concluded that erosion of the soil carried clay minerals off-shore to form the shales and matrix in the Cambrian sediments which were precursors to the authigenic K-feldspar therein.
24. Boron, concentrated towards the top of the alteration profile and in the Cambrian shales, was absorbed into illites from seawater.

25. The boron enrichment identified by the British Geological Survey, which is spatially related to the Cambrian sediments in NW Scotland (see Plate 8.2), is due to the presence of boron-rich muscovite in the shales and sandstone matrix rather than detrital tourmalines as suggested by the BGS.
26. The authigenic K-feldspar and the muscovites in shales in the Cambrian succession formed soon after deposition at $\sim 500 \pm 10$ Ma, i.e. early Ordovician times, as sedimentation continued.
27. K-feldspar in shales of the Lower Member from Eriboll was reset due to the increase in temperature to above the Ar closure temperature. That K-feldspar was reset north of Assynt but not in samples from Assynt or Ullapool following emplacement of the Caledonian nappe pile supports the contention of Downie (1982), Johnson *et al.* (1985) and Ferguson (1987), that burial was deeper in the north than farther south. Since K-feldspar from Eriboll was reset, but biotite and muscovite of the matrix were not, it is concluded that these rocks were subjected to temperatures >150 to 200°C and $<350^\circ\text{C}$. This is also consistent with the findings of Downie (1982), Johnson *et al.* (1985) and Ferguson (1987).
28. It is concluded that pinite, the dominant mineral in the palaeosaprolite, formed at ~ 408 to 422 Ma when temperatures of the footwall reached their maximum after Caledonian thrusting.
29. Pinite (a $2M_1$ muscovite) formed due to the restructuring of illite. The transformation of $1M_d$ illite to $2M_1$ muscovite takes place at $\sim 250^\circ\text{C}$ (Hunziker *et al.* 1986). This temperature and the time at which the transformation occurred are consistent with the findings of Johnson *et al.* (1985). The temperatures are also consistent with those deduced above from $^{40}\text{Ar}/^{39}\text{Ar}$ analyses of shales

(point 26) and with the independent findings of Downie (1982) and Ferguson (1987).

30. Pyrophyllite formed due to reaction between kaolinite and quartz in the weathering profile. Its formation is considered to be contemporaneous with the formation of pinite when temperatures in these rocks reached their maximum of ~245 to 275°C, which is sufficient for this transformation to take place.

31. Agalmatolite is of minor economic importance as a carving stone for a small cottage industry.

REFERENCES

- ALLISON, I. Department of Geology and Applied Geology, University of Glasgow, Glasgow G12 8QQ, Scotland.
- ALLISON, I., FERGUSON, L.K., CARDENAS, S.F.A. AND KRONBERG, B.I. Precambrian muscovite-quartz (agalmatolite) palaeosols from Scotland and Canada. *Canadian Jour. of Earth Sciences*. (In press).
- ANDERTON, R., BRIDGES, P.H., LEEDER, M.R. AND SELLWOOD, B.W. (1979). *A dynamic stratigraphy of the British Isles*. George Allen & Unwin.
- ANON. (1989). China: UN pyrophyllite search. *Industrial Minerals*. 257, p11.
- APPLEYARD, E.C. AND WOOLLEY, A.R. (1979). Fentization: An example of the problems of characterizing mass transfer and volume changes. *Chem. Geol.*, 26, 1 - 15.
- ARMSTRONG, L.C. (1940). Decomposition and alteration of feldspar and spodumene by water. *Am. Mineralogist.*, 25, 810-820.
- BAKER, A.J. AND FALLICK, A.E. (1989). Heavy carbon in two-billion-year-old marbles from Lofoten-Vesteralen, Norway: Implications for the Precambrian carbon cycle. *Geochim. et Cosmochim. Acta.*, 53, 1111-1115.
- BATES, R.L. and JACKSON, J.A. (1987). *Glossary of Geology* (3rd Ed.) American Geol. Inst., Alexandria, Virginia.
- BAYLISS, P., BERRY, L.G., MROSE, M.E. AND SMITH, D.K. (1980). Mineral powder diffraction file. Data book. *JCPDS International Centre for Diffraction Data*.
- BEESON, R., BERG, R.C. AND CRASE, N.J. (1989). Lithogeochemical exploration for shale-hosted lead-zinc deposits: Case studies from the McArthur River and Mount Isa Districts, Northern Australia. *Mineralum Deposita*, 24, 299-307.
- BERMAN, R.G. (1988). Internally-consistent thermodynamic data for stoichiometric minerals in the system $\text{Na}_2\text{O}-\text{K}_2\text{O}-\text{CaO}-\text{MgO}-\text{FeO}-\text{Fe}_2\text{O}_3-\text{Al}_2\text{O}_3-\text{SiO}_2-\text{TiO}_2-\text{H}_2\text{O}-\text{CO}_2$. *J. Petrol.*, 29, 445-522.
- BERMAN, R.G., BROWN, T.H. AND GREENWOOD, H.J. (1985). A thermodynamic data base for minerals in the system $\text{Na}_2\text{O}-\text{K}_2\text{O}-\text{CaO}-\text{MgO}-\text{FeO}-\text{Fe}_2\text{O}_3-\text{Al}_2\text{O}_3-\text{SiO}_2-\text{TiO}_2-\text{H}_2\text{O}-\text{CO}_2$. Atomic Energy Canada Limited. Tech. Rpt. TR-377: 70p.
- BLAMART, D., PICHAVANT, M. AND SHEPPARD, S.M.F. (1988). D/H isotopic fractionation between tourmaline and water: the experimental

- calibration of tourmaline - mineral geothermometers at 500° to 700°C. *Chem. Geol.*, **70**.
- BOLES, J.** Department of Geological Sciences, University of California, Santa Barbara, California 93106, U.S.A.
- BOWIE, S.H.U., DAWSON, J., GALLAGHER, M.J. AND OSTLE, D. (1966).** Potassium rich sediments in the Cambrian of Northwest Scotland. *Trans. Inst. Min. Metal.*, **75B**, 125-145.
- BRINDLEY, G.W. AND BROWN, G. (Eds.) (1980).** *Crystal structures of clay minerals and their X-Ray Identification*. Min. Soc. Monograph. No. 5., Min. Soc., London.
- BROWN, T.H., BERMAN, R.G. AND PERKINS, E.H. (1988).** GEO-CALC : II. PTA-SYSTEM (Version 1.0). Software for calculation and display of pressure-temperature-activity phase diagrams. The University of British Columbia, Vancouver, Canada.
- BRYNDZIA, L.T. (1988).** The origin of diaspore and pyrophyllite in the Foxtrap Pyrophyllite deposit, Avalon Peninsula, Newfoundland: A reinterpretation. *Econ. Geol.*, **83**, 450-453.
- BUTTON, A. (1979).** Early Proterozoic weathering profile on the 2200 m.y. old Hekpoort Basalt, Pretoria Group, South Africa: preliminary results. *University of the Witwatersrand, Johannesburg. Info. Circular No. 133*.
- BUTTON, A. AND TYLER, N. (1979).** Precambrian palaeoweathering and erosion surfaces in Southern Africa: Review of their character and economic significance. *Econ. Geol. Res. Group. Uni. of the Witwatersrand. Info. Circ. 135*.
- BUTTON, A. AND TYLER, N. (1981).** The character and economic significance of Precambrian paleoweathering and erosion surfaces in Southern Africa. *Econ. Geol.*, 75th Anniv. Vol., 686-709.
- BUYCE, M.R. AND FRIEDMAN, G.M. (1975).** Significance of authigenic K-feldspar in Cambrian-Ordovician carbonate rocks of the Proto-Atlantic shelf in North America. *Jour. of Sed. Pet.*, **45**, 808-821.
- CARDENAS, S.F.A. (1986).** The geochemistry of a late Precambrian weathering profile northwest Scotland. Unpublished Ph.D. thesis. Department of Pure and Applied Chemistry, University of Strathclyde, Glasgow.
- CHAPIN, C.E. AND LINDLEY, J.I. (1986).** Potassium metasomatism of igneous and sedimentary rocks in detachment terranes and other sedimentary basins: Economic implications. *Arizona Geol. Soc. Digest. XVI*.

- CHESWORTH, W. (1983).** Phase relationships in the system $\text{SiO}_2\text{-Al}_2\text{O}_3\text{-H}_2\text{O}$, applicable to weathered materials of the surface of the Earth. Prof. Kelkar Mem. Vol. 1-6.
- CHITTLEBOROUGH, D.J. (1991).** Indices of weathering for soils and palaeosols formed on silicate rocks. *Australian Jour. of Earth Sciences.*, **38**, 115-120.
- CLEMMY, H. AND BADHAM, N. (1982).** Oxygen in the Precambrian atmosphere: an evaluation of the geological evidence. *Geology.*, **10**, 141-146.
- COMPSTON, W., WILLIAMS, I.S., RSES, ANU. (1990).** Zircon U-Pb ages relevant to the Cambrian Numerical Time-Scale. In: 7th International Conference on Geochronology and Isotope Geology. *Abstracts - Geol. Soc. of Australia.*
- COX, K.G., PRICE, N.B. AND HARTE, B. (1974).** *The practical study of crystals, minerals and rocks.* Rev. Ed. McGraw Hill, London.
- CRAIG, G.Y. (Ed.) (1983).** *Geology of Scotland.* 2nd Ed. Scottish Academic Press, Edinburgh.
- CRAW, D.** Department of Geology, University of Otago, Box 56, Dunedin, New Zealand.
- CUNNINGHAM, R.J.H. (1841).** Geognostical Account of the County of Sutherland. *Trans. High. Soc. Scot.*, **XIII**.
- DALZIEL, I.W.D. (1991).** Pacific margins of Laurentia and East Antarctica - Australia as a conjugate rift pair: Evidence and implications for an Eocambrian supercontinent. *Geology.*, **19**, 598-601.
- DANA, E.S.B. and FORD, W.E. (1949).** *A Textbook of Mineralogy.* (4th Ed.) John Wiley and Sons.
- DAVIDSON, G. (1992).** Piecing together the Pacific. *New Scientist.*, **133** (1804), 25-29.
- DAY, H.W. (1976).** A working model of some equilibria in the system alumina-silica-water. *Am. J. Sci.*, **276**, 1254-1284.
- DEER, W.A., HOWIE, R.A. AND ZUSSMAN, J. (1962).** *Rock forming minerals - sheet silicates.* v3, 16-18. Longmans, London.
- DEER, W.A., HOWIE, R.A. AND ZUSSMAN, J. (1986).** *Rock forming minerals - Disilicates and Ring Silicates.* VIB. 2nd Ed. Longman Scientific and Technical, England.
- DE JONGH, W.K. (1973).** *X-ray spectrom.*, **2**, 151-158.
- DELIAN, F. (1983).** Polyelements in the Lower Cambrian Black Shale Series in Southern China. In: Augustithis, S.S. (ed.). *The significance of trace elements in solving petrogenetic problems and controversies.* 447-474, Athens : Theophrastus.

- DICKSON, T.E. (1985). North American Pyrophyllite - ceramics leading the way. *Industrial Minerals.*, **218**, 57-59.
- DIPPLE, G.M., WINTSCH, R.P. AND ANDREWS, M.S. (1990). Identification of the scales of differential element mobility in a ductile fault zone. *J. metamorphic Geol.*, **8**, 645-661.
- DOE, B.R., STUCKLESS, J.S., AND DELEVAUX, M.H. (1983). The possible bearing of the granite of the UPH Deep Drill Holes, northern Illinois, on the origin of Mississippi Valley ore deposits: *Jour. Geophys. Res.*, **88**, 7335-7345.
- DOWNIE, C. (1982). Lower Cambrian achritarchs from Scotland, Norway, Greenland and Canada. *Trans. Royal. Soc. Edinburgh : Earth Sciences.*, **72**, 257-285. (esp. p 257).
- DREVER, J.I. (1982). *The geochemistry of natural waters*. Prentice-Hall, Inc., Englewood Cliffs, N.J., U.S.A.
- DUFFIN, M.E. (1989). Nature and origin of authigenic K-feldspar in Precambrian basement rocks of the North American mid-continent. *Geology.*, **17**, 765-768.
- DUFFIN, M.E., LEE, M., KLEIN, G.O. AND HAY, R.L. (1989). Potassic diagenesis of Cambrian sandstones and Precambrian granitic basement in UPH-3 deep hole, Upper Mississippi Valley, U.S.A. *Jour. Sed. Pet.*, **59**(5), 848-861.
- ELIAS, M., DONALDSON, M.J. AND GIORGETTA, N. (1981). Geology, Mineralogy, and Chemistry of Lateritic Nickel-Cobalt Deposits near Kalgoorlie, Western Australia. *Econ. Geol.*, **76**, 1775-1783.
- ELLIOT, D. AND JOHNSON, M.R.W. (1980). Structural evolution in the northern part of the Moine thrust belt, NW Scotland. *Trans. of the Royal Soc. Edinburgh: Earth Sciences.*, **71**, 69-96.
- ERSTAD, K-J. (1990). Adularia feldspar field and greenhouse experiments 1989-91. Annual research report 1989. Report 5/1990. Vol. II. Plant Chemical Analyses, Agricultural University of Norway, Department of Soil Sciences, P.O. Box 28, N-1432 As-NLH.
- ETHIER, V.G. AND CAMPBELL, F.A. (1977). Tourmaline concentrations in the Proterozoic sediments of the southern Cordillera of Canada and their economic significance. *Can. J. Earth Sci.*, **14**, 2348-2363.
- FAURE, G. (1986). *Principles of Isotope Geology*. 2nd Ed. John Wiley & Sons, New York.
- FEAKES, C.R. AND RETELLACK, G.J. (1988). Recognition and chemical characterization of fossil soils developed on alluvium: a Late Ordovician example. In: Reinhardt, J., and Siglio, W.R., (Eds.), *Paleosols and weathering through*

- time: principles and applications: *Geol. Soc. America. Spec. Paper.*, **216**, 35-48.
- FERGUSON, L.K. (1987).** A study of illite crystallinity along the Moine thrust zone of the N.W. Highlands. B.Sc (Hons) dissertation. University of Strathclyde.
- FISHER, R.A. AND YATES, F. (1963).** "Statistical Tables for Biological, Agricultural and Medical Research". 6th Ed. Oliver and Boyd.
- FISK, S. (1986).** An oxygen isotope study of siliceous rocks associated with stratabound mineralization in Scotland and Ireland. Unpub. Ph.D thesis. Department of Applied Geology, University of Strathclyde, Glasgow.
- FOLAND, K.A. (1974).** Ar⁴⁰ diffusion in homogeneous orthoclase and an interpretation of Ar diffusion in K-feldspars. *Geochim. et Cosmochim. Acta.*, **38**, 155-166.
- FORTIER, S. AND DONNAY, G. (1975).** Schorl refinement showing composition dependence of the tourmaline structure. *Canadian Mineralogist.*, **13**, 173-177.
- FRONDEL, C. (1962).** *The system of mineralogy of James Dwight Dana and Edward Salisbury Dana.* v3. 7th Ed., Wiley and Sons, New York and London.
- G-FARROW, C.E. AND MOSSMAN, D.J. (1988).** Geology of Precambrian Paleosols at the base of the Huronian Supergroup, Elliot Lake, Ontario, Canada. *Precamb. Res.* **42**, 107-139.
- GARRELS, R.M. (1984).** Montmorillonite/Illite Stability Diagrams. *Clays and Clay Minerals.*, **32**, 161-166.
- GAVISH, E. AND REYNOLDS, R.C. (1970).** Structural changes and isomorphic substitution in illites from limestones of variable degrees of metamorphism. *Israel J. Chem.*, **8**, 477-485.
- GAY, A.L. AND GRANDSTAFF, D.E. (1980).** Chemistry and mineralogy of Precambrian paleosols at Elliot Lake, Ontario, Canada. *Precamb. Res.*, **12**, 349-375.
- GOLDICH, S.S. (1938).** A study in rock weathering. *J. Geol.* **46**, 17-58.
- GRANDSTAFF, D.E., EDELMAN, M.J., FOSTER, R.W., ZBINBEN, E. AND KIMBERLY, M.M. (1986).** Chemistry and mineralogy of Precambrian paleosols at the base of the Dominion and Pongola groups (Transvaal, South Africa). *Precamb. Res.*, **32**, 97-131.
- GRANT, J.A. (1986).** The Isocon Diagram - A Simple Solution to Gresens' Equation for Metasomatic Alteration. *Econ. Geol.*, **81**, 1976-1982.
- GRESENS, R.L. (1967).** Composition-Volume Relationships of Metasomatism. *Chem. Geol.* **2**, 47-65.

- GRIM, R.E. (1953). *Clay Mineralogy*. New York. p340.
- GRUNER, J.W. (1929). Structural reasons for oriented intergrowths in some minerals. *Amer. Min.* **14**, 227-237.
- HALLIDAY, A.N., STEVENS, W.E. AND HARMON, R.S. (1979). Petrogenetic significance of Rb-Sr and U-Pb isotopic systems in the c.400 Ma old British Isles granitoids and their hosts. *In*: Harris, A.L., Holland, C.H. and Leake, B.E. (eds.). *The Caledonides of the British Isles - reviewed*. Spec. Publ. Geol. Soc. London, **8**, 653-661.
- HALLIDAY, A.N., FALLICK, A.E., DICKIN, A.P., MACKENZIE, A.B., STEPHENS, W.E. AND HILDRETH, W. (1983). The isotopic and chemical evolution of Mount St. Helens. *Earth and Planetary Sci. Letters.*, **63**, 241-256.
- HAMBURGER, G.E. AND BUERGER, M.J. (1948). The structure of tourmaline. *American Mineralogist.*, **33**, p532.
- HARDER, H. (1961). Einbau von Bor in detritische Tonminerale. Experimente zur Erklärung des Borgehalts toniger sedimente. *Geochim. et. Cosmochim. Acta.*, **21**, 284-294.
- HARPER, D.A., LONGSTAFFE, F.J. AND WADLEIGH, M.A. (1991). Unconformity-related K-feldspar and phyllosilicate alteration at the Precambrian-Paleozoic boundary, southwestern Ontario. Programs and abstracts for the Clay Mineral Society, 28th Annual Meeting, Houston, Texas. p66.
- HARLAND, W.B., ARMSTRONG, R.L., COX, A.V., CRAIG, L.E., SMITH, A.G. AND SMITH, D.G. (1990). *A geologic time scale 1989*. Cambridge University Press.
- HARRISON, T.M. AND McDOUGALL, I. (1982). The thermal significance of potassium feldspar K-Ar ages inferred from $^{40}\text{Ar}/^{39}\text{Ar}$ age spectrum results. *Geochim. et Cosmochim. Acta.*, **46**, 1811-1820.
- HARNOIS, L. (1988). The CIW index: A new chemical index of weathering. *Sedimentary Geology.*, **55**, 319-322.
- HARVEY, P.K., TAYLOR, D.M., HENDRY, R.D. AND BANCROFT, F. (1973). An accurate fusion method for the analysis of rocks and chemically related materials by X-ray Spectrometry., **2**, 33-44.
- HARVEY, P.K. AND ATKIN, B.P. (1981). The rapid determination of RB, SR and their ratios in geological materials by X-ray fluorescence spectrometry using a Rhodium X-ray tube. *Chem. Geol.* **32**, 291-301.
- HARVEY, P.K. AND ATKIN, B.P. (1982). The estimation of mass absorption coefficients by Compton scattering-extensions to the use of Rh K_{∞} Compton. *Amer. Mineral.*, **62**, 534-537.

- HEARN, P.P. Jr., SUTTER, J.F. AND BELKIN, H.E. (1987). Evidence for Late-Paleozoic brine migration in Cambrian carbonate rocks of the central and southern Appalachians: Implications for Mississippi Valley-type sulfide mineralization. *Geochim. et Cosmochim. Acta.* **51**, 1323-1334.
- HEDDLE, M.F (1881). The Geognosy and Mineralogy of Scotland. *Min. Mag.*, **4**, 197-254.
- HELGESON, H.C., KIRKHAM, D.H. AND FLOWERS, G.C. (1981). Theoretical prediction of the thermodynamic behaviour of aqueous electrolytes at high pressures and temperatures: IV. Calculation of activity coefficients, osmotic coefficients, and apparent molal and standard and relative partial molal properties to 600°C and 5kb. *Amer. J. Sci.*, **281**, 1249-1516.
- HIGGINS, A.C. (1967). The age of the Durine Member of the Durness Limestone Formation at Durness. *Scott. J. Geol.*, **3(3)**, 382-388.
- HIGGINS, A.C. AND AUSTIN, R.L. (1985). *A stratigraphical index of Conodonts.* p43. Ellis Harwood Limited, W. Sussex.
- HOEVE, J. AND SIBBALD, T.I.I. (1978). On the Genesis of Rabbit Lake and Other Unconformity-type Uranium Deposits in Northern Saskatchewan, Canada. *Econ. Geol.*, **73**, 1450-1473.
- HOLLAND, J.G. AND WINCHESTER, J.A. (1983). The uses of geochemistry in solving problems in highly deformed metamorphic complexes. In: Augustithis, S.S. (Ed.). *The significance of trace elements in solving petrogenetic problems and controversies.* 389-405, Athens: Theophrastus.
- HOLLAND, H.D., FEAKES, C.R. AND ZBINDEN, E.A. (1989). The Flin Flon Paleosol and the composition of the atmosphere 1.8 B.y. B.P. *Am. Jour. of Science.* **2**, 362-388.
- HUNZIKER, J.C., FREY, M., CLAUER, N., DALLMEYER, R.D., FRIEDRICHSEN, H., FLEHMIG, W., HOCHSTRASSER, K., ROGGWILER, P. AND SCHWANDER, H. (1986). The evolution of illite to muscovite: mineralogical and isotopic data from the Glarus Alps, Switzerland. *Contrib. Mineral. Petrol.*, **92**, 157-180.
- Institute of Geological Sciences, (1982). Regional Geochemical Atlas. No. 4., Map 7, Boron.
- JENKINS, R. AND DE VRIES, J.L. (1967). *Practical X-ray spectrometry.* Hazell Watson and Viney Ltd., Bucks, G.B.
- JENNY, H. (1941). *Factors of Soil Formation.* McGraw-Hill, New York. 281p.
- JOHNSON, M.R.W., KELLEY, S.P., OLIVER, G.J.H. AND WINTER, D.A. (1985). Thermal effects of timing of thrusting in the Moine Thrust zone. *Jour. Geol. Soc.*, **142**, part 5, 863-873.

- KALLIOKOSKI, J. (1975).** Chemistry and Mineralogy of Precambrian Paleosols in Northern Michigan. *Geol. Soc. Am. Bull.* **86**, 371-376.
- KASTING, J.F. (1987).** Theoretical constraints on oxygen and carbon dioxide concentrations in the Precambrian atmosphere. *Precamb. Res.*, **34**, 205-229.
- KASTNER, M. AND SEIVER, R. (1979).** Low-Temperature feldspars in sedimentary rocks. *Am. Jour. of Sci.*, **279**, 435-479.
- KELLEY, S.P.** Dept. of Earth Sciences, The Open University, P.O. Box 70, Milton Keynes, NK70 6AA, England.
- KELLEY, S.P. AND POWELL, D. (1985).** Relationships between marginal thrusting and movement on major, internal shear zones in the Northern Highland Caledonides, Scotland. *Journal of Structural Geology.*, **7**, 161-174.
- KIMBERLEY, M.M., TANAKA, R.T. AND FARR, M.R. (1980).** Composition of middle Precambrian uraniferous conglomerate in the Elliot Lake - Agnew Lake area of Canada. *Precamb. Res.*, **12**, 375-392.
- KIMBERLEY, M.M. AND GRANDSTAFF, D.E. (1986).** Profiles of elemental concentrations in Precambrian Paleosols on Basaltic and Granitic Parent Materials. *Precamb. Res.* **32**, 133-154.
- KLAPROTH, M.H. (1797).** Beitrage ur Chemischen Kenntniss der Mineralkorper.
- KORNERUP, A. (1967).** *Methuen handbook of colour (2nd ed.)* Methuen, London.
- KRESTEN, P. (1988).** The chemistry of feniization : examples from Fen, Norway. *Chem. Geol.*, **68**, 329-349.
- KRONBERG, B.I. (1985).** Weathering dynamics and geosphere mixing with reference to the potassium cycle. *Physics of the Earth and Planetary Interiors.*, **41**, 125-132.
- KRONBERG, B.I., FYFE, W.S., LEONARDOS, O.H., Jr. AND SANTOS, A.M. (1979).** The chemistry of some Brazilian soils: element mobility during intense weathering. *Chem. Geol.*, **24**, 211-229.
- KRONBERG, B.I., NESBITT, H.W. AND LAM, W.W. (1986).** Upper Pleistocene Amazon deep-sea fan muds reflect intense chemical weathering of their mountainous source lands. *Chem. Geol.*, **54**, 283-294.
- KRONBERG, B.I., NESBITT, H.W. AND FYFE, W.S. (1987).** Mobilities of alkalis, alkaline earths and halogens during weathering. *Chem. Geol.* **60**, 41-49.
- KRONBERG, B.I., TAZAKI, K. AND MELFI, A.J. (1987).** Detailed geochemical studies of the initial stages of weathering of alkaline rocks: Ilha de São Sebastião, Brazil. *Chem. Geol.* **60**, 79-88.

- LEAKE, B.E., HENDRY, G.L., KEMP, A., PLANT, A.G., HARVEY, P.K., WILSON, J.R., COATS, J.S., AUCOTT, J.W., LÜNEL, T. AND HOWARTH, R.J. (1970). The chemical analysis of rock powders by automatic X-Ray fluorescence. *Chem. Geol.*, **5**, 7-86.
- LEVITAN, M.A., DONTSOVA, E.I., LISITSYN, A.P. AND BOGDANOV, YU.A. (1975). The origin of chert in the sediments of the Pacific Ocean from data of oxygen isotopic analysis and a study of the distribution of chert. *Geochem. Internat.*, **12**, 95-104.
- LIN Fujian Bureau of Geology and Mineral Resources, 58 Hu Dong Road, Fuzhou, China.
- LINDSTRÖM, M. (1971). Lower Ordovician Conodonts of Europe. In : W.C. Sweet and S.M. Bergström (Eds.). *Symp. on Conodont Biostratigraphy, in Mem. Geol. Surv. Am.*, **127**, 21-61.
- LOUGHNAN, F.C. (1969). *Chemical Weathering of the Silicate Minerals*. American Elsevier Pub. Co., Inc., New York.
- MACINTYRE, R.M. AND HAMILTON, P.J. (1984). Isotope Geochemistry of Lavas from sites 553 and 555¹. In: Roberts, D.G., Schnitker, D. *et al.* (1984). Initial Reports of the Deep Sea Drilling Project, Vol. LXXX1, Washington (U.S. Government Printing Office).
- MACINTYRE, R.M. (1986). K/Ar ages of feldspars from the North American Precambrian basement and their possible significance for the genesis of ore deposits of the Mississippi Valley Type. *Terra Cognita*, **6**(2), p227.
- MACKENZIE, F.T. AND GARRELS, R.M. (1966). Chemical mass balance between rivers and oceans. *Am. Jour. of Sci.*, **264**, 507-525.
- MASON, B. (1966). *"Principles of Geochemistry"*. 3rd Ed. Wiley and Sons, Inc. London.
- MATSUHISA, Y., GOLDSMITH, J.R. AND CLAYTON, R.N. (1979). Oxygen isotopic fractionation in the system quartz-albite-anorthite-water. *Geochim. et Cosmochim. Acta.*, **43**, 1131-1140.
- MENSING, T.M. AND FAURE, G. (1983). Identification and Age of Neoformed Paleozoic Feldspar (Adularia) in a Precambrian Basement Core from Scioto County, Ohio, U.S.A. *Contrib. Mineral. Petrol.*, **82**, 327-333.
- McARTHUR, J.M., TURNER, J.V., LYONS, W.B., OSBORN, A.O. AND THIRLWALL, M.F. (1991). Hydrochemistry on the Yilgarn Block, Western Australia: Ferrolysis and mineralisation in acidic brines. *Geochim. et Cosmochim. Acta.*, **55**, 1273-1288.

- McDOUGALL, I. AND HARRISON, T.M. (1988). *Geochronology and thermochronology by the $^{40}\text{Ar}/^{39}\text{Ar}$ method*. Oxford University Press, New York. p212.
- McKIE, T. (1988). The sedimentology of the Cambrian clastic sediments of northwest Scotland. Unpub. Ph.D. thesis. Department of Applied Geology, University of Strathclyde, Glasgow.
- MOORES, E.M. (1991). Southwest U.S. - East Antarctica (SWEAT) connection: A hypothesis. *Geology*, **19**, 425-428.
- NAHON, D., PAQUET, H. AND DELVIGNE, J. (1982). Lateritic Weathering of Ultramafic Rocks and the Concentration of Nickel in the Western Ivory Coast. *Econ. Geol.*, **77**, 1159-1175.
- NESBITT, H.W., MARKOVICS, G. AND PRICE, R.C. (1980). Chemical processes affecting alkalis and alkaline earths during continental weathering. *Geochim. et Cosmochim. Acta.*, **44**, 1659-1666.
- NESBITT, H.W. AND YOUNG, G.M. (1982). Early Proterozoic climates and plate motions inferred from major element chemistry of lutites. *Nature*, **299**, 715-717.
- NICKEL, E.H., ALLCHURCH, P.D., MASON, M.G. AND WILMSHURST, J.R. (1977). Supergene Alteration at the Perseverance Nickel Deposit, Agnew, Western Australia. *Econ. Geol.* **72**, 184-203.
- NORDSTROM, D.K. AND MUNOZ, J.L. (1986). *Geochemical Thermodynamics*. Blackwell Scientific Publications, Oxford, U.K.
- OLLIER, C. (1984). *Weathering*. (2nd Edition). Longman, London and New York.
- OLSEN, S.N. AND GRANT, J.A. (1991). Isocon analysis of migmatization in the Front Range, Colorado, U.S.A. *J. metamorphic Geol.*, **9**, 1 - 14.
- ORIAN, K.J. AND BRULAND, K.W. (1988). Dissolved gallium in the open ocean. *Nature.*, **332**, pp717.
- OXBURGH, E.R. AND TURCOTTE, D.L. (1974). Thermal gradients and regional metamorphism in overthrust terrains with special reference to the eastern Alps. *Schweiz. mineral. petrogr. Mitt.*, **54**, 641-662.
- PAPEZIK, V.S., KEATS, H.F. AND VAHTRA, J. (1978). Geology of the Foxtrap Pyrophyllite Deposit, Avalon Peninsula, Newfoundland. *Econ. Geol.* pp1-9.
- PARK, R.G. AND TARNEY, J. (Ed.) (1973). *The Early Precambrian of Scotland and Related Rocks of Greenland*. University of Keele, Staffordshire, England.

- PEACH, B.N., HORNE, J., GUNN, W., CLOUGH, C.T. and HINXMAN, L.W. (1907). The geological structure of the northwest Highlands of Scotland. *Mem. Geol. Surv. G.B.*
- PETTIJOHN, F.J. (1975). *Sedimentary rocks*, 3rd Edn. New York : Harper and Row.
- PIPER, J.D.A. (1987). *Palaeomagnetism and the Continental Crust*. Halstead Press, 87. John Wiley & Sons, Inc., New York.
- PRASAD, N. AND ROSCOE, S.M. (1991). G.S.C. Report. 91-1C, 43-54.
- RAMDHOR, P. (1969). *The ore minerals and their intergrowths*. Pergamon Press, England.
- RAMKAMA, K. (1955). Geologic evidence of chemical composition of the Precambrian atmosphere. In: A Poldervaart (Ed.), *Crust of the Earth*. *Geol. Soc. Am. Sp. Pap.* 62, Denver, Colorado. 651-664.
- READ, H.H. (1980) *Rutley's elements of mineralogy*. 26th Ed. George Allen and Unwin Ltd., London.
- REIMER, T.O. (1986). Alumina-rich rocks from the early Precambrian of the Kaapvaal Craton as indicators of paleosols and as products of other decompositional reactions. *Precamb. Res.* 32, 155-179.
- RETALLACK, G. (1986). Reappraisal of a 2200M.a.-old paleosol near Waterval Onder, South Africa. *Precamb. Res.* 32, 195-232.
- RETALLACK, G., GRANDSTAFF, D. AND KIMBERLEY, M. (1984). The Promise and Problems of Precambrian Paleosols. *Episodes.* 7 (2), 8-12.
- RILEY, J.P. (1958). Simultaneous Determination of Water and Carbon Dioxide in Rocks and Minerals. *Analyst.*, 83 (982), 42-49.
- ROCK, N.M.S., MACDONALD, R., SZUCS, T. AND BOWER, J. (1986). The comparative geochemistry of some Highland pelites (Anomalous local limestone-pelite successions within the Moine outcrop; II). *Scott. J. Geol.* 22(1), 107-126.
- RODDICK, J.C. (1983). High precision intercalibration of ^{40}Ar - ^{39}Ar standards. *Geochim. et Cosmochim. Acta.*, 47, 887-898.
- ROSE, A.W., HAWKES, H.E. AND WEBB, J.S. (1979). *Geochemistry in mineral exploration*. Academic Press Pub.
- RUSSELL, M.J. and ALLISON, I (1985). Agalmatolite and the maturity of sandstones of the Appin and Argyll groups and Eriboll sandstone. *Scott. Jour. Geol.*, 21, 113-122.
- RUSSELL, M.J. (1985). The evolution of the Scottish mineral sub-province. *Scott. J. Geol.* 21(4), 513-545.

- SCHAU, M. AND HENDERSON, J.B. (1983). Archean chemical weathering at three localities on the Canadian Shield. *Precamb. Res.*, **20**, 189-224.
- SHEPPARD, R.A. AND GUDE, A.J. (1973). Boron-bearing potassium feldspar of authigenic origin in closed-basin deposits. *Jour. Res. U.S. Geol. Surv.*, **1**, 377-382.
- SHEPPARD, S.M.F. (1986). Characterisation and isotopic variations in natural waters. In: Valley, J.W., Taylor, H.P. and O'Neil, J.R. (Eds.). *Stable isotopes in high temperature geological processes. Min. Soc. of Am., Reviews in Mineralogy.*, **16**, 165-184.
- SHIEH, Y.N. (1983). Oxygen isotope study of Precambrian granites from the Illinois Deep Hole Project. *Jour. of Geophys. Research.* **88** (B9), 7300-7304.
- SONG, X-Q. Fujian Bureau of Geology and Mineral Resources, 58 Hu Dong Road, Fuzhou, China.
- SONG, X-Q., AND DONG, B. (1988). The pyrophyllite resource in China. *Geology of China.* (Aug).
- SOPER, N.J. (1971). The earliest Caledonian structures in the Moine Thrust belt. *Scott. J. Geol.*, **7**, 241-247.
- SUTTON, J. AND WATSON, J.V. (1951). The pre-Torridonian metamorphic history of the Loch Torridon and Scourie areas in the northwest Highlands and its bearing on the chronological classification of the Lewisian. *Q.J. Geol. Soc. London.* **106**, 241-307.
- TAYLOR, B.E. AND SLACK, J.F. (1984). Tourmalines from Appalachian-Caledonian Massive Sulfide Deposits: Textural, Chemical, and Isotopic Relationships. *Econ. Geol.*, **79**, 1703-1726.
- TAYLOR, S.R. AND McLENNAN, S.M. (1985). *The Continental Crust: its Composition and Evolution.* Blackwell Scientific Publications, Great Britain.
- THOMPSON, A.B. (1970). A note on the kaolinite-pyrophyllite equilibrium. *Am. J. Sci.*, **268**, 454-458.
- TSUZUKI, Y. (1967) Solubility diagrams for explaining zone sequences in bauxite, kaolin and pyrophyllite-diaspore deposits. *Clays Clay Miner.*, **24**, 297-302.
- TWIST, D. AND CHENEY, E.S. (1986). Evidence for the transition to an oxygen-rich atmosphere in the Rooiberg Group, South Africa - A note. *Precamb. Research.*, **33**, 255-264.
- VEJNAR, Z. (1971). Trioctahedral micas of west Bohemian pluton and their petrogenetic significance. *Krystalinikum*, **7**, 149-164.
- VELDE, B. (1977). *Clays and Clay Minerals in Natural and Synthetic Systems.* Elsevier Scientific Publishing Co., Amsterdam.

- WALSH, J.N. (1985). Determination of Boron at Trace Levels in Rocks by Inductively Coupled Plasma Spectrometry. *Analyst.*, **110**, 959-962.
- WATSON, J.V. (1975). The Lewisian Complex. In: *A correlation of the Precambrian rocks in the British Isles*. A.L. Harris *et al.* (Eds.), **15-19**. Geol. Soc. Lond. Spec. Rep., No. 6.
- WEBSTER, R. (1983). *Gems: their sources, descriptions and identification*. (4th Ed.) Butterworths & Co. Ltd., England.
- WEDEPOHL, K.H. (Ed). (1974). *Handbook of geochemistry*. II/4. 5.8.1-5.0.3.
- WELTON, J.E. (1984). *SEM Petrology atlas*. The American Association of Petroleum Geologists, Oklahoma, U.S.A.
- WILLIAMS, G.E. (1968). Torridonian weathering, and its bearing on Torridonian palaeoclimate and source. *Scott. J. Geol.* **4**(2), 164-184.
- YAALON, D.H. (1963). Weathering and soil development through geologic time: *Isreal Research Council Bull.*, Sec. G., **11** (3), 149-150.
- ZEN, E-AN. (1961). Mineralogy and Petrology of the system $\text{Al}_2\text{O}_3 - \text{SiO}_2 - \text{H}_2\text{O}$ in some pyrophyllite deposits of North Carolina. *The American Mineralogist.*, **46**, 52-66.

APPENDICES

APPENDIX 1

Agalmatolite (Shoushan stone) of China

INTRODUCTION

Much of Chinese agalmatolite is pyrophyllite (Webster 1983), while some is pinite and others steatite (Dana and Ford 1949, Bates and Jackson 1987). Pyrophyllite is found in a number of geological environments, including sub-unconformity settings as an alteration product of Al-rich clay. Although pyrophyllite (with associated minerals known traditionally as Shoushan stone) is used primarily as an industrial mineral in China, it was historically, and is still presently, important as a carving stone.

China is a substantial producer of pyrophyllite, although available statistics are confusing as pyrophyllite figures are integrated with those of talc, steatite and soapstone (Anon 1989). China, however, has the world's third largest known reserves of pyrophyllite after Japan and South Korea (which dominate world production) and together all three have ~75% of the world's reserves (Song and Dong 1988).

Number of deposits and locations in China

To date, there are >100 places where pyrophyllite has been found in China, 16 of which are being exploited. Most of the pyrophyllite reserves are found in Fujian province (56%) followed by Zhejiang (31%) (Song and Dong 1988). Guangdong, Jilin, Beijing and Inner Mongolia also have deposits, with minor amounts in Shandong (Fig. A1.1).

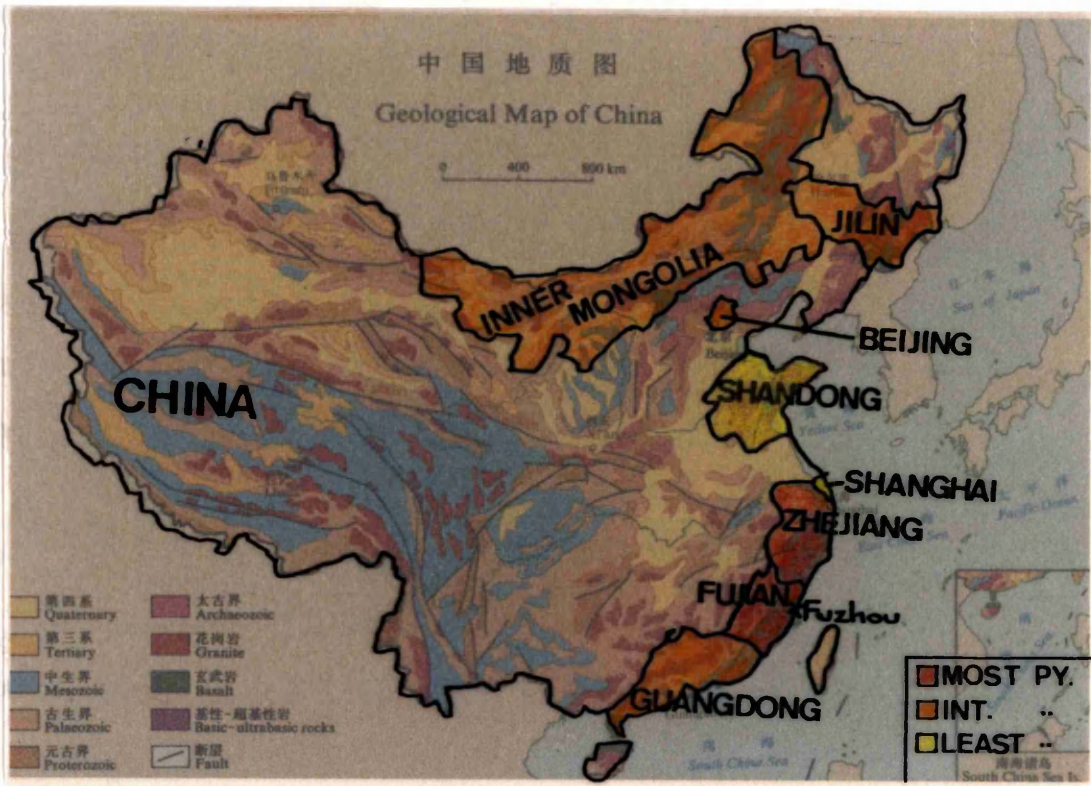


Fig. A1.1
Chinese provinces with known pyrophyllite deposits.

Geological environments of formation

Pyrophyllite in China is divided into two groups dependant on its genesis: 1) hydrothermal and 2) metamorphic.

1. Hydrothermal pyrophyllite

The majority (~90%) of recoverable reserves in China were formed due to hydrothermal alteration of acid to intermediate igneous rocks. Pyrophyllite formed in this environment is usually of high quality, constitutes a large percentage of the rock and formed on a larger scale than that formed in metamorphic environments. Most deposits

are concentrated in SE China (Fig. A1.1). Associated minerals include alunite, dickite, kaolinite and sericite.

2. Metamorphic pyrophyllite

Metamorphic pyrophyllite deposits constitute only a small proportion of recoverable reserves and occur mainly in north and NW China (Fig. A1.1). This category is sub-divided into three groups (Song and Dong 1988): a) dynamic, b) burial and c) regional metamorphism.

a) Dynamic metamorphism

Pyrophyllite formed due to alteration of Al-rich clay during deformation in fault zones. The mineral appears in thin foliated layers.

b) Burial metamorphism

In this case, Al-rich clay is altered on a large scale to pyrophyllite due to the increase in overlying pressure and geothermal gradient during burial (e.g. unconformity related pyrophyllite).

c) Regional metamorphism

Regional metamorphism of acid to intermediate igneous rocks caused secondary pyrophyllite to form.

Pyrophyllite and sericite often occur together and are found in sub-unconformity Proterozoic rocks, as in NW Scotland, in Shandong, Shanxi and Hebei provinces.

Chinese nomenclature

The classification above is based on the genesis of the pyrophyllite. The Chinese call pyrophyllite and its associated minerals "Shoushan stone" which they subdivide into three categories based on quality which is related to genesis (Table A1.1). Altogether there are >100 different varieties dependant on colour, lustre and composition of the rock.

CATEGORY		QUALITY
(1) SHANKENG	Constitutes the main body of pyrophyllite	Poor - suitable only for industrial applications.
(2) SHUIKENG	Common vein association. Often found in caves	Good - can use for carving.
(3) TIANKENG	Of strong yellow/red colour and bright lustre - believed to be due to immergence in water below rice fields for several thousand years!	Very good - best quality carving material.

Table A1.1
Chinese categories of Shoushan stone.

Tianhuang (yellow stone), a variety of Tiankeng, is known as "The King of Shoushan stone" and to the Chinese can be worth three times the price of gold by weight!!

Uses

Traditionally in China, pyrophyllite and related minerals are used for carving. Most, however, is used industrially. Approximately 60% is used in the formation of

porcelain, 23% for refractories and ~10% in plastics. It is also used in glass, concrete, agricultural pesticides, paints, rubber, paper making and cosmetics (Song and Dong 1988).

FUJIAN PROVINCE

A joint venture between the United Nations and China for the exploration for pyrophyllite in Fujian Province was announced in January, 1989 (Anon 1989).

Fujian Province in SE China (Fig. A1.1) is the largest producer of pyrophyllite in China and with 56% contains the country's richest reserves. There are >40 pyrophyllite deposits which are distributed in the east of the province, along the NE striking Mingdong Volcanic belt.

Two of these deposits, Dongzi and Shoushan, were visited in July, 1990.

Dongzi (Pyrophyllite) Deposit

The Dongzi deposit (Plate A1.2) is the largest pyrophyllite deposit in China with reserves of ~18 Mt (Anon 1989). It is situated in Fuqing county, 42 km south of Fuzhou (Fig. A1.1).

Geological setting

The pyrophyllite is found in lenses and was formed due to hydrothermal alteration of Jurassic rhyolitic and dacitic tuffs (Plate A1.1). Pyrophyllite from the Dongzi deposit is of low quality (Shankeng type) due to the often high silica content as well as alunite, pyrite and haematite as impurities.

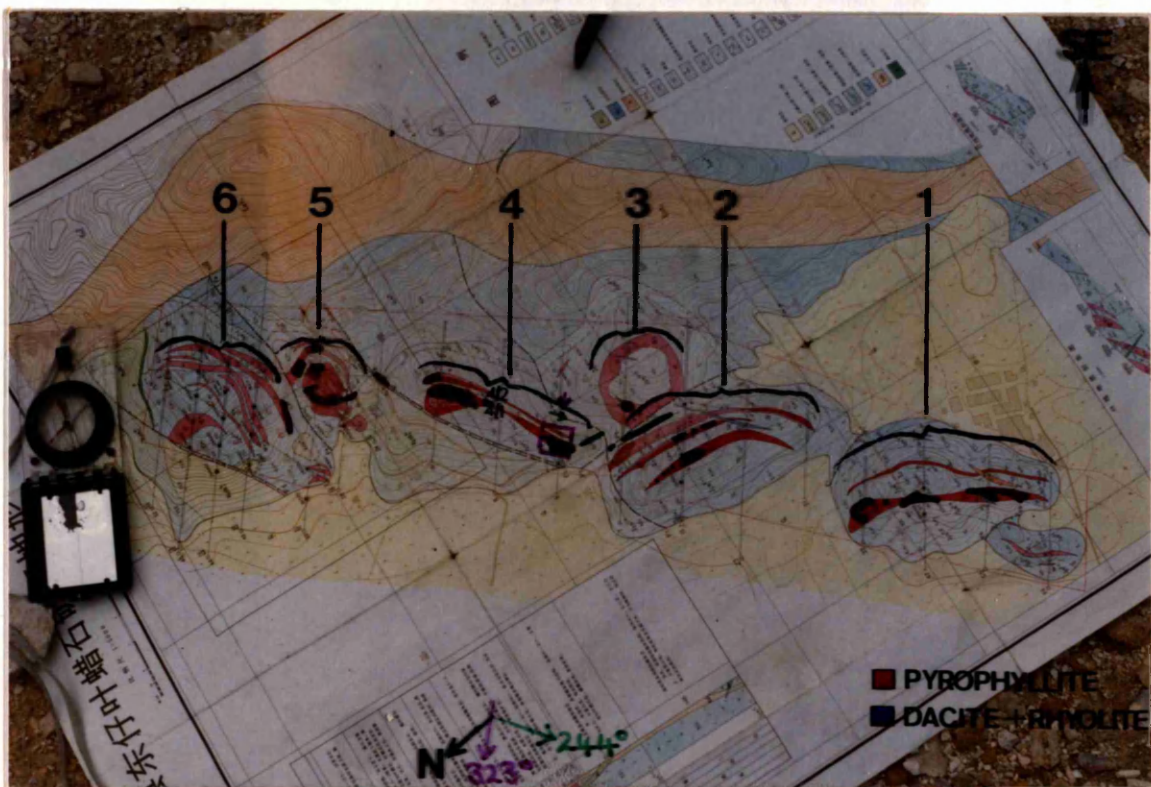


Plate A1.1

Geological map of the Dongzi deposit.

- | | | |
|--------------------|---|---|
| Brown areas | = | Areas of working (cf. Plate A1.2) |
| Purple areas + box | = | As shown on Fig. A1.2 |
| Green area | = | Silicified ridges. Photo (Plate A1.5) taken from green arrow. |
| 1-6 | = | Orebodies. |

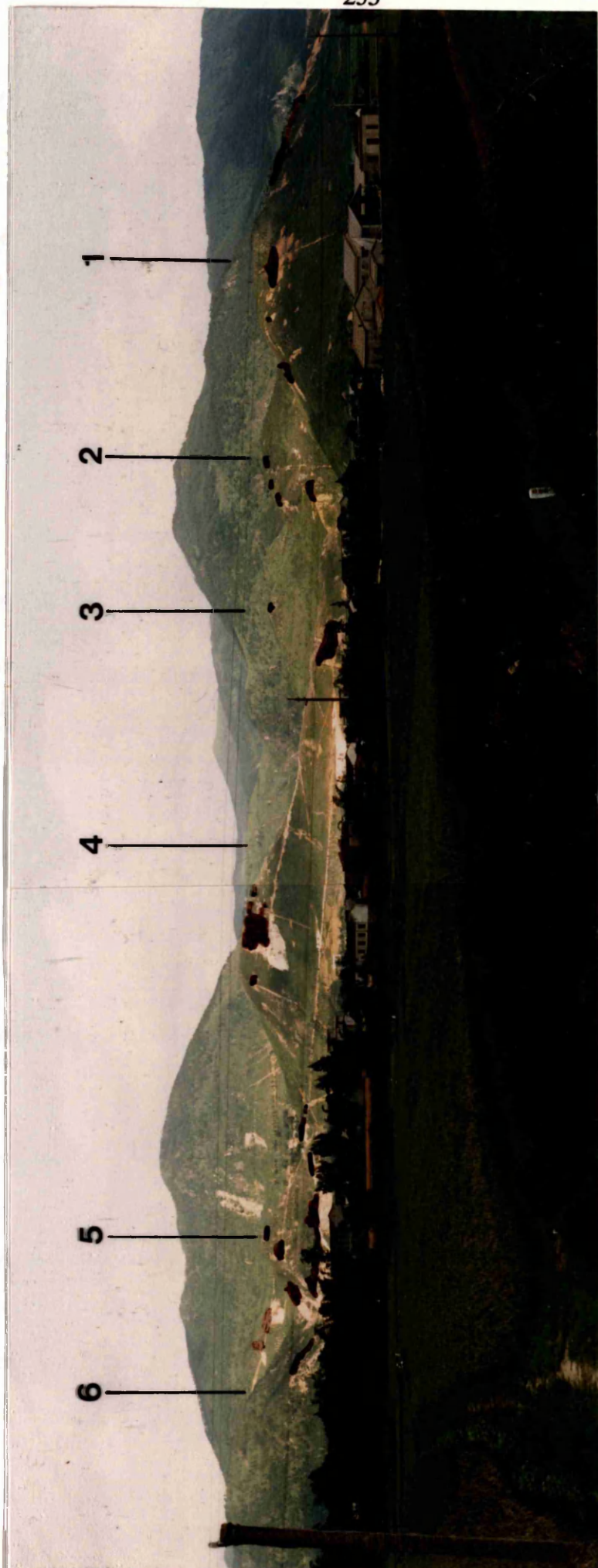


Plate A1.2

Dongzi pyrophyllite deposit - the largest pyrophyllite deposit in China. Nos. 1-6

= orebody numbers

= areas of pyrophyllite workings.

See Plate A1.1 to show their locations on the Geological map.

Orebodies

The Dongzi deposit is divided into six orebodies (Plates A1.1 and A1.2). The pyrophyllite in the upper lens of orebody 4, which has a mineralogy typical of the deposit, is 15m thick, with the purest pyrophyllite in the central zone (Fig. A1.2).

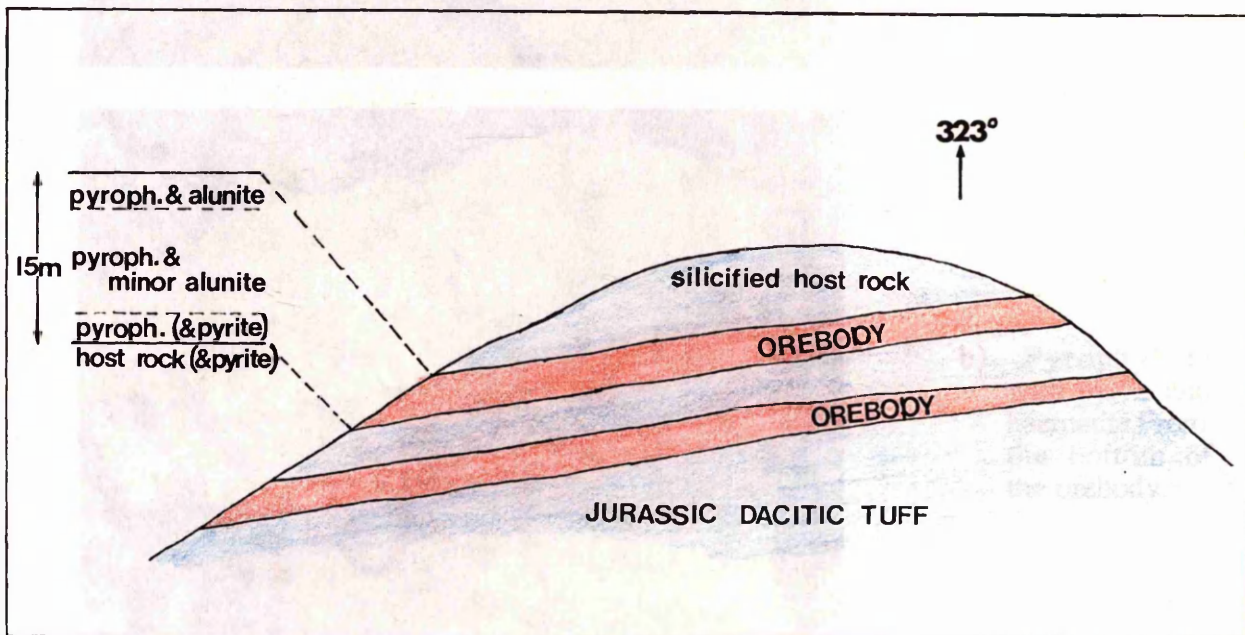


Fig. A1.2

Sketch of orebody 4 and mineralogy of upper lens. (See also Plate A1.1 for area and direction of sketch (purple ink)).

At the edge of the altered zone, the dacite has been oxidised (Plate A1.3c) and pyritized. In the lower zone of the pyrophyllite lens, the pyrophyllite contains pyrite with haematite forming in cracks (Plates A1.3b and A1.4c). The purest zone in the centre contains only minor alunite (Plate A1.4d). In the upper zone, however, alunite becomes more abundant. On close inspection, the alunite and pyrophyllite have a parallel lamination (typical of such minerals in such hydrothermally altered rocks) (Plate A1.4d).



a) Pyrophyllite and alunite.



b) Pyrophyllite with pyrite and haematite. From the bottom of the orebody.



c) Dacite tuff with oxidised margin (host).

Plate A1.3

Field samples from host rock and lower and upper margin of orebody 4/1 respectively.



d) Pyrophyllite from the central area.



c) Pyrophyllite with haematite-rich areas spreading laterally from cracks.



b) Pyrophyllite (above) with haematized host rock (below).



a) Dacitic tuff host rock with pyrophyllite at top. (Pyrite is finely disseminated through the rock).

Fig. A1.4

Rock samples from different parts of the mineralised zone.

The alteration caused the host rock adjacent to the pyrophyllite to become strongly silicified and in general, the stronger the silicification the higher the quality of the adjacent pyrophyllite. These silicified areas form pronounced ridges across the landscape (Plate A1.5).



Plate A1.5

Pronounced silicified ridge.

On left hand side of photo, silicified below orebody 2.

(See Plate A1-1 for position on map (photo taken from position of green arrow)).

Processing the pyrophyllite at Dongzi

Crushing

Crushing is done on site at the Dongzi deposit, employing only a few workers. Initially, cobble to small boulder size rocks are put through a large jaw crusher (Plate A1.6). The resulting chips (~2-5cm long) are then hand picked and those with high Fe content removed - (reducing Fe impurity to ~1%). The chips are then ground to...

200 # - for tiles.

500 # - for ceramics (Plate A1.7)

1000 # - for incorporation into plastics (Plate A1.7).

The 1000 # fines are coated with organic compound to facilitate the pyrophyllite's incorporation into the plastics structure.



Fines ———

— Jaw crusher

— Hand picking
— done at this stage.

Plate A1.6
The two stages of jaw crushing.



← 1000#

Plate A1.7 ↑ 500#
Outlets for the 500# and 1000# pyrophyllite fines.

SHOUSHAN (PYROPHYLLITE) DEPOSIT

The Shoushan deposit is situated in a mountainous region, ~40km WNW of Fuzhou and a few km from the village of Shoushan. As at the Dongzi deposit, the pyrophyllite formed due to hydrothermal alteration of Lower Jurassic volcanic rocks by fluids emanating from the original magma (from isotopic analysis, Lin pers. comm.). The Shoushan deposit, however, is situated in a volcanic caldera. Radial faults around the centre (Plate A1.8) became conduits for the hydrothermal fluids which caused strong alteration of the rhyolitic ignimbrites, forming pyrophyllite, sericite and silica.

The pyrophyllite at Shoushan occurs in layers of parallel lenses \approx 12m thick, similar to that at Dongzi. It formed at $>400^{\circ}\text{C}$ and pH 4-6, and grades into the sericite-rich rocks which formed at lower temperature $<280^{\circ}\text{C}$ and higher pH (Lin pers. comm).

Extraction methods

Most mining is open cast, but there are some adits 100-200m long.



Plate A1.8
Faults associated with the caldera at Shoushan - faults picked out by valleys.

Original site of Shoushan stone

Shoushan stone was originally mined next to the village of Shoushan. This site marks the only known source of the most highly valued variety "Tianhuang" in all China. Tianhuang is quarried by the stream at Shoushan village - but the site is covered over during the rice growing season (Plate A1.9)!



Plate A1.9

Paddy fields at Shoushan village, under which the only known Tianhuang is found.

CARVING 'SHOUSHAN STONE'

The art of carving Shoushan stone has been passed down for more than 1500 years and continued to develop successfully through the cultural revolution. Since the Qing Dynasty (1644-1911), two branches "Xiamen" (West Fuzhou) and "Dongmen" have developed. The "Xiamen" variety is noted for its simplicity and life-likeness, the

"Dongmen" for its delicately and intricately carved pieces. Shoushan stone is very valuable to the Chinese and in "ancient" China, the Emperor had a special seal made from it (Tianhuang). The rarest variety (Tianhuang) can fetch three times the price of gold by weight!

Types of pyrophyllite used for carving

Of the three categories OF Shoushan stone, generally only Tiankeng and Shukeng are used for carving (Table A1.1). These are the purest varieties and contain only dickite and kaolinite impurities.

Carving procedures (Fuzhou Carving Factory).

Rocks of sufficiently high quality are taken to the Fuzhou Carving Factory (Plate A1.10) where skilled workers are employed to carve the Shoushan stone.



Plate. A1.10
Fuzhou Carving Factory.

Workshop procedure for carving

1. At the initial stage, a clay model is made of the specific design.
2. An appropriate rock is then selected and the design is painted onto its surface. Initial sculpting is done along these lines (Plate A1.11).
3. The sample is then passed on for more detailed work (Plate A1.12). To whom it is given depends on the intricacy of the design and the skill of the sculptor.
4. The carving is finally brushed and polished.



Plate A1.11
Sample at initial stages of sculpting.



Plate A1.12
A complicated piece during the final stages of sculpting.

Finished carvings

Plate A1.13a and A1.13b are of two finished products. The carving in Plate A1.13a is made of Tianhuang and is on sale for the equivalent of £3,500!!

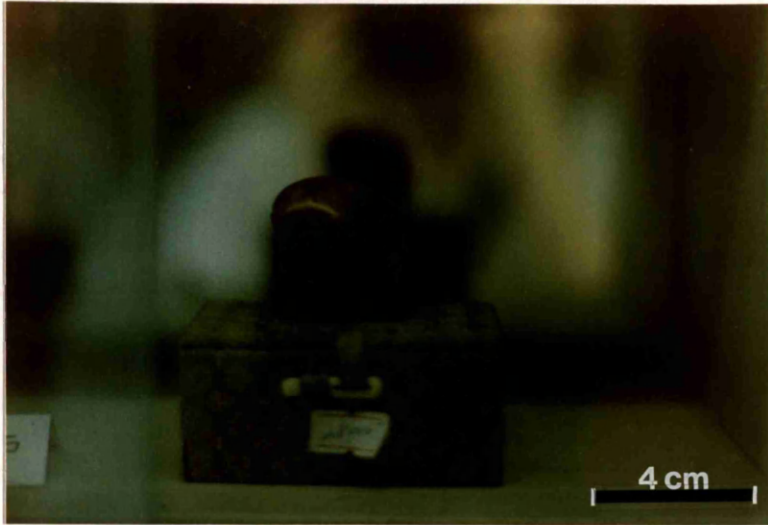


Plate A1.13a
Carving of Tianhuang.



Plate A1.13b
Shoushan stone horse.

APPENDIX 2**Samples used in this project.**

Including; suites and individual samples of fresh and altered Lewisian gneiss, several samples from other Scottish Precambrian rock groups and samples of Cambrian shales.

2a.(1) Lewisian rocks from beneath the unconformity (altered and fresh) - suites.

Name of location	National Grid. Reference	D.B.U. (m)	Rock Type	Sample number		
Cave	NC 4384 6614	2.8	Pegmatite	4988		
		3.9		$\pi 1$		
		4.7		49A		
		8.4		5088		
		10.7		50A		
	NC 4390 6609	14.7		5188		
		~20.0		E		
		~25.0		F		
		NC 4384 6614		1.4	Gneiss	GnA
				2.0		4688
5.0	46A					
7.8	4788					
10.4	47A					
NC 4390 6609	15.0	4888				
	~20.0	G				
	~25.0	H & I				
NC 4384 6614	4.6	Amphibolite	4388			
	8.3		4488			
NC 4390 6609	~20.0		C			
	~25.0		D			
NC 4384 6614	12.5	Pegmatite (Haematized (cf. Plate)	2489/A			

Name of location	National Grid Ref.	D.B.U. (m)	Rock Type	Sample number
Bay 1	NC 434 662	0.5 to 1.0	Gneiss	U
		1.8 to 2.3	Gneiss	T
		1.8 to 2.3	Pegmatite	S
		2.9 to 3.4	Gneiss/Amphibolite	R
		3.4 to 3.8	Amphibolite/Gneiss	Q
		6.6 to 7.1		P
		~18.0	Gneiss	M
		~21.0	Gneiss	L
Bay 1	NC 435 662	0.1	Pegmatite	1
		0.3	Pegmatite	3
		0.1	Pegmatite	6
Small Bay	NC 4348 6619	0.3	Pegmatite	8749
		~17.0	Pegmatite	8752
		~21.8	Pegmatite	8754
		~22.2		8755
		~17.2	Gneiss	8759
Telegraph Hut	NC 4435 6394	4.9 to 7.8	Pegmatite	8740
		6.0 to 8.9	Pegmatite	8742
		7.7 to 10.7	Pegmatite	8744
		9.2 to 12.1	Pegmatite	8745
		9.4 to 12.3	Pegmatite	8746
		5.7 to 8.6	Pegmatite	0690
		6.2 to 9.1	Pegmatite	0590
		8.3 to 11.2	Pegmatite	0490
		8.9 to 11.8	Pegmatite	0390
Cranstackie	NC 348 553	0.35	Pegmatite	3288
	NC 348 553	1.20	Pegmatite	3388
	NC 348 553	10.0	Gneiss	3488 gn
	NC 348 553	10.0	Pegmatite	3488 π
	NC 34 55	24.0	Gneiss (coarse grained)	3588
	NC 34 55	182.0	Gneiss " "	3688
	NC 34 55	270.0	Pegmatite	3788
	NC 34 56	460.0	Pegmatite	3888

2a(II) Lewisian rocks from beneath the unconformity - individual samples.

Name of location	National Grid Ref.	D.B.U. (m)	Rock Type	Sample number
Pod	NC 4387 6611	<1.0	Pegmatite	P3B,P3C PQ, PT
Clachaidh	NC 4361 6240	≤4	Altered Gneiss	2889
	NC 4357 6240	≤4	Quartz/Tourmaline veinlet.	VT + VQ
	NC 4357 6240	≤4	Pink gneiss around VT.	VF
Wheelhouse	NC 4047 6111	≤0.10	Pegmatite	LF Wheelhouse
Arkle	NC 303 444	<2.0	Pegmatite	3088
	NC 3035 4444	<1.0	Pegmatite	3188
E.of L. Glendhu (sheared).	NC 3154 3242	~1.0m	Sheared Agalmatolite	3589

2b. Other Precambrian rocks.

Rock group	Location	Rock type	Sample number.
Lewisian	Laxford Brae		
	NC 232 485	Gneiss	5288
	NC 232 485	Pegmatite	5388+1090
Dalradian	Aberfeldy		
	NN 815 547	Quartz Celsian	AJH/LKF-A
	NN 852 564	Graphitic Schist	" - B
	NN 852 564	Greenish barium muscovite Schist	" - C
	NN 815 547	Carn Mairg Quartzite	" - D
	NN 815 547	Basal Carn Mairg Quartzite	" - E

Moinian	Garve NC 403 645	Psammite	5888
---------	---------------------	----------	------

2c. Cambrian shales and shaly sandstones - predominantly from clastic members.

Member	Rock type	Grid Ref. and location	Sample No
Grudaidh/ Salterella Grit	Shale (Carbonaceous)	NH 142 926 Ullapool	0289 up
		NH 142 926 Ullapool	0289 lo.
Salterella Grit/ Grudaidh	Black shale	NC 43 57 An t-Sron	4288
		NH 142 926 Ullapool	0189
Furoid Beds	Black shale	NC 43 57 An t- Sron	4188
		NC 250 158 Loch Awe	5788
		NH 142 926 Ullapool	0489
Pipe rock	Green shale Sandy shale	NC 240 291 Assynt/Kylesku	5688
		NC 2360 2426 Assynt	1589
Lower member	Black shale	NH 140 955 Ullapool	6188
		NH 137 938 Ullapool	0589
Lower member	Green shale	NC 4395 6374 Eriboll	0988
		NC 231 312 Assynt/Kylesku	3989
		NC 2310 2455 Assynt	1389
		NC 2305 2460 Assynt	1289
		NH 137 938 Ullapool	0689
Lower member	Shaly sandstone	NC 4382 6616 Durness (cave)	1989 -(1)
		NC 4382 6616 Durness (cave)	1989 -(5)
		NC 4382 6616 Durness (cave)	1989 -(6)

APPENDIX 3**Instrument conditions used on the XRD machine.**

Iron filtered $\text{CoK}\alpha$ radiation 36KV; 20mA
 Goniometer scan speed $2\theta/2\theta/\text{min}$ (for most analyses. If more accurate determination of peak positions is required, this may be reduced).
 Chart speed 10mm/min
 Time constants 4
 Range (cps) 2×10^2
 Divergence slit 1° , anti scatter slit 1° , Receiver slit 0.1mm.

APPENDIX 4**Test statistic ('t-test').**

Formulae for the tests of significance for samples of different populations; assuming both sets of results have the same variance.

Test statistic.

$$t = \frac{\bar{x} - \bar{y}}{\sqrt{S^2 \left(\frac{1}{n_x} + \frac{1}{n_y} \right)}}$$

where x and y are mean values of different populations

S = standard deviation.

n_x and n_y = number of values in each population.

(with $n_x + n_y - 2$ degrees of freedom).

$$S^2 = \frac{\sum(X^2) - (\sum X)^2/n_x + \sum(y^2) - (\sum y)^2/n_y}{n_x + n_y - 2}$$

When $t_{\text{crit}} < t_{\text{sample}}$ then there can be x% confidence in a population difference - as given in "t distribution" tables, e.g. Fisher and Yates 1963.

APPENDIX 5**Alteration of Plagioclase (from electron probe analysis)**NOTE: N.A. = not analysed; *n.d.* = not detected.LOCATION CAVE 14.7m below unconformity (NC 4385 6614)
Sample No. 5188DESCRIPTION PLAGIOCLASE
CENTRE OF CRYSTAL

Analysis No.	C1	C2	C3
SiO ₂	66.791	65.799	67.721
Al ₂ O ₃	19.964	20.662	19.374
FeO _{tot}	0.031	0.172	0.056
MgO	0.045	0.149	0.012
CaO	1.055	0.564	0.663
Na ₂ O	11.036	10.170	11.663
K ₂ O	0.509	1.596	0.286
BaO	0.011	<i>n.d.</i>	0.012
TOTAL	99.441	99.111	99.786

LOCATION CAVE 14.7m below unconformity [NC 4385 6614]
Sample No. 5188

DESCRIPTION PLAGIOCLASE - OVERGROWTH MICROCLINE

Analysis No.	B1	B2	B3			A1	A2
SiO ₂	69.111	68.794	67.944			64.346	62.148
Al ₂ O ₃	19.198	19.010	19.939			17.879	17.882
FeO _{tot}	0.022	0.013	0.010			0.027	1.274
MgO	0.002	0.006	0.018			0.017	0.357
CaO	0.265	0.186	1.092			<i>n.d.</i>	<i>n.d.</i>
Na ₂ O	12.045	11.918	11.544			0.392	0.533
K ₂ O	0.082	0.192	0.128			16.151	15.457
BaO	<i>n.d.</i>	<i>n.d.</i>	0.038			0.416	0.419
TOTAL	100.725	100.119	100.713			99.228	98.070

APPENDIX 6

Major element chemistry of Biotites.

LOCATION CAVE 2.0m below unconformity (NC4385 6614)

Sample No. 4688

Analysis No.	6A1	A2	B1	B2	C1	C2	FD2	FE1	FE2	7A1
SiO ₂	47.387	46.482	46.359	46.734	45.838	49.006	47.022	44.518	45.918	45.068
TiO ₂	4.132	3.644	4.452	3.663	4.214	3.321	3.685	4.388	3.859	5.682
Al ₂ O ₃	28.223	28.350	28.563	29.075	28.556	30.541	28.769	27.893	27.860	31.362
FeO	4.776	5.191	4.957	4.917	5.040	3.744	4.760	6.147	6.007	3.018
MnO	0.013	0.008	0.006	0.016	0.022	0.010	0.002	0.021	0.006	<i>n.d.</i>
MgO	0.435	0.467	0.436	0.585	0.461	0.378	0.657	0.544	0.544	0.434
CaO	0.028	0.026	0.025	0.033	0.035	0.032	<i>n.d.</i>	<i>n.d.</i>	<i>n.d.</i>	0.018
Na ₂ O	0.153	0.163	0.144	0.154	0.161	0.165	0.173	0.178	0.184	0.177
K ₂ O	8.772	9.063	8.934	9.128	9.310	8.876	7.945	9.222	9.097	9.033
F	N.A.	N.A.	N.A.	N.A.	N.A.	N.A.	0.225	0.225	0.064	0.174
Cr ₂ O ₃	N.A.	N.A.	N.A.	N.A.	N.A.	N.A.	0.020	0.000	0.044	0.000
TOTAL	93.919	93.392	93.876	94.306	93.637	96.073	93.409	93.378	93.808	95.188

LOCATION CAVE 2.0m Below unconformity

Sample No. 4688

Analysis No.	7A2	A461	A462	A463
SiO ₂	45.301	48.390	46.684	46.146
TiO ₂	3.100	1.130	3.457	3.306
Al ₂ O ₃	29.182	31.037	29.422	26.434
FeO	4.570	2.962	4.698	7.203
MnO	<i>n.d.</i>	0.021	0.033	0.011
MgO	0.613	0.670	0.410	0.548
CaO	0.013	0.023	0.015	0.035
Na ₂ O	0.165	0.148	0.187	0.150
K ₂ O	9.200	8.327	8.475	8.391
Flourine	0.226	0.294	0.165	0.074
Cr ₂ O ₃	<i>n.d.</i>	0.032	0.062	0.008
TOTAL	92.516	93.035	93.608	92.305

LOCATION CAVE 7.8m below unconformity [NC4385 6614]

Sample No. 4788

Analysis No.	A1	B1	B2	B3	B4
SiO ₂	47.403	46.460	47.482	46.088	46.149
TiO ₂	2.928	5.527	2.624	3.684	3.475
Al ₂ O ₃	31.514	32.349	32.168	31.758	32.057
FeO	3.011	2.426	2.559	2.209	2.217
MnO	0.005	0.025	0.022	<i>n.d.</i>	0.011
MgO	0.645	0.332	0.349	0.344	0.340
CaO	0.018	<i>n.d.</i>	0.002	<i>n.d.</i>	<i>n.d.</i>
Na ₂ O	0.148	0.129	0.128	0.168	0.132
K ₂ O	9.850	9.589	9.923	9.486	9.307
F	0.120	0.210	0.131	N.A.	N.A.
Cr ₂ O ₃	0.029	0.019	0.021	N.A.	N.A.
TOTAL	95.669	97.065	95.411	93.737	93.688

LOCATION CAVE ~20m below unconformity (NC 4390 6609)

Sample No.	G										
Analysis No.	2	3	4	5	6	7	8	9	10	11	12
SiO ₂	37.792	38.037	38.025	37.989	37.784	38.009	37.954	38.080	37.891	37.916	37.816
TiO ₂	1.897	1.956	2.010	1.980	2.063	2.198	2.169	1.868	2.404	2.705	2.734
Al ₂ O ₃	16.056	16.207	15.773	16.112	16.029	15.916	15.943	16.329	16.016	15.733	15.881
FeO _{tot}	16.521	15.311	16.366	16.024	16.079	16.149	15.724	15.085	16.036	16.091	16.071
MnO	0.273	0.287	0.261	0.258	0.296	0.273	0.228	0.271	0.250	0.261	0.252
MgO	14.029	14.215	13.791	13.842	13.928	13.633	14.014	14.212	13.624	13.649	13.325
CaO	0.026	0.005			0.010	0.007	0.006	0.011	0.019		
Na ₂ O	0.073	0.081	0.077	0.076	0.090	0.071	0.073	0.098	0.095	0.091	0.084
K ₂ O	9.302	9.808	9.299	9.686	9.432	9.868	9.802	9.723	9.623	9.727	9.690
Cr ₂ O ₃	0.063	0.055	0.084	0.072	0.083	0.039	0.090	0.153	0.106	0.025	0.025
TOTAL	96.471	96.438	96.074	96.643	96.219	96.758	96.520	96.281	96.533	96.769	96.438

LOCATION CAVE ~25m below unconformity (NC 4390 6609)

Sample No.	H										
Analysis No.	1	2	3	4	5	6	7	8	9	10	11
SiO ₂	37.836	38.052	37.760	37.593	37.770	37.805	37.534	37.344	37.770	37.658	37.334
TiO ₂	2.521	2.420	2.406	2.267	2.450	2.418	2.444	2.490	2.751	2.295	2.714
Al ₂ O ₃	16.304	16.268	16.115	16.053	15.827	16.104	15.922	16.169	15.711	15.912	15.843
FeO _{tot}	16.574	16.918	16.652	16.766	17.013	16.685	16.789	17.328	16.786	17.056	16.631
MnO	0.208	0.219	0.238	0.230	0.225	0.252	0.260	0.238	0.238	0.234	0.267
MgO	12.638	12.744	12.781	13.053	13.078	13.004	13.098	12.422	12.937	12.919	12.936
CaO	0.013	0.004	0.005			0.008		0.004		0.010	0.016
Na ₂ O	0.093	0.130	0.072	0.101	0.127	0.109	0.114	0.057	0.078	0.098	0.119
K ₂ O	9.850	9.739	9.535	9.834	9.623	9.829	9.580	9.748	9.674	9.604	9.759
Cr ₂ O ₃	0.019	0.025	0.037			0.050	0.028		0.019	0.046	0.035
TOTAL	96.434	96.952	96.061	96.168	96.473	96.509	96.100	96.081	96.380	96.071	96.028

APPENDIX 7

Major element chemistry of Pinite.

LOCATION

[NC 4426 6394]

Sample No.

8714

Analysis No.	M1A	M1B	M1C	P1	P2	P3	P4	M2A	P5	P6
SiO ₂	45.175	44.429	44.299	44.289	46.861	47.151	44.929	45.458	46.261	45.754
TiO ₂		0.010	0.002	0.009			0.010			0.009
Al ₂ O ₃	37.672	38.031	37.592	34.834	37.171	35.886	35.837	37.544	36.986	34.786
FeO _{tot}	0.341	0.472	0.391	1.901	0.650	1.052	1.293	0.811	0.928	2.212
MnO	0.022	0.000		0.011	0.000	0.017			0.010	0.040
MgO	0.124	0.082	0.046	0.359	0.248	0.560	0.362	0.180	0.230	0.517
CaO		0.101	0.166	0.015	0.108	0.093	0.081	0.079	0.113	
Na ₂ O	0.591	0.790	0.797	0.292	0.665	0.376	0.379	0.520	0.527	0.181
K ₂ O	10.405	10.138	9.839	10.490	9.838	10.519	10.633	10.054	10.013	11.161
TOTAL	94.329	94.053	93.132	92.199	95.540	95.653	93.524	94.944	95.066	94.660
Si	6.035	5.960	5.990	6.116	6.158	6.224	6.097	6.052	6.128	6.176
Ti		0.001	0.000	0.000			0.001			0.000
Al	5.934	6.015	5.993	5.671	5.759	5.584	5.734	5.892	5.776	5.535
Fe	0.038	0.053	0.044	0.219	0.071	0.116	0.147	0.090	0.103	0.250
Mn	0.002	0.000		0.001	0.000	0.002			0.001	0.005
Mg	0.025	0.016	0.009	0.074	0.048	0.110	0.073	0.036	0.045	0.104
Ca		0.014	0.024	0.002	0.015	0.013	0.012	0.011	0.016	
Na	0.153	0.206	0.209	0.078	0.169	0.096	0.100	0.134	0.135	0.047
K	1.773	1.735	1.697	1.848	1.650	1.771	1.841	1.708	1.692	1.922
Mole Ratio K ₂ O/Al ₂ O ₃	0.299	0.288	0.283	0.326	0.287	0.317	0.321	0.290	0.293	0.347
Mole Ratio SiO ₂ /Al ₂ O ₃	2.034	1.982	1.999	2.157	2.139	2.229	2.127	2.054	2.122	2.232

Major element chemistry of pinite cont'd....

LOCATION

[NC 4426 6394]

Sample No.

8714

Analysis No.	P7	M3A	P8	P9	P10	P11	P12	P14	P15	P17
SiO ₂	46.005	45.578	44.943	46.435	46.383	45.569	46.500	45.705	45.261	45.926
TiO ₂	<i>n.d.</i>	<i>n.d.</i>	0.015	0.016	0.007	<i>n.d.</i>	<i>n.d.</i>	0.005	0.002	<i>n.d.</i>
Al ₂ O ₃	35.023	35.213	33.989	34.974	35.212	36.126	35.000	35.177	34.300	34.953
FeO	2.286	2.317	2.304	1.909	1.977	1.315	2.376	2.113	2.511	2.485
MnO	0.052	0.033	0.011	0.003	0.009	0.025	0.044	0.026	0.020	0.031
MgO	0.521	0.423	0.461	0.458	0.512	0.252	0.466	0.509	0.449	0.391
CaO	<i>n.d.</i>	0.021	<i>n.d.</i>	0.046	<i>n.d.</i>	0.105	<i>n.d.</i>	0.032	0.008	0.013
Na ₂ O	0.207	0.221	0.205	0.250	0.190	0.499	0.238	0.217	0.213	0.203
K ₂ O	11.331	11.112	11.250	10.507	11.409	10.278	11.291	10.691	11.134	11.136
TOTAL	95.425	94.916	93.179	94.597	95.697	94.169	95.914	94.475	93.898	95.139
Si	6.167	6.139	6.179	6.228	6.187	6.125	6.198	6.160	6.174	6.173
Ti	<i>n.d.</i>	<i>n.d.</i>	0.002	0.002	0.000	<i>n.d.</i>	<i>n.d.</i>	0.001	0.000	<i>n.d.</i>
Al	5.535	5.591	5.509	5.530	5.537	5.725	5.500	5.589	5.516	5.539
Fe	0.256	0.261	0.265	0.214	0.220	0.148	0.265	0.238	0.286	0.279
Mn	0.006	0.004	0.001	0.000	0.001	0.003	0.005	0.003	0.002	0.004
Mg	0.104	0.085	0.095	0.091	0.102	0.050	0.092	0.102	0.091	0.078
Ca	<i>n.d.</i>	0.003	<i>n.d.</i>	0.007	<i>n.d.</i>	0.015	<i>n.d.</i>	0.005	0.001	0.002
Na	0.054	0.058	0.055	0.065	0.049	0.130	0.062	0.057	0.056	0.053
K	1.938	1.909	1.973	1.798	1.942	1.762	1.920	1.838	1.938	1.910
Mole ratio K ₂ O/Al ₂ O ₃	0.350	0.341	0.358	0.325	0.351	0.308	0.349	0.329	0.351	0.345
Mole ratio SiO ₂ /Al ₂ O ₃	2.228	2.196	2.243	2.252	2.235	2.140	2.254	2.204	2.239	2.229

Major element chemistry of pinite cont'd....LOCATION *inside of* [NC 4426 6394]

Sample No. 8714

Analysis No.	P18	P19	P20	P21	Average Pinite
SiO ₂	46.972	46.098	46.060	45.579	45.734
TiO ₂	0.011	0.010	0.015	<i>n.d.</i>	0.005
Al ₂ O ₃	36.724	36.741	35.396	34.920	35.837
FeO	1.564	0.740	2.544	2.324	1.617
MnO	0.016	0.013	0.030	0.007	0.018
MgO	0.238	0.431	0.411	0.426	0.361
CaO	0.044	0.061	<i>n.d.</i>	<i>n.d.</i>	0.045
Na ₂ O	0.351	0.470	0.247	0.232	0.369
K ₂ O	10.602	10.520	11.349	11.104	10.700
TOTAL	96.521	95.084	96.052	94.592	94.698
Si	6.161	6.121	6.142	6.159	6.135
Ti	0.001	0.001	0.002	<i>n.d.</i>	0.000
Al	5.679	5.751	5.564	5.563	5.668
Fe	0.172	0.082	0.284	0.263	0.182
Mn	0.002	0.001	0.003	0.000	0.002
Mg	0.047	0.085	0.082	0.086	0.072
Ca	0.006	0.009	<i>n.d.</i>	<i>n.d.</i>	0.006
Na	0.089	0.121	0.064	0.061	0.096
K	1.774	1.782	1.931	1.914	1.832
Mole Ratio K ₂ O/Al ₂ O ₃	0.312	0.310	0.347	0.344	0.324
Mole Ratio SiO ₂ /Al ₂ O ₃	2.170	2.129	2.208	2.214	2.167

APPENDIX 8

Major element chemistry of Tourmaline.

Wt.% oxide of major elements - determined by electron probe analysis.

8a - Vein Tourmaline.

LOCATION

[NC 4357 6240]

Sample No.

Veinlet VT

Analysis No.	T1	T2	T3	T4	T5	T8	T9	T10	T11	T16
SiO ₂	36.788	36.732	36.449	36.524	35.912	36.413	36.657	36.491	36.534	36.465
TiO ₂	0.287	0.679	1.305	0.635	0.500	0.499	0.388	0.646	0.243	0.553
Al ₂ O ₃	29.562	27.561	27.075	26.962	27.329	27.060	27.394	27.576	27.024	27.613
FeO _{tot}	9.968	12.356	12.283	12.995	12.746	12.815	12.281	11.737	12.313	11.855
MnO	0.032	0.057	0.026	0.045	0.082	0.078	0.071	0.059	0.069	0.052
MgO	6.756	6.808	6.865	6.846	6.594	6.925	7.046	6.886	7.143	6.805
CaO	0.372	0.337	0.472	0.248	0.448	0.202	0.218	0.261	0.116	0.492
Na ₂ O	2.642	2.708	2.516	2.673	2.636	2.717	2.760	2.627	2.773	2.492
K ₂ O	0.061	0.086	0.047	0.082	0.070	0.069	0.082	0.058	0.068	0.093
Cr ₂ O ₃	0.009	0.021	0.000	0.000	0.041	0.000	0.000	0.033	0.000	0.000
TOTAL	86.771	87.547	87.060	87.076	86.460	87.001	86.899	86.450	86.283	86.419
Na ₂ O (Na ₂ O+K ₂ O+ CaO)	0.859	0.865	0.829	0.890	0.836	0.909	0.902	0.892	0.934	0.810
FeO (FeO+MnO +MgO)	0.595	0.643	0.641	0.653	0.656	0.647	0.633	0.628	0.631	0.634

Analysis No.	T17	T18	T19	T20
SiO ₂	37.295	35.637	36.180	36.255
TiO ₂	0.258	2.672	1.371	0.353
Al ₂ O ₃	26.172	25.642	26.325	29.298
Fe ₂ O ₃				
FeO	12.609	12.941	12.874	10.384
MnO	0.028	0.038	0.011	0.012
MgO	6.373	6.476	6.448	6.506
CaO	0.392	0.452	0.344	0.427
Na ₂ O	2.523	2.485	2.536	2.558
K ₂ O	0.723	0.259	0.048	0.096
Cr ₂ O ₃	0.023	0.046	0.000	0.000
TOTAL	86.532	86.648	86.306	86.059
Na ₂ O (Na ₂ O+K ₂ O+CaO)	0.694	0.778	0.866	0.830
FeO (FeO+MnO+MgO)	0.663	0.665	0.666	0.614

8b Blue 'sun' tourmaline rosettes.

LOCATION CAVE SUITE ~2m below unconformity [NC4385 66140]

Sample No. 4688

Analysis No.	A6	A9	FA1	FA2
SiO ₂	36.846	35.771	35.538	35.664
TiO ₂	0.106	0.079	0.068	0.042
Al ₂ O ₃	36.242	35.080	35.989	35.920
FeO _{tot}	9.047	8.429	8.517	8.171
MnO	<i>n.d.</i>	0.022	0.036	0.028
MgO	2.598	3.295	3.375	3.658
CaO	0.022	0.027	0.031	0.025
Na ₂ O	0.661	0.722	0.794	0.720
K ₂ O	0.068	0.045	0.039	0.033
F	0.231	0.096	<i>n.d.</i>	0.041
BaO	<i>n.d.</i>	0.011	0.006	0.017
TOTAL	85.820	83.575	84.387	84.319
Na ₂ O (Na ₂ O+K ₂ O+CaO)	0.880	0.909	0.919	0.925
FeO (FeO+MnO+MgO)	0.777	0.718	0.714	0.689

LOCATION 'POD' : <1m below unconformity [NC 4387 6611]

Sample No. P3B

Analysis No.	3	TB1	TB7	TB10	TBA	TBB	TB12	TB13
SiO ₂	37.073	37.380	37.427	37.126	36.675	37.100	36.994	36.987
TiO ₂	0.036	0.050	0.051	0.036	0.051	0.019	0.042	0.048
Al ₂ O ₃	35.440	35.463	35.805	35.280	35.063	36.085	35.813	36.072
FeO _{tot}	10.776	9.173	9.162	8.840	9.989	9.635	9.147	9.383
MnO	0.012	0.013	0.011	0.009	0.000	0.010	0.000	0.000
MgO	2.310	2.724	2.622	2.840	2.419	2.343	2.472	2.398
CaO	0.032	0.006	0.016	0.009	0.020	0.020	0.015	0.008
Na ₂ O	0.729	0.756	0.835	1.089	0.692	0.566	0.741	0.656
K ₂ O	0.040	0.019	0.043	0.020	0.015	0.000	0.028	0.014
Cr ₂ O ₃	0.000	0.000	0.025	0.030	0.030	0.002	0.000	0.007
TOTAL	86.604	85.618	85.995	85.312	84.954	85.781	85.275	85.639
Na ₂ O (Na ₂ O+K ₂ O+CaO)	0.910	0.968	0.934	0.974	0.952	0.966	0.945	0.968
FeO (FeO+MnO+MgO)	0.823	0.770	0.777	0.756	0.805	0.804	0.787	0.796

LOCATION

'POD' : ~1m below unconformity (NC4387 6611)

Sample No

P3C

Analysis No	TB40	TBA	TBB	TBC	TBD	TB41	TB43	TB44	TB45	TB46	TB47
SiO ₂	36.682	38.475	36.883	36.749	36.938	37.236	36.748	36.950	36.784	37.258	37.487
TiO ₂	0.055	0.087	0.047	0.064	0.039	0.032	0.051	0.039	0.000	0.036	0.052
Al ₂ O ₃	34.960	33.710	35.685	34.852	35.002	35.588	34.168	35.468	36.317	36.056	36.116
FeO _{tot}	10.299	11.196	9.896	10.609	10.530	10.311	9.971	9.566	9.046	8.244	9.471
MnO	0.000	0.032	0.009	0.003	0.000	0.000	0.050	0.000	0.003	0.019	0.023
MgO	2.092	2.234	2.116	2.193	2.099	2.317	2.583	2.469	2.374	2.934	2.682
CaO	0.011	0.004	0.023	0.021	0.028	0.033	0.018	0.021	0.009	0.021	0.000
Na ₂ O	0.788	0.948	0.619	0.743	0.802	0.688	1.055	0.700	0.710	0.873	0.731
K ₂ O	0.025	0.003	0.000	0.000	0.013	0.025	0.043	0.047	0.030	0.017	0.021
Cr ₂ O ₃	0.004	0.000	0.010	0.044	0.000	0.000	0.018	0.010	0.024	0.004	0.000
TOTAL	84.925	86.747	85.422	85.278	85.642	86.297	84.761	85.438	85.377	85.585	86.694
Na ₂ O (Na ₂ O+ K ₂ O+CaO)	0.956	0.933	0.964	0.973	0.951	0.922	0.945	0.911	0.948	0.958	0.972
FeO (FeO+MnO +MgO)	0.831	0.832	0.823	0.829	0.834	0.817	0.791	0.795	0.792	0.736	0.778

8c Green tourmaline

LOCATION 'POD' : <1m below unconformity [NC4387 6611]

Sample No.

P3B

Analysis No.	TG5	TG5A	TG6	TG6A	TG6B	TG6C	TG6D
SiO ₂	37.267	36.924	36.643	36.857	36.834	36.311	37.061
TiO ₂	0.057	0.088	0.022	0.083	0.021	0.051	0.056
Al ₂ O ₃	34.229	33.391	33.979	34.317	33.927	33.322	33.792
FeO _{tot}	9.584	10.212	11.372	9.573	10.385	12.035	9.841
MnO	0.003	0.000	0.001	0.008	0.036	0.000	0.000
MgO	2.806	2.701	2.112	2.812	2.674	2.213	2.922
CaO	0.011	0.001	0.012	0.027	0.000	0.007	0.017
Na ₂ O	1.490	1.839	2.186	1.450	2.144	1.788	1.684
K ₂ O	0.013	0.023	0.023	0.027	0.032	0.019	0.030
Cr ₂ O ₃	0.038	0.000	0.000	0.000	0.025	0.006	0.008
TOTAL	85.499	85.201	86.493	85.342	86.299	85.828	85.411
Na ₂ O (Na ₂ O+K ₂ O+CaO)	0.984	0.987	0.984	0.964	0.985	0.986	0.973
FeO (FeO+MnO+MgO)	0.773	0.791	0.843	0.772	0.793	0.845	0.771

APPENDIX 9

Major element chemistry of pyrophyllite

LOCATION

NC4385 6614

NC4387 6611

Sample No.

4688

P3C

Analysis No.	3A1	3A3	5A1		Py1	Py2	DG1
SiO ₂	65.844	65.615	67.330		68.682	68.169	68.236
TiO ₂	0.020	0.009	n.d.		0.013	0.018	0.025
Al ₂ O ₃	26.580	27.968	28.349		28.129	27.887	27.822
FeO	0.320	0.281	0.215		0.416	0.356	0.312
MnO	0.003	0.016	n.d.		0.004	0.007	0.000
MgO	0.012	0.017	0.037		0.021	0.032	0.007
CaO	0.017	0.023	0.022		0.045	0.028	0.021
Na ₂ O	0.095	0.110	0.064		0.080	0.048	0.070
K ₂ O	0.065	0.055	0.085		0.058	0.043	0.051
F	0.152	n.d.	N.A.		0.000	0.000	0.000
Cr ₂ O ₃	n.d.	n.d.	N.A.		0.005	0.000	0.003
TOTAL	93.109	94.095	96.102		97.453	96.714	96.546
Si	8.085	7.969	8.000				
Ti	0.002	0.000	n.d.				
Al	3.848	4.004	3.981				
Fe	0.033	0.029	0.021				
Mn	0.000	0.002	n.d.				
Mg	0.002	0.003	0.007				
Ca	0.002	0.003	0.003				
Na	0.023	0.026	0.015				
K	0.010	0.009	0.013				
TOTAL	12.064	12.045	12.029				
Mole K ₂ O/Al ₂ O ₃ ratio	0.003	0.003	0.002				
Mole SiO ₂ /Al ₂ O ₃ ratio	4.202	4.023	3.981				

Detection limits are as follows:

0.002	0.002	0.002
0.002	0.002	0.002
0.002	0.002	0.002

Inks Systems Ltd.

Printed on 10/10/00

of Lake at 10/10/00

APPENDIX 10

Analytical methods for whole rock geochemical analyses.

Methods

The methods used for whole rock geochemical analysis were those used by the Department of Geology & Applied Geology, University of Glasgow. Full details are given in their "XRF analysis handbook" compiled by Farrow 1982.

Whole rock geochemical analysis was determined using a Philips PW1450/20 automatic X-ray fluorescence (XRF) spectrometer, with a 60 position sample changer and on-line Superbrain microcomputer for data processing.

Major elements (weight % oxide)

Fused glass discs were prepared for major element analysis (full method outlined by Harvey *et al.* (1973), with influence factors to correct for remaining absorption-enhancement effects (Jenkins 1969, De Jongh 1973). Calibration coefficients are established from internal Glasgow standards, with periodic checks made against international standards - e.g. USGS standards G-1, MAG-1, SOC-1 etc.. Ten major element oxides were determined using this technique, i.e. SiO₂, TiO₂, Al₂O₃, FeO_{tot}, MnO, MgO, CaO, Na₂O, K₂O, P₂O₅ (with total iron determined as Fe₂O₃).

Detection limits are as follows:-

Oxide	SiO ₂	TiO ₂	Al ₂ O ₃	Fe ₂ O ₃	MnO	MgO	CaO	Na ₂ O	K ₂ O	P ₂ O ₅
Detection Limit	0.086	0.018	0.087	0.045	0.012	0.165	0.006	0.155	0.002	0.018

Trace elements (ppm)

Pressed powder pellets were prepared for trace element determination, using the method of Leake *et al.* (1968), with correction for absorption (Harvey 1981, 1982). All were

analysed with a Mo tube. All available international standards were used to establish the calibration. Sixteen trace elements were determined, i.e. Ba, Ce, Co, Cr, Cu, Ga, La, Ni, Pb, Rb, Sr, Th, U, Y, Zn, Zr.

Upper and detection limits are as follows:-

Element	Zr	Y	Sr	U	Rb	Th	Pb	Ga
Upper limit	300	150	800	100	600	400	100	100
Detection limit	2.7	1.4	1.5	9.4	1.7	11.5	11.6	2.4
Element	Zn	Cu	Ni	Co	Cr	Ce	Ba	La
Upper limit	1400	400	2500	250	3200	500	2500	250
Detection limit	1.8	4.4	4.8	3.2	1.9	3.2	12.3	3.9

H₂O/CO₂

The technique of "simultaneous determination of water and carbon dioxide in rocks and minerals" of Riley (1958), was used for this analysis.

FeO

Ferrous iron values were determined by dichromate titration after decomposition in platinum crucible with sulphuric acid and hydrofluoric acid in a non-oxidative atmosphere. Ferric iron was then ascertained using the equation:-

$$\text{Fe}_2\text{O}_3 = \text{FeO}_{\text{tot}} - (1.112 \times \text{FeO}).$$

APPENDIX 11

Whole rock major, minor and trace element compositions of samples analysed in this project.

Suites from various locations at interval depths beneath the unconformity.

CAVE [NC 448 661]

Sample No. Depth below unc(m)	GNEISS										PEGMATITE						AMPHIBOLITE			
	GnA	4688	46A	4788	47A	4888	G	H	I	4988	P1	49A	5088	50A	5188	E	F	4388	C	D
	1.4	2.0	5.0	7.8	10.4	15.0	~20	~25	~25	2.8	3.9	4.7	8.4	10.7	14.7	~20	~25	4.6	~20	~25
SiO ₂	64.40	66.81	65.25	62.39	65.39	68.08	67.37	71.02	62.35	60.27	70.98	54.87	62.99	64.21	70.96	74.02	73.49	47.05	48.23	48.62
TiO ₂	0.32	0.30	0.22	0.26	0.19	0.17	0.31	0.22	0.40	0.02	0.02	0.05	0.02	0.05	0.02	0.06	0.04	0.68	0.60	0.67
Al ₂ O ₃	25.58	24.77	21.86	24.66	18.51	17.88	15.88	15.86	17.22	26.46	17.93	25.95	23.33	18.32	15.58	15.29	14.78	15.84	14.19	13.52
Fe ₂ O ₃		0.59		1.50		0.94	0.83	0.57	1.39	0.93			1.71		0.18	0.45	0.55	4.55	3.32	3.60
FeO		0.04		0.04		0.51	1.74	1.33	2.56	0.07			0.15		0.07	0.09	0.02	6.20	6.53	6.88
MnO	0.00	0.00	0.00	0.00	0.03	0.01	0.07	0.02	0.08	0.00	0.04	0.04	0.02	0.04	0.00	0.00	0.00	0.19	0.17	0.20
MgO	0.40	0.45	0.84	0.38	1.70	1.14	1.83	1.23	2.81	0.56	1.21	2.19	1.00	1.42	0.48	0.24	0.16	8.61	9.47	8.70
CaO	0.01	0.19	0.00	0.00	0.03	1.83	2.66	2.92	4.06	0.00	0.00	0.00	0.00	0.03	0.75	1.52	1.18	8.45	12.92	11.84
Na ₂ O	0.00	0.00	0.07	0.08	0.21	4.56	4.63	5.10	4.47	0.36	0.00	0.21	0.18	0.14	3.10	4.17	3.39	1.13	1.87	2.54
K ₂ O	4.77	5.64	6.78	7.61	10.21	4.33	2.60	1.33	1.80	8.22	5.49	6.72	7.69	11.56	7.93	3.79	5.35	3.05	0.80	0.91
P ₂ O ₅	0.01	0.02	0.01	0.02	0.01	0.08	0.11	0.07	0.14	0.03	0.01	0.03	0.03	0.02	0.05	0.00	0.01	0.07	0.05	0.06
H ₂ O+				2.60		1.02	0.91	0.76	0.90	3.55			2.23			0.04	0.80	2.44	0.74	1.78
CO ₂				0.04		0.18	0.02	0.14	0.16	0.08			0.06			0.01	0.13	0.00	0.00	0.09
TOTAL			99.58			100.84	98.42	100.57	98.34	100.55		99.41			99.68	99.90		98.26	98.85	99.41

Appendix JI cont'd...

Sample No.	GnA	4688	46A	4788	47A	4888	G	H	I	4988	PI	49A	5088	50A	5188	E	F	4388	C	D
Cr	8	13	8	12	8	17	72	30	1475	3	5	12	6	12	10	8	32	260	263	225
Ni	5	8	31	7	15	10	28	22	64	29	36	41	23	17	1	2	2	129	135	124
Co	5	1	9	0	10	1	9	5	16	2	21	37	1	6	0	0	0	58	51	55
Cu	0	2	0	1	0	1	19	10	13	9	0	0	5	0	9	18	14	76	140	40
Zn	1	6	3	8	33	35	57	35	78	2	10	9	5	25	2	7	3	80	75	91
U	0	2	0	3	0	2	0	0	0	2	0	0	3	0	0	0	2	4	2	4
Th	3	0	0	0	0	0	5	4	5	1	1	32	19	6	0	0	0	0	0	0
Pb	2	3	3	1	3	17	18	20	16	0	1	3	1	6	34	54	36	2	3	4
Rb	59	75	107	93	146	58	89	51	69	90	108	115	93	146	131	83	113	56	25	29
Sr	24	39	11	10	61	387	389	310	415	37	26	73	15	65	364	292	356	51	161	138
Ba	55	73	155	159	607	316	575	313	431	181	260	234	179	398	781	422	841	145	75	73
Zr	143	92	130	96	89	98	111	84	116	92	1	59	118	27	16	55	89	46	37	44
Y	6	6	5	4	3	1	6	4	8	15	1	7	14	1	2	2	4	17	16	17
Ca	27	28	25	25	18	20	19	20	24	37	20	35	36	21	23	23	25	15	11	14
La	7	19	6	6	1	4	22	6	25	19	7	67	5	11	4	0	1	4	1	0
Ce	15	14	5	2	3	1	46	14	40	30	17	121	13	29	4	9	5	1	2	0
SG		2.66		2.64		2.77	2.71	2.67	2.72	2.67			2.78			2.61	2.62	2.98	3.08	3.04
K/Na			108.4	106.5	54.41	1.06	0.63	0.29	0.50	25.55		35.81	47.81	92.40	2.86	1.02	1.77	3.02	0.48	0.40
K/Rb	671	624	526	679	580	620	243	217	217	758	422	485	686	657	503	379	393	452	266	260
K/Ba	720	641	363	679	140	114	38	35	35	377	175	238	357	241	84	75	53	175	89	103
K/Sr	1650	1200	5117	6318	1390	93	55	36	36	1844	1753	764	4256	1476	181	108	125	496	41	55
Rb/Sr	246	1.92	9.73	9.30	2.39	0.15	0.23	0.17	0.17	2.43	4.15	1.58	6.20	2.25	0.36	0.28	0.32	1.10	0.16	0.21
Al/Ga	5015	4682	4628	5221	5443	4732	4424	4197	3798	3785	4745	3924	3430	4618	3585	3519	3129	5589	6828	5112
Fe ³⁺ /Fe ²⁺		13.27		33.74		1.66	0.43	0.39	0.49	11.95			10.26		2.31	4.50	24.74	0.66	0.46	0.47

Appendix II cont'd...

Sample No.	TELEGRAPH HUT : [NC 4435 6394] AMPH PEGMATITE				CRANSTACKIE : [NC 34 55] GNEISS & PEGMATITE				[NC 3154 3242] SHEARED AGAL.						
	8739	8740	8742	8744	8745	8746	3288	3488	3488	3588	3688	3788	3888	3888	3589
Depth below unc.(m)	-1	0	1.1	2.9	4.3	4.5	0.35	10	10	24	182	270	460		
SiO ₂	58.48	64.81	62.58	73.62	67.79	64.57	69.72	68.53	67.63	71.68	73.04	73.33	66.03	67.14	
TiO ₂	1.00	0.25	0.19	0.02	0.11	0.13	0.18	0.33	0.06	0.22	0.11	0.21	0.09	0.32	
Al ₂ O ₃	22.23	21.09	23.85	16.15	18.57	20.48	16.48	15.45	17.29	14.33	14.96	13.73	20.53	19.72	
Fe ₂ O ₃	3.55	1.00	1.32	1.11	1.39	1.47	1.14	3.06	0.22	0.65	1.35	0.70	0.50	1.24	
FeO	0.18	0.19	0.21	0.04	0.04	0.04	0.70	1.61	0.13	1.03	0.59	1.10	0.41	0.03	
MnO	0.00	0.01	0.01	0.04	0.00	0.00	0.01	0.04	0.00	0.03	0.02	0.03	0.00	0.02	
MgO	1.86	0.81	1.01	1.06	0.98	0.84	0.67	1.37	0.26	0.67	0.18	0.75	0.38	0.86	
CaO	0.00	0.02	0.00	0.03	0.00	0.00	1.24	2.32	0.08	0.90	0.96	0.57	2.40	0.09	
Na ₂ O	0.00	0.05	0.06	0.22	0.17	0.00	2.97	3.68	1.69	2.39	3.35	2.38	6.24		
K ₂ O	8.47	8.27	8.47	5.95	8.25	8.71	6.09	2.97	11.15	6.28	5.20	6.62	2.94	6.32	
P ₂ O ₅	0.02	0.01	0.04	0.06	0.07	0.03	0.06	0.12	0.00	0.06	0.04	0.02	0.01	0.14	
H ₂ O ⁺							0.11	0.52	0.31	0.51	0.50	0.36	0.72		
CO ₂							0.13	0.03	0.17	0.15	0.16	0.11	0.28		
TOTAL							99.50	100.03	98.99	98.90	100.46	99.91	100.53		

Appendix II Cont'd...

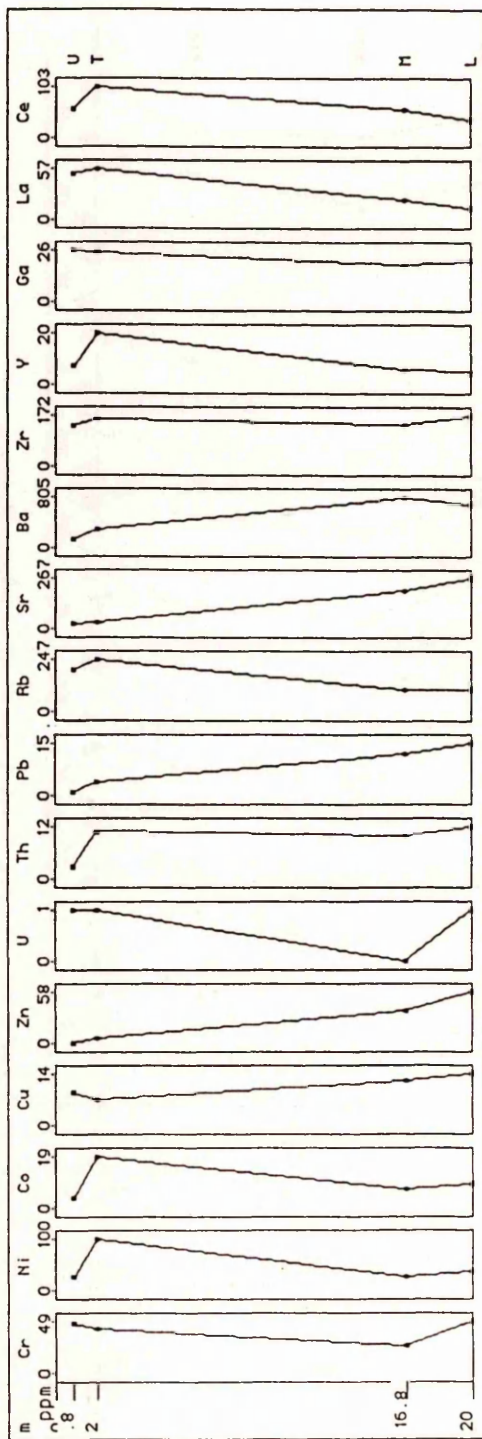
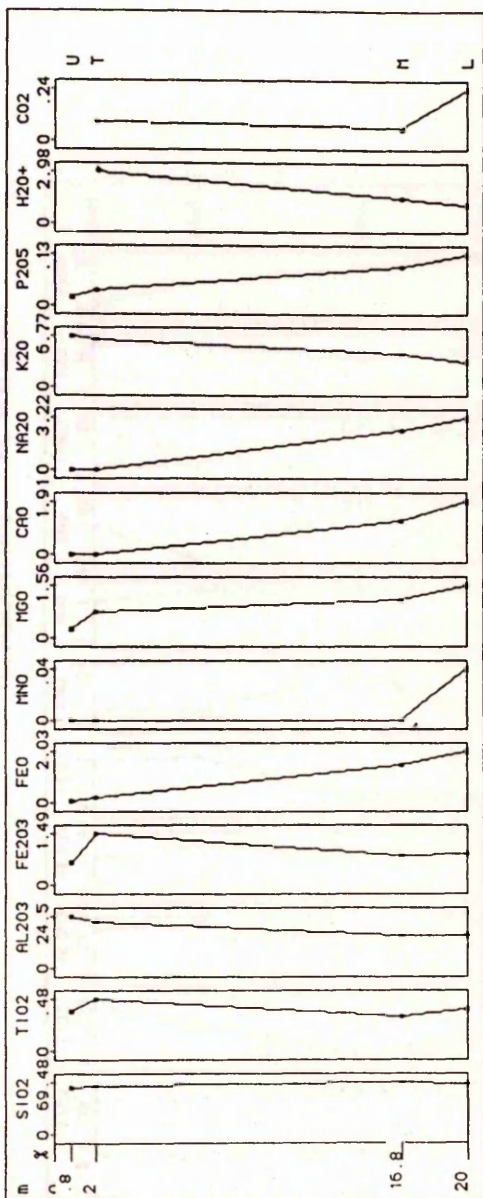
Sample No.	8739	8740	8742	8744	8745	8746	3288	3488	3488	3588	3688	3788	3888	3589
Cr	180	10	4	4	6	17	10	15	0	3	10	11	28	14
Ni	55	3	0	5	3	3	2	6	5	4	2	6	3	18
Co	10	1	2	0	1	0	0	5	8	4	0	1	6	3
Cu	2	2	2	2	4	0	13	17	4	11	9	10	0	1
Zn	14	14	17	14	13	14	20	45	6	30	13	29	10	1
U	3	2	2	1	1	2	0	0	0	1	0	1	0	2
Th	0	14	0	0	0	0	24	10	0	53	6	3	5	1
Pb	1	20	10	8	19	18	28	18	39	28	30	25	21	0
Rb	150	134	134	88	138	141	131	65	233	129	121	230	72	61
Sr	9	118	71	45	144	95	543	566	930	503	402	493	1048	19
Ba	268	682	501	229	686	650	2160	1069	7505	1924	1320	1938	1059	627
Zr	194	34	23	13	49	29	177	72	0	325	338	14	0	188
Y	4	2	1	0	2	1	4	9	0	7	2	0	2	10
Ga	35	26	31	23	27	28	18	21	13	19	19	18	24	24
La	86	8	7	2	6	0	67	24	0	108	29	21	11	28
Ce	73	17	2	0	7	0	145	66	2	223	56	35	27	57
S.G.							2.69	2.69	2.60	2.72	2.66	2.60	2.66	
K/Na	185.1	157.97		30.26	54.31									μ
K/Rb	469	512	525	561	496	513	386	379	397	404	357	239	339	860
K/B a	262	101	140	216	100	111	23	23	12	27	33	28	23	84
K/Sr	7813	582	990	1098	476	761	93	44	100	104	107	112	23	2762
Rb/Sr	16.67	1.14	1.89	1.96	0.96	1.48	0.24	0.11	0.25	0.26	0.30	0.47	0.07	3.21
Al/Ga	3362	4293	4072	3717	3640	3871	4846	3894	7040	3992	4168	4037	4528	4349
Fe ³⁺ /Fe ²⁺	17.75	4.74	6.29	24.97	31.27	33.07	1.47	1.71	1.52	0.57	2.06	0.57	1.10	37.19

Appendix II cont'd.....

Sample No.	BAY I [NC 434 662]				BAY I [NC 435 662]			SMALL BAY [NC 433 663]							
	U	T	S	R	Q	P	M	L	1	3	6	8749	8754	8755	8759
Depth below unconformity (m)	-0.8	2.0	2.0	3.1	3.5	6.8	16.8	20.0	0.1	0.3	0.1				
SiO ₂	62.00	64.06	67.48	62.45	67.10	62.86	69.48	67.38	68.07	70.38	92.93	67.53	71.49	59.47	
TiO ₂	0.37	0.48	0.32	0.59	0.25	0.51	0.32	0.39	0.05	0.01	1.79	0.35	0.05	0.40	
Al ₂ O ₃	24.50	21.68	21.23	22.46	18.09	15.28	15.51	15.24	19.58	17.34	2.99	15.55	15.85	17.13	
Fe ₂ O ₃	0.63	1.49	0.83	1.79	2.02	2.49	0.84	0.91	1.09	0.52	0.45	1.09	0.46	1.47	
FeO	0.05	0.19	0.04	0.25	0.41	2.45	1.46	2.03	0.16	0.08	0.10	0.05	0.03	1.94	
MnO	0.00	0.00	0.02	0.00	0.02	0.06	0.00	0.04	0.00	0.02	0.02	0.05	0.05	0.13	
MgO	0.28	0.79	0.29	0.77	1.15	2.86	1.12	1.56	0.66	0.34	0.36	2.01	0.63	2.86	
CaO	0.00	0.00	0.00	0.00	0.00	0.04	1.19	1.91	0.00	0.00	0.00	2.60	0.83	4.89	
Na ₂ O	0.00	0.00	0.00	0.06	0.01	0.09	2.42	3.22	0.00	0.00	0.00	3.97	3.69	4.16	
K ₂ O	6.77	6.43	5.97	6.50	6.00	9.88	4.58	3.37	7.59	9.31	1.37	3.01	6.09	2.42	
P ₂ O ₅	0.02	0.04	0.04	0.01	0.01	0.12	0.10	0.13	0.01	0.01	0.02	0.12	0.01	0.21	
H ₂ O ⁺	2.98			2.45	2.45	1.32	1.52	1.06	2.27	1.22	0.37	0.89	0.83		
CO ₂	0.09			0.18	0.18	0.08	0.06	0.24	0.26	0.10	0.24	0.15	0.18		
TOTAL	98.23			98.01	98.04	98.60	97.48		99.74	99.33	100.64	99.16			

Appendix 11 cont'd...

	U	T	S	R	Q	P	M	L	1	3	6	8749	8754	8755	8759
Cr	48	42	34	35	29	310	26	49	8	6	44	11	50	5	82
Ni	27	100	26	50	35	82	27	38	12	7	3	8	12	0	46
Co	4	19	3	9	5	20	7	9	4	9	1	10	12	0	16
Cu	9	7	7	8	12	7	12	14	10	1	9	9	4	3	5
Zn	0	5	2	4	24	67	36	58	12	6	4	9	61	12	67
U	1	1	0	2	3	3	0	1	1	0	2	3	1	2	1
Th	3	11	9	3	15	3	10	12	0	1	24	0	2	0	10
Pb	1	4	2	2	5	3	12	15	11	30	6	25	31	42	19
Rb	195	247	170	326	191	190	108	103	109	144	24	134	91	128	56
Sr	28	33	48	15	20	49	209	267	88	173	26	197	483	415	638
Ba	137	291	160	237	246	595	805	690	474	869	163	707	684	840	835
Zr	140	159	125	143	126	110	142	172	46	39	919	45	131	87	158
Y	7	20	11	5	13	5	6	5	9	6	25	4	8	1	7
Ga	26	25	30	26	28	18	19	21	32	20	2	14	22	23	19
La	51	57	71	20	17	19	23	14	12	15	55	8	19	0	32
Ce	58	103	105	35	45	41	57	37	9	24	119	22	41	3	62
K/Rb	288	216	292	166	261	432	352	272	578	537	474		275	395	359
K/Ba	410	183	310	228	202	139	47	41	133	89	70		37	60	24
K/Sr	2007	1618	1033	3598	2491	1674	182	105	716	447	437		52	122	32
Rb/Sr	6.96	7.48	3.54	21.73	9.55	3.88	0.52	0.39	1.24	0.83	0.92	0.68	0.19	0.31	0.09
Al/Ga	4988	4590	3746	4572	3420	4493	4321	3841	3239	4589	7913		3741	3648	4772

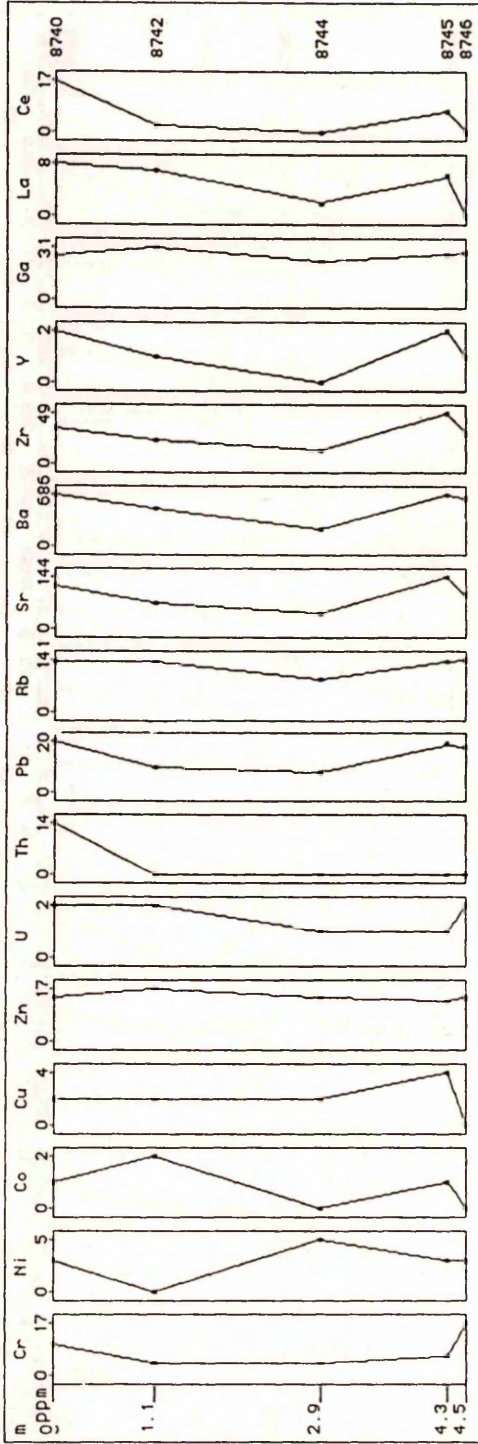
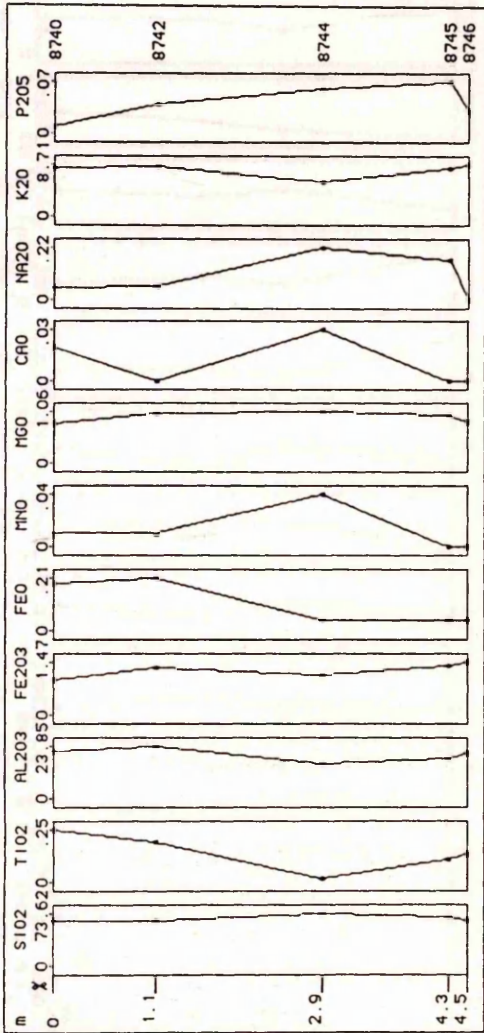


APPENDIX J2a

APPENDIX J2

Variation diagrams showing changes in major element oxides and trace elements with depth below the unconformity: from (a) Bay 1 [NC 434 662], (b) Telegraph Hut [NC 4435 6394] and (c) Cranstackie [NC 34 55].

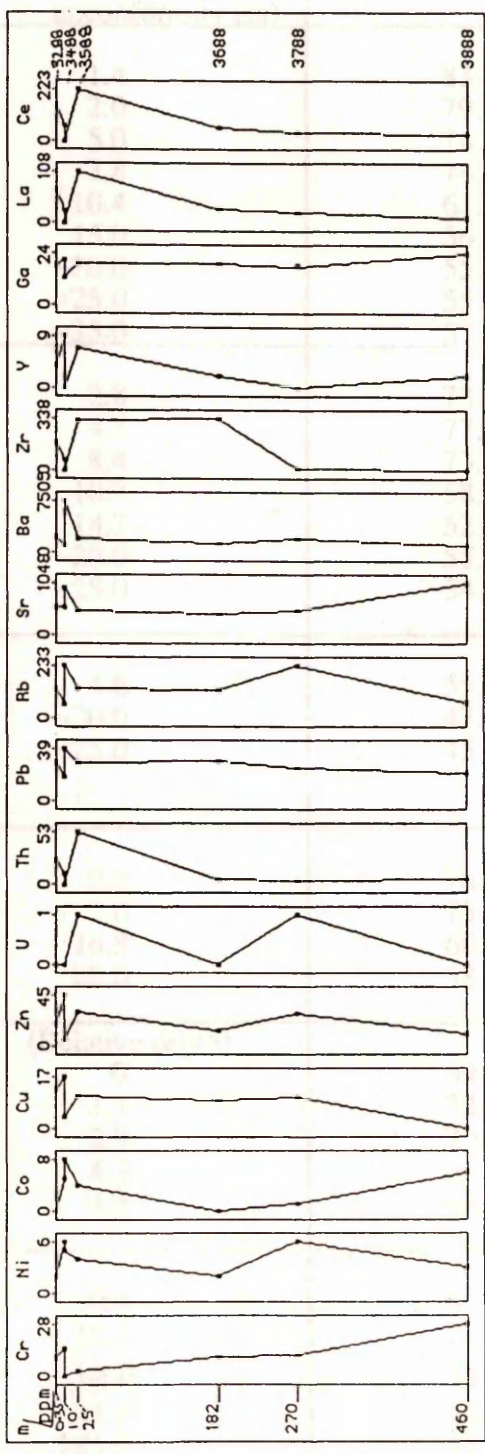
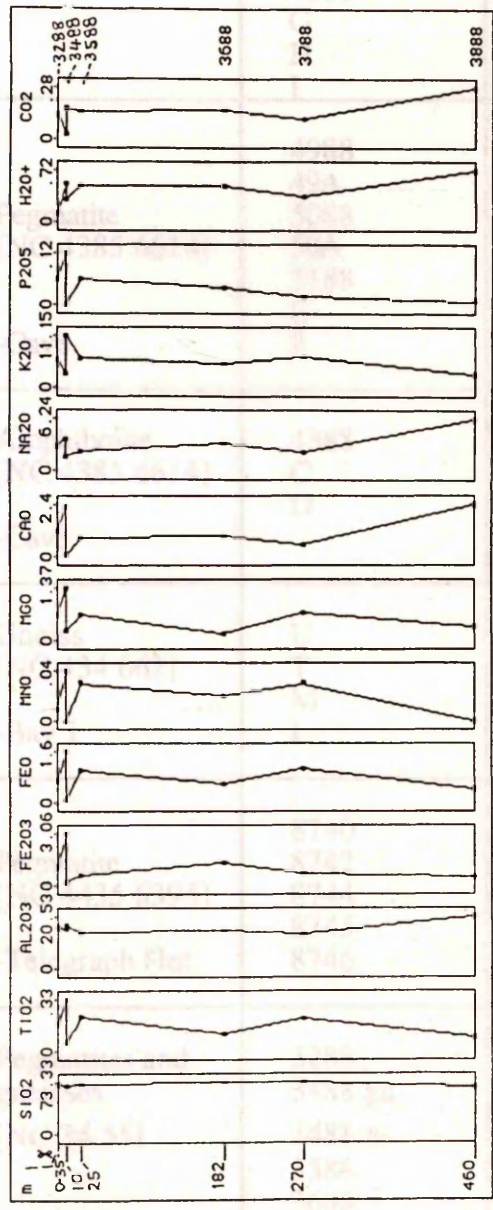
TELEGRAPH HUT NC 4435 6394



APPENDIX 11

Chemical Index of Alteration (CIA) values for samples shown in Fig. 9.1

CRANSTACKIE NC 34 55



APPENDIX 13Chemical Index of Alteration (CIA) values for samples shown in Fig. 6.2

Suite location and name	Sample	Depth below unconformity (m)	CIA
Gneiss [NC 4385 6614] -Cave	GnA	1.4	83.17
	4688	2.0	79.78
	46A	5.0	74.59
	4788	7.8	74.67
	47A	10.4	61.84
	4888	15.0	56.35
	G	~20.0	55.28
	H	~25.0	55.96
	I	~25.0	57.28
Pegmatite [NC 4385 6614] -Cave	4988	2.8	73.60
	49A	4.7	77.29
	5088	8.4	73.01
	50A	10.7	58.93
	5188	14.7	52.03
	E	~20.0	55.33
	F	~25.0	54.30
Amphibolite [NC 4385 6614] -Cave	4388	4.6	55.23
	C	~20.0	47.49
	D	~25.0	45.91
Gneiss [NC 434 662] -Bay 1	U	0.8	76.98
	T	2.0	75.69
	M	16.8	60.75
	L	20.0	58.79
Pegmatite [NC 4435 6394] -Telegraph Hut		(Relative depth)	
	8740	0	69.97
	8742	1.1	72.03
	8744	2.9	70.28
	8745	4.3	66.85
8746	4.5	68.48	
Pegmatites and gneisses [NC 34 55] -Cranstackie	3288	0.4	56.66
	3488 gn	10.0	57.59
	3488 π	10.0	53.68
	3588	25.0	55.38
	3688	182.0	55.47
	3788	270.0	54.21
3888	460.0	56.78	

Precambrian paleosols referenced in the text (especially Chapter 6).

Reference	Age of Palaeosol	Protolith	Mineralogy of palaeosol	Country & locality
Button, 1979	~2.2 Ga	basalt	sericite (at top) iron-rich chlorite, quartz, sericite magnetite (at base)	Republic of South Africa
Button & Tyler, 1979	3.0 Ga	granite	sericite, quartz	Republic of South Africa. Pongola, Transvaal
Button & Tyler, 1981	2.8 Ga	rhyolite	pyrophyllite, chloritoid, rutile, muscovite	Republic of South Africa. Transvaal
	2.75 Ga	felsite	sericite, opaques	Republic of South Africa. Transvaal
	>2.2 Ga	basalt	sericite, chloritoid, rutile	Republic of South Africa. Transvaal
	2.7 Ga	diabase	sericite	Republic of South Africa. Eastern Transvaal
G-Farrow & Mossman, 1988	>2.29 Ga	granite	sericite, quartz	Canada: NAN claim, Elliot Lake, Ontario
	>2.29 Ga	greenstone	sericite, quartz, chlorite, rutile	Canada: Denison mine, Elliot Lake, Ontario
	>2.29 Ga	greenstone	chlorite, biotite, quartz, silica, veinlets, feldspar, rutile	Canada: Stanleigh mine, Elliot Lake, Ontario
Gay & Grandstaff, 1988	>2.29 Ga	granite	sericite, quartz, microcline, pyrite	Canada: Pronto mine, Elliot Lake, Ontario
	>2.29 Ga	greenstone	sericite, quartz, biotite, Fe-chlorite	Canada: Denison mine, Elliot Lake, Ontario

Appendix 14 Cont'd...

Reference	Age of Palaeosol	Protolith	Mineralogy of palaeosol	Country & locality
Grandstaff <i>et al.</i> 1986	>2.8 Ga	granite	quartz, sericite, andalusite	Republic of South Africa: Jerico Dam, Transvaal
	>2.5 Ga	granodiorite	sericite, quartz, iron, chlorite, leucoxene	Republic of South Africa: Otrosdal, Transvaal
Holland <i>et al.</i> 1989	1.8 Ga	pillow basalt	muscovite, haematite, quartz, illite	Canada: Flin Flon, Manitoba
Kalliokoski, 1975	~900- 1100 Ma	granodiorite	sericite-chlorite, vermiculite illite, haematolite K-feldspar, dolomite cemented zones	Canada: Presque Isle Point, Marquette, Michigan
	~900- 1100 Ma	peridotite	chlorite, vermiculite, dolomite, quartz, haematite, talc	"
	~900- 1100 Ma	diabase	haematite, quartz, chlorite-vermiculite	"
Kimberley <i>et al.</i> 1980				
Kimberley & Grandstaff, 1986	>2.9-3.0Ga >2.8-2.9Ga >2.7 Ga >2.3 Ga	granodiorite granodiorite basalt basalt	Lime-green sericite	Republic of South Africa Republic of South Africa Canada: Blanche River, Ontario Republic of South Africa
Rankama, 1955				
Reimer, 1986				Republic of South Africa.

Appendix 14 Cont'd...

Reference	Age of Paleosol	Protolith	Mineralogy of palaeosol	Country & locality
Retallack, 1986	2.2 Ga	basalt		Republic of South Africa, Waterval Order, Transvaal
Schau & Henderson, 1983	>2.7 Ga	granite	paragonite, muscovite, chlorite, quartz opaques	Canada: Steep Rock Lake, Atikokan, Ontario
	>2.65 Ga	granite	feldspars extremely altered	Canada: Point Lake, NW Territories
	>2.95 Ga	gneiss	no regolith but composition of overlying sediments \Rightarrow weathering	Canada: Laughland Lake, NW Territories
Williams, 1968	pre-	gneiss/ pegmatite	Primary quartz & microcline. Plagioclase partly altered to pale-green fine micaceous matrix & patches of carbonate are present. Biotite altered giving haematite. Also epidote. (Amphibolite contains secondary chlorite, carbonate and iron oxide.)	Scotland, U.K.: Sheigra, Sutherland.

Appendix 15 Cont'd...

Sample No.	0689	1289	1389	3989	0988	1989 1	1989 5	1989 6	0589	6188	0489	4188	5788	0189	0289 Up	0289 Lo	4288
Cr	26	247	27	192	72	13	10	16	153	195	71		89	34	83		88
Ni	7	64	6	36	14	6	4	0	32	16	19		25	15	41		25
CO		9	7	7	2		6	1	12	4	11		8	5	46		14
Cu	10	33	0	22	14	3		5	40	23	12		9	5	10		34
Zn	0	46	3	10	6		2	2	8	10	8		36	27	10		15
U	0	1		5	2	0		0	2	3	1		3	2			3
Th		3	0	12	14	8	2	2	6	10	5	8	15	1	10		12
Pb	8	12	5	10	14	1	3	4	16	8	11		15	2	38		18
Rb	79	179	18	130	129	9	6	23	131	106	140		177	80	137		130
Sr	108	93	30	56	183	15	27	36	98	65	76		95	72	97		79
Ba	1045	658	173	559	1298	31	284	258	937	555	573		669	617	599		405
Zr	110	267	87	897	663	215	63	131	376	168	234		215	142	371		135
Y	4	5	5	16	16	7	5	6	8	9	27	53	26	10	18		16
Ga	12	47	4	33	20	3	1	2	31	32	18		22	11	12		20
La	5	22	4	33	55	38	2	15	22	43	51		53	11	28		43
Ce	13	45	12	65	100	70		39	46	80	122		107	18	68		85
K/Na	110	508	∞	∞	∞	∞	46	∞	626	765	280	385	∞	2.98	136	10.73	∞
K/Rb	1030	421	881	455	687	590	2159	563	709	1071	594		595	395	515		667

APPENDIX 16**16a Detailed preparation procedure for determination of trace levels of Boron, by inductively coupled plasma spectrometry (ICPS)- after Walsh, 1985.****A. WEIGHING ROOM.**

1. Palau (or platinum) crucibles used in the experiment should ideally be kept (although not crucial for this job) in the weighing room for 1/2 an hour before weighing. Weighing room should be draught-free. Pay special attention that spatulas are CLEAN - with lithium borates FAR AWAY.

2. 0.200g of sample, i.e. powder crushed to 250 # or 100 #, is weighed into crucible. 1.000g of potassium carbonate is weighed on top (viz. after sample). (Hence if too much is added, it should be easy to remove excess without removing other material). The two substances should then be gently mixed, until the sample is approximately homogeneous.

3. Crucibles and lids should be placed into a desiccator.

N.B. Do not put crucible down on organic material (bench etc.). A clean tile should be used for such. May touch outside rim of crucible with clean hands. (There should not be significant contamination from hands).

First four crucibles.....potassium carbonate only - i.e. blanks.

Second four crucibles.....different standards.

Subsequent four crucibles.....three samples and one standard or blank.

B. BUNSENS.

1. Using platinum tipped tongues, crucibles are then transferred from desiccator to silica triangles above bunsens. (Palau crucibles will glow red). Crucibles should be kept over bunsens for 30 to 60 minutes.

NOTE. The material inside will become very viscous and there should be no need to swirl the contents during heating. (Want a 'cake' of material at the bottom after this heating and subsequent cooling).

2. After required time, bunsens are turned off and crucibles allowed to cool.

N.B. The whole bench area around bunsens should be well wiped to avoid contamination. (Asbestos tiles, bunsens etc. should all be clean). New glass silica triangles and new platinum tongues or very clean ones NOT USED FOR LITHIUM BORATE should be used. (Platinum tongues should be placed (facing upwards) on CLEAN ceramic tile when not in use).

C. HOT PLATE.

1. Move cooled crucibles to CLEAN hot plate.
2. Distilled water is then added from water bottle to cover 'cake' of fused material. As this heats up, the fused material will disintegrate and dissolve. (Some fused material which may have adhered to the lid of the crucible should be washed off into the crucible using a couple of drops of water).

3. PTFE rods are used to stir the solution.

4. After all the material has dissolved, the solutions are poured into PTFE centrifuge tubes (with 10, 15 and 20ml marked off) and made up to 10-15ml.

NOTE Use water added to and swirled in the crucibles to make up to maximum volume. This will collect the remainder of the solid material from the crucibles.

5. The solution is then centrifuged at 3000rpm for approximately 1 minute. (After this time the liquid can be gently moved round the inside of the centrifuge tube to collect any solid material left on the side of the tube. The solution is centrifuged again for another minute/1/2 minute).

6. The liquids are then decanted into other PTFE centrifuge tubes and made up to ~17ml max.

(To make up to the final volume, extra DIW is put into the first centrifuge tube down the edge. This small volume of material is again centrifuged for ~1 minute and the liquid then poured into the respective second tube).

N.B. Length of time in centrifuge not critical.

PTFE centrifuge tubes should be for BORON ANALYSIS ONLY.

PTFE centrifuge tubes finished with are emptied, rinsed with DIW and dried.

D. FUME CUPBOARD.

1. Put the four centrifuge tubes in fume cupboard and add 3ml of perchloric acid to each. (Again, exact amount not critical).
2. After solutions have stopped effervescing and cooled down (approximately 1 hour) they should be put in the centrifuge again for ~1 minute. (Again, tube may be gently rotated to pick up any material on the sides, and recentrifuged for ~1 minute). The solid will now be compact.

E. FINAL PREPARATION.

1. Clean ICP bottles (flat at both ends, with caps) are placed on a 2 d.p. balance and zeroed. (Balance should be in a draught-free place).
2. Centrifuged solution is poured into a clearly labeled bottle and solution is made up to 20.50g. To make up to 20.50g, put DIW down PTFE tube and repour. To make up final few points, a pipette (new) can be used to drop in DIW. IF MASS IS ACCIDENTALLY EXCEEDED (e.g. 20.54g), the mass should be recorded and later calculation adjusted accordingly.

N.B. Bottles should only have been used previously in trace element analysis and should have been standing in DIW to leach any elements remaining.

Sample is now ready to be run on ICP.

16b. Operating conditions for the ICP (Walsh, 1985).**Gas flow counts**

Coolant	-	151 min ⁻¹
Auxiliary	-	0.51 min ⁻¹
Injector	-	1.11 min ⁻¹
Power	-	1.1 kw
Solution uptake rate	-	2.1 ml min ⁻¹
Analytical observation : zone height above work coil.	-	12-16mm.

Appendix 16c. Intensities determined by ICP spectrometry.

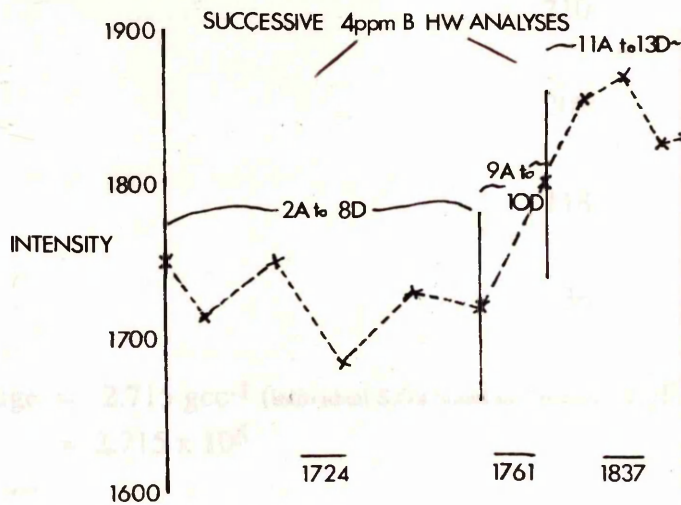
Analysis No.	Sample	Intensity	Mass of Sol ^I	Bppm	Analysis No.	Sample	Intensity	Mass of Sol ^{II}	Bppm
	Distilled H ₂ O	38			7A	0689	242	20.51	44
	Distilled H ₂ O	42			B	1289	910	20.50	204
	Distilled H ₂ O	42			C	0589	784	20.52	174
	4ppm B HW	1738			D	KC 14 standard	134	20.52	18
	Water	40			8A	1189	442	20.52	92
	KC11	144			B	5788	912	20.54	205
	4ppm B BDH	1752			C	0489	572	20.50	123
	4ppm HW K ₂ CO ₃ Std	1688			D	SY-3 standard	388	20.50	79
	40ppm B HW	17,250				4ppm B HW	1720		
	40ppm B BDH	16,992			9A	4288	632	20.52	135
14A	1889 Fusion	136			B	0289	262	20.55	48
B	4988 Fusion	166			C	1589	304	20.96	59
C	4688 Fusion	152			D	KC 10 standard	54	20.52	
D	9888 Fusion	142			10A	5088	940	20.51	207
	4ppm B HW	1714			B	4788	886	20.50	194
1A	Blank	74	20.48		C	4388	544	20.51	114
B	Blank	60	20.51		D	MAG 1 standard	670	20.53	144
C	Blank	54	20.51			4ppm B HW	1802		
D	Blank	56	20.71		11A	0289	254	20.64	44
2A	KC 10 (standard)	62	20.50	1	B	5088	1072	20.53	228
B	KC 11 (standard)	434	20.53	90	C	LKF (A)	102	21.00	10
C	KC 12C (standard)	92	20.51	8	D	SCO 1 standard	392	20.51	75
D	KC 14 (standard)	134	20.51	18		4ppm B HW			
	4ppm B HW	1750			12A	1889	4524	20.51	1004
3A	5288	98	20.81	10	B	4988	992	20.52	210
B	3488 Gn	174	20.52	28	C	4688	1006	20.51	213
C	H	112	20.50	13	D	SGR 1 standard	368	20.50	69
D	Blank	48	20.49	0		4ppm B HW	1870		
4A	Z	116	20.51	14	13A	1889	4338	21.18	994
B	G	96	20.52	9	B	9888	1012	20.51	214
C	F	86	20.58	7	C	9988	1054	20.52	224
D	KC 10 (standard)	50	20.49	0	D	C	194	20.97	31
	4ppm B HW	1684				4ppm B HW	1826		
5A	E	98	20.52	9		Water (DIW)	42		
B	3788/2	70	20.53	3	1A	Blank	62		
C	5188 (fsp)	82	20.51	6		4ppm B HW	1830		
D	KC 11 (standard)	430	20.51	89					
6A	D	180	20.94	30					
B	5188	144	20.51	20					
C	4888	208	20.52	36					
D	KC 12C (standard)	96	20.56	9					
	4ppm B HW	1728							

16d. Determination of B concentration (ppm) from intensity given from ICP spectrometry.

$$B(\text{ppm}) = \left(\text{Intensity}_{(\text{sample})} \cdot \frac{\text{Mass of final liquid}}{20.50} - \text{Intensity}_{(\text{blank})} \right) \cdot \left(\frac{X(\text{ppm known}) \cdot 100}{\text{Intensity at Xppm} - \text{Intensity}_{(\text{blank})}} \right)$$

The average blank intensity throughout the whole analyses was 59ppm.

The intensity for the 4ppm B HW sample fluctuated, with values increasing towards the end of the run (see sketch below). Values were averaged over the ranges shown and these numbers used in determination of Bppm over the respective ranges.



Hence for samples

2A to 8D	Bppm = (Intensity _(s) $\frac{\text{Mass of liquid}}{20.50}$ - 59) $\frac{400}{1665}$
9A to 10D	Bppm = (Intensity _(s) $\frac{\text{Mass of liquid}}{20.50}$ - 59) $\frac{400}{1702}$
11A to 13D	Bppm = (Intensity _(s) $\frac{\text{Mass of liquid}}{20.50}$ - 59) $\frac{400}{1878}$

e.g. Sample 7A.

$$B\text{ppm} = \left(242 \cdot \frac{20.51}{20.50} - 59 \right) \cdot \frac{400}{1665}$$

$$\Rightarrow B\text{ppm} = 44$$

APPENDIX 16e**Determination of seawater column required to supply boron concentration found in agalmatolite.**

B content = 4.6 mg/l in seawater
 = 0.0046 g l⁻¹ assuming boron level in
 Proteozoic/Cambrian seawater was similar
 to that in post-Cambrian seawater (after
 Ethier and Campbell 1977).

Depth below unconformity	B content (ppm)
2m	220
4m	210
6m	
8m	200
10m	
12m	118
14m	
15m	36

S.G - average = 2.715 g cc⁻¹ (individual S.G's noted in Appendix 11)
 $\Rightarrow 1\text{m}^3 = 2.715 \times 10^6$ B content = 150 $\mu\text{g g}^{-1}$
 = 150 x 10⁻⁶ g
 in every g of rock.

Hence in 15m = 40.725 x 10⁶g of rock

Hence total B content = 150 x 10⁻⁶ x 40.725 x 10⁶
 = 6108.75g of boron

Seawater B = 4.6mg/l
 = 0.0046g/l

To satisfy B requirement in altered rock need

How many metres? = $\frac{6108.75}{0.0046}$ litres
 = 1327989
 = $\frac{1327989}{1000}$
 = 1328m
~1.3km of seawater

1l = 1000cm³
 \Rightarrow 1000l in 1m³

If an enrichment of 1000ppm (as found in the pure pinite sample analysed) is assumed as the concentration for the rock in the first metre beneath the unconformity, and individual rather than an average specific gravities are considered, then the depth of seawater determined is ~1.9km.

APPENDIX 17**Experimental methods for $^{40}\text{Ar}/^{39}\text{Ar}$ laser probe investigation.**

1. Thick sections (~1 to 3mm thick) of the rock samples were cleaned ultrasonically in methanol.
2. Samples were wrapped in pure Al foil and irradiated in the Petten reactor, Holland, (row 1, position 3 of the high flux pool side facility, with neutron dose of approximately 10^{18}n cm^{-2} (irradiation EK5)). Samples were rotated half-way through irradiation to minimise the horizontal flux gradient.
3. About 10 to 20 grains of flux monitor Hb3gr (a hornblende) wrapped in aluminium foil was positioned in the central region of each shale slab, in order to measure the J values. These were determined using the laser extraction method.

The 'J' value, $J = \frac{e^{-\lambda t} - 1}{(^{40}\text{Ar}/^{39}\text{Ar})_{\text{HB3gr}}}$

where λ = decay constant ($= 5.543 \times 10^{-10}$)
 $t = 1072$ m.y. (from Roddick, 1983)
 $(^{40}\text{Ar}/^{39}\text{Ar})_{\text{HB3gr}}$ is determined on analysis.

e.g. for the black shale (0589) monitor $J = \frac{e^{5.543 \times 10^{-10} \cdot 1072 \times 10^6} - 1}{144.605}$
 $= 0.005613$

(For shales 0988 and 0589, the J values are 0.00739 ± 0.00007 and 0.00561 ± 0.00003 respectively).

4. Following irradiation, the shales were placed in a laser port connected to a noble gas extraction system. During evacuation to ultra high vacuum, samples were heated with a lamp for 34 hours at $\sim 100^\circ\text{C}$.
5. The laser used was a Nd:YAG continuous wave laser ($\lambda = 1064$ nm) used in TEM₀₀ mode. The laser beam was steered into a modified petrographic microscope and focussed through a 10x objective lens.
6. Laser shots lasting <1 second were fired at the sample, producing melt pits of 50 to 100 μm diameter.
7. The argon gas emitted was purified using a SAES GP10 getter at 400°C for 5 minutes.
8. At the end of this time, the argon was equilibrated into a MAP 215 mass spectrometer for isotopic analysis. Measurements were made on seven masses (35,36,37,38,39,40,41) using an electron multiplier, in 11 successive cycles, lasting a total of ~ 20 minutes. After analysis the peaks were projected to the inlet time. Masses 41 and 35 were measured to assess the hydrocarbon background and Cl content respectively.
9. Blanks were determined using the same procedure as above, but without firing any laser shots. Blanks were measured after every second sample analysis.
10. Corrections applied to the data were; nuclear interference corrections (for details see Roddick, 1983), corrections for mass discriminations, ^{37}Ar decay and background

amounts (obtained from the blanks). Levels of ^{36}Ar released were used to apply a small air correction, i.e.

$$\begin{array}{c}
 \text{Oxide} \\
 \text{NiO} \\
 \text{MgO} \\
 \text{Al}_2\text{O}_3 \\
 \text{SiO}_2 \\
 \text{P}_2\text{O}_5 \\
 \text{TiO}_2 \\
 \text{K}_2\text{O} \\
 \text{CaO} \\
 \text{FeO} \\
 \text{H}_2\text{O} \\
 \text{TOTAL}
 \end{array}
 \begin{array}{c}
 40\text{Ar} = \\
 \uparrow \\
 \text{radiogenic}
 \end{array}
 =
 \begin{array}{c}
 40\text{Ar (meas)} \\
 \uparrow \\
 \text{measured}
 \end{array}
 -
 \begin{array}{c}
 (36\text{Ar(meas)} \times 295.5) \\
 \uparrow \\
 \text{measured}
 \end{array}$$

11. Hence, having determined the value of $^{40}\text{Ar}/^{39}\text{Ar}$ for an analysis, the age could then be determined from the formula.

$$t = 1/\lambda \ln [1 + J (^{40}\text{Ar}/^{39}\text{Ar})]$$

knowing λ , J and $^{40}\text{Ar}/^{39}\text{Ar}$.
(re-arranged formula from (3)).

12a) Quantities K₂O, Na₂O, CaO, MgO, FeO, TiO₂, SiO₂, P₂O₅, NiO, Al₂O₃, H₂O

Oxide	Weight %	Molar %
NiO	0.00	0.00
MgO	0.00	0.00
Al ₂ O ₃	0.00	0.00
SiO ₂	0.00	0.00
P ₂ O ₅	0.00	0.00
TiO ₂	0.00	0.00
K ₂ O	0.00	0.00
CaO	0.00	0.00
FeO	0.00	0.00
H ₂ O	0.00	0.00
TOTAL	0.00	0.00

APPENDIX 18**18a) Quantitative EDS analyses of 0988 matrix material.**

Oxide	%Oxide	Formula	=Formula on 24 O	%Oxide	Formula	=Formula on 24 O
Na2O	0.077	0.026	0.020	0.185	0.069	0.052
MgO	3.614	0.950	0.713	3.271	0.934	0.701
Al2O3	29.972	6.231	4.673	27.211	6.142	4.607
SiO2	56.180	9.909	7.432	51.845	9.927	7.445
P2O5	0.000	0.000	0.000	0.124	0.020	0.015
ClO2	0.009	0.001	0.001	0.041	0.007	0.005
K2O	11.369	2.558	1.919	10.338	2.525	1.894
CaO	0.057	0.011	0.008	0.088	0.018	0.014
TiO2	0.486	0.064	0.048	0.457	0.066	0.050
MnO2	0.000	0.000	0.000	0.012	0.002	0.002
FeO	3.061	0.451	0.338	3.030	0.485	0.364
O		32.000	24.000		32.000	24.000
TOTAL	104.825	20.201	15.152	96.602	20.195	15.149

18b) Quantitative EDS analyses of 0988 K-feldspar clasts.

Oxide	%Oxide	Formula	%Oxide	Formula
Na2O	0.450	0.161	0.252	0.091
MgO	0.068	0.019	0.026	0.007
Al2O3	18.861	4.104	18.883	4.121
SiO2	64.333	11.877	64.100	11.868
P2O5	0.222	0.035	0.235	0.037
ClO2	0.004	0.001	0.027	0.004
K2O	15.603	3.675	15.677	3.703
CaO	0.045	0.009	0.132	0.026
TiO2	0.141	0.020	0.174	0.024
MnO2	0.000	0.000	0.000	0.000
FeO	0.101	0.016	0.014	0.002
O		32.000		32.000
TOTAL	99.828	19.917	99.520	19.883

APPENDIX 19

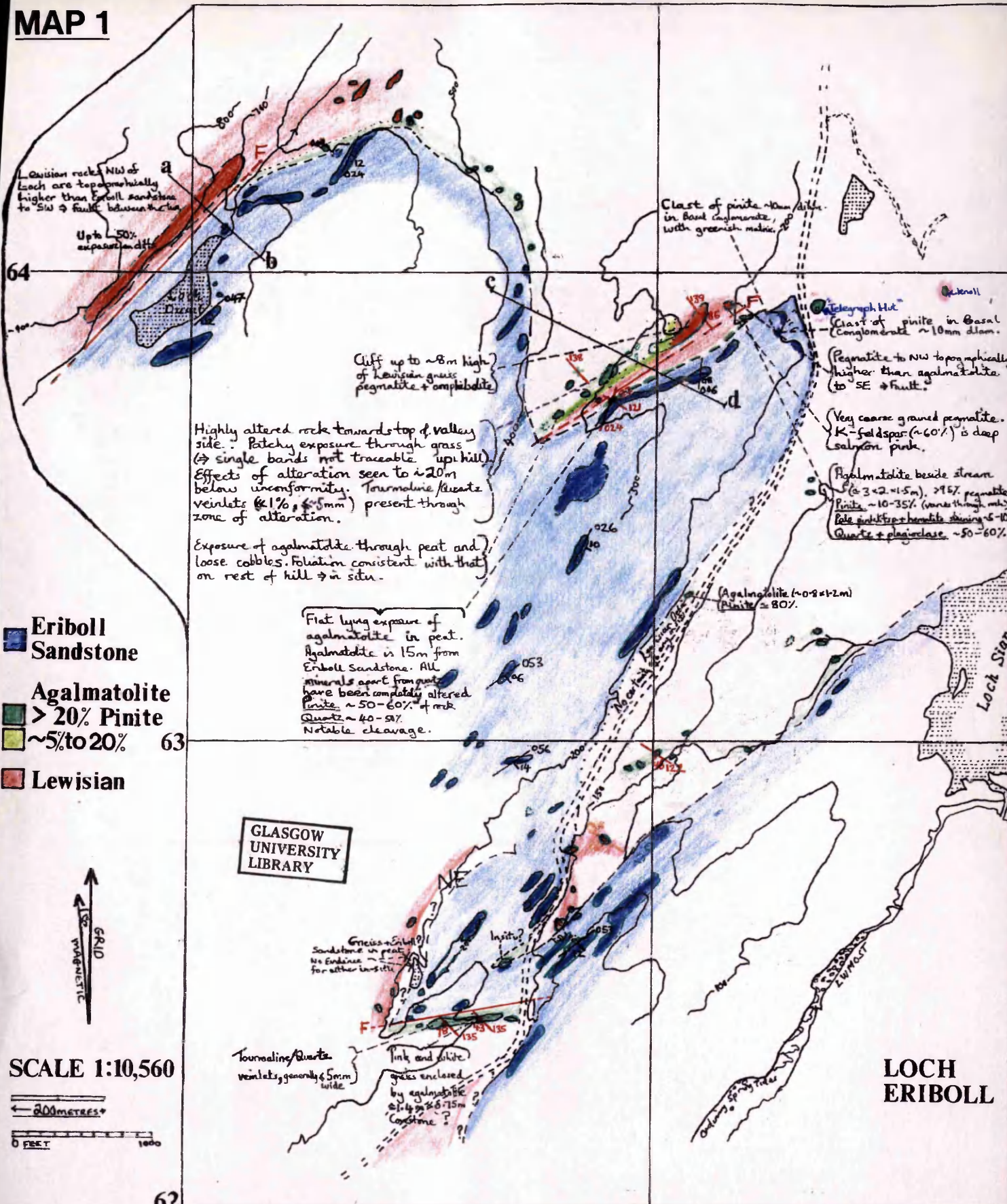
Ages determined from $^{40}\text{Ar}/^{39}\text{Ar}$ laser probe analysis.

Sample	Description of analysed spot	^{40}Ar (cc volt ⁻¹)	^{39}Ar (cc volt ⁻¹)	$^{40}\text{Ar}/^{39}\text{Ar}$	AGE (Ma)	Error (Ma)
0988	White clast (feldspar)	9.2988 x10 ⁻¹⁰	2.3931 x10 ⁻¹¹	38.9	434	
		1.26 x10 ⁻¹²	1.67 x10 ⁻¹³	0.3		3
		5.4306 x10 ⁻¹⁰	1.3604 x10 ⁻¹¹	39.9	445	
		7.2 x10 ⁻¹³	1.37 x10 ⁻¹³	0.4		4
		1.0825 x10 ⁻⁹	2.6894 x10 ⁻¹¹	40.3	448	
		1.08 x10 ⁻¹²	1.57 x10 ⁻¹³	0.2		3
		5.1282 x10 ⁻¹⁰	1.2634 x10 ⁻¹¹	40.6	451	
		7.20 x10 ⁻¹³	8.64 x10 ⁻¹⁴	0.3		3
	Brownish White clast (fsp)	3.2112 x10 ⁻¹⁰	7.8282 x10 ⁻¹²	41.0	455	
		5.4 x10 ⁻¹³	1.03 x10 ⁻¹³	0.5		6
	Light brown clast (Fsp & matrix)	1.5829 x10 ⁻⁹	3.8347 x10 ⁻¹¹	41.3	458	
		1.44 x10 ⁻¹²	2.41 x10 ⁻¹³	0.3		3
	Reddish brown (Haematite stain?)	9.7524 x10 ⁻¹⁰	2.2608 x10 ⁻¹¹	43.1	476	
		9.00 x10 ⁻¹³	1.28 x10 ⁻¹³	0.2		3
	(feldspar)	3.1950 x10 ⁻¹⁰	7.2252 x10 ⁻¹²	44.2	487	
		5.40 x10 ⁻¹³	7.02 x10 ⁻¹⁴	0.4		5
	Brown matrix	6.8238 x10 ⁻¹⁰	1.5363 x10 ⁻¹¹	44.4	488	
		3.60 x10 ⁻¹³	1.28 x10 ⁻¹³	0.4		4
		2.1348 x10 ⁻¹⁰	4.7898 x10 ⁻¹²	44.6	490	
		3.60 x10 ⁻¹³	6.30 x10 ⁻¹⁴	0.6		6
		9.4698 x10 ⁻¹⁰	2.1004 x10 ⁻¹¹	45.1	495	
		1.26 x10 ⁻¹²	1.57 x10 ⁻¹³	0.3		4
		7.7904 x10 ⁻¹⁰	1.6798 x10 ⁻¹¹	46.4	507	
		1.08 x10 ⁻¹²	9.90 x10 ⁻¹⁴	0.3		3
		1.0643 x10 ⁻⁹	2.3108 x10 ⁻¹¹	46.1	510	
		1.26 x10 ⁻¹²	1.24 x10 ⁻¹³	0.3		3
	White clast (feldspar)	1.8828 x10 ⁻⁹	3.6709 x10 ⁻¹¹	51.3	553	
		9.00 x10 ⁻¹³	9.72 x10 ⁻¹⁴	0.1		2
		8.0478 x10 ⁻¹⁰	1.5547 x10 ⁻¹¹	51.8	558	
		1.44 x10 ⁻¹²	8.28 x10 ⁻¹⁴	0.3		3
	Dark brown mineral -feint cleavage	5.9706 x10 ⁻¹⁰	1.0879 x10 ⁻¹¹	54.9	587	
		1.08 x10 ⁻¹²	9.36 x10 ⁻¹⁴	0.5		5
	Biotite	9.5490 x10 ⁻¹⁰	5.6214 x10 ⁻¹²	169.9	1427	
		1.08 x10 ⁻¹²	4.86 x10 ⁻¹⁴	1.5		10

Appendix 19 cont'd...

		1.5795 $\times 10^{-9}$	8.7750 $\times 10^{-12}$	180.0	1471	
		1.44 $\times 10^{-12}$	1.03 $\times 10^{-13}$	2.1		13
0589	Brown	7.3350 $\times 10^{-10}$	1.2589 $\times 10^{-11}$	58.3	506	
		5.40 $\times 10^{-13}$	1.55 $\times 10^{-13}$	0.7		6
	Black vfg material	3.7152 $\times 10^{-10}$	5.4486 $\times 10^{-12}$	68.2	580	
		3.60 $\times 10^{-13}$	4.14 $\times 10^{-14}$	0.5		4
		9.5814 $\times 10^{-10}$	1.3043 $\times 10^{-11}$	73.5	618	
		1.44 $\times 10^{-12}$	8.28 $\times 10^{-14}$	0.5		4
		2.6334 $\times 10^{-10}$	3.4524 $\times 10^{-12}$	76.3	638	
		3.60 $\times 10^{-13}$	6.48 $\times 10^{-14}$	1.4		10
		1.6700 $\times 10^{-9}$	1.9319 $\times 10^{-11}$	86.4	708	
		2.70 $\times 10^{-12}$	1.28 $\times 10^{-13}$	0.6		5
		1.1453 $\times 10^{-9}$	1.1243 $\times 10^{-11}$	101.9	810	
		3.60 $\times 10^{-13}$	6.48 $\times 10^{-14}$	0.6		4
		4.5450 $\times 10^{-10}$	4.1634 $\times 10^{-12}$	109.2	856	
		7.20 $\times 10^{-13}$	6.30 $\times 10^{-14}$	1.7		11
		1.2919 $\times 10^{-9}$	1.0321 $\times 10^{-11}$	125.2	953	
		1.08 $\times 10^{-12}$	8.64 $\times 10^{-14}$	1.1		7
	White clasts (feldspar)	8.9046 $\times 10^{-10}$	1.1614 $\times 10^{-11}$	76.7	641	
		7.20 $\times 10^{-13}$	8.64 $\times 10^{-14}$	0.6		4
		1.8792 $\times 10^{-9}$	2.3267 $\times 10^{-11}$	80.8	669	
		1.62 $\times 10^{-12}$	2.0 $\times 10^{-13}$	0.7		5
		4.1112 $\times 10^{-10}$	5.0652 $\times 10^{-12}$	81.2	672	
		7.20 $\times 10^{-13}$	6.66 $\times 10^{-14}$	1.1		8
		2.3906 $\times 10^{-9}$	2.0066 $\times 10^{-11}$	119.1	917	
		7.02 $\times 10^{-12}$	1.26 $\times 10^{-13}$	0.8		6
		8.7768 $\times 10^{-10}$	5.5332 $\times 10^{-12}$	158.6	1141	
		1.26 $\times 10^{-12}$	9.72 $\times 10^{-14}$	2.8		5

MAP 1



Lewisian rocks NW of Loch are topographically higher than Eriboll sandstone to SW \rightarrow fault between them

Up to 50% exposure in diff.

Clast of pinite 10cm diam. in Basal conglomerate with greenish matrix

Cliff up to ~8m high of lewisian gneiss pegmatite + amphibolite

Highly altered rock towards top of valley side. Patchy exposure through grass (\rightarrow single bands not traceable up hill). Effects of alteration seen to ~20m below unconformity. Tourmaline/Quartz veinlets (1%, \pm 5mm) present through zone of alteration.

Exposure of agalmatolite through peat and loose cobbles. Foliation consistent with that on rest of hill \rightarrow in situ.

Flat lying exposure of agalmatolite in peat. Agalmatolite is 15m from Eriboll Sandstone. All minerals apart from quartz have been completely altered. Pinite ~50-60% of rock. Quartz ~40-50%. Notable cleavage.

Telegraph Hill (Clast of pinite in Basal Conglomerate ~10cm diam.)

(Pegmatite to NW topographically higher than agalmatolite to SE \rightarrow fault.)

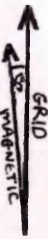
(Very coarse grained pegmatite. K-feldspar (~60%) is deep salmon pink.)

Agalmatolite beside stream (3x2x1.5m), 75% pegmatite. Pinite ~10-35% (varies through rock). Late pink feldspar hornblende staining ~10%. Quartz + plagioclase ~50-60%.

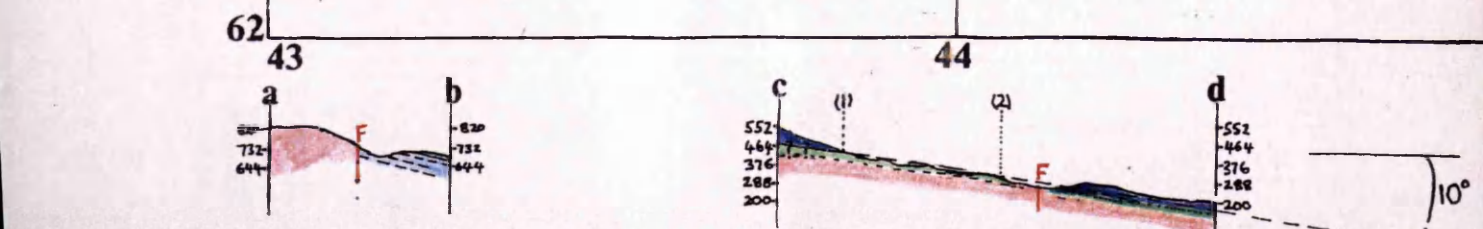
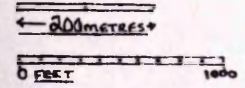
(Agalmatolite ~0.8x1.2m) Pinite ~80%.

- Eriboll Sandstone
- Agalmatolite
- > 20% Pinite
- ~5% to 20%
- Lewisian

GLASGOW UNIVERSITY LIBRARY



SCALE 1:10,560



If unconformity dips at 10° to SE at (1), then (2) would be \equiv projection of point (1). i.e. rocks immediately beneath the unconformity. The large area of exposed agalmatolite SE of (1) is, approximately, the Lewisian surface beneath the unconformity. Assuming no faults between (1) and (2), then the rocks SE of the fault marked must have been down-thrown at least ~35'. (More if angle of unconformity < 10°).

MAP 2

This is a pink, green yellow white and grey, very coarse grained pegmatite.

PINK - K-feldspar ~50% of rock.
 - Crystals up to 25cm long. Very little alteration except along cracks where it is yellowish to lime green. Generally, the smaller the crystal, the greater % alteration.

GREEN - Altered feldspar / pinite ~30% of rock.
 - Feldspars partially altered - lime green. (Generally do not find olive green agalmatolite, except at joints).

GREY - Quartz ~20% of the rocks.
 - Crystals up to 8cm diam. Some crystals have slight greenish tinge due to pinite penetrating along cracks.

WHITE - <5% - Recent bleaching - surficial alteration of feldspars.

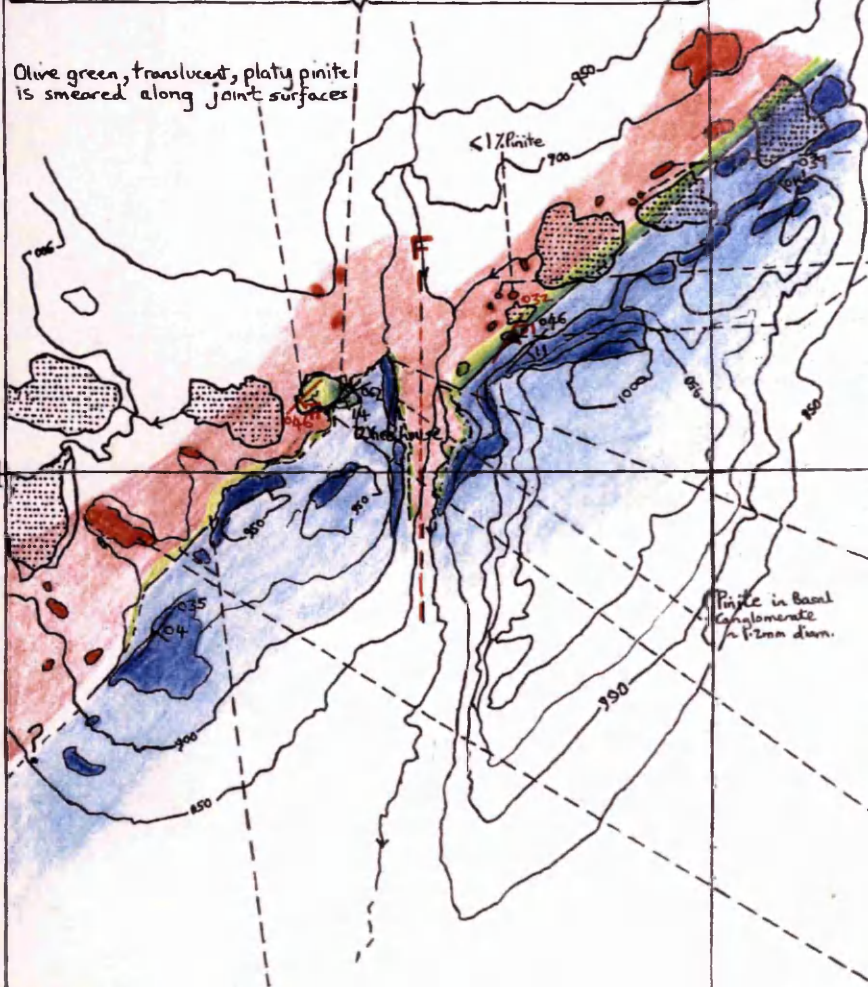
The most notable/distinct feature at this locality is the freshness of so many feldspars immediately beneath the unconformity. Contrast with the exposure at NC 4385 (274). Pink K-feldspar just below the unconformity has vermicular intergrowths of quartz. On close examination, pinite is seen between the K-feldspar and the quartz intergrowths.

K-FELDSPAR ~ 0.18 x 0.16 m. : **QUARTZ INTERGROWTH** up to 1x18 mm - most < 0.5mm wide.

PINITE < 0.1mm.

~50 to 80% of this exposure is composed of pinite (15 x 9 x 2 m). The whole rock is very altered, with all but some remnant quartz changed. Original texture is still discernable (e.g. large precursor feldspar crystals >10cm can be picked out - although now completely green). Different bands maintain original structure although strong foliations have developed - parallel to and perpendicular to the unconformity. The varying shades of green are dependent on the precursor mineralogy.

Olive green, translucent, platy pinite is smeared along joint surfaces



~1% Pinite. Recent - surficial alteration also visible - much harder than pinite.

Slight greenish tinge to micas - but still hard.

Altered lewisian - 0 to 18 cm / 6cm to 24 cm below unc. This is a pink, green, white and translucent grey, fine grained gneiss.

PINK - K-feldspar ~60-70% of rock. Crystals up to 2x1-5mm

GREEN - Pinite ~20-30% of rock. Area ~ 1-5mm diam

Dark green - more definite shapes
 light " - less " (~60-70%) (between crystals)

WHITE/PINKISH WHITE - Recently altered feldspar up to 20% in areas

TRANSLUCENT GREY - Quartz ~10%. Up to 2mm diam.

On exposed surface, pinite stands out more proud than feldspar. (? Perhaps interlocking nature of very fine grained crystals makes pinite more resistant - even though softer?)

(% Difficult to estimate % pinite due to lichen on rock surface. % pinite may be overestimated/ ~3-4 metres below unconformity lewisian almost fresh but feldspars salmon pink (some whitish where exposed conglomerate layer above at base of lower member layer ~3cm thick).

CLASTS: Quartz. Clasts >2mm, ~40% of rock. Up to 15mm

K-FELDSPAR ~ 62mm ~ 5%

MATRIX: Can be very greenish in places

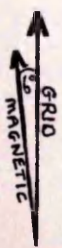
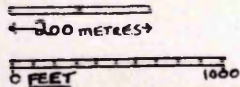
(Lowermost reaches of alteration horizon upstanding, with fresher gneiss surrounding this exposure. "Cut-off" taken at contour line).

No exposure immediately beneath unconformity but 5% pinite <20% inferred due to similarity in depth below unconformity and proximity to exposure at [pic 404 611].

Lewisian - predominantly pegmatite. Large salmon pink feldspars. <5% pinite, but alot of recently altered plagioclase crystals on the surface (creamish yellow).

GLASGOW UNIVERSITY LIBRARY

SCALE 1:10,560



- Eriboll Sandstone
- Agalmatolite: >20% Pinite
- " ~5% to 20% "
- Lewisian